AD-A129 320 PLASMA WAVE TURBULENCE AND PARTICLE HEATING CAUSED BY ELECTRON BEAMS RADI..(U) COLORADO UNIV AT BOULDER DEPT OF ASTRO-GEOPHYSICS M V GOLDMAN 01 JAN 83 CU-1533201 1/3

UNCLASSIFIED AFOSR-TR-83-0498 AFOSR-80-0022 F/G 20/9 NL

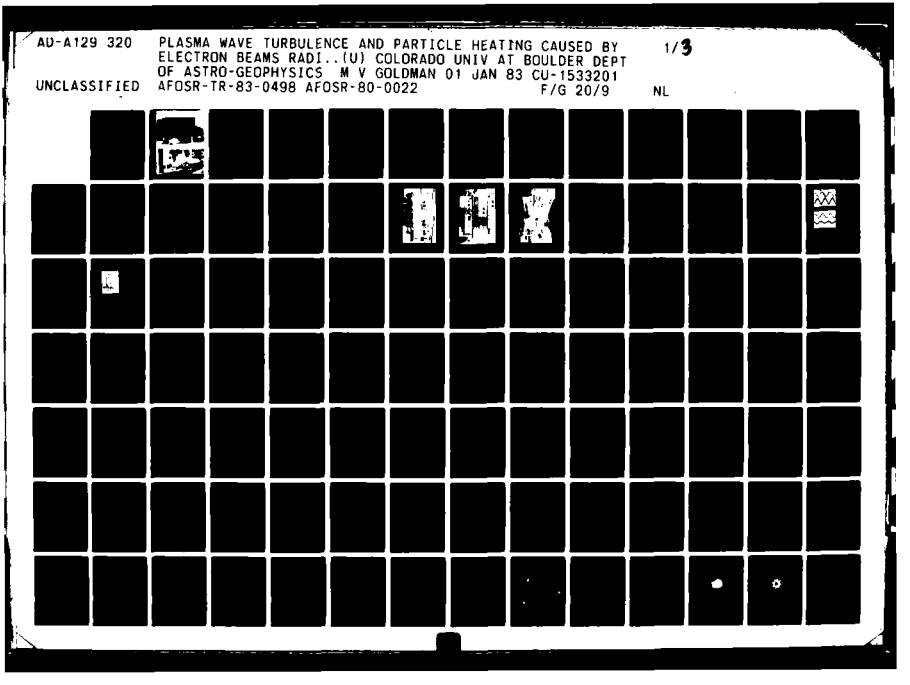

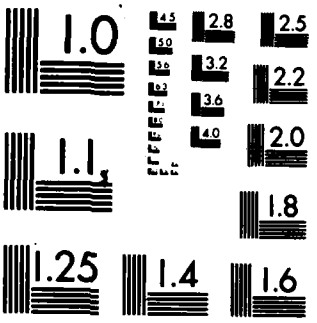

AIR FORCE OFFICE OF SCIENTIFIC RESEARCH

Interim Report: October 1981 - September 198

Plasma Wave Turbulence and Particle Heating

Caused by Electron Beams, Radiation, and Pinch

Martin V. Goldman, Principal Investigator

AIR FORCE OFFICE OF SCIENTIFIC RESEARCH

Interim Report: October 1981 - September 1982

Plasma Wave Turbulence and Particle Heating Caused by Electron Beams, Radiation, and Pinches

Martin V. Goldman, Principal Investigator

AFOSR-80-0022

CU#-1533201

January, 1983

UNCLASSIFIED

SECURITY CLASSIFICATION OF THIS PAGE (When Data Entered)

REPORT DOCUMENTATION PAGE		READ INSTRUCTIONS BEFORE COMPLETING FORM
1. REPORT NUMBER AFOSR-TR- 83-0498	2. GOVT ACCESSION NO. AD-A129320	3. RECIPIENT'S CATALOG NUMBER
4. TITLE (and Subtitle) PLASMA WAVE TURBULENCE AND PARTICLE HEATING CAUSED BY ELECTRON BEAMS, RADIATION, AND PINCHES		5. TYPE OF REPORT & PERIOD COVERED ANNUAL 1 Oct 81 - 30 Sep 82 6. PERFORMING ORG. REPORT NUMBER
7. AUTHOR(s) Martin V. Goldman		8. CONTRACT OR GRANT NUMBER(s) AFOSR 80-0022
9. PERFORMING ORGANIZATION NAME AND ADDRESS University of Colorado Department of Astro-Geophysics Boulder, Colorado 80309		10. PROGRAM ELEMENT, PROJECT, TASK AREA & WORK UNIT NUMBERS 61101F 2301/A8
11. CONTROLLING OFFICE NAME AND ADDRESS AFOSR/NP BUILDING 410 BOLLING AFB, DC 20332		12. REPORT DATE 1 January 83 13. NUMBER OF PAGES
14. MONITORING AGENCY NAME & ADDRESS(if different from Controlling Office)		15. SECURITY CLASS. (of this report) UNCLASSIFIED 15a. DECLASSIFICATION/DOWNGRADING SCHEDULE

16. DISTRIBUTION STATEMENT (of this Report)

Approved for public release;
distribution unlimited.

17. DISTRIBUTION STATEMENT (of the abstract entered in Block 20, if different from Report)

18. SUPPLEMENTARY NOTES

19. KEY WORDS (Continue on reverse side if necessary and identify by block number)

20. ABSTRACT (Continue on reverse side if necessary and identify by block number)

This report covers research performed from 1 Oct 81 through 30 Sep 82 on electron beam excited plasma turbulence and electromagnetic emission, on propagation of intense electromagnetic radiation in the earth's ionosphere, and on laboratory experiments on particle beams and plasma waves.

DD FORM 1 JAN 73 1473 EDITION OF 1 NOV 65 IS OBSOLETE

UNCLASSIFIED

SECURITY CLASSIFICATION OF THIS PAGE (When Data Entered)

LIST OF APPENDICES

A. "Beam-Plasma Instability in the Presence of Low Frequency Turbulence," M.V. Goldman and D.F. DuBois, Phys. Fluids, 25, 1062-1072 (1982).

B. "Steady State Turbulence with a Narrow Inertial Range," J.C. Weatherall, D.R. Nicholson and M.V. Goldman, accepted by Physics Fluids.

C. "Backscatter Cascade of Beam Modes off Ambient Density Fluctuations," D.A. Russell and M.V. Goldman, submitted to Physics Fluids.

D. "Preliminary Results Concerning Compton Conversion of Langmuir Waves into High Frequency Electromagnetic Waves in the Presence of an Ultra Relativistic Electron Beam," David Newman.

E. Solitons and Ionospheric Modification," J.P. Sheerin, J.C. Weatherall, D.R. Nicholson, G.L. Payne, M.V. Goldman, and P.J. Hansen, submitted to J. Atmos. Terr. Phys. (March 1982).

F. "Beam-Plasma Interactions in a Positive Ion-Negative Plasma," T. Intrator, N. Hershkowitz, and R.A. Stern, submitted to Physics of Fluids.

G. "Intense Ion Transport in Electrostatic Ion Cyclotron Waves," R.A. Stern and N. Rynn, Proceedings of the 1982 International Conference on Plasma Physics, October, 1982.

H. "Direct Ion Transport Measurements by Optical Tagging," R.A. Stern, D.N. Hill, and N. Rynn, accepted for publication in Physics Letters A.

ABSTRACT

This interim report covers research performed from October 1, 1981 through September 30, 1982, on electron-beam excited plasma turbulence and electromagnetic emission, on propagation of intense electromagnetic radiation in the earth's ionosphere, and on laboratory experiments on particle beams and plasma waves.

TABLE OF CONTENTS

I. Introduction

This interim report describes work performed under AFOSR grant #80-0022 during the period October 1, 1981 to September 30, 1982. The subject of research has been the theory of "Plasma Wave Turbulence and Particle Heating Caused by Electron Beams, Radiation, and Pinches." The period covered is the third stage of a comprehensive research program concerned with the nonlinear behavior of plasma subjected to intensely energetic sources.

One of the significant developments in plasma physics over the past decade has been the theoretical and experimental progress made in our understanding of nonlinear plasma wave evolution in response to external sources: A wide variety of radiation sources such as lasers,[1,2] microwaves,[3,4] and radar,[5,6] and of electron beam sources, such as solar electron streams[7,8] and laboratory beams[9] can excite plasma wave instabilities in target plasmas. The waves saturate into a turbulent spectrum,[10] and may heat the plasma, accelerate plasma particles, and/or emit their own radiation. Such processes have been linked to inertial[11] and magnetic[12] controlled thermonuclear fusion schemes, radar communications in the earth's ionosphere, and electromagnetic emissions from beam-plasma systems in the solar wind[7,8] and in the laboratory.[15] The phenomena also bear heavily on certain fundamental questions of plasma turbulence, such as wave collapse in phase space, electric-field envelope-soliton evolution,[13,14] and the nature of the so-called "strong turbulence."[13]

II. Summary of Accomplishments

In the following summary, we include the accomplishments of our program from October, 1981 to September 1982. The foundation for the present program of research was laid during earlier sponsorship, under AFOSR #F49620-76-C-0005, from August, 1976 through September, 1979, and under AFOSR 80-0022 during the period from October, 1979 through September, 1981.

Our research has been divided into three main areas:

1. Radiation and turbulence created by electron beams incident upon plasmas.
2. Turbulence created by radiation incident upon plasmas.
3. Laboratory studies of beam-plasma systems and plasma turbulence.

We shall discuss recent accomplishments in each of these areas separately. Details can be found in the Appendices.

A. Turbulence and Radiation Due to Beams

i) Plasma Wave Turbulence Excited by Beams

Our research has centered upon fundamental properties of the Langmuir turbulence excited by a warm electron beam passing through a pre-existing plasma, and the electromagnetic emission from such turbulence. It is essential to note that the spectrum and intensity of the radiation cannot be predicted without a thorough knowledge of the spectrum and intensity of the underlying plasma wave turbulence.

In past years, we have demonstrated that the dominant nonlinear physical effect governing the plasma wave turbulence is the ponderomotive force of the plasma waves on the density. In our studies of the resulting wave-wave interactions, we considered the background plasma traversed by the electron beam to be in thermal equilibrium.

More recently, we have studied effects associated with a background plasma possessing ambient non-thermal low-frequency density fluctuations and a non-thermal electron distribution. Some of these effects are described in Appendices A, B and C. We now briefly summarize the resulting picture of beam-excited Langmuir turbulence:

In the absence of significant background density fluctuations, the waves grow until they are large enough to undergo an induced scatter down to a low wave-number "condensate" of spectral energy. The condensate is eventually unstable to modulational instability, which causes energy flow to higher wave numbers, where the waves are damped by an enhanced (nonthermal) level of background plasma electrons with phase velocities lower than the beam velocity. Due to Landau damping off this nonthermal feature of the background electron distribution, the Langmuir spectrum cuts off abruptly at wavenumbers which are only a few times the wavenumber of the beam-resonant waves. Hence, the nonthermal feature prevents the self-focusing, or "collapse" of electron plasma waves down to very small scale sizes. The resulting steady state turbulence is described in

Appendix B. Based on the numerical analysis, we have also made a movie of the evolution of this turbulence in two dimensions, which dramatically shows wave packet evolution and the spatial structure of the turbulence.

It is worth noting that precisely such a nonthermal feature has been found experimentally in real plasmas, such as the background solar wind plasma in which electron beams excite Langmuir waves and electromagnetic emission during Type III solar radio bursts. For this case, we find steady state turbulence with the correct intensity (on the order of the largest spacecraft-measured turbulent intensities), and predict a scale size for electron plasma wave turbulence on the order of 5 or 10 km, also in agreement with measurement. The virtues of studying beam-excited electromagnetic emission during Type III bursts is that the best measurements of beam properties, emission, and Langmuir turbulence exist for such a beam-plasma system.

In two-dimensional numerical work, we have studied the effect of enhanced background density fluctuations (e.g. low-frequency turbulence) on the nonlinear evolution of the beam-unstable Langmuir waves. By solving the Zakharov equations with initial low-frequency turbulence present, it has been found that background density fluctuations on the order of one ten-thousandth of the background density can stabilize the wave growth. The physical basis for this stabilization is the fast scattering of waves out of resonance with the beam as a

result of interaction with the density fluctuations. The requisite level of density fluctuations increases with the growth rate (proportional to the beam density).

A new statistical theory [Appendix A], which we have developed with Dr. D.F. DuBois for electron plasma wave evolution in the presence of a near-gaussian distribution of background density fluctuations, tends to confirm our numerical results. The kinetic equation which we have developed for plasma waves contains the physical effects of absorption, emission, scattering and diffusion of the wave spectrum. Our point of departure is the coupling between dynamically active high-frequency waves and passive (given) low frequency turbulence. The development is very general, encompassing both resonant and nonresonant processes, with careful attention to the conditions for validity of the statistical treatment.

We have solved the kinetic equations for a number of special cases. In the case of density fluctuations of scale size much longer than the wavelength of the beam-modes, a process of small-angle scattering or diffusion occurs, spreading the Langmuir waves into an isotropic distribution of angles. Since waves propagating oblique to a (warm) beam are damped by it rather than amplified, an isotropic distribution is stable. We have calculated the Langmuir wave spectrum under these conditions [Appendix A].

In very recent work [Appendix C], we have solved the kinetic equations for the case of a spectrum of density fluctuations containing scale sizes equal to and shorter than

the wavelength of the beam-modes. Here, there occurs a process of multiple back-scatters off the ambient density fluctuations. Energy is carried to higher wavenumbers, where it is dissipated by thermal or non-thermal Landau damping by the background plasma electrons (we consider both thermal and nonthermal background electron distributions). Even for very small levels of background density fluctuations, the amplification of plasma waves by the beam may be saturated linearly by this scattering process. For still smaller levels, nonlinearity is responsible for saturation, but even in this case, the early scattering by the background fluctuations will alter the nonlinear evloution (work in progress).

It is possible that such scattering plays an important role in relativistic beam-plasma systems, where Buneman and ion-acoustic turbulence may be excited by return currents. This low-frequency turbulence can then suppress the beam-excited Langmuir turbulence and affect the level of electromagnetic emission (work in progress).

We have also explored the basis for a statistical theory of the dynamical (Zakharov) equations of the beam-driven plasma turbulence, by studying intrinsically chaotic behavior of the solutions to the dynamical equations as a function of the beam growth rate. These studies were performed under assumed conditions of adiabatic ions, and with a truncation to a few Fourier modes. With three coupled modes, strange attractors and limit cycles were observed in phase space. With up to seven modes included, limit cycles and chaos and

intermittency were also observed, as well as the development of fast (non-adiabatic) time-scale behavior. It is likely that a statistical treatment of the electron plasma-wave turbulence is only possible in regimes that show chaos.

ii) Radiation from Beam-Plasma Systems

In Appendix D, we describe preliminary results of a calculation of emission of intense high-frequency radiation from a relativistic beam incident upon a plasma. This work is highly relevant to the recent experiments of Benford[15] in which megawatts of radiation at tens-of-gigahertz frequencies were found to emanate from laboratory beam-plasma systems. The mechanism considered here is Compton up-conversion of relativistic-beam-excited Langmuir waves into high-frequency transverse radiation, which has been proposed tentatively by Benford as a possible explanation for his experimental results. The detailed calculation has been undertaken by an advanced graduate student, David Newman. Further work will form part of his PhD thesis.

The preliminary result is that this mechanism may not be as efficient as previously thought. One problem is that although (weak) amplification is predicted for radiation emitted by Langmuir waves parallel to the beam axis, the radiation associated with oblique Langmuir waves experiences damping. Hence, for a beam widely dispersed in angle (as in the Benford experiments), there will be a competion at each angle between amplification and dissipation. This competion will hinder or suppress the emission and may render this particular mechanism less viable as a theoretical explanation for the experiments.

In the case of low density sub-relativistic beams, for which we have developed a deep understanding of the underlying Langmuir turbulence (see Section IIA.(ii) and Appendices A - C

in this proposal), we have carried out calculations of the emission near the plasma frequency and the second harmonic. A manuscript is currently in preparation, but we include here a brief summary of our findings. We have taken our best numerically-determined beam-excited Langmuir spectra and used them as input for calculations of emission of radiation, both in the presence and absence of weak levels of background density fluctuations.

In a quiescent plasma, second-harmonic emission is enabled kinematically by the broad shape of the long-wavelength (condensate) part of the Langmuir spectrum. The intensity of this part of the spectrum is sufficient to enable second harmonic generation by plasma coalescence to be a reasonably efficient emission mechanism. Fundamental emission seems most likely to occur by parametric instability of the condensate into radiation and ion-acoustic waves. The thresholds and mean free paths for this process are favorable.

In the presence of a low level of density fluctuations, fundamental emission can occur by conversion of the Langmuir waves off the local density gradients associated with the fluctuations. We have developed a kinetic equation which describes this process. It also includes anomalous absorption of the emitted radiation by the inverse (so-called Dawson-Oberman) process. Conditions have been determined when this reabsorption is sufficiently strong that the plasma is "optically thick" to this conversion mechanism, and emission is reduced.

Finally, we remark on the progress of our research concerning emission mechanisms which are independent of Langmuir waves in beam-plasma systems. Our statistical theory [Appendix A] contains a preliminary treatment of the so-called plasma laser effect, in which long wavelength waves (Langmuir or electromagnetic) are destabilized by nonresonant interaction with beam-excited Langmuir waves, in the presenece of low-frequency turbulence. The preliminary result is that this effect is weak, unless the low frequency spectrum happens to be narrowly centered upon the beam-resonant part of the Langmuir spectrum.

B. Intense Radiation Incident on Plasmas

Prior work on the modification of the ionosphere by high power HF radar has now appeared as a publication ("Solitons and Ionospheric Heating"--see Publications since October, 1981). Related work has just been submitted for publication [Appendix E]. This research was described in the last interim report.

C. Laboratory Program on Beam-Plasma Interaction - R. Stern

i) Background

As a bridge between experiments and theory, a new laboraconfiguration has been explored and developed, in which beam-plasma interactions can be measured under conditions which are especially suitable for computational modeling. This work, carried out in collaboration with Prof. N. Hershkowitz (U. of Wisconsin) during his sabbatical stay at the University of Colorado as a visiting professor, is being reported as a Ph.D. thesis at the University of Colorado by T. Intrator (now a post-doc at Wisconsin), and was submitted for publication (see Appendix F).

The laboratory program on beam-plasma interactions is intended to measure the production of electromagnetic emission due to the passage of electron beams through plasmas. The purpose of the experiments is to set up, under controlled conditions, a variety of electron beam/plasma configurations which will enable the dominant parameters of the interaction to be measured. These measurements can then be compared with the theoretical predictions, and also generate new information for further consideration.

The appropriate apparatus in which such a study can be carried out is the DP device. Although limited to relatively low beam energies, it has several unique advantages. First, it is a quasi-steady-state instrument, in which beams are

generated at precisely synchronized intervals with a high repetition rate (KHz). This allows the time-evolution of the beam/plasma interaction to be followed exactly. This contrasts with single-shot experiments, in which the shot-to-shot variation can completely mask the time dependence. Secondly, the beam and the plasma properties are independently variable. Finally, it is the only configuration in which complete and self-consistent measurements of the important properties, including low-frequency density fluctuations and particle distribution functions, can be carried out.

The basic device was acquired from Bell Laboratories in October 1981, and is now fully instrumented. Figure 1 illustrates the device; shown are two chambers, respectively an electron-beam source and a plasma generator section, axially connected to each other. Figure 2 is a photograph of the chambers integrated with the instrumentation module, consisting of 1) vacuum pumps and controls, 2) gas handling circuit, 3) power supplies and 4) probes. Figure 3 shows the overall experimental configuration, including electronics and input/output devices. Every one of the experimental segments is fully operational; calibration runs have been completed, and a program of systematic measurements is now in progress.

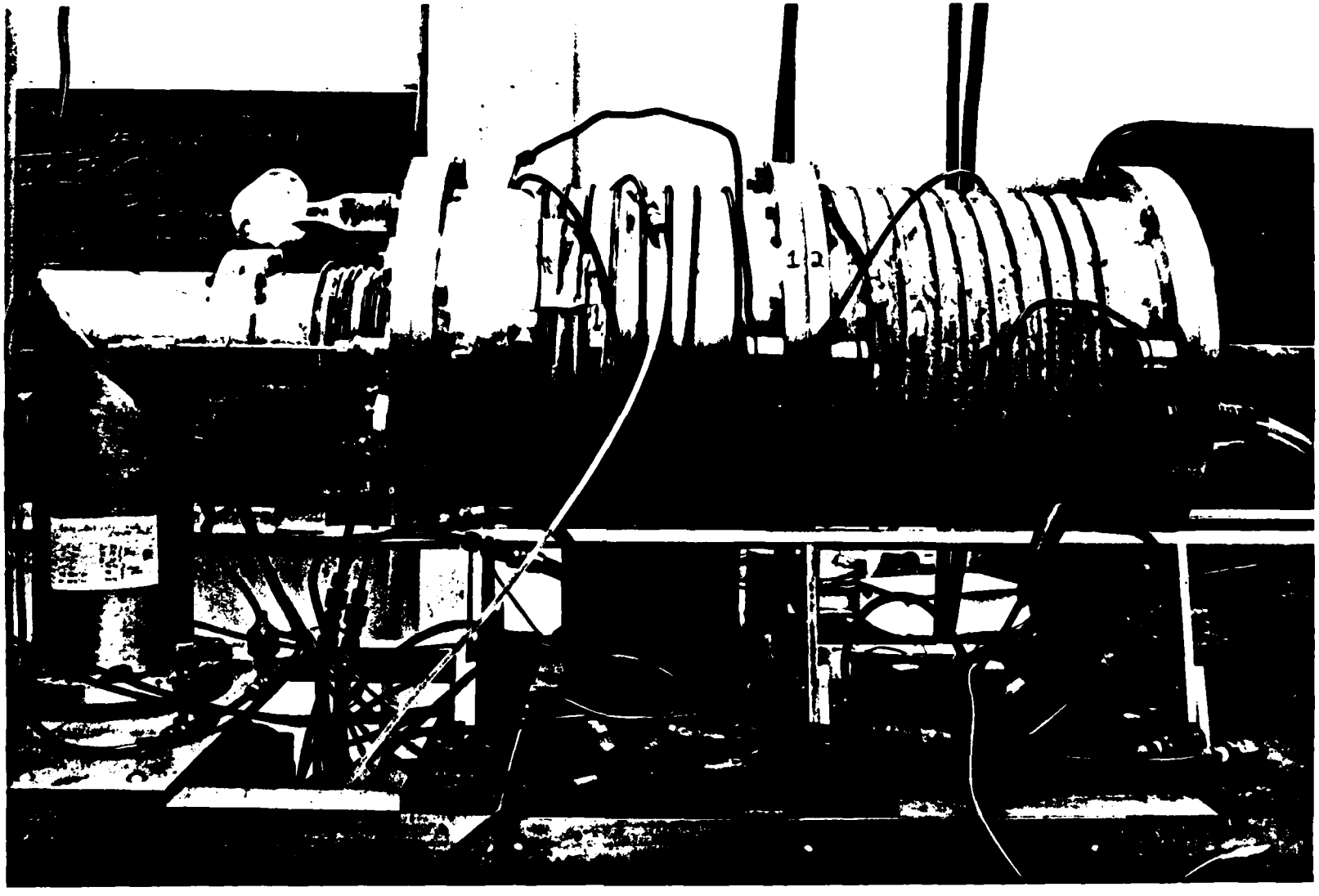

Figure 1

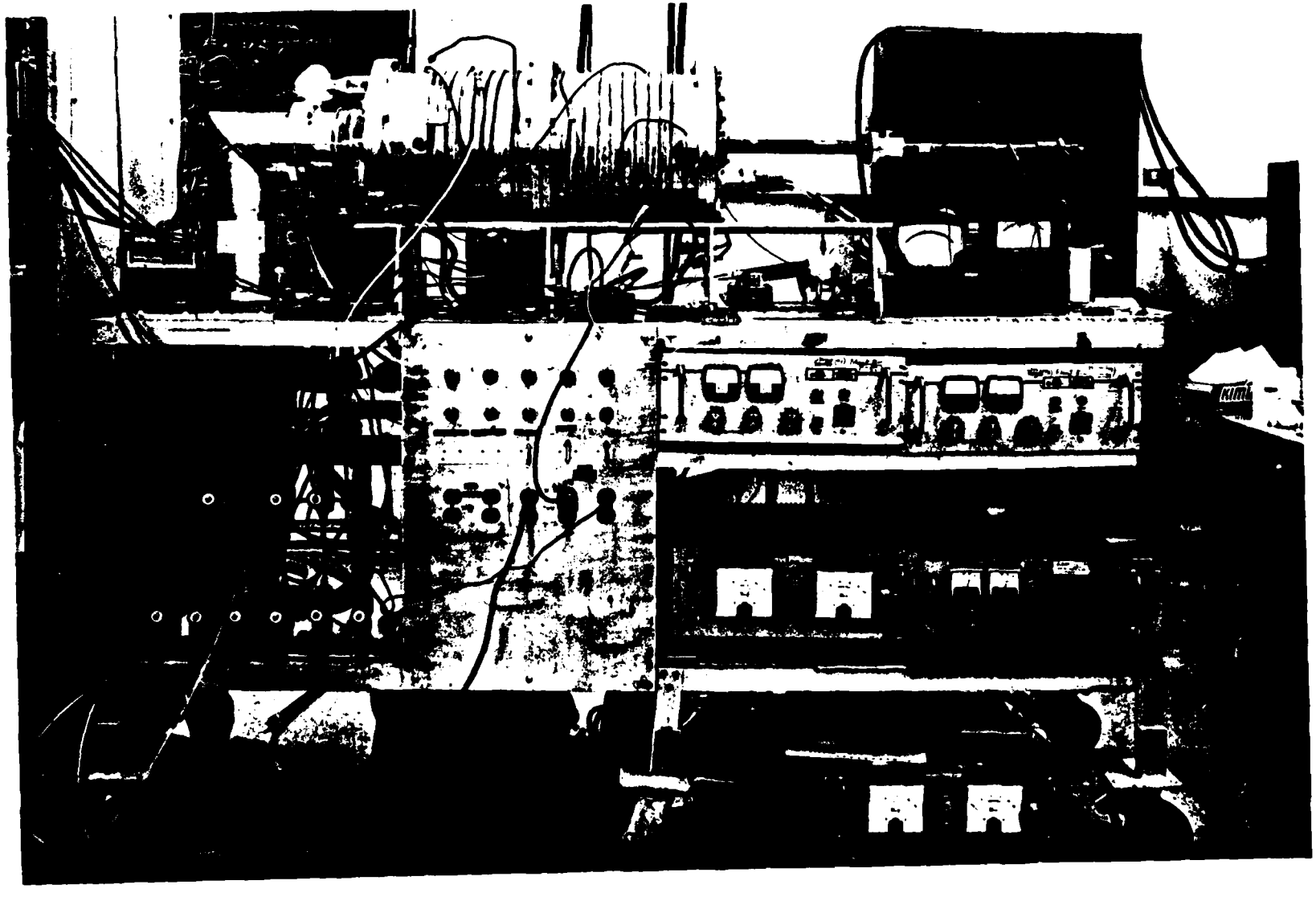

Figure 2

Figure 3

ii) Beam Properties

Tests on plasma generation and electron beam injection were initiated in January, 1982. We have successfully operated the experiment in its basic mode, single-sided injection of an electron beam into a plasma. Figure 4 shows typical Langmuir probe traces in the "target" plasma. These are records of the current drawn to a small, one-sided metal disc in the plasma, as a function of the voltage difference between the disc and the plasma container. Trace A corresponds to the background plasma, in the absence of a beam, with an electron density of 10^8 cm^{-3} and an electron temperature of 1.4 eV. Note that as the voltage sweeps downwards from the right, the large electron current is "turned off," with the current decreasing in an exponential curve below the plasma potential (about 1.5V), leaving only the smaller ion current below about -15V.

During the beam injection, the probe trace changes to B. The effect of the beam can be seen in the lower graph, which plots the difference (B-A) between the above traces. The beam introduces an additional current due to streaming electrons, which is seen to be fairly constant between -3 and -18V. This current represents a beam density of 20% of the background density. Below -18V, the additional current "turns off" (just as the background plasma electrons did below 1.5V), corresponding to an electron beam energy of about 20 eV. Note that the probe traces represent integrals of the electron velocity distribution functions, so that their energy voltage derivatives can provide the functions directly.

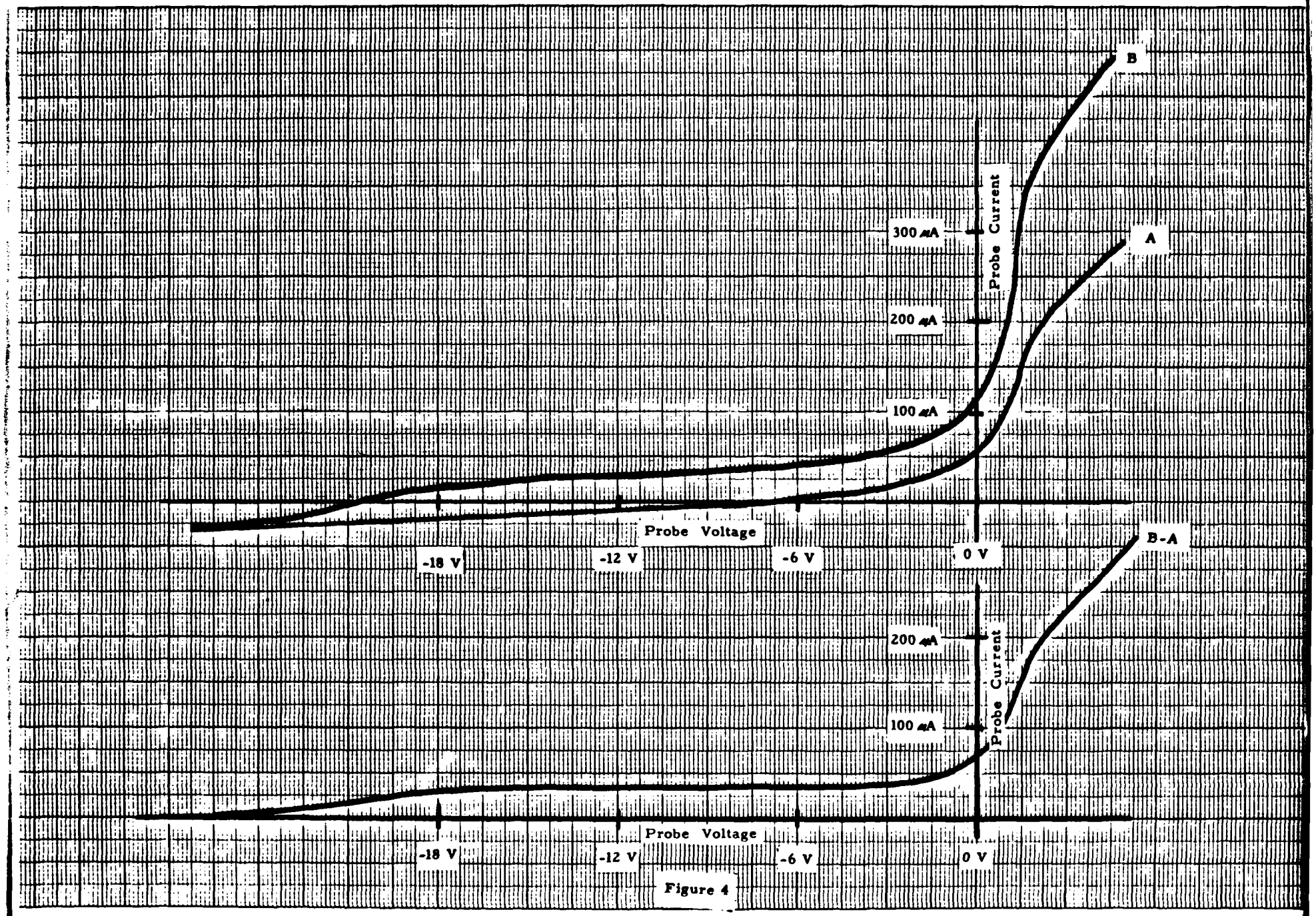
B
300 μA
A
Probe Current
200 μA
100 μA
Probe Voltage
-18 V
-12 V
-6 V
0 V
B-A
200 μA
Probe Current
100 μA
Probe Voltage
-18 V
-12 V
-6 V
0 V

Figure 4

It should be noted that the data in Figure 4 illustrates a high density and high energy beam in which the salient properties are clearly visible. Most of our work utilizes a lower density beam which can be classified as a warm beam, or bump-on-tail. We can, at this point, generate a reproducible beam of 40 eV or more, with a density of up to 20% of the background plasma. Extension of this to greater energies, if necessary, should present no technical difficulties.

iii) Wave Excitation

Tests on wave generation and diagnostics were initiated in June. We have begun to study both externally driven and nonlinearly generated (beam-excited) ion-acoustic waves in the plasma. Figure 5 shows a plot of the measured dispersion relation for these waves when driven externally. The solid line represents the predicted dispersion relation based on the electron temperature as measured by a Langmuir probe, corresponding in this case to a wave phase velocity of 2×10^5 cm/sec. (The dotted lines show the approximate accuracy of this prediction, ± 20%). The plotted points correspond to measurements of the wavelengths at varying frequencies, obtained by measuring phase changes while physically displacing the probe, illustrated in Figure 6.

Wave excitation by the injected electron beams has been attained, and is illustrated below. We recall that the velocity of a 20 eV electron beam is nearly 3×10^8 cm/sec, more than 3 orders of magnitude higher than the ion acoustic wave phase velocity. The electron beam therefore couples

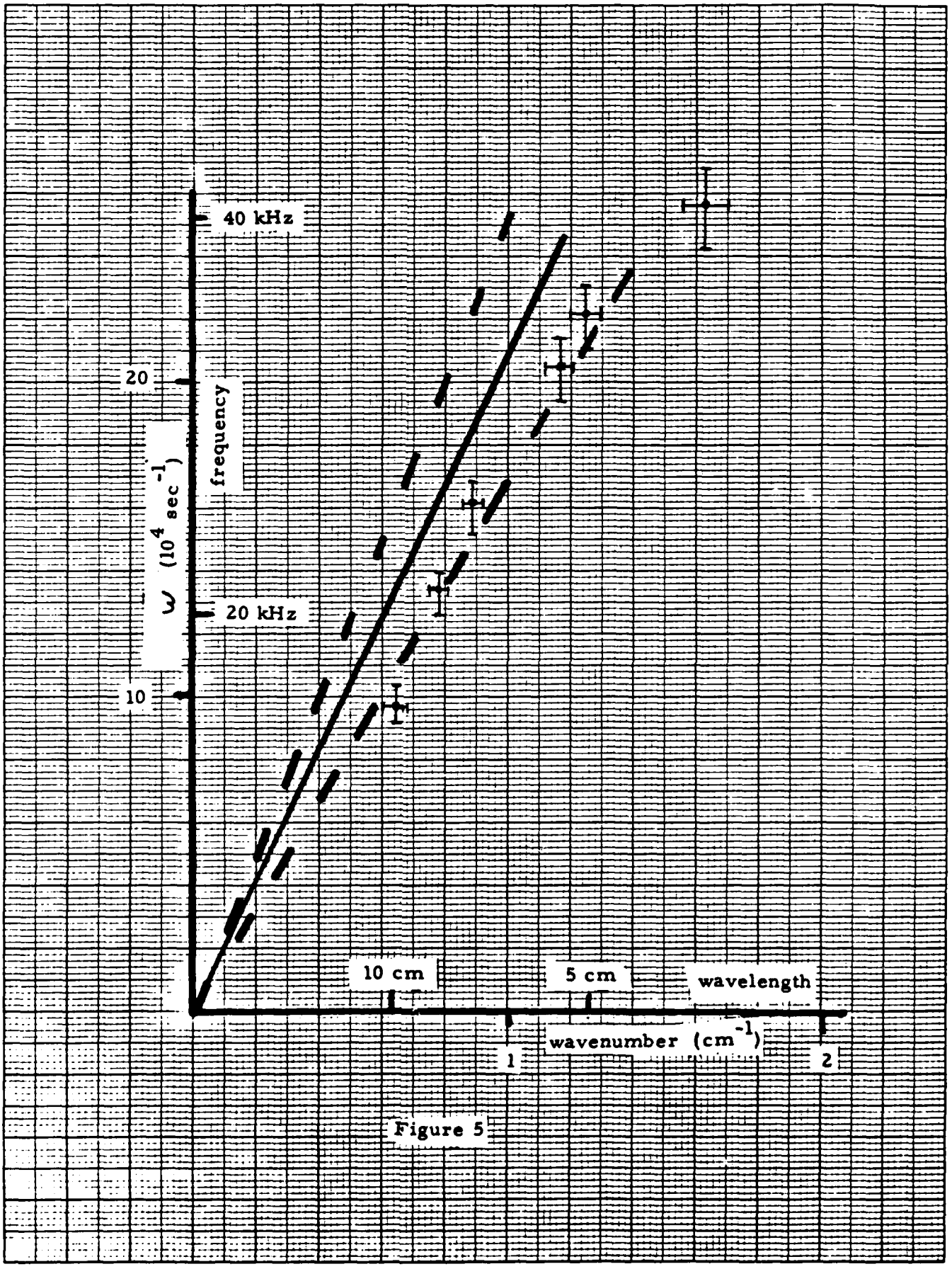
40 kHz
20
frequency
ω (10^4 sec^-1)
20 kHz
10
10 cm
5 cm
wavelength
wavenumber (cm^-1)
1
2

Figure 5

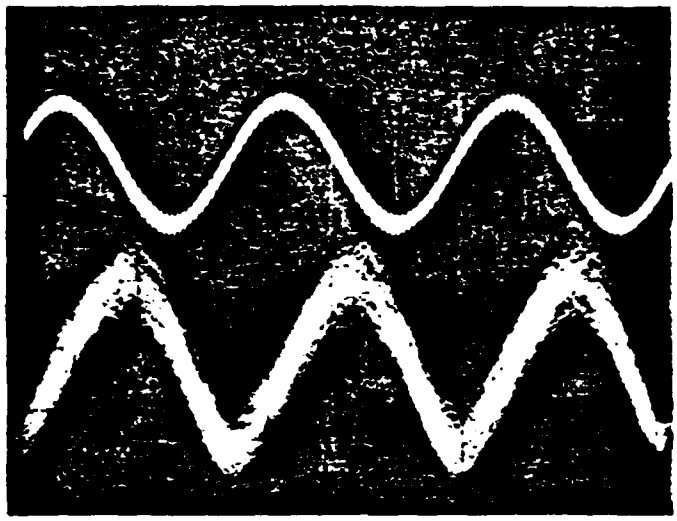

Probe Voltage ---->

$V_{driving}$ 100mv/cm

probe current fluctuations
across 1 kOhm, 1mv/cm
probe distance = 0

Time ---->

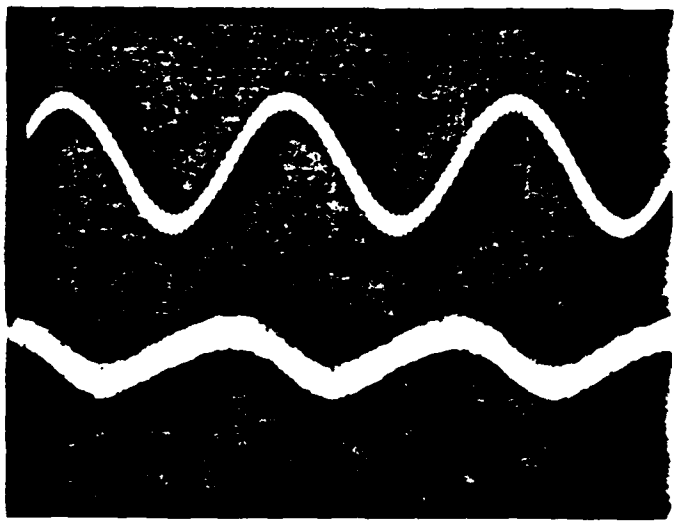

Probe Voltage ---->

$V_{driving}$ 100mv/cm

probe current fluctuations
across 1 kOhm, 1mv/cm
probe distance = 7.2 cm

Time ---->

(v_{phase} = 4.8×10^5 cm/sec)

10 microsec/cm

Figure 6 - Phase Distance Relations for Driven Waves

directly to an electron-plasma wave of very high frequency, GHz in our case. This, in turn, gives rise to secondary excitations, including ion-acoustic waves at the lower end of the spectrum. Figure 7 shows a spectral analysis of the low frequency response of the plasma during electron beam injection. The response at 300 KHz is ion acoustic turbulence which may be associated with parametric instability of fundamental emission driven by the nonlinear Langmuir wave spectrum (see Section II.A(ii) of this report). The response at 580 KHz may be the ion acoustic turbulence from the nonlinear scatter of beam-excited Langmuir waves into lower wavenumbers (see Section II.A(i) of this report).

iv) Work in Progress

Current work involves continued construction of wave diagnostics, especially at higher frequencies. Wave generation and observation for high frequency modes, both electrostatic and electromagnetic, will complete instrumentation for full observation of the beam/plasma interaction.

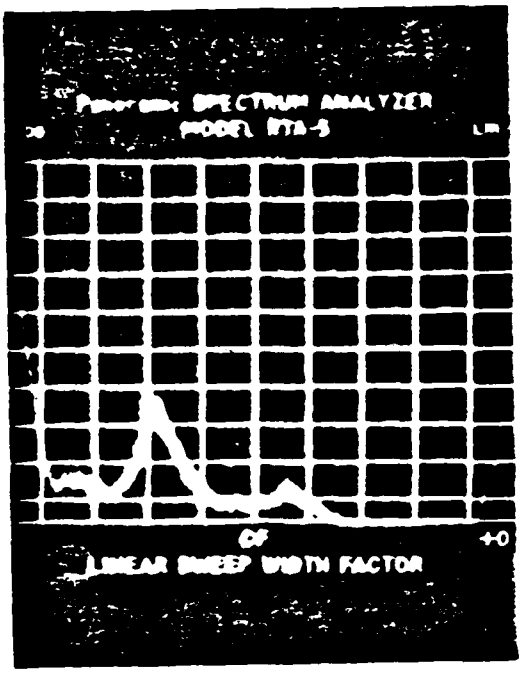

Intensity ---->

Log scale
(arbitrary units)

Frequency ---->

0 Hz

500 kHz

1 MHz

Figure 7 - Low Frequency Spectral Response of Target Plasma

III. Publications and Presentations During this Grant Period

A. Publications since October, 1981

"Scattering and Collapse of Langmuir Waves Driven by a Weak Electron Beam," B. Hafizi, J. Weatherall, M.V. Goldman, and D. Nicholson, Phys. Fluids 25, 392-401 (February, 1982).

"Beam-Plasma Instability in the Presence of Low Frequency Turbulence," M.V. Goldman and D.F. DuBois, Phys. Fluids 25, 1062-1072 (1982).

"Solitons and Ionospheric Heating," J. Weatherall, J. Sheerin, D. Nicholson, G. Payne, and M.V. Goldman, J. Geophys. Res. A 87, 823-842 (1981).

"Intense Ion Transport in Electrostatic Ion Cyclotron Waves," R.A. Stern and N. Rynn, Proceedings of the 1982 International Conference on Plasma Physics (October, 1982).

"Chaotic (Strange) and Periodic Behavior in Instability Saturation by the Oscillating Two-Stream Instability," D.A. Russell and E. Ott, Phys. Fluids 24, 1976-1988 (November, 1981).

B. Papers Submitted for Publication During the Period of this Report

"Steady State Turbulence with a Narrow Inertial Range," J.C. Weatherall, D.R. Nicholson, and M.V. Goldman, accepted for publication by Physics Fluids (1982).

"Direct Ion Transport Measurements by Optical Tagging," R.A. Stern, D.N. Hill, and N. Rynn, accepted for publication in Physics Letters A (1982).

"Solitons and Ionospheric Modification," J.P. Sheerin, J.C. Weatherall, D.R. Nicholson, G.L. Payne, M.V. Goldman, and P.M. Hansen, accepted for publication by J. Atmos. Terr. Phys. (March 1982).

"Backscatter Cascade of Beam-Modes off Ambient Density Fluctuations," D.A. Russell and M.V. Goldman, submitted to Physics Fluids (1982).

C. Preliminary Reports

"Preliminary Results Concerning Compton Conversion of Langmuir Waves into High Frequency Electromagnetic Waves in the Presence of an Ultra Relativistic Electron Beam," David Newman.

D. Invited Papers Presented Between October, 1981 and September, 1982

"Emission of Electromagnetic Waves from Beam-Plasma Systems," M.V. Goldman, University of California at Berkeley, April, 1982.

"Theory of Emission of Radiation from Beam-Plasma Systems," M.V. Goldman, Institute for Theoretical Physics, University of California at Santa Barbara, Goleta, California, March 1982.

"Status of Observations of Type III Solar Radio Wave Emission," M.V. Goldman, Institute for Theoretical Physics, University of California at Santa Barbara, Goleta, California, March, 1982.

"Turbulence and Wave Particle Interaction in Solar Terrestrial Plasmas," M.V. Goldman, G. Dulk, J. Toomre, and D. Smith, invited paper at AGU Meeting, San Francisco, December, 1981.

--This list does not include the invited talks of Prof. Stern. A complete list will be furnished with our next proposal.--

E. Abstracts of Contributed Talks

"Steady State Langmuir Turbulence," J.C. Weatherall, M.V. Goldman, and D.R. Nicholson, paper 8F6, Bull. Am. Phys. Soc., vol. 26, pg. 1026, October 1981. (New York meeting of the Plasma Physics Division of the American Physical Society.)

"Beam Instability in a Plasma with Low Frequency Turbulence," Martin V. Goldman and D.F. DuBois, paper 9U3, Bull. Am. Phys. Soc. vol. 26, pg. 1062, October 1981. (New York meeting of the Plasma Physics Division of the American Physical Society.)

"Evolution of Bump-on-Tail Instability During Type III Solar Radio Bursts," M.V. Goldman, D. Smith, B. Hafizi, J. Weatherall, and D. Nicholson, paper 4T18, Bull. Am. Phys. Soc., vol. 26, pg. 940, October 1981. (New York meeting of the Plasma Physics Division of the American Physical Society.)

"Effect of Density Fluctuations on Beam Unstable Langmuir Waves," M.V. Goldman, J.C. Weatherall, and D.F. Smith, AGU Fall Meeting, San Francisco, December, 1981.

"Scattering and Collapse of Langmuir Waves During Type III Solar Radio Bursts," B. Hafizi, J.C. Weatherall, M.V. Goldman, and D.R. Nicholson, AGU Fall Meeting, San Francisco, December, 1981.

"Intrinsic Stochasticity of Beam-Driven Langmuir Waves," D. Russell and M.V. Goldman, AGU Fall Meeting, San Francisco, December, 1981.

"Solitons and Ionospheric Modification," D.R. Nicholson, P.J. Hansen, G.L. Payne, J.C. Weatherall, M.V. Goldman and J.P. Sheerin, URSI XXth General Assembly, Washington, D.C., August 10-19, 1981, Symposium on Active Experiments, Ionospheric Modification Session.

"Modulational Interaction of Nonlinear Waves and Recurrence," B. Hafizi, 23rd Annual Meeting of Plasma Physics Division of APS, October, 1981.

F. Conferences Organized

Martin V. Goldman was organizer of an International Workshop on Plasma Physics, at the Aspen Center for Physics, June, 1980, 1981, 1982.

IV. References

1. S. Jackel, B. Perry, and M. Lubin, Phys. Rev. Lett. 37, 95 (1976).
2. M.J. Forrest, P.D. Morgan, N.J. Peacock, K. Kuriki, M.V. Goldman, and T. Rudolph, Phys. Rev. Lett. 37, 1681 (1976).
3. R.P.H. Chang, M. Porkolab, and B. Grek, Phys. Rev. Lett. 28, 206 (1972).
4. R. Stenzel and A.Y. Young, Phys. Rev. Lett. 28, 274 (1972).
5. F.W. Perkins and P.K. Kaw, J. Geophys. Res. 76, 282 (1971).
6. H.C. Carlson, W.E. Gordon, and R.L. Showen, J. Geophys. Res. 77, 1242 (1972).
7. K. Papadopoulos, G.L. Goldstein, and R. Smith, Astrophys. J. 190, 1242 (1972).
8. S. Bardwell and M.V. Goldman, Astrophys. J. 209, 912 (1976).
9. A.Y. Wong and B.H. Quon, Phys. Rev. Lett. 34, 1499 (1975).
10. D.F. DuBois and M.V. Goldman, Phys. Rev. Lett. 28, 218 (1972).
11. P.K. Kaw and J.M. Dawson, Phys. Fluids 12, 2585 (1969); D.W. Forslund et al., Phys. Rev. Lett. 36, 35 (1975).
12. W.M. Hooke and S. Barnabei, Phys. Rev. Lett. 29, 1218 (1972).
13. V.E. Zakharov, Sov. Phys. JETP 35, 908 (1972).
14. G.J. Morales and Y.C. Lee, Phys. Fluids 19, 690 (1976).
15. G. Benford, D. Tzach, K. Kato, and D.F. Smith, Phys. Rev. Lett. 45, 1182 (1980).

APPENDIX A

A. "Beam-Plasma Instability in the Presence of Low Frequency Turbulence"

M.V. Goldman and D.F. DuBois
Physics of Fluids 25, 1062-1072 (1982)

Beam-plasma instability in the presence of low-frequency turbulence

Martin V. Goldman
Department of Astro-Geophysics, University of Colorado, Boulder, Colorado 80309

D. F. DuBois
Theoretical Division, Los Alamos National Laboratories, Los Alamos, New Mexico 87545

(Received 18 August 1981; accepted 26 March 1982)

General equations are derived for a linear beam-plasma instability in the presence of low-frequency turbulence. Within a "quasilinear" statistical approximation, these equations contain Langmuir wave scattering, diffusion, resonant and nonresonant anomalous absorption, and a "plasma laser" effect. It is proposed that naturally occurring density irregularities in the solar wind may stabilize the beam-unstable Langmuir waves which occur during type III solar emissions.

I. INTRODUCTION

The saturation of beam-induced instabilities of electron plasma waves can occur through a wide variety of different mechanisms. Cold beams can produce relatively coherent waves which saturate by electron trapping.[1,2] Warm beams, or cold beams which have broadened,[2] are traditionally expected to saturate by quasilinear plateau formation.[3] Yet, under certain circumstances, nonlinear wave–wave interactions are faster, and can dominate. Such ponderomotive force effects include induced scatter off screened ions,[4–6] modulational instability,[7,6] and collapse.[8,9] The first process can be treated statistically by weak turbulence wave–wave interaction techniques,[4] and the latter two processes are currently being studied by "strong" turbulence methods such as the direct interaction approximation.[10]

These nonlinear saturation processes are usually studied in a spatially homogeneous plasma. Conditions often arise, however, when random background density inhomogeneities are important, and may even predominate over nonlinear mechanisms in the saturation of beam instabilities.

Refraction and scattering in the random index of refraction variations may cause the regions of nonlinearity to be isolated and sporadic.[11,12]

Nishikawa and Ryutov[13] have studied the relaxation of a relativistic electron beam in a plasma with random density inhomogeneities. Their statistical treatment is based on the angular Fokker–Planck diffusion of Langmuir rays into an almost isotropic distribution of spectral energy density. A key point in their analysis is that the angle-averaged quasilinear growth rate is always negative. Hence, angular diffusion provides access to dissipative regions of phase space which can stabilize the instability.

However, Fokker–Planck diffusion explicitly assumes that the density inhomogeneities have a characteristic scale size q_n^{-1} which is much larger than the Langmuir wave scale size, k_L^{-1}. When this inequality is relaxed, the density inhomogeneities may cause anomalous resistivity to occur. This can be due to resonant large angle scattering, or to nonresonant beating to large wavenumbers. The first process is related to the Dawson–Oberman resistivity.[14] The second has been invoked as a mechanism which stabilizes Langmuir collapse.[15]

The purpose of this paper and its sequel[16] is to present a unified treatment of the effects of a given "external" distribution of density fluctuations on the evolution of beam-unstable Langmuir waves. Since we do not make the WKB approximation ($k_L \gg q$), both anomalous resitivity and Fokker–Planck diffusion effects are contained in appropriate limits of what turns out to be a relatively simple, general integral equation for the Langmuir spectral energy density. In addition, this equation contains "beat" emission due to the Langmuir wave scattering off the density fluctuation. Such scattering to higher wavenumbers has been suggested as playing an important role in the observed evolution of beam-driven Langmiur waves in the presence of external ion-acoustic turbulence in the vicinity of Jupiter's bow shock.[17] Our equation provides a quantitative basis for studying this evolution. It is also highly relevant to the phenomenon of type III solar radio waves,[18] since background low-frequency turbulence is always present in the solar wind,[19] and is often at such high levels that an electron stream passing through them will be influenced in Langmuir-wave and radio-wave emission. Still another potential application is to laboratory relativistic beam-plasma systems in which a return current can excite ion-acoustic fluctuations, or in which the beam significantly disturbs the density homogeneity. Here also, Langmuir and electromagnetic emission may be affected.

In the second paper[16] we will show that our equations are relevant to the effect known as plasma laser emission.[20] This effect is closely related to anomalous resistivity. When the beam disturbance and the density spectrum are centered about wavenumbers for which the damping rate is negative (i.e., at phase speeds in the up-slope portion of a bump-on-tail electron velocity distribution function), then the anomalous resistivity changes sign. The existence and nature of this effect depends strongly on the spectral shape of the low-frequency turbulence, and may also be sensitive to higher-order renormalization.

There is an interesting analogy between the present theory in the WKB limit, and statistical theories of Vlasov turbulence. The Langmuir ray plays the role of the electron trajectory. The ray moves in the effective external "field" which is the varying refractive index associated with the external density fluctuations. The simplest closure for the Langmuir kinetic equation is analogous to the quasilinear closure for the electron distribution function in a given ran-

 0031-9171/82/061062-11$01.90

dom external field. The conditions for a simple Markoffian quasilinear description require a broad spectrum of ion density fluctuations which provides a small correlation time, again analogous to the Vlasov case. When $q_n \ll k_L$, this gives the quasilinear diffusion of Langmuir rays.[13] However, when $2k \lesssim q_n$, large angle scattering and anomalous resistivity effects are obtained.

For both the Vlasov equation and the Langmuir equation the effects of higher-order renormalization in the random external fields are analogous. Even a closure approximation which contains such renormalization relies on the assumption that the statistics of the external fields (or density fluctuations) are near Gaussian.[21,22] Effects such as particle (or ray) trapping are ignored. This assumption is much easier to justify when the density fluctuations are indeed external. In the more general formulation, self-consistency must be addressed,[10] and this means that the statistics of the fluctuations can no longer be taken as ad hoc. In the case of Vlasov turbulence, this means that Poisson's equation for the field fluctuations must be taken into account. This finds its analog in Langmuir turbulence in the second Zakharov equation for ion-acoustic fluctuations driven by the Langmuir pondermotive force. When a self-consistent treatment of the density fluctuations is required, we should be more suspicious of closure approximations, in general. However, there are no guarantees that the statistics of external fluctuations will be near Gaussian in any given application.

In many respects, our theory is quite general, since we do not specify the nature of the coupling between the waves and the beam or background particles, but merely represent such coupling by a fixed wave damping rate, which may be positive or negative. Many of the present considerations will apply, with only trivial modifications, to other kinds of waves in a dissipative medium with random irregularities. Since we do not make the WKB approximation, our treatment is more general in this respect than the work of Besieries and Tappert,[23] who performed careful, systematic studies of geometrical-optic ray propagation in random media.

The plan of this paper is as follows: In Sec. II we shall set up the basis for a statistical theory, and set forth the essential and convenient approximations to be employed. In Sec. III we shall make the simplest quasilinear closure and show its consequences in the case of a short density-fluctuation correlation time: a simple integral equation for the Langmuir spectral function. Section IV is devoted to estimates of the consequences of the basic equation for the Langmuir waves driven by a stream of solar electrons during type III bursts. It is found that these waves can be stabilized by density fluctuations with $q_n \ll k_L$ and $q_n \approx 2k_L$. The Appendix contains a solution of the kinetic equations for an isotropic distribution of Langmuir waves in the presence of long-wavelength density fluctuations.

In a second paper[16] we will discuss in more detail a number of technical points such as the criteria for the validity of the Markoff quasilinear description, the nonresonant cases including the plasa-laser effect, the complications of long density correlation times (or narrow spectra), higher renormalization schemes, and the generalization of this approach to include transverse radiation.

II. GENERAL STATISTICAL THEORY

Let us assume that the given spectrum of density fluctuations is spatially homogeneous (in the statistical sense). Then the Langmuir spectral function will also be spatially homogeneous, and is given in terms of the Langmuir field $\mathbf{E}(\mathbf{r},t)$ by

$$W(\mathbf{k};t) \equiv \frac{1}{4\pi}\int \frac{d^3\mathbf{r}}{(2\pi)^3}\exp(-i\mathbf{k}\cdot\mathbf{r})\langle \mathbf{E}(\mathbf{r},t)\cdot\mathbf{E}(0,t)\rangle. \tag{1}$$

We wish to work entirely in terms of the slowly time-varying complex envelope field, $\mathscr{E}$ which is related to the Langmuir field $\mathbf{E}$ by

$$\mathbf{E} = \tfrac{1}{2}[\mathscr{E}\exp(-i\omega_p t) + \mathscr{E}^*\exp(+i\omega_p t)]. \tag{2}$$

If we insert (2) into (1), and neglect oscillations at $2\omega_p$, then

$$W(\mathbf{k};t) = (1/16\pi)[F(\mathbf{k},t) + F(-\mathbf{k},t)], \tag{3}$$

where the Langmuir envelope correlation function is

$$F(\mathbf{k};t) \equiv \int \frac{d^3\mathbf{r}}{(2\pi)^3}\exp(-i\mathbf{k}\cdot\mathbf{r})\langle \mathscr{E}(\mathbf{r},t)\cdot\mathscr{E}(0,t)\rangle = \lim_{V\to\infty}\langle|\mathscr{E}(\mathbf{k},t)|^2\rangle/V. \tag{4}$$

Our object is to write a suitable equation for the envelope, $\mathscr{E}$, from which a kinetic equation may be derived for the distribution function, F. Then, W may be found, using (3). We shall make the following essential assumptions:

(A). The external density fluctuations δn are known statistically, and have properties which enable a closure of the equation for F. The averaging, $\langle\ \rangle$, is assumed to be over an ensemble of realizations of the random density δn.

(B). Coupling to the beam and background particles shall be through a fixed linear external "damping" rate, γ_k, which may be negative or positive in appropriate regions of $\mathbf{k}$ space. Since γ_k is given and fixed, we are ignoring the reaction of the waves back on the particles, and there will be no quasilinear plateau formation or particle trapping. Although our treatment is perfectly general, we shall often have in mind the situation where γ_k is given in terms of the electron distribution function, by the usual (quasilinear) expression,

$$\gamma_k = \frac{-\pi}{2n}\frac{\omega_p^3}{k^2}\int d^3\mathbf{v}\,\mathbf{k}\cdot\partial_{\mathbf{v}} f\,\delta(\omega_p - \mathbf{k}\cdot\mathbf{v}). \tag{5}$$

(C). We shall assume that there are no mean fields, that is,

$$\langle\delta n\rangle = \langle\mathscr{E}\rangle = 0. \tag{6}$$

(D). As already mentioned, we assume spatially homogeneous turbulence.

For convenience in the present treatment, we also make a number of additional assumptions, which can be relaxed in a more general treatment.

(E). the envelope field $\mathscr{E}$ is taken as electrostatic, so that $\mathscr{E} = -\nabla\phi$.

(F). Nonlinearities in $\mathscr{E}$ (or F) will be neglected; that is, δn will be considered as entirely external. In general, there is a self-consistent contribution, δn, which is nonlinearly driven by the Langmuir field. Put more simply, we neglect the ponderomotive force. Some of the consequencies of ponderomotive force are simple, and can be inserted trivially as corrections to the linear kinetic equations if necessary. For

example, the weak turbulence effect of induced scattering off ions can easily be added.[13] Modulation instability and collapse, however, are not easily incorporated.[10]

(G). We shall assume that γ_k is not sensitive to the variation δn. This can be justified explicitly for the case of ion-acoustic turbulence in the solar wind ($\delta n/n = 10^{-4}$). This restriction can be lifted, in general, as shown by Besieris and Tappert.[23]

Our starting equation for the Langmuir field envelope $\mathscr{E}$ incorporates all of these assumptions, and furthermore, makes strong contact with previous work on the Zakharov equation. In fact, our basic dynamical equation is precisely the first Zakharov equation, in which the density fluctuation δn is treated as external:

$$\nabla_1\cdot[i(\partial_t + \hat{\gamma}_1) + \nabla_1^2 + \delta n(\mathbf{r}_1,t)]\,\mathscr{E}(\mathbf{r}_1,t) = 0. \tag{7}$$

Here, $\hat{\gamma}_1\mathscr{E}$ has the Fourier transform $\gamma_k\mathscr{E}(\mathbf{k})$, where γ_k is the (growth or) damping given by (5), with δn neglected (or by any other expression independent of δn and of $\mathscr{E}$). The units are the same as in previous work, although $\mathscr{E}$ can be considered to have dimensional units since the equation is linear and homogeneous in $\mathscr{E}$. The transformation to convert (7) into dimensional units is

$$t\to\omega_p t, \quad \mathbf{r}\to\sqrt{2}k_D\mathbf{r}/\sqrt{3}, \quad \delta n\to\delta n/2n, \tag{8}$$

where ω_p and k_D are the plasma frequency and Debye wavenumber, respectively.

The field $\mathscr{E}$ is assumed to be longitudinal. We have taken the divergence to remove explicit coupling to the envelope of the transverse plasma waves. Alternately, we can take the longitudinal part of $\delta n\mathscr{E}$ to accomplish this. In Fourier space, Eq. (7) is then equivalent to

$$[i(\partial_t + \gamma_{k_1}) - k_1^2]\,\mathscr{E}(\mathbf{k}_1) + \frac{1}{V}\sum_q \delta n(\mathbf{q})\hat{\mathbf{k}}_1\hat{\mathbf{k}}_1\cdot\mathscr{E}(\mathbf{k}_1 - \mathbf{q}) = 0. \tag{9}$$

Next, multiply by $\mathscr{E}(\mathbf{k}_2)^*$, and subtract the complex conjugate equation, with $\mathbf{k}_1$ and $\mathbf{k}_2$ interchanged. The result may be written as

$$G^{-1}(\mathbf{k}_1,\mathbf{k}_2)\mathsf{f}(\mathbf{k}_1,\mathbf{k}_2) = -\frac{1}{V}\sum_q \delta n(\mathbf{q})[\hat{\mathbf{k}}_1\hat{\mathbf{k}}_1\cdot\mathsf{f}(\mathbf{k}_1 - \mathbf{q},\mathbf{k}_2) - \mathsf{f}(\mathbf{k}_1,\mathbf{k}_2 + \mathbf{q})\cdot\hat{\mathbf{k}}_2\hat{\mathbf{k}}_2] \tag{10}$$

where f is the dyadic

$$\mathsf{f}(\mathbf{k}_1,\mathbf{k}_2) \equiv \mathscr{E}(\mathbf{k}_1)\mathscr{E}(\mathbf{k}_2)^*, \tag{11}$$

and G^{-1} is the operator

$$G^{-1}(\mathbf{k}_1,\mathbf{k}_2) = i(\partial_t + \gamma_{k_1} + \gamma_{k_2} + (k_2^2 - k_1^2). \tag{12}$$

We now take the ensemble average of (10), noting that,

$$(1/V)\mathsf{f}(\mathbf{k}_1,\mathbf{k}_2) \equiv \mathsf{F}(\mathbf{k}_1)\delta_{\mathbf{k}_1,\mathbf{k}_2} + (1/V)\delta\mathsf{f}(\mathbf{k}_1,\mathbf{k}_2), \tag{13}$$

by the assumed translational invariance of the statistically averaged plasma, here, $\langle\delta\mathsf{f}\rangle = 0$. The quantity $F(\mathbf{k})$ defined by Eq. (4) is simply

$$F(\mathbf{k}) \equiv \mathrm{Tr}\,\mathsf{F}(\mathbf{k}), \tag{14}$$

which, from the average of (10), obeys

$$i(\partial_t + 2\gamma_k)F(\mathbf{k}) = -\frac{1}{V}\sum_q \langle\delta n_q\hat{\mathbf{k}}\cdot[\delta\mathsf{f}(\mathbf{k} - \mathbf{q},\mathbf{k}) - \delta\mathsf{f}(\mathbf{k},\mathbf{k} + \mathbf{q})]\cdot\hat{\mathbf{k}}\rangle. \tag{15}$$

The equation for $\delta\mathsf{f}$ is obtained by subtracting the average of Eq. (10) from Eq. (10) itself

$$\begin{aligned} G^{-1}(\mathbf{k}_1,\mathbf{k}_2)\delta\mathsf{f}(\mathbf{k}_1,\mathbf{k}_2) &= -\frac{1}{V}\delta n_{\mathbf{k}_1-\mathbf{k}_2}[\hat{\mathbf{k}}_1\hat{\mathbf{k}}_1\cdot\mathsf{F}(\mathbf{k}_2) - \mathsf{F}(\mathbf{k}_1)\cdot\hat{\mathbf{k}}_2\hat{\mathbf{k}}_2] \\ &\quad - \left\{\frac{1}{V}\sum_q \delta n_q[\hat{\mathbf{k}}_1\hat{\mathbf{k}}_1\cdot\delta\mathsf{f}(\mathbf{k}_1 - \mathbf{q},\mathbf{k}_2) - \delta\mathsf{f}(\mathbf{k}_1,\mathbf{k}_2 + \mathbf{q})\cdot\hat{\mathbf{k}}_2\hat{\mathbf{k}}_2]\right. \\ &\quad \left. - \left\langle\frac{1}{V}\sum_q \delta n_q[\hat{\mathbf{k}}_1\hat{\mathbf{k}}_1\cdot\delta\mathsf{f}(\mathbf{k}_1 - \mathbf{q},\mathbf{k}_2) - \delta\mathsf{f}(\mathbf{k}_1,\mathbf{k}_2 + \mathbf{q})\cdot\hat{\mathbf{k}}_2\hat{\mathbf{k}}_2]\right\rangle\right\}. \end{aligned} \tag{16}$$

Equations (15) and (16) are our basic statistical equations. Together, they generate a hierarchy very similar to the Klimontovich equation hierarchy in Vlasov turbulence. The operator G^{-1} is analogous to the Vlasov operator, F is analogous to the particle distribution function, and δn to the field. The term on the right side of Eq. (15) is analogous to the usual correlation function associated with fluctuations in the acceleration term. When the two terms in the braces, are ignored, we have $\delta\mathsf{f}$ proportional to $\delta n\mathsf{F}$, which, when inserted into (15), gives the usual quasilinear closure. In the next section, we discuss the consequences of this simple closure scheme.

The conditions for the validity of this closure are similar to the usual Vlasov quasilinear case. Some complications arise because of the dispersive nature of Langmuir waves and will be discussed in a second paper.[16] For completeness we merely list these criteria here with only a brief discussion:

(i) The density fluctuations are a quasi-Gaussian random process.[21,22]

(ii) $(\langle\delta n^2\rangle/n^2)^{1/2}\,\tau_c\omega_p \ll 1$ (17)

where the appropriate correlation time of the density fluctuations is

$$\tau_c = [\inf|2(k \pm q_0) \pm \partial\omega_q/\partial q|\Delta q]^{-1}, \tag{18}$$

where Δq is the half-width of the density fluctuation spectrum which is centered about $q = q_0$. [Note that the inf in Eq. (18) indicates that one takes the combination of signs which gives the smallest value of the expression within the absolute value signs.]

(iii) $(\Delta q)^2\tau_c \ll 1$. (19)

The last criterion which does not arise in Vlasov quasilinear theory appears because of the dispersive nature of Langmuir waves [i.e., the q^2 term in Eq. (25)]. It turns out to be necessary so that the density correlation function decays to a negligible value for $\tau > \tau_c$.

Conditions (i) and (ii) are sufficient for the neglect of terms in the weak turbulence perturbation expansion beyond the quasilinear terms. Condition (i) allows the neglect of the effect of irreducible correlation functions of order greater than two provided condition (ii) is satisfied. The strict definition of a quasi-Gaussian process is given in Refs. 21 and 22.

III. QUASILINEAR CLOSURE

We neglect the two terms in braces in Eq. (16). The solution may then be written as

$$\delta\hat{t}(t;\mathbf{k}_1,\mathbf{k}_2) = +\frac{1}{V}\int d\bar{t}\, G(t-\bar{t};\mathbf{k}_1,\mathbf{k}_2)\delta n_{\mathbf{k}_1-\mathbf{k}_2}(\bar{t}) \times \hat{\mathbf{k}}_1\hat{\mathbf{k}}_2(\hat{\mathbf{k}}_1\cdot\hat{\mathbf{k}}_2)[F(\bar{t},\mathbf{k}_2) - F(\bar{t},\mathbf{k}_1)], \quad (20)$$

where we have used the results that

$$F(\mathbf{k}_2) \equiv \langle \mathscr{E}(\mathbf{k}_2)\mathscr{E}(\mathbf{k}_2)^*\rangle = -\hat{\mathbf{k}}_2\hat{\mathbf{k}}_2 F(k_2).$$

The Green's function G is obtained from (12):

$$G(t-\bar{t};\mathbf{k}_1,\mathbf{k}_2) = \begin{cases} -i\exp[\gamma_{\mathbf{k}_1} - \gamma_{\mathbf{k}_2} + i(k_2^2 - k_1^2)(t-\bar{t}), & t>\bar{t} \\ 0, & t<\bar{t} \end{cases}$$

(causal condition). (21)

Combining (20) with (15) gives us a kinetic equation in the quasilinear approximation:

$$i(\partial_t + 2\gamma_{\mathbf{k}})F(\mathbf{k},t) = \frac{1}{V}\sum_{\mathbf{q}}\int d\bar{t}\, C(\mathbf{q};t-\bar{t},(t+\bar{t})/2) \cdot(\hat{\mathbf{k}}\cdot\widehat{(\mathbf{k}-\mathbf{q})})^2[G(t-\bar{t};\mathbf{k}-\mathbf{q},\mathbf{k}) + G(t-\bar{t};\mathbf{k},\mathbf{k}-\mathbf{q})][F(\mathbf{k},\bar{t}) - F(\mathbf{k}-\mathbf{q},\bar{t})], \quad (22)$$

and where the density correlation function is

$$C(\mathbf{q};t-\bar{t},(t+\bar{t})/2) \equiv (1/V)\langle \delta n_{+\mathbf{q}}(t)\delta n_{-\mathbf{q}}(\bar{t})\rangle.$$

Here, the dependence on $t-\bar{t}$ is associated with the spectral frequency (i.e., the ion-acoustic timescale, if these are ion-acoustic waves), and the dependence on $(t+\bar{t})/2$ represents an evolution time scale for the entire correlation function.

We shall assume that C is independent of $t+\bar{t}$ and that its dependence on $\tau \equiv t-\bar{t}$ is known and may be expressed in the following simple general form:

$$C(q,\tau) = C_{\mathbf{q}}\exp(-\nu_{\mathbf{q}}\tau)\cos\omega_{\mathbf{q}}\tau,$$

where $\omega_{\mathbf{q}}$ is an oscillation frequency, $\nu_{\mathbf{q}}$ is a relaxation rate, and $C_{\mathbf{q}}$ is the spectral function for density correlations $\delta n_{\mathbf{q}}$. All of the quantities in (22) are assumed to be set by external conditions and given independently. For example, if we are dealing with ion-acoustic waves, $\omega_{\mathbf{q}} = c_s q$ and $\nu_{\mathbf{q}}$ represents the damping rate of such waves (in appropriate units). Another possibility is purely relaxing density fluctuations, for which $\omega_{\mathbf{q}} = 0$. The shape and magnitude of the spectral function $C_{\mathbf{q}}$ is also taken to be given or measured. We shall employ various models of $C_{\mathbf{q}}$.

In terms of the above equation for $C_{\mathbf{q}}$ and (21) for G, the basic kinetic equation may be written as

$$(\partial_t + 2\gamma_{\mathbf{k}})F_{\mathbf{k}}(t) = -2\int_0^t d\bar{t}\int\frac{d^3q}{(2\pi)^3}K_{\mathbf{q}}(t-\bar{t}) \times [F(\mathbf{k},\bar{t}) - F(\mathbf{k}-\mathbf{q},\bar{t})], \quad (23a)$$

where

$$K_{\mathbf{q}}(\tau) = \mu_-^2 C_{\mathbf{q}}\exp(-\tau\Gamma)(\cos\tau R_+ + \cos\tau R_-)/2, \quad (23b)$$

$$\mu_-^2 \equiv [\hat{k}\cdot\widehat{(\mathbf{k}-\mathbf{q})}]^2, \quad (23c)$$

$$\Gamma \equiv \gamma_{\mathbf{k}-\mathbf{q}} + \gamma_{\mathbf{k}} + \nu_{\mathbf{k}}, \quad (23d)$$

$$R_\pm \equiv |\mathbf{k}-\mathbf{q}|^2 - k^2 \pm \omega_{\mathbf{q}}. \quad (23e)$$

The first term on the right side of (23a) is the "scattering-out" term, and the second is the "scattering-in" term. In the basic three-wave interaction, $\mathbf{k}$ is the "incident" wave, $\mathbf{k}-\mathbf{q}$ is the scattered wave, and $\mathbf{q}$ belongs to the density fluctuation. The angular factor μ_-^2 is largest in the forward or backscattered direction. The quantity Γ represents the sum of the damping rates of the three waves; one or more of these may be negative. The quantity $R_\pm$ represents the total frequency mismatch between the three waves. Resonant processes correspond to $R_\pm$ close to zero.

We note that Eq. (23a) is intrinsically non-Markoffian, however, since it is an integral equation of the convolution type, it may be solved by Laplace transform. This method, and its implications will be treated later.[16]

A. Time asymptotic Markoffian resonant limit

If conditions (i) and (ii) for the quasilinear approximation are satisfied, then Eq. (23a) can be further simplified by a Markoffian approximation if $F_{\mathbf{k}}(t)$ is sufficiently slowly varying on a scale determined by τ_c:

$$\text{(iv)}\quad \frac{\partial}{\partial t}\ln|F_{\mathbf{k}}(t)|\cdot\tau_c \ll 1. \quad (24)$$

In this case $F_{\mathbf{k}}(\bar{t})$ and $F_{\mathbf{k}-\mathbf{q}}(\bar{t})$ in Eq. (23a) can be replaced by $F_{\mathbf{k}}(t)$ and $F_{\mathbf{k}-\mathbf{q}}(t)$. The details of this argument will be presented in the second paper.

This equation can be further simplified in the time asymptotic limit $t \gg \tau_c$ for the case where the resonance conditions

$$R_\pm = q^2 - 2\mathbf{k}\cdot\mathbf{q} \pm \omega_{\mathbf{q}} = 0 \quad (25)$$

can be satisfied over some range of the $\mathbf{q}$ spectrum.

The result is independent of the sign and magnitude of Γ provided the following condition is met

$$\text{(v)}\quad \Gamma\tau_c \ll 1. \quad (26)$$

The derivation of this condition will be discussed in more detail in the second paper.[16] Condition (v) states that the decay or growth of the kernel $K_{\mathbf{q}}^{\pm}(t)$ is inconsequential on the scale of the decay due to phase mixing with correlation time τ_c.

If conditions (i) through (v) are satisfied, Eq. (23a) reduces to a simple Markoffian equation for the evolution of $F(\mathbf{k},t)$

$$(\partial_t + 2\gamma_{\mathbf{k}})F(\mathbf{k},t) = -2\gamma_{\mathbf{k}}^{\text{eff}}F(\mathbf{k},t) + S_{\mathbf{k}}^{\text{eff}}(t), \quad (27a)$$

$$\gamma_{\mathbf{k}}^{\text{eff}} = \frac{\pi}{2}\int\frac{d^3q}{(2\pi)^3}C_{\mathbf{q}}\mu_-^2[\delta(R_+) + \delta(R_-)], \quad (27b)$$

$$S_{\mathbf{k}}^{\text{eff}} = \pi\int\frac{d^3q}{(2\pi)^3}C_{\mathbf{q}}\mu_-^2[\delta(R_+) + \delta(R_-)]F(\mathbf{k}-\mathbf{q},t). \quad (27c)$$

The significance of the δ-function condition (25), $R=0$, in this limit, is that it guarantees energy conservation between the Langmuir wave at wave vector $\mathbf{k}$, the low-frequency turbulence at frequency, $\omega_\pm \equiv \pm\omega_{\mathbf{q}}$ and wave vector $\mathbf{q}$, and the (scattered) Langmuir wave at $\mathbf{k}-\mathbf{q}$. In physical units this condition is

$$\omega_p[1 + \tfrac{3}{2}k^2/k_D^2] = \omega_\pm + \omega_p[1 + \tfrac{3}{2}|\mathbf{k}-\mathbf{q}|^2/k_D^2]. \quad (28)$$

When the low-frequency turbulence is ion acoustic, we have $\omega_\pm = \pm c_S q$, where $c_S = (\theta_e/M)^{1/2}$ is the ion sound speed. When the density fluctuations are on a large spatial scale

compared with the Langmuir wavelength, we have the diffusion limit.

1. Diffusion limit ($q_n \ll k_L$) [Fig. 1(a)]

This limit corresponds precisely to quasilinear diffusion in Vlasov turbulence, and could have been obtained by using geometric optics approximations (based on the slow variation of δn) in the original equation (7). We expand the δ functions by assuming $q \ll k$:

$$\delta(R_{\pm}) \approx \delta(\omega_{\pm} - 2\mathbf{k}\cdot\mathbf{q}) - \frac{q_j}{2}\frac{\partial}{\partial k_j}\delta(\omega_{\pm} - 2\mathbf{k}\cdot\mathbf{q}). \quad (29)$$

We also expand $F(\mathbf{k}-\mathbf{q})$ in Eq. (23) for $S_{\mathbf{k}}^{\text{eff}}$, to second order in $\mathbf{q}$. The result may be put in the standard form

$$-2\gamma_{\mathbf{k}}^{\text{eff}} F(\mathbf{k}) + S_{\mathbf{k}}^{\text{eff}} = \frac{\partial}{\partial k_j} D_{jl} F(\mathbf{k}), \quad (30)$$

where the diffusion coefficient, D is $[(D^{(+)} + D^{(-)})]/2$, and

$$D_{jl}^{+}(\mathbf{k}) \equiv \pi \int \frac{d^3\mathbf{q}}{(2\pi)^3} C(\mathbf{q}) q_j q_l \delta(\omega_{\pm} - 2\mathbf{k}\cdot\mathbf{q}). \quad (31)$$

The kinetic equation (27) now becomes a diffusion equation, and is completely analogous to the quasilinear diffusion in Vlasov turbulence. In the limit $|\omega_{\pm}| \approx c_S q \ll kq$, or, in dimensional units when

$$(m/M)^{1/2} \ll k/k_D, \quad (32)$$

the frequency $\omega_{\pm}$ in (25) is negligible, and the underlying scattering is elastic. The corresponding diffusion was studied by Niskikawa and Ryutov,[13] in their work on beam-plasma interaction. In this limit, the diffusion occurs in angle only [see Fig. 1(a)]. The density fluctuations then drive the Langmuir spectrum toward isotropy. This may stabilize the beam modes.[13] For the case of shorter scale density fluctuations the elastic scattering limit may also be taken, and both anomalous absorption and isotropization take place.

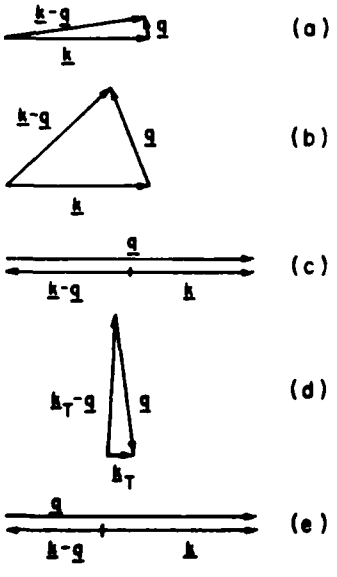

FIG. 1. Momentum matching configurations for various resonant three-wave interactions involving low-frequency turbulence at wave vector $\mathbf{q}$. In each case, $\mathbf{k}$ is the momentum of the incident wave, and $\mathbf{k}-\mathbf{q}$ of the scattered wave: (a) Diffusion limit, $q \ll k$. (b) General elastic scattering, $|\mathbf{k}-\mathbf{q}| = k$. (c) Elastic backscatter. (d) Conversion of a transverse wave at $\mathbf{k}_T$ off "long" wavelength turbulence, $\mathbf{q}$, into a Langmuir wave at $\mathbf{k}_T - \mathbf{q}$. (e) Inelastic backscatter: $|\mathbf{k}-\mathbf{q}|$ is shorter than k by an amount $\sim(m/M)^{1/2}$.

2. General elastic scattering ($|\omega_q| \ll q_n^2$, $k_L q_n$) and anomalous absorption from intermediate scale density fluctuations ($q_n \lesssim 2k_L$)

We see from Eq. (27), that, when ω_q is neglected in $R_{\pm}$, the steady-state kinetic equation becomes

$$-2\gamma_{\mathbf{k}}^{\text{eff}} F + S_{\mathbf{k}}^{\text{eff}} = \pi \int \frac{d^3\mathbf{q}}{(2\pi)^3} C(\mathbf{q}) \mu_{-}^2 \delta[(\mathbf{k}-\mathbf{q})^2 - k^2] \times [F(\mathbf{k}) - F(\mathbf{k}-\mathbf{q})]. \quad (33)$$

It is evident that (33) vanishes for an isotropic Langmuir distribution

$$F(\mathbf{k}) = F(|\mathbf{k}|).$$

Even though we are not in the diffusion limit $q_n \ll k_L$, the scattering-off density fluctuation is now in angle only, and may drive the Langmuir waves towards isotropy [Fig. 1(b)]. The condition for the neglect of $|\omega_{\pm}|$ is Eq. (32) in the limit of small q, or the limit of large q,

$$(m/M)^{1/2} \ll q/q_D. \quad (34)$$

It is instructive to examine $\gamma_{\mathbf{k}}^{\text{eff}}$ alone, in the general elastic limit. We may write

$$\gamma_{\mathbf{k}}^{\text{eff}} = \pi \int \frac{d^3\mathbf{q}}{(2\pi)^3} C(\mathbf{q}) \mu_{-}^2 \delta(q^2 - 2\mathbf{k}\cdot\mathbf{q}). \quad (35)$$

For an isotropic density fluctuation spectrum, $C(\mathbf{q}) = C(|\mathbf{q}|)$, the angular integrations may be performed, leading to

$$\gamma_{\mathbf{k}}^{\text{eff}} = \frac{1}{4\pi} \int_0^{\infty} dq\, C(q) f(q/2k), \quad (36)$$

where the function $f(x)$ is defined by

$$f(x) \equiv x(1-2x^2)^2, \quad x<1,$$
$$\equiv 0, \quad x>1.$$

$f(x)$ rises to a local maximum of about 0.2 at $x = 1/\sqrt{10}$, falls to a minimum of zero at $x = 1/\sqrt{2}$, and rises monotonically to a value of 1 at $x = 1$, before cutting off discontinuously to zero at larger x. Next, we suppose that $C(q)$ is peaked at $q_n < 2k$, and has a width $\Delta q < k/2$. Then,

$$\gamma_{\mathbf{k}}^{\text{eff}} \approx \frac{\pi}{2} f(q_n/2k) \langle |\delta n(\mathbf{r})|^2 \rangle q_n^2, \quad (37a)$$

or, in dimensional units,

$$\gamma_{\mathbf{k}}^{\text{eff}} \approx \frac{\pi}{18} f \frac{\langle |\delta n|^2 \rangle}{n^2} \frac{k_D^2}{q_n^2} \omega_p. \quad (37b)$$

This represents anomalous absorption, and is very similar to the formula derived by Dawson and Oberman[14] for the anomalous resistivity of electromagnetic waves near the plasma frequency. An important difference for the Langmuir wave case is the function $f(q_n 2k)$, which is negligibly small unless $q_n \approx 2k$. The condition $q_n = 2k$ corresponds to backscatter, in which the wave vectors $\mathbf{k}$ and $\mathbf{k}-\mathbf{q}$ are equal and opposite [see Fig. 1(c)]. This configuration is favored because of the angular factor, μ_{-}^2. This condition is very restrictive on the relation between k_L and q_n. For example, if

$q_n > 2k_L$, the factor f vanishes identically. The electromagnetic case is much less restrictive. In this case, there appears on the left of Eq. (28), the electromagnetic wave dispersion relations, $\omega_p[1 + c^2k^2/2]$, rather than the Langmuir wave dispersion relation, $\omega_p[1 + 3k^2/2k_D^2]$. As a consequence, the condition $R = 0$ becomes, in the elastic limit

$$q^2 = (c^2/3v_e^2)k_T^2. \tag{38}$$

Hence, $k_T \ll q_n$, and the scattered (or, more precisely, the "converted" wave) wave vector is $-\mathbf{q}$ [see Fig. 1(d)]. For this case, one has

$$\gamma^{\text{eff}} = C(q_n)\pi \int \frac{d^3q}{(2\pi)} (\hat{\mathbf{e}}\cdot\hat{\mathbf{q}})^2 \delta(q^2 - c^2k^2/3v_e^2),$$

or

$$\gamma^{\text{eff}} \approx \frac{\pi}{9} \frac{\langle|\delta n|^2\rangle}{n^2} \frac{k_D^2}{q_n^2} \omega_p, \tag{39}$$

a result which has been derived by Dawson.[14] This formula, which is valid for transverse waves with $k_T \ll q_n$, is much less restrictive than (34). In the literature,[24,25] Eq. (39), rather than Eq. (37) appears to have been applied to Langmuir waves. In these applications, the role of the emission terms, S_k^{eff}, has also been ignored.

3. Inelastic scattering and cascade [Fig. 1(c)]

For wavenumbers close to $(m/M)^{1/2}$, the frequency ω can no longer be neglected, and changes in wavenumber are associated with the scattering process. Then the (energy conserving) delta functions in Eq. (27) tells us that

$$q = 2\mathbf{k}\cdot\hat{\mathbf{q}} \pm c_S \tag{40a}$$

Hence, for backscatter ($\mathbf{q} \| \mathbf{k}$ and $q > k$), this gives

$$q = 2k \pm c_S, \tag{40b}$$

or

$$k - q = -k \mp c_S. \tag{40c}$$

The scattered wavenumber can therefore be increased or decreased by $c_S = 0.82\,(m/M)^{1/2}$, relative to the incident wavenumber. This effect is most pronounced when k is not significantly higher than c_S. We note from Eq. (40b) that, in order for q to be positive, k cannot be less than $c_S/2$. It appears from Eqs. (27a) and (27b) that steady state may result from a cascade of scatterings which may occur toward both higher and lower wavenumbers (subject to $k > c_S/2$). A cascade to higher wavenumbers has been suggested for beam-driven Langmuir waves in the presence of ion-acoustic turbulence near Jupiter.[17]

B. Nonresonant anomalous absorption ($\Gamma > 0$) for short scale density fluctuations ($k_L \ll q_n$)

All of the time-asymptotic phenomena discussed so far were resonant, and could have been obtained from semi-classical "Golden-rule" arguments involving Feynman diagrams for creation and annihilation of Langmuir waves (plasmons) and ion-acoustic waves (phonons).

However, another class of phenomena is present for which the resonant conditions $R^{\pm} = 0$ cannot be satisfied. The first example occurs for $q_n > 2k$ and $q_n > c_S$. In the nonresonant case, again assuming conditions (i)–(v), the first nonzero term is obtained by keeping the terms proportional to τ in $\exp(-\Gamma\tau) \simeq 1 - \Gamma\tau + \ldots$, $F_k(t-\tau) = F_k(t) - \tau(\partial/\partial t)F_k(t)\ldots$, etc. in the τ integration of Eq. (23). The full result will be reported in the second paper. Here, we will discuss only one special case in detail.

Let us assume $\Gamma \approx \gamma_{-\mathbf{q}} = \gamma_{\mathbf{q}}$, corresponding, for example, to Landau damping at high q_n. We further assume $R \approx q^2 \gg \Gamma, c_S^2$. Then, the nonresonant contributions to Eqs. (27a) and (27b) can be written as

$$\gamma_k^{\text{eff}} = \int \frac{d^3q}{(2\pi)^3} C(\mathbf{q})(\hat{\mathbf{k}}\cdot\hat{\mathbf{q}})^2 \frac{\gamma_q}{q^4}, \tag{41}$$

$$S_k^{\text{eff}} = \int \frac{d^3q}{(2\pi)^3} C(\mathbf{q})(\hat{\mathbf{k}}\cdot\hat{\mathbf{q}})^2 \frac{\gamma_q}{q^4} F(\mathbf{q}). \tag{42}$$

The emission term S_k^{eff} will be small because F is small at the (high) wavenumber q_n where C peaks (recall F peaks at $k_L \ll q_n$.) The anomalous absorption term γ_k^{eff} given by Eq. (41), in this limit, was written down without derivation by Galeev *et al.*,[15] in connection with Langmuir mean fields damped by ion-acoustic waves. In their case, the ion-acoustic waves arise due to sound wave emission from density cavities driven by ponderomotive force. We note that γ_k^{eff} is independent of $|\mathbf{k}|$ as long as $|\mathbf{k}| \ll q_n$, so this constitutes a uniform damping of long wavelength Langmuir turbulence by short wavelength ion-acoustic waves. According to Galeev *et al.*,[15] this damping can stop the collapse[8,9] of Langmuir solitons in fully developed Langmuir turbulence.

Here we consider a different application, in which a bump-on-tail electron distribution drives resonant Langmuir waves unstable in a certain equation of k space. Hence, in the kinetic equation, (27), we may consider wave vectors $\mathbf{k}$ for which γ_k is negative. If, then, $C(\mathbf{q})$ peaks at $q_n \gg k$, and q_n lies in the region of strong Landau damping, γ_q, then γ_k^{eff}, as given by expression (41), will tend to stabilize the beam modes. In order to estimate the size of γ_k^{eff}, let us assume that $C(\mathbf{q})$ is isotropic, and has a width Δq about q_n. We may then aproximate (41) as

$$\gamma_k^{\text{eff}} \lesssim \frac{\gamma_{q_*}}{q_n^4} \int \frac{d^3q}{(2\pi)^3} C(\mathbf{q})(\hat{\mathbf{k}}\cdot\hat{\mathbf{q}})^2 \approx \gamma_{q_*} \frac{\langle|\delta n(r)^2|\rangle}{3q_n^4}, \tag{43}$$

where $q_* \cong q_n + \Delta q$ is the point of maximum Landau damping, γ_{q_*}. The largest γ_{q_*} can be is of order ω_p for q_n of order $\frac{1}{2}k_D$, so, in dimensional units, the maximum value of γ_k^{eff} is

$$\gamma_k^{\text{eff}}\big|_{\max} = \frac{8}{27}\left|\frac{\delta n}{n}\right|^2 \omega_p. \tag{44}$$

Very weak beam-mode growth rates, γ_k, may be stabilized by the effective damping, γ_k^{eff}. If γ_k^{eff} is not large enough to provide stabilization, we must consider nonlinear contributions to the effective damping and emission terms.

In the second paper[16] we will consider the plasma laser effect; this is a situation where the density fluctuation spectrum is peaked about a value q_n which lies in the range of wave vectors $\Delta\mathbf{k}$ which correspond to unstable beam modes near ω_p/v_b. Then it appears possible to destabilize very long

wavelength Langmuir waves by a plasma laser effect,[20] in which $\gamma_{k\ll\omega_p/v_{th}}^{eff}$ is negative. We consider expression (41) once more (assuming $|\gamma|_{k=0} \ll |\gamma_q| \ll q^2$). Now, γ_q will be negative, since q lies in the range of momenta corresponding to unstable beam modes (i.e., waves whose phase velocity lies in the up-slope portion of the electron distribution function). For the broad spectrum ($\tau_c \to 0$) case considered in this paper the plasma laser effect can be wiped out on integration over q, which averages over stable and unstable regions of γ_q; it appears that the stable regions will dominate over the unstable regions, and the system will be stable in this case. The plasma laser effect can work in principle for a narrow band width spectrum. In Sec. IV, we discuss some applications of the stabilization of beam modes already discussed (cases A and B).

IV. APPLICATION TO BEAMS ASSOCIATED WITH TYPE III SOLAR RADIO EMISSION

A type III solar radio burst occurs when a stream of electrons, emanating from the sun, propagates into the solar wind. The sequence of events leading to the observed burst is thought to be this: The stream excites Langmuir waves by a bump-on-tail instability;[26] the Langmuir waves saturate by nonlinear mechanisms such as quasilinear plateau formation[27] and/or ponderomotive force effects;[18] and the turbulent Langmuir waves emit electromagnetic radiation by two-plasmon coalescence and/or conversion off (ambient) ion-acoustic waves.[28] The effect of independently generated low-frequency turbulence on this sequence of events has not been studied systematically. Such turbulence may saturate the Langmuir waves linearly or in conjunction with the nonlinear mechanisms. It may also affect the emission and propagation of the electromagnetic waves.

A. Short density fluctuations

Gurnett *et al.*[19] have shown that nonthermal levels of ion-acoustic waves are very common in the ambient solar wind. The Helios 1, 2 spacecraft antennae have picked up sporadically intense electric fields in the frequency range from 1 to 10 kHz at 0.47 a.u. These fields have been interpreted as ion-acoustic waves, Doppler-shifted by the solar wind speed, $v_s = 500$ km sec$^{-1} \pm 100$ sec^{-1}. Since v_s is much greater than the ion sound speed, the wavelength of this turbulence is $\lambda_n \simeq 100$ m. Typical electric field peaks are between 10 and 100 μV m^{-1}. The spacecraft instrumentation measures the average of the logarithm of the intensity of the waves, but is limited by a characteristic resolving time of 50 msec. For stationary broadband structures convecting past the antenna at the solar wind speed, this implies that scale sizes smaller than or equal to 25 km register only in terms of a logarithmic average. Hence, the measured electric fields associated with the 100 m ion-acoustic turbulence may be grossly underestimated.

If we assume that the electrons respond adiabatically to the low-frequency fields, then the associated density fluctuation level is

$$\left|\frac{\delta n}{n}\right| = \frac{e\lambda_n E}{2\pi k_B T_e} = 1.85\times 10^{-4}\left(\frac{\lambda_n}{100\text{ m}}\right)\left(\frac{E}{100\,\mu\text{V/m}}\right)\left(\frac{10^5\,^\circ\text{K}}{T}\right), \tag{45}$$

where e is the electron charge, T_e is the electron temperature ($1-2\times 10^5$ °K at $\frac{1}{2}$ a.u.), and E is the electric field.

Let us now consider the consequences of a type III burst electron stream passing through these density fluctuations at 0.5 a.u. Assuming an ambient plasma electron density of 15 cm^{-3}, and therefore an electron plasma frequency of $f_p \simeq 35$ kHz, an electron stream of velocity one-third the speed of light will give rise to Langmuir waves of wavelength, $\lambda_L = v_0/f_p = 3$ km. Hence, we are in the regime $\lambda_L \gg \lambda_n$, or $q_n \gg k_L$, which is the limit of nonresonant anomalous absorption, discussed in Sec. IIIB. The Debye length is $\lambda_D \simeq 7$ m at this density and $T = 10^5$ °K, so $q_n\lambda_D \simeq \frac{1}{2}$, and we are in the regime of heavy Landau damping, where Eq. (44) gives the applicable anomalous absorption of long wavelength modes. With $|\delta n/n| \simeq 2\times 10^{-4}$, we find $\gamma^{eff}/\omega_p = 10^{-8}$. This is too low to stabilize typical growing beam modes, for which the growth rate is $\gamma_g/\omega_p = 10^{-7}$–$10^{-6}$. On the other hand, if $|\delta n/n|$ has been underestimated by an order of magnitude or more (due to the logarithmic averaging of intensities) stabilization by anomalous absorption may occur. We note that the damping rate, ν_q, of ion-acoustic waves in always larger than $(m/M)(q\lambda_D) \simeq 10^{-3}$. This is sufficient to guarantee the condition $\Gamma > 0$ required for stabilization (in the linear approximation) even without phase mixing effects.

B. Large scale density fluctuations

An altogether different possibility arises when we consider the possible effect of very large scale density fluctuations. Measurements[29,30] of interplanetary scintillations have established[11] the existence of density fluctuations with q_n^{-1} between 50 and 200 km, and $\delta n/n$ of order 10^{-3}. Hence, $q_n \ll k_L$, and the effect on the Langmuir waves is Fokker–Planck diffusion. In the elastic limit, the k space diffusion occurs in angle only. We treat this case, for simplicity, assuming $(m/M)^{1/2} \ll k_L/k_D$. As shown by Nishikawa and Ryutov,[13] the diffusion coefficient [given by our Eq. (31), with $\omega_q = 0$] for a cylindrically symmetric Langmuir spectrum diffusing in polar angle θ only, is

$$D_k(\theta) = \frac{\omega_p{}^3 m}{6\pi k^3 T}\int_0^\infty q^3\,dq \int_{|\cos\theta'|<|\sin\theta|} d\theta' \times \frac{C(q,\theta')\sin\theta'\cos^2\theta'}{\sin^2\theta\,(\sin^2\theta\sin^2\theta' - \cos^2\theta\cos^2\theta')^{1/2}}. \tag{46}$$

For a spherically symmetric density fluctuation spectrum, $C(q,\theta') = C(q)$, peaking at q_n, this reduces to

$$D_\perp = \frac{\omega_p}{12}\frac{q_n}{k}\left(\frac{1}{k\lambda_D}\right)^2\frac{\langle|\delta n(r)|^2\rangle}{n^2}, \tag{47}$$

and the Fokker–Planck equation resulting from (27) and (30) becomes (in physical units)

$$(\partial_t + 2\gamma_k)F(k,\cos\theta) - \frac{1}{\sin\theta}\partial_\theta D_\perp \sin\theta\partial_\theta F(k,\cos\theta) = S(k,\cos\theta). \quad (48)$$

Here, we have added an electron spontaneous emission term, S, on the right side. For the case of a bump-on-tail in a background plasma, this consists of two pieces: Cerenkov emission from the beam, and combined Cerenkov and bremsstrahlung emission from the background plasma.

For the type III bursts under consideration $k\lambda_D = 1.5\times10^{-2}$, $q_n/k \approx 5\times10^{-3}$, so the characteristic diffusion time is $D_k^{-1} \approx 1$ sec. One e-folding time for a beam mode is on the order of 10 sec, so the diffusion should be rapid.

We first look for a steady-state solution to the linear diffusion equation (48), in which the spectrum is close to isotropic:

$$F(k,\mu) = F_0(k) + F_1(k,\mu), \quad (49a)$$

$$|F_1| \ll F_0, \quad \mu \equiv \cos\theta. \quad (49b)$$

Insert this into Eq. (48) and average over the polar angle θ

$$2\bar{\gamma}F_0 + 2\,\overline{\gamma_1 F_1} = \bar{S}. \quad (50)$$

A bar indicates a polar angle average

$$\overline{f(\mu)} \equiv \frac{1}{2}\int_{-1}^{+1} d\mu\, f(\mu). \quad (51)$$

The anisotropic part of the damping-growth rate γ_1, is

$$\gamma_1 \equiv \gamma - \bar{\gamma}. \quad (52)$$

The kinetic equation for the anisotropic part of the distribution function, $F_1(\mu)$ is obtained by subtracting (50) from (48):

$$2\gamma_1 F_0 - \frac{1}{\sin\theta}\partial_\theta D \sin\theta\partial_\theta F_1 = S_1 - 2\bar{\gamma}F_1 - 2(\gamma_1 F_1 - \overline{\gamma_1 F_1}). \quad (53)$$

The general procedure is to solve Eq. (53) for F_1, and insert into (50) to enable the evaluation of $\overline{\gamma_1 F_1}$. The last terms in parentheses on the right side of Eq. (53) can be neglected, since $|F_1| \ll F_0$, by assumption. In our particular problem, the angle-averaged growth rate, $|\bar{\gamma}|$ is much smaller than the anisotropic part of the growth rate, $|\gamma_1|$, at most angles, so the term $\bar{\gamma}F_1$ is also negligible. Finally, we assert that $|S_1| \ll |\gamma_1 F_0| \simeq \bar{S}\,|\gamma_1/\bar{\gamma}|$, which can also be shown to be true at almost all polar angles, θ. Hence, the right side of (53) is negligible, and may be set equal to zero. A first integral of (53) then gives

$$\partial_\theta F_1 = \frac{2F_0}{D\sin\theta}\int_\mu^1 d\mu'\,\gamma_1. \quad (54)$$

Furthermore, the quantity $\overline{\gamma_1 F_1}$, required in (50) is easily shown, with the help of (53) and (54), to be

$$\overline{\gamma_1 F_1} = -F_0 g_1^2, \quad (55)$$

where

$$g_1^2 \equiv \frac{2}{D}\overline{\left[(1-\mu^2)^{-1/2}\int_\mu^1 d\mu'\,\gamma_1\right]^2} > 0. \quad (56)$$

The solution to the kinetic equation (50) for the (dominant) angle-averaged Langmuir distribution is, therefore,

$$F_0 = \bar{S}/2(\bar{\gamma} - g_1^2). \quad (57)$$

A realizable stationary state requires $q_1^2 < \bar{\gamma}$. For sufficiently large $|\delta n/n|^2$, D becomes large, and $g_1^2 \ll \bar{\gamma}$. In that case, (57) represents a detailed balance between the angle-averaged spontaneous emission, $\bar{S}$, and the angle-averaged damping. Even though γ_k is negative at forward angles for k near ω_p/v_b, the angle-averaged, $\bar{\gamma}_k$, will always[13] be positive, for any quasilinear distribution of electrons, and stabilization can be achieved.

In the Appendix we have numerically evaluated the Langmuir energy density, $W_0(k)$, using (57), and (3), and shown that the condition for $g_1^2 \ll \bar{\gamma}$, is $|\delta n/n| > 3\times10^{-4}$, which is well satisfied for the irregularities observed[11,29,30] in scintillation measurements. Typically,[11] $\delta n/n$ is measured at 10^{-3}.

Under conditions associated with a type III burst, (A16), we obtain the isotropic spectra shown in Fig. 2. Only the case $\Delta v/v_0 \equiv 1/3$ is of interest to us here. The spectral energy rises to $W_0(k) = 3\times10^4\ k_B T$ in the interval $1.5 < kv_0/\omega_p < 13.5$. Note, these are larger wavenumbers than the wavenumber $kv_0/\omega_p = (1-\Delta v/v_0)^{-1} = 1.5$ of the fastest growing beam mode. For this case, the integrated, or spatial energy density, is

$$\frac{E^2}{4\pi n k_B T} = \int \frac{d^3\mathbf{k}}{(2\pi)^3}\frac{W_0(\mathbf{k})}{nk_B T} = 3\times10^{-10}, \quad (58)$$

which is only two orders of magnitude larger than the equilibrium value. Hence, when this linear diffusive saturation mechanism operates, it is extremely effective at limiting the energy density in Langmuir waves. Langmuir energy densi-

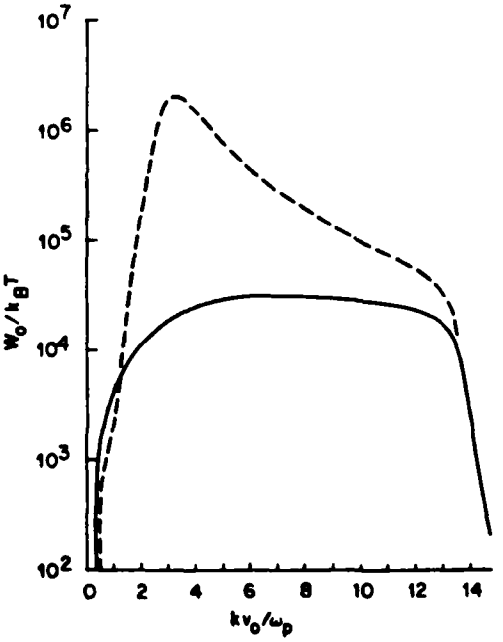

FIG. 2. Solution to Eq. (A23) for the isotropic spectral energy density in Langmuir waves under conditions appropriate to type III solar radio emission. The solid line spectrum corresponds to the set of parameters in (A16). The dashed line spectrum corresponds to the same set of parameters, except with $\Delta v/v_0 = \frac{1}{4}$.

ties this low are not uncommon[31] during type III bursts. It is unlikely, however, that such levels can give rise to electromagnetic emission, even though the isotropic distribution of Langmuir waves at large wavenumbers does permit the kinematics of second harmonic emission to be satisfied.

In steady state we find that conditions (ii)–(v) are well satisfied in this case.

C. Density fluctuations with $q_n = \mathcal{O}(2k_L)$

The cases we have just considered were based on measured density fluctuations at $q_n \ll k_L$, and $q_n \gg k_L$. In both cases, levels of $|\delta n/n|$ on the order of 10^{-3} were required to saturate the beam-unstable modes. Such levels appear to have been observed by scintillation techniques, for the case $q_n \ll k_L$.

In the limit $q_n \gg k_L$, spacecraft measurements yield $|\delta n/n|$ values which appear to be marginally too small. Here, the nonresonant effective damping, (44), applied. If we compare this with the resonant effective damping, (37), we note that the resonant damping is larger by the factor $k_D^2/4k_L^2$. This is true, however, only provided we interpret $|\delta n/n|^2$ in (37) to be $|\delta n/n|_*^2$, defined by

$$\left|\frac{\delta n}{n}\right|_*^2 \equiv \frac{4\pi}{(2\pi)^3}\int_{0\,q/2k\,1} dq\, q^2\, C(q). \tag{59}$$

This is necessary, in order for the function $f(q/2k)$ to be set equal to one. Since $k_D^2/4k_L^2$ is typically 2×10^3, the requirement on $|\delta n/n|_*$ for saturation is

$$|\delta n/n|_* > 4\times 10^{-5}. \tag{60}$$

Such low-frequency density fluctuations are required at $\lambda_n \simeq 1$ km. Convecting past a spacecraft antenna by the solar wind, these fluctuations would appear at about 400 Hz. Unfortunately, Gurnett *et al.*[19] find instrumental difficulties in resolving these frequencies in the solar wind.

The anomalous damping given by Eq. (37), is also a likely candidate for stabilizing Langmuir waves. Our derivation of that formula was based upon an isotropic density fluctuation spectrum. For a spectrum peaked along the beam axis, the damping should be even larger.

Finally, we note that this process is really scattering, rather than damping, and the emission term ought to be taken into account. Moreover, the scattering is not elastic, for k_L/k_D is only slightly above $(m/M)^{1/2}$. The scattering rate does appear to be fast enough to prevent a buildup of resonant beam modes, as in the case of long-wavelength density fluctuations. We are currently studying both processes, numerically.

V. CONCLUSION

We have derived general statistical equations governing the evolution of beam-unstable Langmuir waves in the presence of low-frequency (external) turbulence. These equations include the physical effects of scattering, diffusion, resonant and nonresonance broadening. For a broad spectrum of density fluctuations a simple Markoffian quasilinear description is obtained.

One important application has been developed in detail. It has been found that the Langmuir waves driven by solar electron streams during type III solar radio emissions can be stabilized by ambient solar wind density fluctuations at levels of $\delta n/n = 10^{-3}$, observed at wavenumbers $q_n \ll \omega_p/v_b$ or $q_n \simeq 2\omega_p/v_b$. It is likely that the Langmuir wave intensities are saturated by the density fluctuations at rather low levels.

This has important implications for the theory of type III electromagnetic emission. The emissions below 1 MHz have traditionally been interpreted as second harmonic emissions, arising from Langmuir wave coalescence. Recent spacecraft measurements have cast considerable doubt both as to the identity of the emissions as second harmonic,[26] and as to whether the Langmuir waves are sufficiently intense to produce either fundmental or harmonic emission.[31] Both Lin *et al.*[23] and Goldman[32,33] have suggested that density fluctuations in the ambient solar wind may be affecting the propagation of fundamental emission, thus causing it to be misinterpreted as second harmonic emission.

If the emissions below 1 Mhz are indeed at the fundamental, it may be possible to produce them independently of Langmuir waves. Melrose[34] has suggested that the electromagnetic version of the plasma laser effect could lead to the production of fundamental emission by the beam in the presence of the density fluctuations. Our result that the Langmuir waves are kept at low intensities by measured density fluctuations makes this idea worth pursuing.

The nonresonant extention of this theory as described in the second paper also describes the electromagnetic plasma laser effect. The major difficulty with this effect is that only the density fluctuations with wave vector $\mathbf{q}$ in a narrow range (with $q \gtrsim \omega_p/v_b$) contribute to the growth of long-wavelength electromagnetic waves; density fluctuations with nearby and remote wave vectors will stabilize the waves. Evidently, there is a need for further detailed work in this area.

It is worth commenting upon the relationship of our present results to earlier work on nonlinear saturation[9,18,35] of bump-on-tail instabilities, such as those associated with type III bursts. Studies of spatial collapse, or self-focusing of Langmuir waves by density fluctuations driven self-consistently by ponderomotive force, show that $\delta n/n$ is of order $\langle E^2\rangle 4\pi n k_B T$. At the threshold for collapse, this implies $\delta n/n$ of order 10^{-5}, which is far below the levels of "external" density fluctuations in the solar wind, whose effects we have studied here. It would appear, therefore, that the solar wind is not sufficiently homogeneous for some of these nonlinear saturation mechanisms to operate globally, and that scattering off external density fluctuations (with $\delta n/n$ between 10^{-4} and 10^{-3}) is the dominant mechanism for saturating the beam-unstable Langmuir waves. A word of caution is in order, however.

The theory of Langmuir wave self-focusing and collapse is dynamical in nature, whereas the present theory is statistical. The validity of the statistical external density fluctuations have statistics which are close to Gaussian.

It is not known whether this is the case for the density fluctuations in the solar wind; Gaussianity is probably unlikely, because long time average values of $\delta n/n$ are orders of magnitude below peak (50 msec average) values.[19] Numerical studies of dynamical Langmuir ray trajectories in the

presence of large scale density fluctuations, with $\delta n/n = 10^{-3}$, clearly reveal spatial pockets in which Langmuir wave levels are nonlinear.[11] It may be that such regions have been detected by spacecraft and play a role in type III emissions. However, recent[36] two-dimensional numerical studies of the dynamical Zakharov equations in the presence of external density fluctuations show a pervasive linear saturation of beam-unstable modes for relatively low values of $\delta n/n$.

The general area is clearly worth pursuing further, not only for its implications for the type III problem, but also for its relevance to other beam-plasma systems, such as the beams and Langmuir waves produced by Jupiter's bow shock,[17] and relativistic laboratory electron beams capable of producing intense electromagnetic emission.[37]

ACKNOWLEDGMENTS

We gratefully acknowledge conversations with H. Rose, D. Pesme, and G. Pelletier, and the hospitality of the Aspen Center for Physics where a portion of this work was performed. One of us (M.V. G.) wishes to acknowledge conversations with R. Lin and to thank him for an early preprint version of Ref. 23 on type III emission, which directly motivated this research, and also to acknowledge valuable conversations with F. Tappert, and the hospitality of the Physics Department and Marine Laboratories of the University of Miami, where another portion of this research was performed. Other important conversations were with D. Smith, J. Weatherall, G. Dulk, D. Melrose, K. Sheridan, and the Commonwealth Scientific Industrial Research Organization Solar Radio Physics Group.

This work was supported by the Air Force Office of Scientific Research (Grant No. 80-0022), the National Aeronautics and Space Administration (Grant No. NAGW-91), by the National Science Foundation, Atmospheric Sciences Section (Grant No. ATM-7916837), to the University of Colorado, and by the U.S. Department of Energy. One of us (D. F. D.) was partially supported by a Guggenheim Foundation Fellowship.

APPENDIX: ISOTROPIZATION DUE TO ANGULAR DIFFUSION OF LANGMUIR WAVES OFF LARGE SCALE DENSITY IRREGULARITIES

In this appendix, we evaluate the linear isotropic detailed balance result for the Langmuir spectral function

$$F_0 = \bar{S}/2\bar{\gamma}, \tag{A1}$$

for conditions relevant to the interplanetary electron stream associated with type III solar radio bursts. In addition, we estimate a lower bound on $\delta n/n$, in order for the quantity g_1^2, defined by Eq. (56) to satisfy

$$g_1^2 < \bar{\gamma}, \tag{A2}$$

as required for the steady state found in Eq. (57). Finally we show that (A2) guarantees the condition for the anisotropic part of the distribution function, F_1 to be small, namely,

$$|F_1| \ll F_0. \tag{A3}$$

Let us assume a gentle bump distribution function of the form

$$f_b(\mathbf{v}) = \frac{n_b}{(2\pi)^{3/2}\Delta v^3} \exp\left(-\frac{(\mathbf{v}-\mathbf{v}_0)^2}{2\Delta v^2}\right). \tag{A4}$$

The quasilinear growth rate formula, Eq. (5), then yields

$$\gamma_{\mathbf{k}}^{b1} = \Omega\,(v_0/\Delta v) z \exp(-z^2/2), \tag{A5}$$

where

$$\Omega \equiv (\pi/8)^{1/2}\omega_p (n_b/n)\omega_p^2/k^2 v_0 \Delta v, \tag{A6}$$

$$z \equiv (v_0/\Delta v)(\omega_p/k v_0 - \mu), \tag{A7}$$

and $\mu = \cos\theta$, where θ is the polar angle between $\mathbf{k}$ and $\mathbf{v}_0$. The maximum beam growth rate, $\gamma_{\mathbf{k}}^{b1}|_m$, corresponds to $z = -1$ and $\mu = 1$, and is given by a negative damping,

$$\gamma_{\mathbf{k}}^{b1}|_m = -\Omega e^{1/2} v_0/\Delta v. \tag{A8}$$

For typical type III burst conditions, $|\gamma_{\mathbf{k}}^{b1}|_m^{-1}$ is on the order of 1–10 sec. The angle average of the "damping" rate given by Eq. (A5) is

$$\bar{\gamma}_{\mathbf{k}}^{b1} = \Omega b_- > 0, \tag{A9}$$

where

$$b_\pm \equiv [\exp(z^2/2) \pm \exp(-z_\pm^2/2))]/2,$$

and

$$z_\pm = (v_0/\Delta v)(\omega_p/k v_0 \pm 1). \tag{A10}$$

We note that $\gamma_{\mathbf{k}}^{b1}$ is positive and $\ll |\gamma_{\mathbf{k}}^{b1}|_m$ at most wave numbers, due to the exponential factor b_-. Stabilization occurs because the beam takes more energy from the waves (at angles such that $z > 0$) than it gives to them ($z < 0$) in an isotropic distribution.

In order to evaluate g_1^2, we need the quantity

$$\int_\mu^1 d\mu'\,\gamma_1 = \Omega\,[\exp(-z^2/2) + b_+ - \mu b_-]. \tag{A11}$$

We shall find a spectrum, F_0 which peaks at $\omega_p/k v_0 < 1$, so (A11) is largest for $|z| \ll 1$, or for $0 < \mu \ll 1$. Hence, from Eq. (56),

$$g_1^2 < \pi^{1/2}\Omega^2 (\Delta v/v_0)/D. \tag{A12}$$

The inequality (A2) then implies the condition for a stationary isotropic state, as

$$(\Omega/b_-)(\Delta v/v_0) \ll D, \tag{A13}$$

or, using Eq. (48),

$$\left(\frac{n_b}{n}\right)^{1/2} \frac{v_e}{v_0} \left(\frac{k}{q_n}\right)^{1/2} b_-^{-1/2} \ll \left|\frac{\delta n}{n}\right|. \tag{A14}$$

This gives us a lower bound on $|\delta n/n|$ for the validity of the isotropic detailed balance result, (A1).

It is easy to verify that this lower bound also guarantees that $|F_1| \ll F_0$. From Eqs. (50), (53), and (55) it follows that

$$\overline{F_1^2/F_0^2} = \mathcal{O}[(g_1^2/\bar{\gamma})(\bar{\gamma}/D)]. \tag{A15}$$

Since (A13) guarantees that $g_1^2/\bar{\gamma} \ll 1$ and $\bar{\gamma}/D$ is generally also small (in our case $\bar{\gamma} \ll |\gamma|_{max} \lesssim D$), it follows that the anisotropic part, F_1, is small compared with F_0.

How large must $|\delta n/n|$ be in order to satisfy the condition (A14)? We consider typical conditions for an electron beam associated with a type III burst

$$n_b/n = 10^{-7} - 10^{-6},$$
$$v_e/v_0 = 10^{-2}, \tag{A16}$$
$$\Delta v/v_0 = 1/3,$$
$$k/q_n = 100.$$

Thus, we must have

$$\left.\frac{\delta n}{n}\right|_{\min} = 3\times 10^{-4} \tag{A17}$$

which is *below* the mean level of density fluctuations observed by scintillation measurements.[11,29,30] This mean level, as quoted by Smith and Sime,[11] is $\delta n/n = 10^{-3}$.

For fluctuations smaller than $|\delta n/n|_{\min}$, nonlinearity must be taken into account in the saturation of the beam modes. Assuming that the conditions for validity of (A1) are met, what kind of spectrum results? The Cerenkov emission produced by the beam given in Eq. (A4) is

$$S_b = 16\pi\Omega\,\theta_e(v_0/v_e)(k_D/k)\exp(-z^2/2). \tag{A18}$$

The angle-averaged emission is

$$\overline{S_b} = 16\pi\Omega\theta_e\frac{\Delta v}{v_e}\frac{k_D}{k}\left(\frac{\pi}{2}\right)^{1/2}[\Phi(z_+) - \Phi(z_-)], \tag{A19}$$

where $\theta_e = k_B T_e$ is the electron temperature, in energy units, and where, the Gaussian error integral is defined as

$$\Phi(z) = (2\pi)^{-1/2}\int_{-\infty}^{z} du\exp(-u^2). \tag{A20}$$

In order to join smoothly to the equilibrium distribution at large and small k_- values, we include, in the denominator of (A1), both Landau and collisional damping,

$$\gamma_L \equiv (\pi/8)^{1/2}\omega_p^4/k^3 v_e^3\exp(-\omega_p^2/2k^2v_e^2), \tag{A21a}$$

$$\gamma_c \equiv (12\pi\sqrt{2\pi})^{-1}\omega_p(k_D^3/n)\ln\Lambda, \tag{A21b}$$

and the corresponding spontaneous emission terms which can be defined by the detailed balance condition. They are, respectively, Cerenkov and bremmstrahlung emission from the background plasma

$$S_L \equiv 2\theta\gamma_L, \quad S_c \equiv 2\theta\gamma_c. \tag{A22}$$

From Eq. (3), the energy density in Langmuir waves is $W_0 = F_0/8\pi$. In Fig. 2, we plot

$$W_0(k)/\theta = \frac{\bar{S}_b/2\theta + (\gamma_L + \gamma_c)}{8\pi(\bar{\gamma} + \gamma_L + \gamma_c)}, \tag{A23}$$

as a function of $u \equiv kv_0/\omega_p$, for the parameters of (A16), and also for $v_0/\Delta v = 6$. Throughout the enhanced region, beam emission dominates the background emission processes (A22). Beam damping is the main dissipation process, except at small k values, where collision-damping is dominant, and at large k, where Landau damping is dominant. In the curve with $\Delta v/v_0 = 6$, the beam damping is dominated by collision damping for $\mu > 3$. In the enhanced region we see mode energy from four to six orders to a magnitude greater than the equilibrum value of θ_e per mode.

[1]T. M. O'Neil, J. H. Winfrey, and J. H. Malmberg, Phys. Fluids **14**, 1204 (1971); T. M. O'Neil and J. H. Winfrey, *ibid.* **15**, 1514 (1972).
[2]R. Jones, W. Carr, and M. Seidl, Phys. Fluids **19**, 548 (1976).
[3]K. W. Gentle and J. Lohr, Phys. Fluids **16**, 1464 (1973).
[4]B. B. Kadomtsev, *Plasma Turbulence* (Academic, New York, 1965).
[5]R. Z. Sagdeev and A. A. Galeev, *Nonlinear Plasma Theory*, revised and edited by T. M. O'Neil and D. L. Book (Benjamin, New York, 1969).
[6]S. Bardwell and M. V. Goldman, Astrophys. J. **209**, 912 (1976).
[7]K. Nishikawa, J. Phys. Soc. Jpn. **24**, 916, 1152 (1976).
[8]V. E. Zakharov, Zh. Eksp. Teor. Fiz. **62**, 1745 (1972) [Sov. Phys.-JETP **35**, 908 (1972)].
[9]M. V. Goldman and D. R. Nicholson, Phys. Rev. Lett. **41**, 406 (1978).
[10]D. F. DuBois and H. A. Rose, Phys. Rev. **24**, 1476 (1981).
[11]D. F. Smith and D. Sime, Astrophys. J. **233**, 998 (1979).
[12]M. Berry, J. Phys. A **10**, 2061 (1977).
[13]K. Nishikawa and D. Ryutov, J. Phys. Soc. Jpn. **41**, 1757 (1976).
[14]J. Dawson and C. O. Oberman, Phys. Fluids **6**, 394 (1963); J. Dawson, in *Advances in Plasma Physics*, edited by A. Simon and W. B. Thompson (Interscience, New York, 1968), Vol. 1, p. 1.
[15]A. A. Galeev, R. Z. Sagdeev, V. D. Shapiro, and V. J. Shevchenko, Pis'ma Zh. Eksp. Teor. Fiz. **24**, 25 (1976) [JETP Lett. **24**, 21 (1977)].
[16]D. F. DuBois and M. V. Goldman (to be published).
[17]D. A. Gurnett, J. E. Maggs, D. L. Gallagher, W. S. Kurth, and F. L. Scarf, J. Geophys. Res. **86**, 8833 (1981).
[18]D. Nicholson, M. V. Goldman, D. Hoyng, and J. C. Weatherall, Astrophys. J. **223**, 605 (1978).
[19]D. A. Gurnett, E. Marsch, W. Pilipp, R. Schwenn, and H. Rosenbauer, J. Geophys. Res. **84**, 2029 (1979).
[20]A. T. Lin, K. Kaw, and J. W. Dawson, Phys. Rev. A **8**, 2618 (1973).
[21]J. C. Adams, G. Laval, and D. Pesme, Ann. de Phys. (Paris) **6**, 319 (1981).
[22]D. Pesme and D. DuBois, in *Proceedings of Conference on Nonlinear Problems: Present and Future* (North-Holland, Amsterdam, to be published).
[23]J. M. Besieris and F. Tappert, J. Math. Phys. **17**, 734 (1976).
[24]R. A. Smith, M. L. Goldstein, and K. Papadopoulos, Astrophys. J. **234**, 348 (1979).
[25]L. Vlahos and K. Papadopoulos, Astrophys. J. **234**, L217 (1979).
[26]R. P. Lin, D. W. Potter, D. A. Gurnett, and F. L. Scarf, Astrophys. J. **251**, 324 (1981).
[27]G. R. Mageissen and D. F. Smith, Solar Phys. **55**, 211 (1977).
[28]D. B. Melrose, *Plasma Astrophysics* (Golden and Breach, New York, 1980), Chap. 11.
[29]W. A. Coles and J. K. Harmon, J. Geophys. Res. **83**, 1413 (1978).
[30]J. W. Armstrong, Ph.D. thesis, University of California at San Diego, 1975.
[31]D. A. Gurnett, R. R. Anderson, and R. L. Tokar, in *IAU Symposium No. 86, Radio Physics of the Sun*, edited by M. R. Kundu and T. E. Gergely (Reidel, Dordrecht, 1980), p. 369.
[32]M. V. Goldman (to be published).
[33]M. V. Goldman and D. F. Smith, in *Physics in the Sun* (National Academy of Sciences, Washington, DC, 1982), Chap. 12.
[34]D. B. Melrose, Aust. J. Phys. **35**, 67 (1982).
[35]B. Hafizi, J. C. Weatherall, M. V. Goldman, and D. R. Nicholson, Phys. Fluids **25**, 392 (1982).
[36]J. C. Weatherall, M. V. Goldman, and D. Smith, in *AGU Fall Meeting*, SS4-1-A 9, San Francisco, 7–11 Dec. 1981.
[37]G. Benford, D. Tzach, H. Kato, and D. Smith, Phys. Rev. Lett. **45**, 1182 (1980).

APPENDIX B

B. "Steady State Turbulence with a Narrow Inertial Range"

J.C. Weatherall, D.R. Nicholson and M.V. Goldman
Accepted by Physics of Fluids

Steady State Turbulence with a Narrow Inertial Range

J.C. Weatherall, D.R. Nicholson*, and M.V. Goldman
Department of Astro-Geophysics
University of Colorado

and

*Department of Physics & Astronomy
University of Iowa

Abstract

Coupled two-dimensional wave equations are solved on a computer to model Langmuir wave turbulence excited by a weak electron beam. The model includes wave growth due to beam-plasma interaction, and dissipation by Landau damping. The inertial range is limited to a relatively small number of modes such as could occur when the ratio of masses between the negative and positive ions is larger than in a hydrogen plasma, or when there is damping in long wavelength Langmuir waves. A steady state is found consisting of quasi-stable, collapsed wave packets. The effects of different beam parameters, and the assumed narrow inertial range are considered. The results may be relevant to plasma turbulence observed in connection with type III solar bursts.

I. Introduction

There are many examples of plasmas in astrophysics and in the laboratory in which Langmuir turbulence[1-3] is produced either by charged particle streams or intense electromagnetic radiation. This turbulence is thought to have an important role in limiting the growth of instabilities and providing a mechanism for the dissipation of energy through particle heating, as well as enabling the emission of electromagnetic radiation at the plasma frequency and its harmonics. For these reasons, an understanding of the nonlinear behavior of Langmuir waves has been sought in connection with type III solar radio bursts,[4-6] which are produced by a beam of electrons ejected into the corona during a flare; plasma wave emission from Jupiter[7] due to electrons streaming from Jupiter's bow shock; ionospheric modification[8] caused by intense radio pulses sent into the ionosphere; and the radiation and heating in laboratory beam and laser plasmas.[9,10]

In the case when an electron beam passes through the plasma, the development of Langmuir wave turbulence is believed to be the result of nonlinear wave-wave interaction: namely, as the waves which are unstable because of the presence of the electron stream grow in amplitude, they begin to couple nonlinearly to other waves. Another possibility involves the interaction of the waves back on the beam particles. This is studied by quasi-linear theory. Generally, the difficulties with the theory for particle-wave saturation of the beam instability is that it predicts energy levels of

Langmuir waves in excess of the thresholds for nonlinear wave processes.[11] Furthermore, the beam appears to lose a substantial fraction of its energy to Langmuir waves within some 100 beam instability growth times.[12] This is inconsistent with the observed propagation of particle streams; for example, type III streams persist out to the earth, well beyond the 20,000 km they propagate during 100 beam instability growth times. Quasi-linear calculations[13] which allow for the finite duration of the stream show that reabsorption of the waves by beam particles can permit the beam to propagate further. Nonetheless, since the reabsorption is slow and involves nonlinear wave energies, wave-wave interaction will occur and will probably be the dominant process. Here, we will consider only turbulence due to wave-wave processes.

The theoretical ideas on the nonlinear plasma wave evolution are the following. First, there is the exponential growth of waves which are unstable because of the electron beam or radiation. When these waves reach a critical amplitude, various wave instabilities can occur. In the case of the beam plasmas, these instabilities can remove energy from resonance with the beam so as to limit the loss of beam energy to Langmuir waves. A further consequence of the instabilities is the formation of a broad distribution of Langmuir waves.[14] The nonlinear stage of this wave-wave interaction was discovered by Zakharov[15] to cause the localization of plasma waves by trapping in regions

of low plasma density. This process leads to the collapse[15,16] of wave packets to very small dimension, at which dissipation (for example by Landau damping or Langmuir wave breaking) can occur.

The general features[3] of the energy spectrum of a turbulent system of Langmuir waves are indicated schematically in Figure 1a. We identify three ranges of wavenumbers. First, there is a small wavenumber region (labelled the "condensate") which is formed by a cascade of energy from the injection wavenumber, k_o. into wavenumbers below k_o. Second, there is a dissipation region of wavenumbers greater than $k \sim .2k_D$ for which Landau damping is significant (k_D is the Debye wavenumber). In analogy with fluid turbulence, the intermediate region of wavenumber space is called the inertial range, and is involved in the transfer of wave energy from the injection to the dissipative regions. Computer solutions[17-19] of the nonlinear wave equations (as written in Sec. II) suggest that the wave-wave process outlined above, including collapse, can produce such an energy spectrum. (We should add, however, that in systems which are very strongly pumped[19-21] or which have significant ion-acoustic noise[22,23] collapse may not be essential to the turbulent equilibrium. In addition, for systems with other sources of dissipation besides Landau damping by thermal electrons, an equilibrium state may be possible without catastrophic collapse.)

In this paper, we will present results of two-dimensional computer solutions which demonstrate that a steady state can be maintained by the collapse of wave packets. Previous two-dimensional models[5,16,18,24] of beam-plasma systems have not included damping, so they do not describe a steady state. In our model, the injection of energy is through the beam-plasma instability caused by a weak electron beam; the dissipation is due to Landau damping from thermal electrons. We will limit the size of the inertial range in order to accomodate the finite number of modes in the numerical grid. As discussed in Sec. III, this can be accomplished by adopting a mass ratio of m/M = 1/25. With this mass ratio, the inertial range is compressed, as indicated in Fig. 1(b). The presence of nonthermal electrons with phase velocities *less* than the beam velocity can also reduce the inertial range by damping small wavenumber modes; this is depicted in Fig. 1(c). These two ways of shortening the inertial range are mathematically equivalent. We will present our numerical results in Secs. IV and V in the context of the m/M = 1/25 model. Applications to physical systems (such as the type III plasma) can be sought through a transformation of variables; these will be presented later in Sec. VI.

The steady state we find consists of quasi-stable collapsed wave packets. We will study in Sec. V how the wave energy in the turbulent state scales with the beam parameters of intensity

and temperature. Using scaling arguments, we will further comment (in Sec. VI) on the characteristic length scales in the turbulent system; namely, whether most of the wave energy will be found in the long wavelength condensate or in the small compact wave packets.

II. The Nonlinear Wave Equations

The mathematical description of nonlinear Langmuir waves which we shall use is due to Zakharov,[15] who derived two coupled equations describing the slow time scale behavior of the envelope of the electric field and the plasma density fluctuations;

$$\bar{\nabla}\cdot\left(i\frac{\partial \bar{E}}{\partial t} + \frac{i\nu_e \bar{E}}{2} + \frac{3}{2}\,\omega_p \lambda_e^2\,\bar{\nabla}\,\bar{\nabla}\cdot\bar{E}\right) = \frac{\omega_p}{2n_o}\,\bar{\nabla}\cdot n\bar{E} \tag{1a}$$

$$\frac{\partial^2 n}{\partial t^2} + \nu_i \frac{\partial}{\partial t} n - \frac{\kappa T_e}{M}\nabla^2 n = \frac{1}{16\pi M}\,\nabla^2 |\bar{E}|^2 \quad . \tag{1b}$$

$\bar{E}$ is the envelope field; the total electric field is given by

$$\bar{\mathcal{E}} = \frac{1}{2}[\bar{E}(t,\bar{r})e^{-i\omega_p t} + \bar{E}^*(t,\bar{r})e^{i\omega_p t}] \quad ; \tag{2}$$

n is the variation of the ion density from its average, n_o; ω_p is the background electron plasma frequency, $\omega_p = (4\pi n_o e^2/m)^{\frac{1}{2}}$, m and M are the electron and ion masses, respectively; the electron Debye length is $\lambda_e = k_D^{-1} = \left(\frac{4\pi n_o e^2}{\kappa T_e}\right)^{\frac{1}{2}}$; T_e is the electron temperature, assumed here to be much greater than the ion temperature; and κ is the is Boltzmann's constant.

These equations contain all of the physics of electrostatic Langmuir waves and quasi-neutral ion sound waves; in addition, they include the refraction of Langmuir waves by the density variation, and the effects on plasma density due to the ponderomotive force of the inhomogeneous electric field. These equations can be derived from a simple fluid model by separating all quantities into high and low frequency components (the plasma electrostatic oscillations are high frequency, and the ion-acoustic fluctuations are low frequency), and by assuming that the displacement of electrons in the high frequency motion is much less than the scale length of the slow variations. The electric field energy density must necessarily be small compared to the thermal energy density; $|\bar{E}|^2/8\pi << n_o \kappa T_e$.

The damping terms ν_e and ν_i are operators in real space which represent Landau damping. The term ν_e can be negative for waves which are driven by an external source, such as a beam of particles.

Equation (1) describes a wide variety of nonlinear wave-wave phenomena. For a turbulent system of waves, an analytic description is very difficult, and a statistical treatment[25] of turbulence arising from the ponderomotive force is not completely developed. In this paper, we will use a computer to model the Langmuir wave turbulence.

III. A Computer Model of Langmuir Turbulence

Many of the computer solutions[19,20,26] for Langmuir turbulence based on equation (1) are done in one dimension. However, it is well known that one dimensional calculations do not produce all the physical phenomena contained in the wave equations. The most significant difference is that the nonlinear evolution of wave packets can result in a spatial collapse only in more than one dimension. The authors[19,20] of the one dimensional work overcome this difficulty by resorting to a powerful electromagnetic pump which adds energy to the system so fast that the one dimensional soliton structures are forced to smaller and smaller sizes. Nonetheless, in weakly pumped systems that are of interest in astrophysical plasmas, it has been shown by direct comparison[24] of one and two dimensional solutions that the collapse time in two dimensions is much faster than the evolution of the soliton structures in one-dimension.

Although it is desirable to study Langmuir turbulence in more than one dimension, finding solutions to the Zakharov equations in just two dimensions is a formidible task for a computer in terms of the time and memory required. The best two dimensional solutions utilize a system with 64^2 grid points, but these do not begin to incorporate all of the important length scales. This difficulty is similar to the problem in fluid turbulence in which the dynamic scale lengths are determined by

the largest eddies, while the dissipation occurs in the smallest eddies. In the plasma, energy is injected by a beam or electromagnetic pump into waves with relatively long wavelength. For example, Langmuir waves resonant with an electron stream travelling at velocity v_b will have a wavelength

$$\frac{\lambda_1}{2\pi} \sim \left(\frac{v_b}{v_e}\right)\lambda_e \quad , \tag{3}$$

where v_e is the thermal velocity of the background plasma electrons. The initial evolution of these waves is likely to involve a cascade or scattering into other wavemodes.[24] When the pump is relatively weak (i.e., $W < (\lambda_1/\lambda_e)^{-2}$, m/M; where W is the pump energy in dimensionless units, $W = |E|^2/8\pi n_o \kappa T_e$), this scattering will produce a "condensate"[3,27] of Langmuir waves which exhibits wave packets propagating more slowly than the ion sound speed; this condensate can be characterized by wavelengths

$$\frac{\lambda_2}{2\pi} \gtrsim 3\sqrt{M/m}\ \lambda_e \quad . \tag{4}$$

Eventually, the wave energy may become large enough to drive modulational instabilities and produce self-focusing. The result would then be a "collapse" of wave packets to smaller sizes, which according to theory, proceeds at an accelerating rate until they reach such small scales that they become rapidly

Landau damped by thermal electrons:

$$\frac{\lambda_3}{2\pi} \sim 5\lambda_e \quad . \tag{5}$$

Therefore a realistic solution must include all of the length scales λ_1, λ_2, and λ_3 which span a couple of orders of magnitude.

Fortunately, some important physics can be learned by using a grid which includes only those scale lengths λ_1 and λ_2. This is often the case when the grid spacing is chosen to accommodate the wavelength of the pump at the expense of the shortest length scales which constitute the dissipation region. This approach[5,18,24] has been successful in describing the initial development of weakly pumped systems, including the nonlinear saturation of the beam instability and the formation of collapsing wave packets. Of course, the grid is too coarse to follow the evolution of the collapsing wave structures. Therefore an understanding of the asymptotic steady state is lacking from these solutions.

The way in which we overcome this problem of disparate length scales is to use a mass ratio, M/m = 25. As can be seen from Eq. (4) , this will effectively reduce the condensate length scale to such an extent that it can be included in a 64x64 point grid with a grid spacing determined by the small dissipation

length scale, which is of the order of a Debye length. We are then able to solve a model problem for Langmuir turbulence in two-dimensions which contains all of the relevant physics of the beam-plasma instability, nonlinear wave-wave interaction, and wave dissipation through Landau damping. Although the choice of the mass ratio is a matter of convenience, this solution may have a physical realization in the laboratory[28] with heavy negative and positive ion plasmas.

The numerical calculation is performed on complementary grids in real space and wavenumber space. The fields n and ψ (where $\bar{E} = \bar{\nabla}\psi$) are defined at each point on a grid in x,y space having $N \times M$ points with a separation Δx and $\Delta y = \Delta x$. These fields can be represented in terms of their Fourier components on grids in k_x, k_y space with $\Delta k = 2\pi/N\Delta x$. For a field $A_{\bar{x}}$ at the grid point (m,j) such that $x = (m-1)\Delta x$, $y = (j-1)\Delta y$, the transform is given by

$$A_{\bar{k}} = \frac{1}{N^2} \sum_{m=1}^{N} \sum_{j=1}^{N} A_{\bar{x}} \exp[-i(2\pi/N)(m-1)(k_x-1)] \exp[-i(2\pi/N)(j-1)(k_y-1)] \quad . \tag{6}$$

All quantities in real space are periodic with period $N\Delta x$ and $N\Delta y$. A certain segment in $\bar{k}$ space is not allowed to contain any energy; this step is taken to avoid the problem of aliasing. In this paper, we will use $N = 64$.

The numerical technique is known as the split-step Fourier method[29] and was invented by Tappert to solve the Korteweg deVries and nonlinear Schrodinger equations. It combines features of the "splitting" method,[30] which was used by G.I. Marchuk on the diffusion equation, and the Fourier method[31] used by Orsag on the Navier-Stokes equation. The technique has been applied specifically to the Zakharov equations by Pereira, Sudan, and Denavit,[17,32] and by the present authors in other papers.[5,8,16,18,24]

The basic concept is the following. The Zakharov equations are cast into the form of a vector equation

$$\frac{\partial \tilde{A}}{\partial t} + \tilde{\tilde{L}}\tilde{A} = \tilde{N}$$

where $\tilde{A}$ is a very large vector consisting of the components E_o^x, E_o^y (the k = 0 components of the electric field, ψ (the electric potential), n (the ion density), and $\dot{n}$ (the time derivative of the ion density. L is a linear operator, actually a constant in k-space, and N is a nonlinear operator, which is in real space. Therefore, we solve for $\partial\tilde{A}/\partial t$ in two parts at each time step: one part in k-space involving only the operator $\tilde{\tilde{L}}$, and a second part involving only the nonlinear term, $\tilde{N}$. The advantage in doing this is that it allows the spatial derivatives to be evaluated very accurately in k-space, while at the same time forming nonlinear products, such as $n\tilde{E}$ and $|\tilde{E}|^2$, in coordinate space.

Using the analytically known stationary soliton as an example, the method proves to be stable and accurate. Also, in initial value solutions with no growth or damping of waves, conservation laws for $|E|^2$ and n are checked and found to hold true. The code has been used successfully to study parametric instability and Langmuir wave collapse, giving results which have been supported with analytic theories.[16,18]

The problem is set up as follows. In wavenumber space, the 64^2 Fourier components of the electric field can be plotted as a function of their wavenumbers k_x and k_y. The beam-induced emission of Langmuir waves amplifies those wavevectors centered around the wavevector $\bar{k}_o$ having a bandwidth δk (see Fig. 2). The interaction of these modes with the beam is given by the growth rate γ. The dissipation processes affect those Langmuir wavevectors which have relatively large wavenumbers ($k \gtrsim \frac{1}{5} k_D$) where the Landau damping, ν_e, becomes important. In our simple model, changes in the particle distribution functions[19,33,34] due to the waves are not included. The ions are assumed to be cold ($T_e >> T_i$) so that the weak damping of ion-acoustic waves, ν_i, is due to Landau damping by electrons. As an initial condition, all the Langmuir modes are given a small amount of randomly phased electric field amplitude; there are no externally applied density fluctuations. With this prescription, equations (1) are solved in time by the split-step Fourier method.

The numerical values for these parameters are given as

$$\begin{aligned} k_o &= 0.11\, k_D & \frac{M}{m} &= 25 \\ \gamma &= 0.002\, \omega_p & \Delta k &= 0.018\, k_D \\ \delta k &= 0.072\, k_D & \Delta x &= 5.4\, \lambda e \end{aligned} \qquad (7)$$

and the damping rates by the formulae

$$\nu_e = 0.22\sqrt{\pi}\left(\frac{1}{k\lambda_e}\right)^3 \exp\left(\frac{-1}{2k^2\lambda_e^2}\right)\omega_p \tag{8}$$

$$\nu_i = \left(\frac{\pi}{8}\right)^{\frac{1}{2}}\left(\frac{m}{M}\right)^{\frac{1}{2}}\left(\frac{T_e}{M}\right)^{\frac{1}{2}}k \quad . \tag{9}$$

Although these Landau damping rates are derived using a Maxwellian electron distribution and straight line particle trajectories, we will continue to use them even when the fields are large. The choice of growth rate γ has no special meaning, but it will turn out to be a good selection for the statistical steady state on this grid size - other solutions with different γ will be discussed later.

The central beam-driven wavenumber, $\lambda_1 = 2\pi/k_o = 60\ \lambda_e$, is such that it lies between the subsonic condensate, $\lambda_2 > 90\ \lambda_e$, and the dissipation region, $\lambda_3 < 30\ \lambda_e$. The bandwidth δk corresponds to beams with significant dispersion in velocity. It should also be noted that although 64^2 wavenumbers are present, in practice only 42^2 modes are used because of the aliasing technique. Because these modes include both forward and backward wavevectors, the largest wavenumber is given by $k_{max} = 0.42\ k_D$.

IV. Numerical Results

The numerical calculation follows the evolution of Langmuir waves from their initial noisy conditions to a quasi-steady state driven by the beam-plasma interaction.[35]

Those waves which are unstable because of the beam initially experience a period of exponential growth. During this time, wave packets appear in the coordinate space grid with increasing amplitude and size $2\pi/\delta k$ associated with the bandwidth, δk, of the pump waves. These wave packets travel at the Langmuir group velocity in the direction of the beam.

The first indication of nonlinear wave interaction is seen in wavenumber space as a spreading of wave energy into modes adjacent to the pump modes (see Fig. 3). As described by a perturbation theory,[36] this process is due to a four wave interaction involving three pump modes and a fourth wave whose frequency mismatch with the pump waves is not too large, i.e. no greater than the frequency bandwidth in the pump. As the wave spectrum broadens, this effect causes the wave packets to contract in real space. However, at the time of Fig. 3, this interaction is slower than the beam instability growth time.

There is evidence for other types of nonlinear interaction at later times. As seen in Fig. 4, as the wave energy spreads into a large number of modes, it tends to "condense" into smaller wavenumbers. This may be associated with an induced scattering process,[24] because each time a Langmuir wave scatters or decays, it will lose energy and momentum to ion modes.

As the wave energy is passed into the smaller wavenumbers, the beam instability is saturated and the pump waves stop growing. In real space, wave packets affected by these long wavelength

instabilities distort and may break up into parts, but they do not disperse. Instead of propagating at the group velocity of the pump waves, these wave packets are nearly stationary. Because of this feature, they can be identified with the low wavenumber condensate, rather than the beam modes.

As more energy fills the condensate, these long wavelengths also become unstable. In coordinate space, the wave packets steepen by refracting into density wells created by their own ponderomotive force. The collapsing wave packets are stablized when they reach scale sizes where Landau damping can occur. Surprisingly, the resulting wave structures are relatively stable, and exist over many periods of beam growth time, γ^{-1}. In fact, they tend to disappear only when they are disrupted by the density well of a nearby wave packet.

The collection of collapsed wave packets trapped in density cavities. represents the final state of the system. The electric field amplitude appears as in Fig. 5. A comparison of Fig. 5 with Fig. 6, which is a simultaneous plot of density contours, shows the correspondence between regions of large electric field amplitude and low density. Over the course of time, these wave packets vary in shape, but remain roughly the same size. As mentioned before, they will occasionally interact with each other, and either coalesce or break up. Sometimes new wave structures are born. On the average, there is a constant number of collapsedwave structures in the system.

The steady state continues over several beam growth periods γ^{-1} for which the calculation is continued. During this time, the electrostatic energy in the beam modes, $W_p = \sum_k^{beam} |E_k|^2/8\pi n_o \kappa T$, remains fairly constant, as seen in Fig. 7a. The acoustic wave energy, $W_s = \sum_k n_k^2/n_o^2$ also saturates at a low value, as shown in Fig. 7b.

The steady state was also investigated on a grid of 32x32 points using a smaller time step. On the average, 2 to 3 collapsed wave packets occurred in the grid, which was 1/4 as large in area as the one reported here. The saturated values of W_p, W, and W_s are consistent with those in Fig. 7a and Fig. 7b, although fluctuations around the mean values are larger. We followed this steady state for 100 beam growth periods, and found no evidence of any change.

The steady state implies that the rate at which energy is generated in the pump modes is matched by the transfer and damping of energy in the dissipation regions. The evidence that the transfer of energy does not occur directly, but involves many intermediate modes and perhaps a number of distinct processes, is found in the wave spectra of the electric field and density. Figs. 8 and 9 show the Fourier components of the electric field and density averaged over two growth periods γ^{-1} spanning the steady state. The electric field amplitude tends to decrease monotonically from small to large k despite the fact that the pump modes have intermediate wavenumbers. This suggests that a considerable fraction of the energy removed from the beam waves

finds its way into the low wavenumber condensate. The interesting feature of the density spectrum is that it is peaked in a ring centered at $k = 0$ with radius $k_n = 0.05\ k_D$.

In real space the length scale $2\pi/k_n$ will be the average distance of separation between wave packets (the highest real space plasma density occurs in the region between wave packets which is filled with the plasma expelled by the ponderomotive force. These density fluctuations, which are generated by the collapsing wave packet, could have a role in scattering the Langmuir waves.[19]

The final transfer of energy from the condensate into the damped region seems to be accomplished by modulational processes; as energy accumulates in the low wavenumber modes, it spills out into higher and higher wavenumbers until it becomes damped. This nonlinear interaction is of the same nature as the one described in the context of Fig. 3 as the mechanism for broadening the pump bandwidth, except now the condensate modes replace the pump modes as the source of wave energy. The manifestation of this process in real space is the collapsed wave packets.

Given the two-dimensional spectrum of the electric field in Fig. 8, we can construct the one-dimensional energy spectrum for this problem. This is done by first calculating partial sums, Σ_i, of energy contained in modes between wavenumbers $k_i - \frac{\Delta k_i}{2} < |\tilde{k}| \leq k_i + \frac{\Delta k_i}{2}$. The interval Δk_i is

chosen so that the volume in k-space is constant, i.e., the interval contains N points, and volume $N\Delta k^2$, where Δk is the spacing of the grid. The one-dimensional energy spectrum, $W(k_i)$ is then given by

$$W(k_i) = \frac{\Sigma_i}{N\Delta k^2} 2\pi k_i \quad . \tag{10}$$

This function is plotted, using sums over N = 20 points, in Fig. 10 (after multiplying by k_D to make it dimensionless). The area under this curve gives the total energy, W. Because the inertial range is very small, we do not compare the scaling with the conventional Kolmogoroff power law. However, it is extremely interesting that the two-dimensional energy distribution $\varepsilon(k_i) = \frac{\Sigma_i}{N\Delta k^2}$, seems to decrease exponentially with increasing wavenumber. For this spectrum we find

$$\varepsilon(k) \sim (1.2/k_D^2) \exp(-k/.059\ k_D) \quad . \tag{11}$$

Finally, we wish to identify the characteristic length scales of this turbulent system. For example, the contour plot of electric field amplitude in Fig. 5 could be misleading if the small, collapsed wave structures contained only a small fraction of energy, despite their large amplitude. Therefore, we analyze the distribution of energy (as distinguished from the energy density) in Fig. 11. Fig. 11 is constructed by defining two contour levels of electric field amplitude, E_1 and E_2

(where $E_1 > E_2$). The region of real space with electric field amplitude $|E| > E_1$ contains 1/3 of the total electrostatic energy; it is most lightly shaded in the figure. The region with amplitude $|E| < E_2$ also contain 1/3 of the total electrostatic energy, and is most darkly shaded. Fig. 11 shows that a large fraction of wave energy in this system is contained in the small wave packets. We will discuss this feature of turbulence again in Sec. VI.

V. Further Numerical Results with Different Beam Parameters

The complexity of the nonlinear interaction makes it difficult to establish by analytic argument the above interpretation of the numerical results. However, we can test some of these ideas by changing parameters in the model and noting the effects on the final turbulent state. We are free to change certain parameters which affect the characteristics of the beam; these are the beam-plasma growth rate and the bandwidth of the beam modes.

The same numerical experiment as described in the previous section was done for seven different beam-plasma growth rates ranging from $\gamma/\omega_p = 0.00025$ through $\gamma/\omega_p = 0.005$. The maximum growth rate of the kinetic beam instability due to a Maxwellian bump-on-tail electron distribution having density $n_b << n_o$, central velocity $v_b >> \frac{\kappa T_e}{m}$, and temperature $\frac{\kappa T_b}{m} = \Delta v_b^2$ such that $(\Delta v_b/v_b)^3 >> n_b/n_o$ is given by

$$\gamma = \sqrt{\pi/8}\, \frac{n_b}{n_o} \left(\frac{v_b - \Delta v_b}{\Delta v_b}\right)^2 e^{-\frac{1}{2}}\, \omega_p \quad . \tag{12}$$

Because the growth rate is proportional to the number density in the beam, by changing γ we are effectively studying different strength beams. As in the earlier example, a steady state is established in all these cases consisting of collapsed, quasi-stable wave packets. The values of peak electric field amplitude, the depth of the density depletion, and the average number N of the wave packets in the grid area are given as a function of the growth rate in table I. Although it would be desirable to study a wider range of growth rates, we are again faced with certain numerical limitations. At the lower range of growth rates, there are only a small number of collapsed wave packets in the system. In order to simulate smaller growth rates, it would be necessary to increase the grid area to accomodate the small density of wave packets, which means increasing the number of modes. At the larger range of growth rates, the electric field amplitudes are very intense and the density fluctuations are no longer small ($n \sim n_o$), so that the model Eqs. (1) are no longer valid. Therefore, we must be satisfied with this range of growth rates.

The total electrostatic energy in the final steady state is plotted as a function of growth rate, γ, in Fig. 12. The energy density increases approximately linearly with γ.

The other feature of the beam instability which can be changed is the bandwidth, which is related to the temperature of the beam. For the Gaussian bump-on-tail electron distribution the bandwidth δ is approximately $(\Delta v_b/v_b)k_o$.[37] The bandwidth can be changed by adding (or subtracting) pump modes. The examples up to this point were done with 25 pump modes. Now we do other cases involving 49 pump modes and 16 pump modes, keeping the same central wavevector,

$\bar{k}_o$, as before. In general, the energy in the system is greater with a given growth rate for the larger bandwidths. These results are plotted in Fig. 13 as a function of growth rate.

Let us attempt to understand these results as a balance between the rate at which energy is added to the pump modes by the beam-plasma instability, and the rate at which energy is lost from the pump modes by scattering processes. The addition of energy, Λ_{in}, proceeds at a rate proportional to the beam-plasma instability growth rate, γ, and the energy in the pump modes,

$$\frac{d\Lambda_{in}}{dt} = 2\gamma \sum_{\alpha} |\bar{E}(\bar{k}_\alpha)|^2/8\pi \tag{13}$$

where the index α denotes all the pump modes. Furthermore, if we assume that the scattering of pump waves is described by a three wave decay instability, then the rate at which energy is lost from the pump waves into the decay waves is given as

$$\frac{d\Lambda_{out}}{dt} = 2 \sum_{\beta} \omega_i(\bar{k}_\beta) |\bar{E}(\bar{k}_\beta)|^2/8\pi \tag{14}$$

where the index β denotes all the decay modes, and $\omega_i(\bar{k}_\beta)$ is the instability growth rate at the wavevector $\bar{k}_\beta$. An energy balance is found by equating (13) and (14):

$$\gamma \sum_{\alpha} |\bar{E}(\bar{k}_\alpha)|^2 = \sum_{\beta} \omega_i(\bar{k}_\beta) |\bar{E}(\bar{k}_\beta)|^2 \quad . \tag{15}$$

To some extent, the spectrum $\bar{E}(\bar{k})$ can be regarded as uniform over a broad region of k space: $|\bar{E}(\bar{k})| \sim E_o$. Therefore, the sum on the left side of Eq. (15) can be approximated as

$$\sum_{\alpha} |\bar{E}(\bar{k}_\alpha)|^2 \sim E_o^2 N_\alpha \tag{16}$$

where $N_\alpha = \sum_\alpha 1$ is the number of pump modes. For the right side of equation (15), we adopt for $\omega_i(\bar{k}_\beta)$ the maximum growth rate for the decay instability,[38] $\omega_i \sim W_p/16$, and write

$$\sum_\beta \omega_i(\bar{k}_\beta)\,|\bar{E}(\bar{k}_\beta)|^2 \sim \frac{W_p}{16}\,E_o^2 N_\beta \tag{17}$$

where $N_\beta = \sum_\beta 1$ is the number of decay modes. The number of pump modes N_α is equal to the bandwidth of the pump, δk^2, times the density of modes. The scatter of Langmuir waves will be into wavevectors with $|\bar{k}_\beta| < |\bar{k}_o|$, since this interaction necessarily involves a loss of wave momentum to the ions. Thus, we estimate the number of decay modes, N_β, to be this volume of k space, πk_o^2, times the density of modes. The ratio of the number of pump modes to decay modes is given by

$$\frac{N_\alpha}{N_\beta} \sim \frac{\delta k^2}{\pi k_o^2} \quad . \tag{18}$$

By substituting (16) and (17) into Eq. (15), and using Eq. (18), we find the relation

$$W_p \sim \frac{16}{\pi}\,\gamma\left(\frac{\delta k}{k_o}\right)^2 \quad , \tag{19}$$

W_p is plotted as a function of $\gamma(\frac{\delta k}{k_o})^2$ in Fig. 14 for all of the steady state solutions found by the computer. The straight line shows that the scaling law is appropriate to this set of numerical experiments.

From Eq. (19), together with Eq. (12), which gives the dependence of γ on n_b and T_b, we may conclude that the rate, γW_p, at which a beam loses energy in a fully evolved turbulent plasma is proportional to the square of the beam number density and inversely proportional to the beam temperature.

Next we discuss to what extent these results can be generalized to real mass ratio plasmas.

VI. Comments on Turbulence in Physical Systems

Most astrophysical systems affected by streaming electrons (such as the solar corona during type III bursts) are hydrogen plasmas with electron to ion mass ratio of 1/1836. In this section we will examine how the above results, based on light to heavy mass ratio of 1/25, can be scaled to real beam-plasma systems.

In practice, Eqs. (1a) and (1b) are solved in dimensionless form, and the realization of a physical system is made by the appropriate transformations[5] of the time, length, electric field, and density. These transformations contain explicit dependence on the mass ratio. By using $m/M = 1/25$, we produce an injection region such that both it and the region which is Landau damped ($k > 0.2\ k_D$) can be contained in the same limited grid [see Fig. 1(b)]. If, instead, we make the transformation using the mass ratio $m/M = 1/1836$, then we have a more typical injection region, but now there is damping in relatively small wavenumbers ($k > 0.02\ k_D$) as in Figure 1(c). These are both valid ways of interpreting the numerical results. In order to make the connection between the case when $m/M = 1/1836$ and our model solutions, we make the following transformation:

$$(\omega_p t)' = \left(\frac{1836}{25}\right)\omega_p t \quad , \qquad \left(\frac{x}{\lambda_e}\right)' = \left(\frac{1836}{25}\right)\left(\frac{x}{\lambda_e}\right) \quad ,$$

$$W' = \left(\frac{25}{1836}\right)W \quad , \qquad \left(\frac{n}{n_o}\right)' = \left(\frac{25}{1836}\right)\left(\frac{n}{n_o}\right) \quad ,$$

$$\left(\frac{m}{M}\right)' = \frac{1}{1836} \quad . \tag{20}$$

While both cases have the advantage of supplying the damping necessary to produce an assymptotic steady state, they each deprive the system of an extended inertial range. Let us consider the effect the assumed narrow inertial range might have on the physics of the turbulence.

Our model demonstrates the saturation of the beam instability by scattering of Langmuir waves, the creation of a condensate, and the formation of collapsing wave packets. This development of wave turbulence is observed in other computer solutions[24] which do not have the damping, so effectively have larger (though still incomplete) inertial range. Therefore, we are encouraged to believe that this behavior is physically relevant, independent of the size of the inertial range.

On the other hand, the characteristics of the final turbulent state are probably sensitive to the distribution of energy throughout k space. For example, it is likely that the lack of a large inertial range in our model will tend to exaggerate the fraction of energy which is contained in the smallest scales. Evidence from self-similar solutions[39] suggests that while collapsing wave packets may have spectacular amplitude, they will contain a relatively small fraction of the wave energy by the time they reach their

smallest size. This could mean that the dominant length scale in the system is the relatively long wavelength "background" condensate length scale rather than the short scale of the collapsed wave packet.

We can make the following physical argument regarding the fraction of the total energy contained in the collapsed wave packets. The energy in the smallest length scales can be determined by balancing the dissipation in the short wavelengths with the energy produced in the pump waves:

$$\nu_c W_c = \gamma W_p \quad . \tag{21}$$

As before, W_p is the energy in the pump waves and γ is the beam-plasma instability growth rate. W_c is the energy in the small length scales, estimated as

$$W_c = \frac{1}{8\pi n \kappa T_e} \sum_{\zeta} |\bar{E}(\bar{k}_\zeta)|^2 \tag{22}$$

where the index ζ denotes those modes associated with the smallest wavelengths. We identify W_c with the energy in the core of the collapsed wave packets. The effective damping rate, ν_c, can be estimated by the Landau damping rate at the wavenumber $k_* = 2\pi/\lambda_c$, where λ_c is the characteristic dimension of the collapsed wave packets. We will assume that λ_c is not sensitive to the rate of energy

injection, γ. Forming the ratio of W_c to the total energy W we obtain

$$\frac{W_c}{W} = \frac{W_p}{W} \frac{\gamma}{\nu_c} \quad . \tag{23}$$

For the turbulent state described in Sec. III we found $\frac{W_p}{W} = .15$; the size of the wave packets is about $5\Delta x$, which gives $\lambda_c = 25\ \lambda_e$; and the growth rate is $\gamma = .002\ \omega_p$. The damping ν_c is given by Eq. (8) evaluated for the wavenumber $k = 2\pi/\lambda_c$. For these parameters, Eq. (23) implies that about 15% of the total energy is found in the small length scales. This is consistent with Fig. 11 which shows that about 1/3 of the energy is contained in the cores of the collapsed wave packets.

Using real electron and ion masses, the ratio γ/ν_c will be smaller because γ will transform according to Eq. (20) but unless the dissipation region is to be different from the usual Landau damping, the length λ_c (and therefore the damping rate, ν_c) should not be transformed. From this we conclude that with a realistic inertial range, the ratio $\frac{W_c}{W}$ would be smaller by a factor of 25/1836. Therefore, very little energy may actually be in the smallest length scales.

With the mass ratio m/M = 1/1836, the example in section III corresponds to a beam instability with growth rate $\gamma = 3 \times 10^{-5} \omega_p$ and principle wavenumber $k_o = 0.013\ k_D$, in which there is a large amount of damping for wavenumbers $k > 0.02\ k_D$. Despite the fact that γ is very large ($10^{-6} \omega_p$ is more realistic), this has some semblance of reality for the type III case because the

nonthermal component observed[40] in the electron distribution function in the ambient solar wind will introduce damping in wavenumbers such as the above. With these parameters, the electrostatic energy in Langmuir waves saturates at $W = 2.0 \times 10^{-4}$ and the wave packets will have dimensions of the order of 300 λ_e. With a Debye length at 1/2 A.U. of about 5 m, the wave packet scale sizes will be of the order of 1 or 2 km. Unfortunately, this is still less than the resolution of interplanetary spacecraft measuring type III bursts[4,11] (the smallest observable size is of the order of 10 km).

Finally, it should be pointed out that although the two dimensional calculations are an improvement over one dimension, the real behavior of collapsing wave packets in three dimensions might be significantly different from our model. One might expect from analytic arguments[16] that wave packets would collapse much faster in three dimensions, and might even contain a smaller fraction of the total wave energy than in the two-dimensional case.

VII. Conclusions

We have shown that in a simple two-dimensional model of beam-induced Langmuir turbulence consisting of a long wavelength regime in which instability adds energy to the system, and a short wavelength regime which provides damping, an equilibrium turbulent state is possible in which the collapse of wave packets enables the transfer of energy between the two regimes. This steady state consists of quasi-stable collapsed wave packets trapped in density cavities, which persist over a period much longer than the collapse time. The final turbulent energy level is found to be a function of the intensity of the beam and the beam temperature.

From the wave spectra we found that the greatest concentration of wave energy tends to occur in the wavenumber region of the condensate. This brings up the question of how important the smallest wave structures are to the gross properties of the turbulent system. Unfortunately, the answer is not provided by the present work because of the inadequate resolution in the grid. However, it seems possible from physical arguments that the ratio of energy in the collapsed wave packets to the total energy in weakly pumped systems will be small.

Acknowledgments

We thank F.D. Tappert, M.L. Goldstein, and R.A. Smith for helpful conversations.

This work was supported by the National Science Foundation, Atmospheric Research Section (Grant No. ATM 7916837), the Air Force Office of Scientific Research (Grant No. 80-0022), and the National Aeronautics and Space Administration (Grant No. NAGW-91). One of us (D.R.N.) was also supported by the National Science Foundation, Atmospheric Research Section (Grant Nos. ATM-79-18778 and ATM 81-11126), by the U.S. Department of Energy (Grant No. DE-AC02-76ET53034), and by the National Aeronautics and Space Administration (Grant No. NS6-7632). We thank the National Center for Atmospheric Research, supported by the National Science Foundation, for computer time used in this study. A portion of this work was completed at the Institute for Theoretical Physics at Santa Barbara, whose hospitality we gratefully acknowledge.

References

1. B.B. Kadomstev, Plasma Turbulence, (Academic Press, N.Y., 1965).
2. V.N. Tsytovich, An Introduction to the Theory of Plasma Turbulence (Pergamon Press, N.Y., 1972).
3. R.Z. Sagdeev, Rev. of Mod. Phys. 51, 1 (1979).
4. D.A. Gurnett and R.R. Anderson, Science 194, 1159 (1976).
5. D.R. Nicholson, M.V. Goldman, P. Hoyng, and J.C. Weatherall, Astrophys. J. 223, 605 (1978).
6. R.A. Smith, M.L. Goldstein, and K. Papadopoulos, Astrophy. J. 234, 348 (1979).
7. F.L. Scarf, D.A. Gurnett, and W.S. Kurth, Science 204, 991 (1979).
8. J.C. Weatherall, J.P. Sheerin, D.R. Nicholson, G.L. Payne, M.V. Goldman, and P.J. Hansen, J. Geophys. Res. 87, 823 (1982).
9. A.Y. Wong and B.H. Quon, Phys. Rev. Lett. 34, 1499 (1975).
10. D.A. Whelan and R.L. Stenzel, Phys. Rev. Lett. 47, 95 (1981).
11. D.F. Smith and D.R. Nicholson, in Wave Instabilities in Space Plasmas, p. 225 (Dordrecht: D. Reidel Pub. Co., 1979).
12. R.J.-M. Grognard, Aust. J. Phys. 28, 731 (1975).
13. G.R. Magelssen and D.F. Smith, Solar Phys. 55, 211 (1977).
14. A.A. Vedenov and L.I. Rudakov, Dokl. Akad. Nauk, SSSR 159, 767 (1964) [Sov. Phys. Dokl. 9, 1073 (1965)].
15. V.E. Zakharov, Zh. Eksp. Teor. Fiz. 62, 1745 (1972) [Sov. Phys. - JETP 35, 908 (1972)].

16. M.V. Goldman and D.R. Nicholson, Phys. Rev. Lett. 41, 406 (1978).

17. N.R. Pereira, R.N. Sudan, and J. Denavit, Phys. of Fluids 20, 936 (1977).

18. D.R. Nicholson and M.V. Goldman, Phys. of Fluids 21, 1766 (1978).

19. L.M. Degtyarev, R.Z. Sagdeev, G.I. Solovev, V.D. Shapiro, and V.I. Shevchenko, Fiz. Plazmy 6, 485, (1980) [Sov. J. Plasma Phys. 6, 263 (1980)].

20. B.A. Al'terkop, A.S. Volokitin, and V.P. Tarakanov, Fiz. Plazmy 3, 59 (1977). [Sov. J. Plasma Phys. 3, 34 (1977)].

21. A.A. Galeev, R.Z. Sagdeev, V.D. Shapiro, and V.I. Shevchenko, Zh. Eksp. Teor. Fiz. 73, 1352 (1977) [Sov. Phys. - JETP 46, 711 (1977)].

22. A.A. Galeev, R.Z. Sagdeev, V.D. Shapiro, and V.I. Shevchenko, Pis'ma Zh. Eksp. Teor Fiz. 24, 25 (1976) [JETP Lett. 24, 21 (1976)].

23. M.V. Goldman and D.F. DuBois, Phys. of Fluids 25, 1062 (1982).

24. B. Hafizi, J.C. Weatherall, M.V. Goldman, and D.R. Nicholson, Phys. of Fluids 25, 392 (1982).

25. D.F. DuBois, Phys. Rev. A., 23, 865 (1981).

26. K. Papadopoulos and H.D. Freund, Comments Plas. Phys. 5, 113 (1979).

27. K. Nishkikawa, Y.C. Lee, and C.S. Liu, Comments Plas. Phys. 2, 63 (1975).

28. N. Hershkowitz and T. Intrator, Rev. Sci. Instrum. 52, 1629 (1981).

29. R.H. Hardin and F.D. Tappert, SIAM Rev. 15, 423 (1973).

30. G.I. Marchuk, Methods of Numerical Mathematics (Springer-Verlag, New York, 1975).

31. D. Gottlieb and S. Orszag, Numerical Analysis of Spectral Methods (SIAM, Philadelphia, 1977).

32. J. Denavit, N.R. Pereira, and R.N. Sudan, Phys. Rev. Lett. 33, 1435 (1974).

33. T.F.J. van Gunsven, P. Hoyng, and D.R. Nicholson, Astron. Astrophys. 91, 7 (1980).

34. H.L. Rowland, J.C. Lyon, and K. Papadopoulos, Phys. Rev. Lett. 46, 346 (1981).

35. J.C. Weatherall, "Beam-excited Langmuir Wave Turbulence", computer movie produced at NCAR (1981).

36. J.C. Weatherall, Phys. of Fluids 25, 212, (1982).

37. M.V. Goldman, G.F. Reiter, and D.R. Nicholson, Phys. of Fluids 23, 388 (1980).

38. S. Bardwell and M.V. Goldman, Astrophys. J. 209 (1976).

39. M.V. Goldman, K. Rypdal, and B. Hafizi, Phys. of Fluids 23, 945 (1980).

40. R.P. Lin, D.W. Potter, D.A. Gurnett, and F.L. Scarf, "Energetic Electrons and Plasma Waves Associated with a Solar Type III Radio Burst", Astrophys. J. 251, 346 (1981).

TABLE I

Turbulence parameters with different beam growth rates

γ/ω_p	$E_{max}/(8\pi n_o kT_e)^{\frac{1}{2}}$	n_{max}/n_o	N
0.25×10^{-3}	0.3	0.16	1
0.50×10^{-3}	0.4	0.2	3
0.93×10^{-3}	0.4	0.32	4
1.3×10^{-3}	0.4	0.32	5
2.0×10^{-3}	0.5	0.50	9
2.5×10^{-3}	0.6	0.64	13
5.3×10^{-3}	1.0	1.6	15

FIGURE CAPTIONS

Fig. 1: Energy spectra of Langmuir waves:
a) hypothetical spectrum for a turbulent plasma;
b) turbulent spectrum with a small mass ratio;
c) turbulent spectrum allowing for Landau damping due to a suprathermal tail on the electron distribution.

Fig. 2: Numerical grid of Langmuir wavevectors in the beam-plasma model. There is a region in wavenumber space of 25 modes growing at a constant rate due to the beam. Larger wavenumber modes are Landau damping.

Fig. 3: Early nonlinear development of Langmuir waves in wave-number space. Numbers represent relative electric field amplitude (those less than 3 are not plotted). The box outlines the 25 pump modes, each one having relative amplitude of 240. The total pump wave energy is $W_p = 0.001$.

Fig. 4: Later nonlinear development of Langmuir waves shows the tendency of wave energy to be scattered into small wavenumber modes. The units of electric field amplitude are ten times larger than Fig. 3. (Numbers less than 50 are not plotted). Total pump wave energy is $W_p = 0.010$.

Fig. 5: Contours of electric field amplitude in real space grid at the time of the steady state. The highest contour (in the center of the collapsed wave packets) has amplitude $E = 0.5(8\pi n_o \kappa T_e)^{\frac{1}{2}}$. The lowest contour has amplitude $E = 0.08(8\pi n_o \kappa T_e)^{\frac{1}{2}}$.

Fig. 6: Contours of ion density at the same time as Fig. 5. The contours with the largest magnitude are found in the center of the density cavities: $\delta n = -0.5\ n_o$.

Fig. 7: Development of the turbulent state

a) The electrostatic energy in the pump modes (W_p) and the total electrostatic energy in Langmuir waves (W) as a function of time. (Time is in units of ω_p^{-1}).

b) Mean squared density, $(n/n_o)^2$, as a function of time.

Fig. 8: Root mean squared Langmuir wave spectrum. The amplitude per mode goes from $E_k/(8\pi n_o \kappa T_e)^{\frac{1}{2}} \leq 1.2 \times 10^{-3}$ (the lightest shading) to $E_k/(8\pi n_o \kappa T_e)^{\frac{1}{2}} \geq 1.1 \times 10^{-2}$ (the darkest shading).

Fig. 9: Root mean squared density spectrum. n_k/n_o goes from .0005 (the lightest shading) to .005 (the darkest shading).

Fig. 10: One-dimensional energy spectrum, $k_D W(k)$, as a function of wavenumber, k/k_D.

Fig. 11: Distribution of electrostatic energy in the turbulent system. Each of the shaded regions contains 1/3 of the total energy. The lightest shade has the larger values of electric field amplitude.

Fig. 12: Total electrostatic energy in Langmuir waves in the final turbulent state for various beam instability growth rates.

Fig. 13: Total electrostatic energy in Langmuir waves for three different pump bandwidths and various beam growth rates. The middle curve is the same as Fig. 11.

Fig. 14: Final electrostatic energy in Langmuir waves plotted as a function of $\gamma\delta k^2$ for eleven different numerical examples of steady state turbulence.

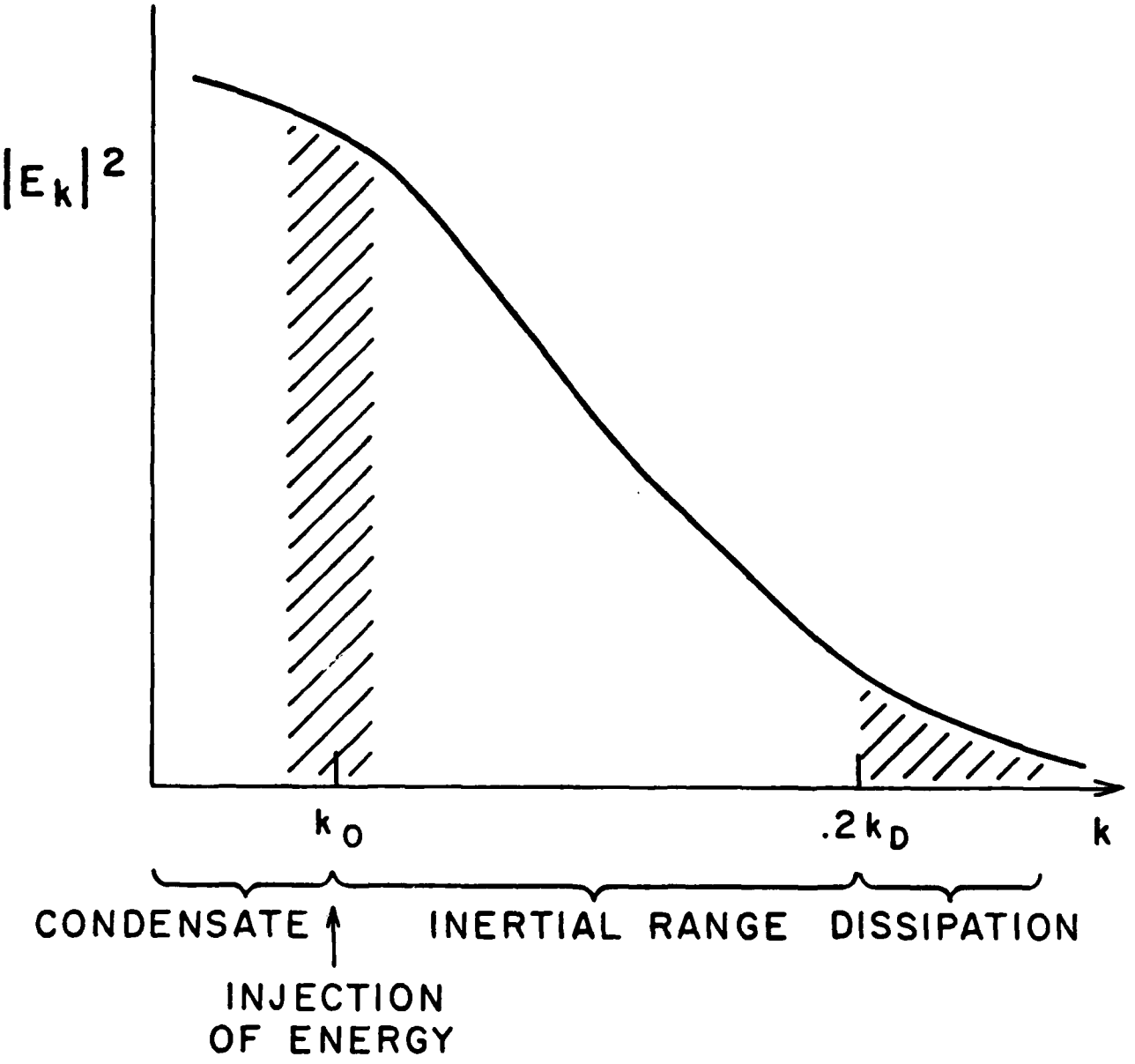
$|E_k|^2$
k_0
$.2k_D$
k
CONDENSATE
INERTIAL RANGE
DISSIPATION
INJECTION
OF ENERGY

FIGURE 1a

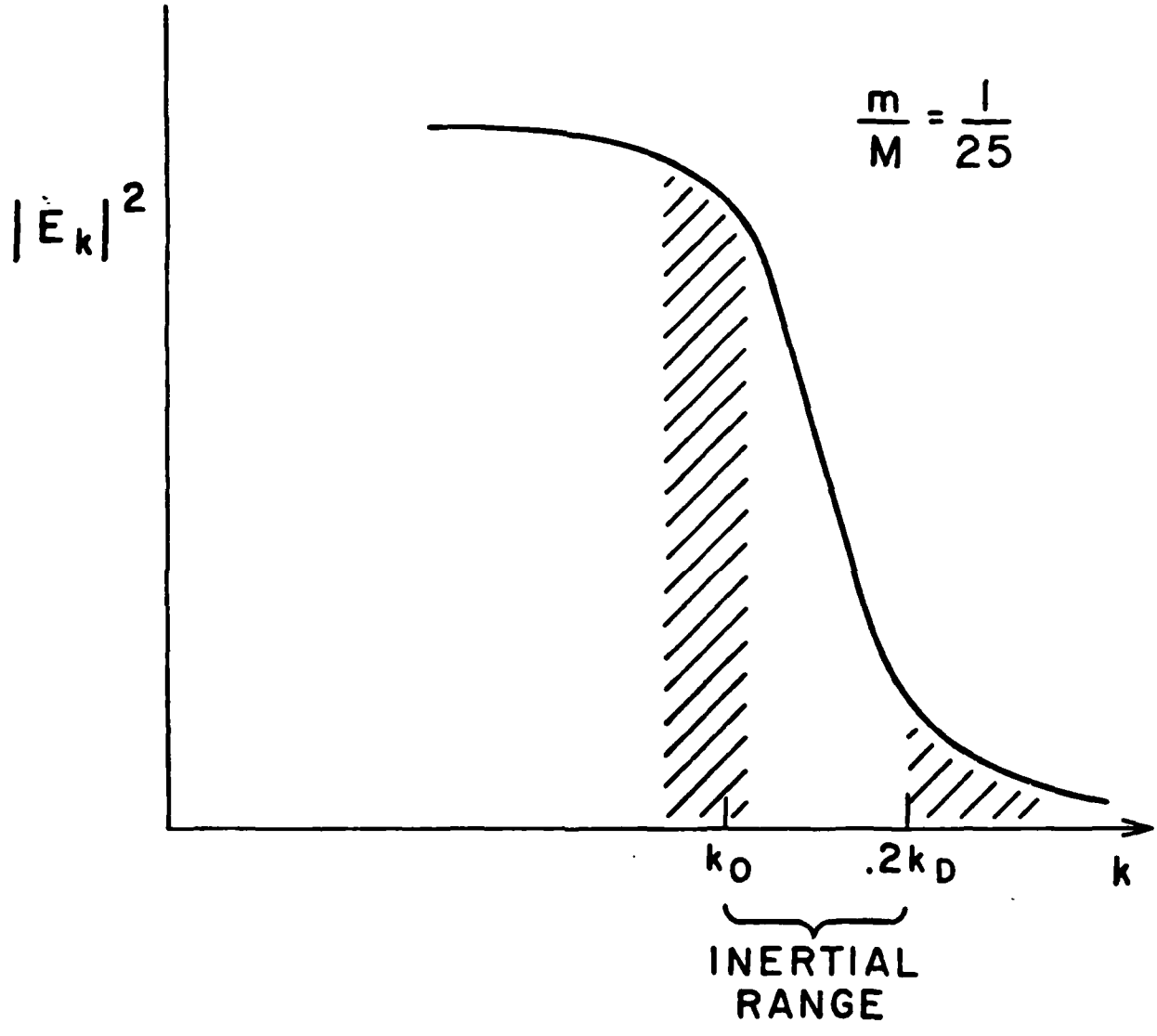

FIGURE 1b

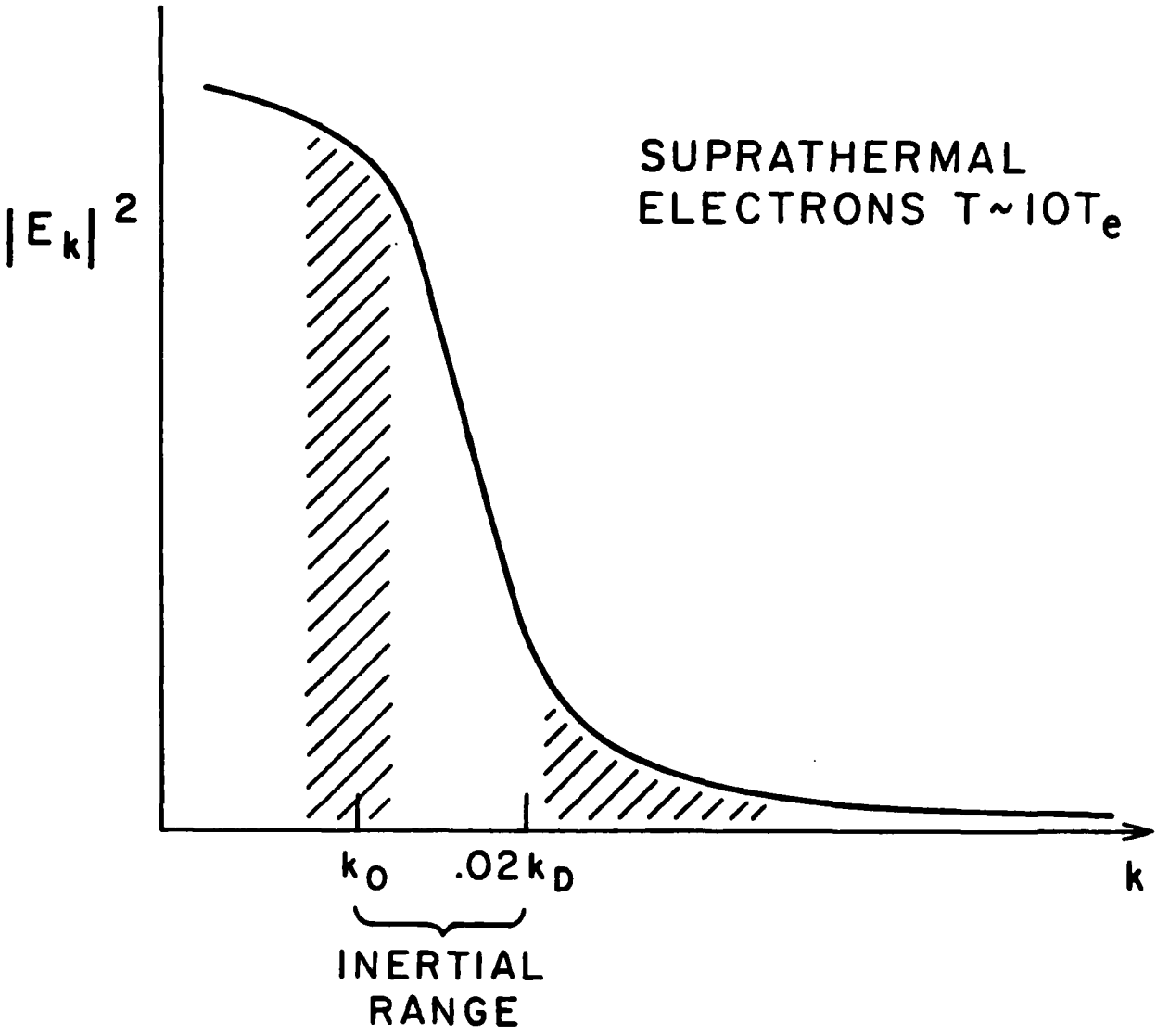
$|E_k|^2$
SUPRATHERMAL
ELECTRONS $T \sim 10T_e$
k_0
$.02k_D$
k
INERTIAL
RANGE

FIGURE 1c

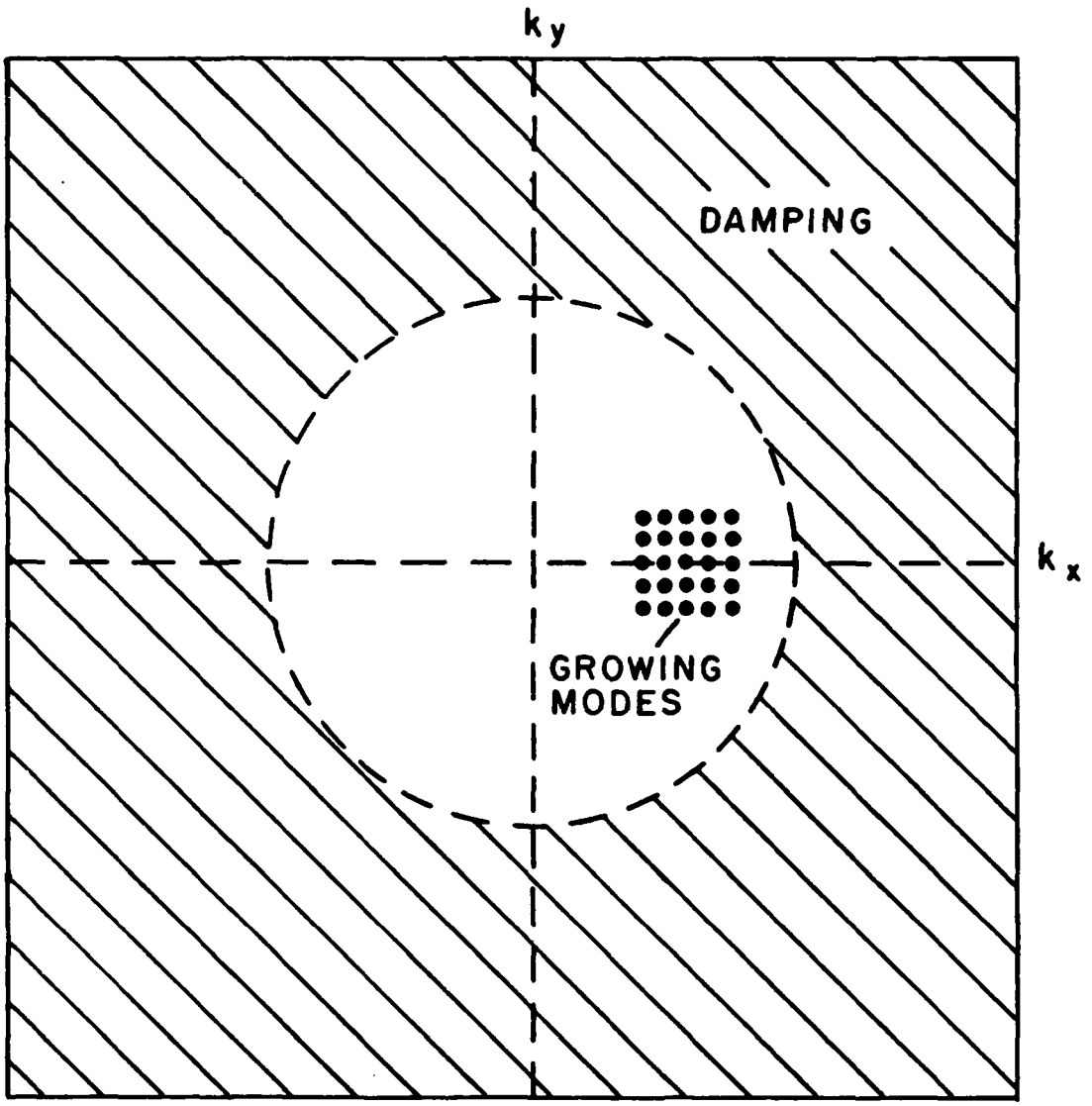

FIGURE 2

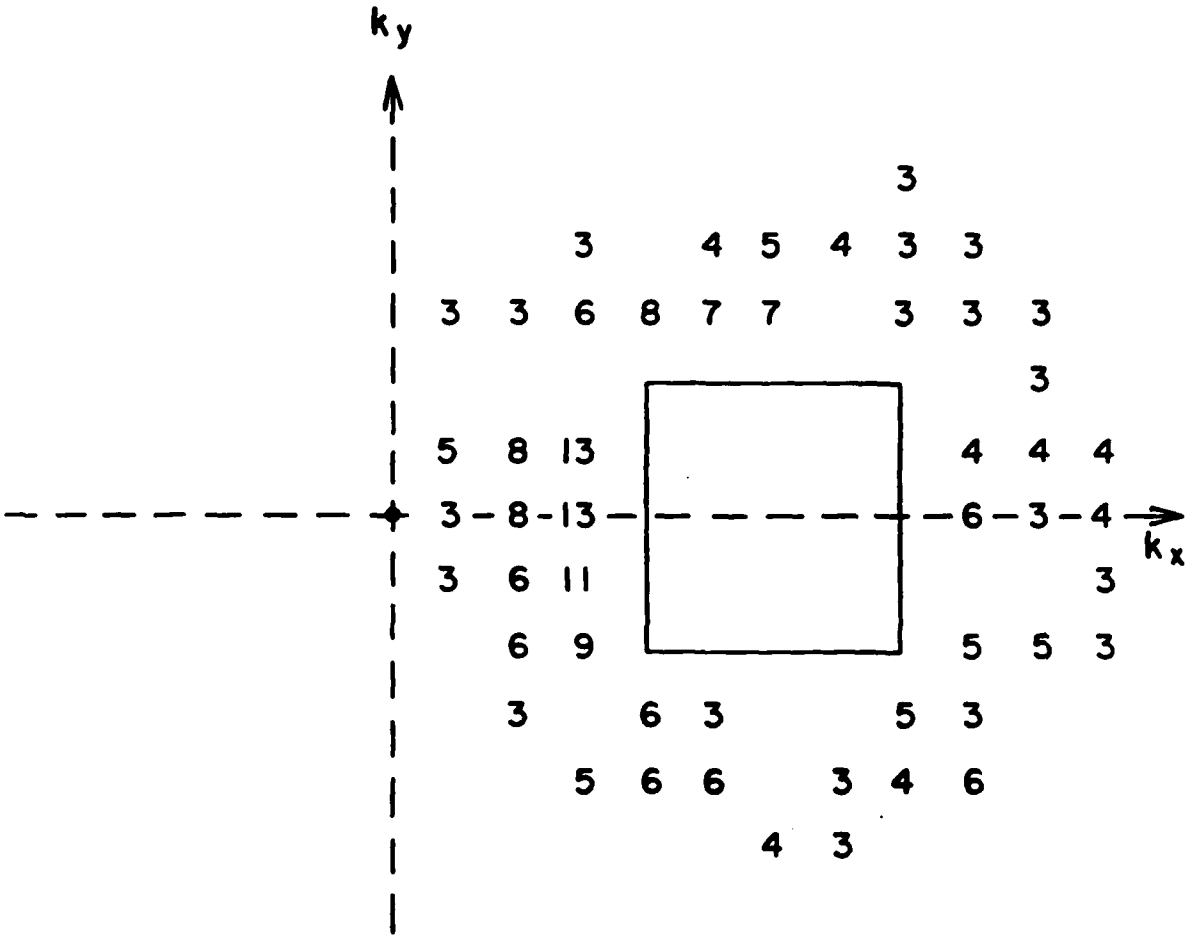
k_y
k_x
3
3 4 5 4 3 3
3 3 6 8 7 7 3 3 3
3
5 8 13 4 4 4
3 8 13 6 3 4
3 6 11 3
6 9 5 5 3
3 6 3 5 3
5 6 6 3 4 6
4 3

FIGURE 3

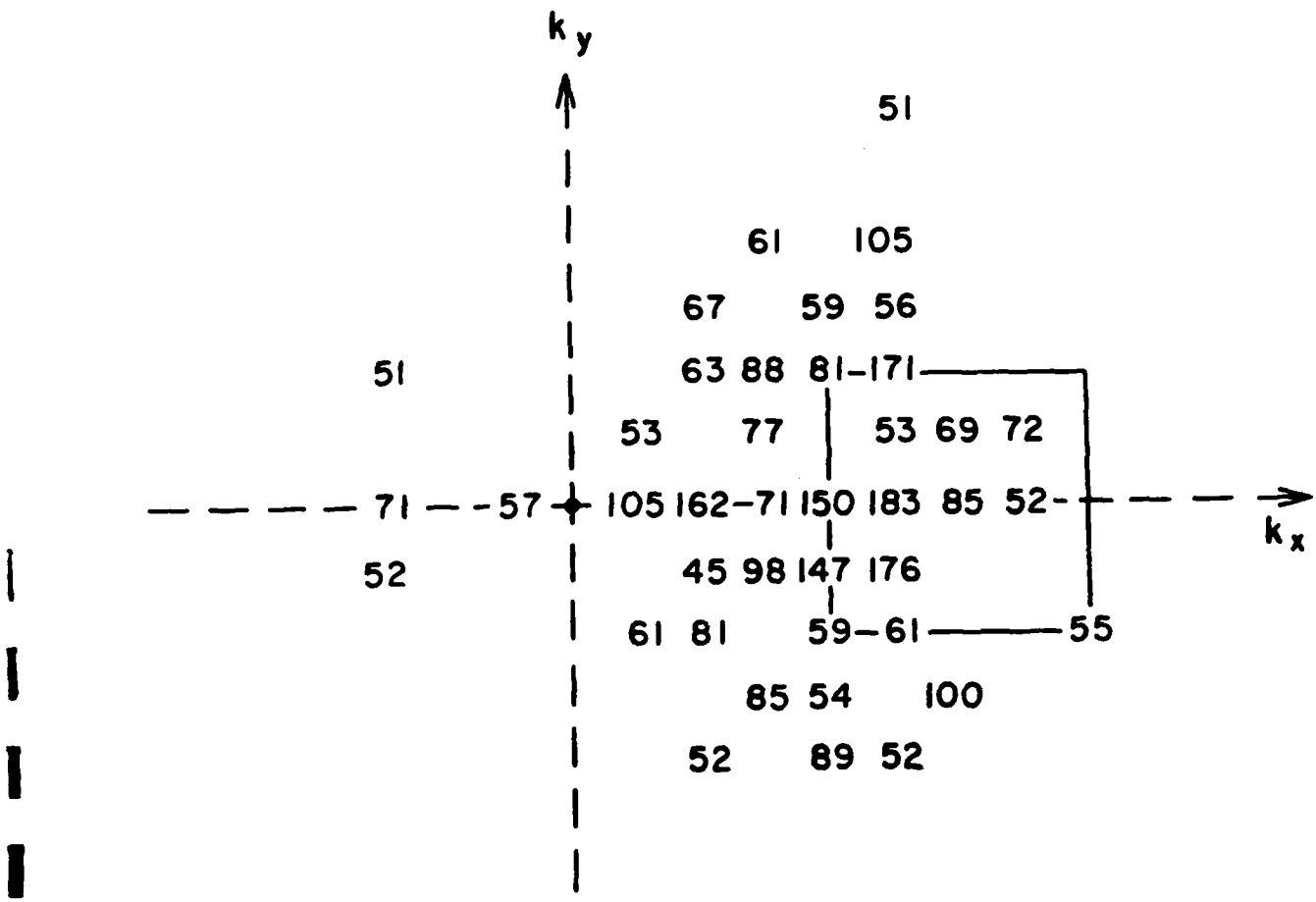
k y
k x
51
61 105
67 59 56
51 63 88 81 171
53 77 53 69 72
71 57 105 162 71 150 183 85 52
52 45 98 147 176
61 81 59 61 55
85 54 100
52 89 52

FIGURE 4

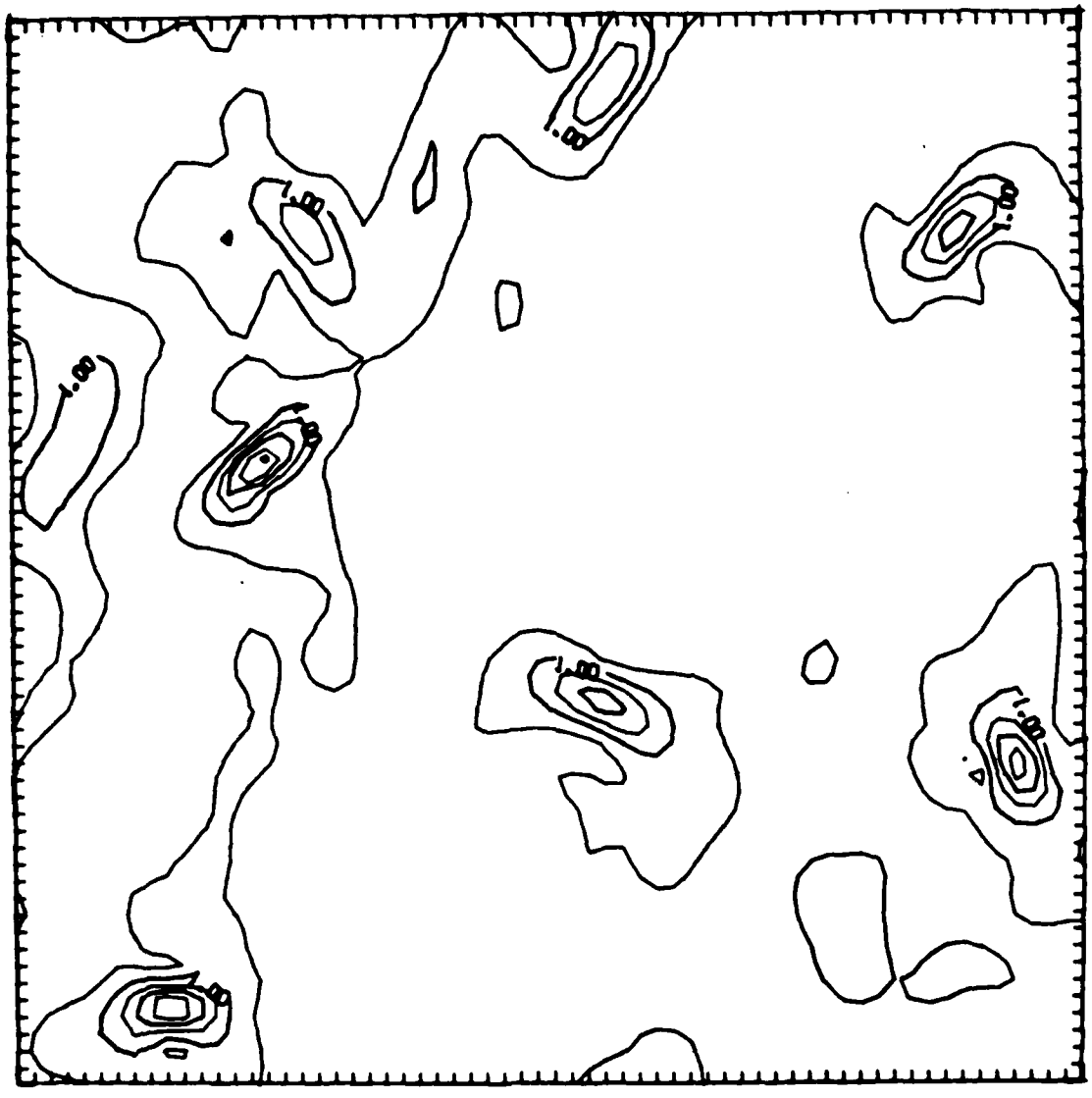

FIGURE 5

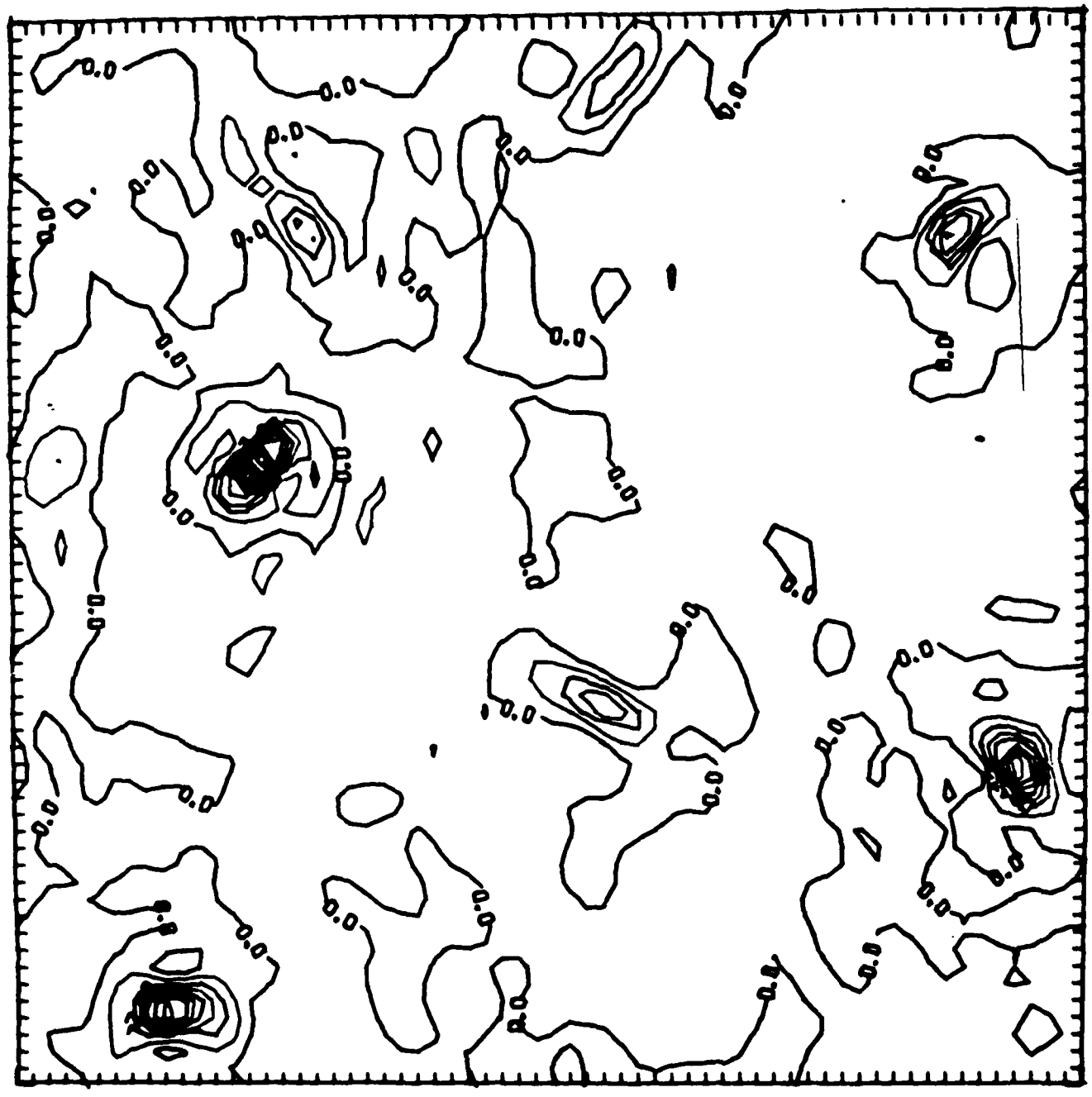

FIGURE 6

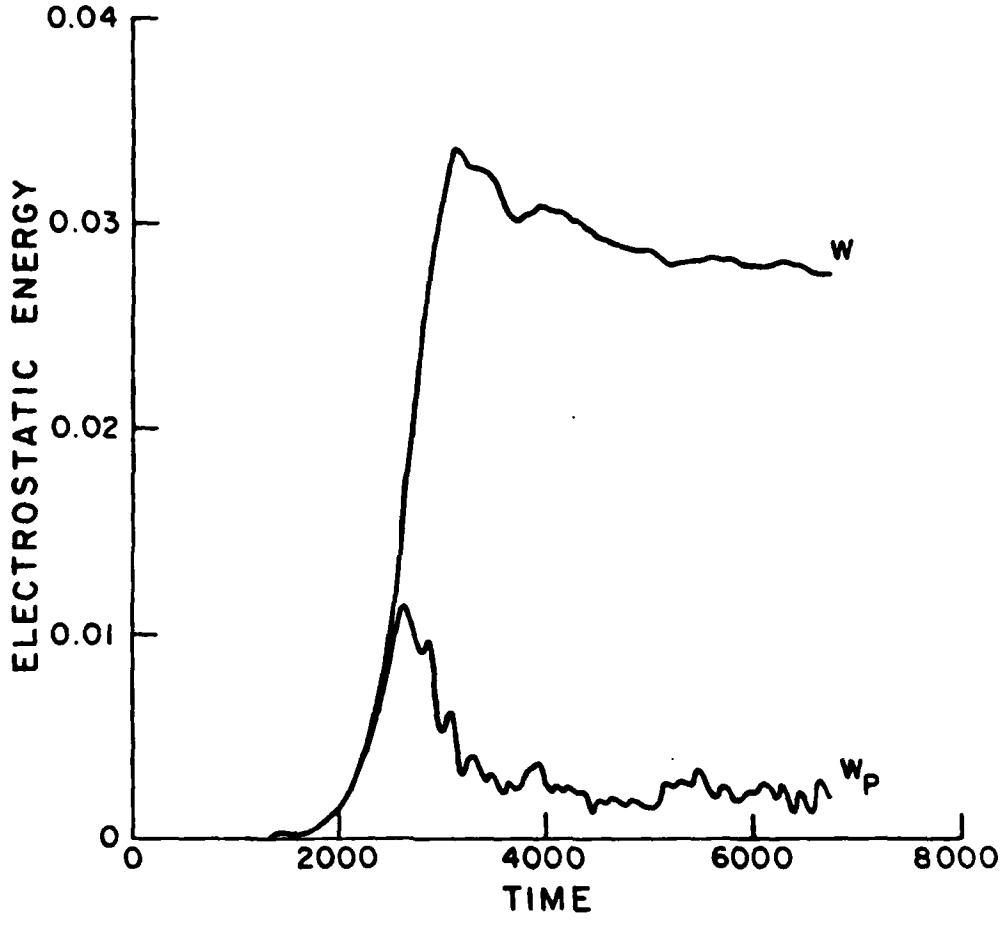
0.04
0.03
0.02
0.01
0
ELECTROSTATIC ENERGY
W
W_P
0
2000
4000
6000
8000
TIME

FIGURE 7a

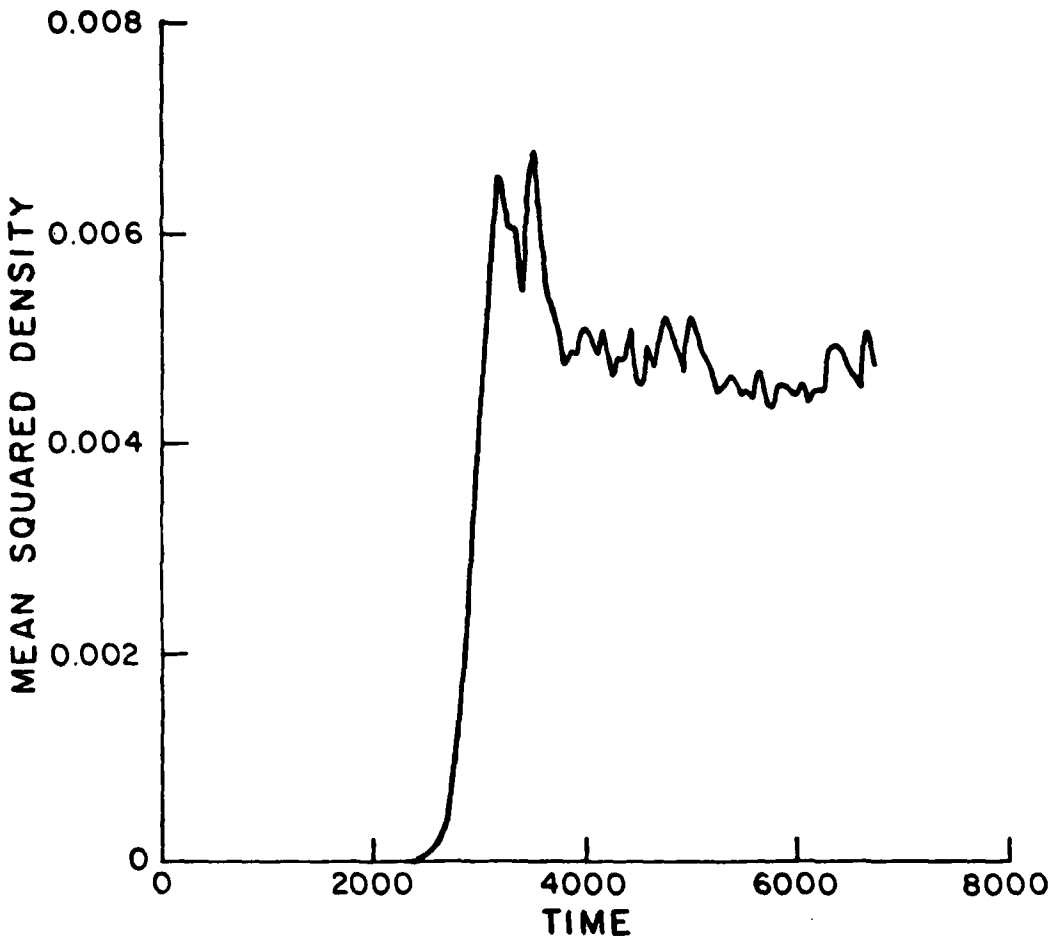
0.008
0.006
0.004
0.002
0
MEAN SQUARED DENSITY
0
2000
4000
6000
8000
TIME

FIGURE 7b

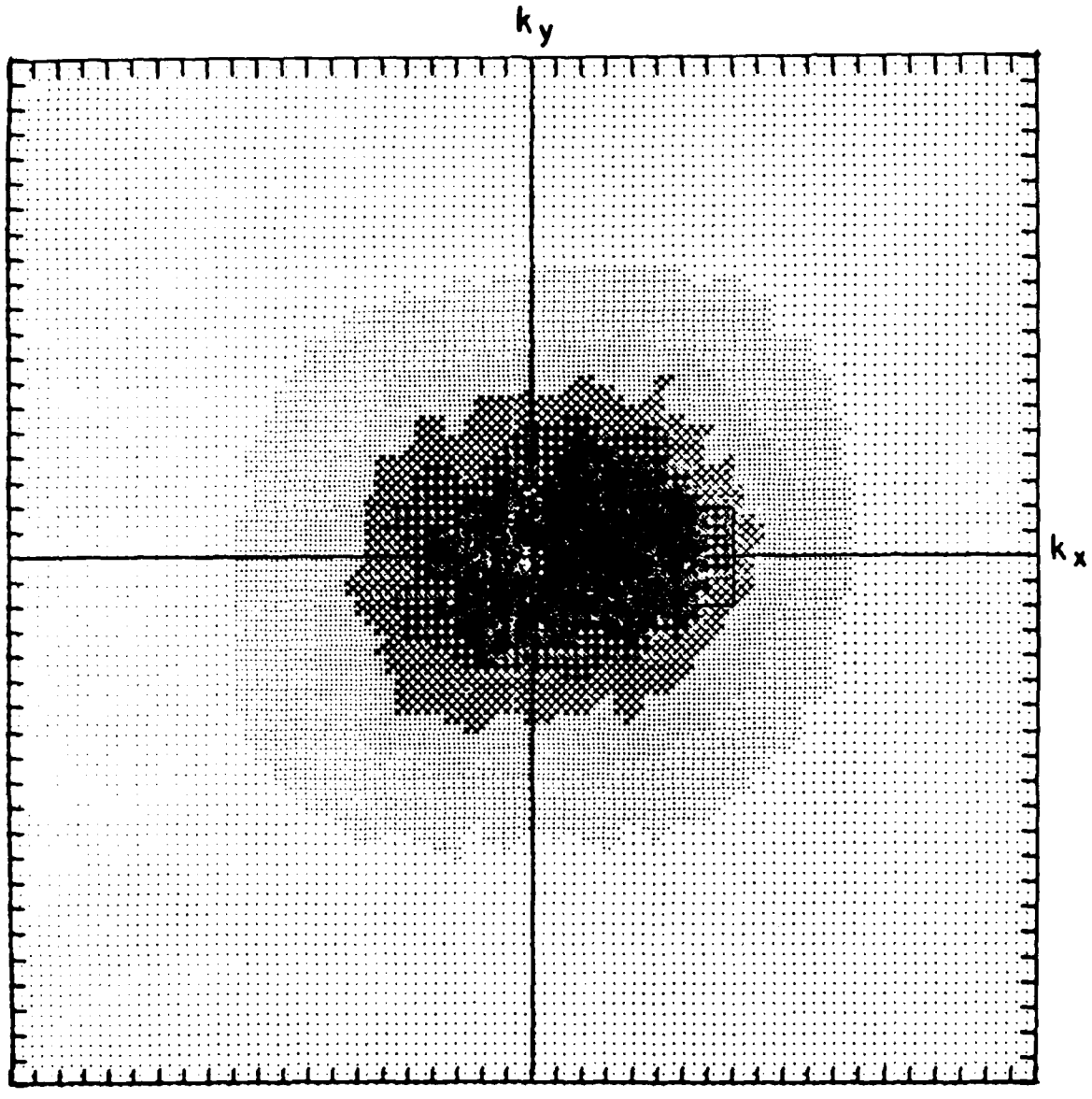

FIGURE 8

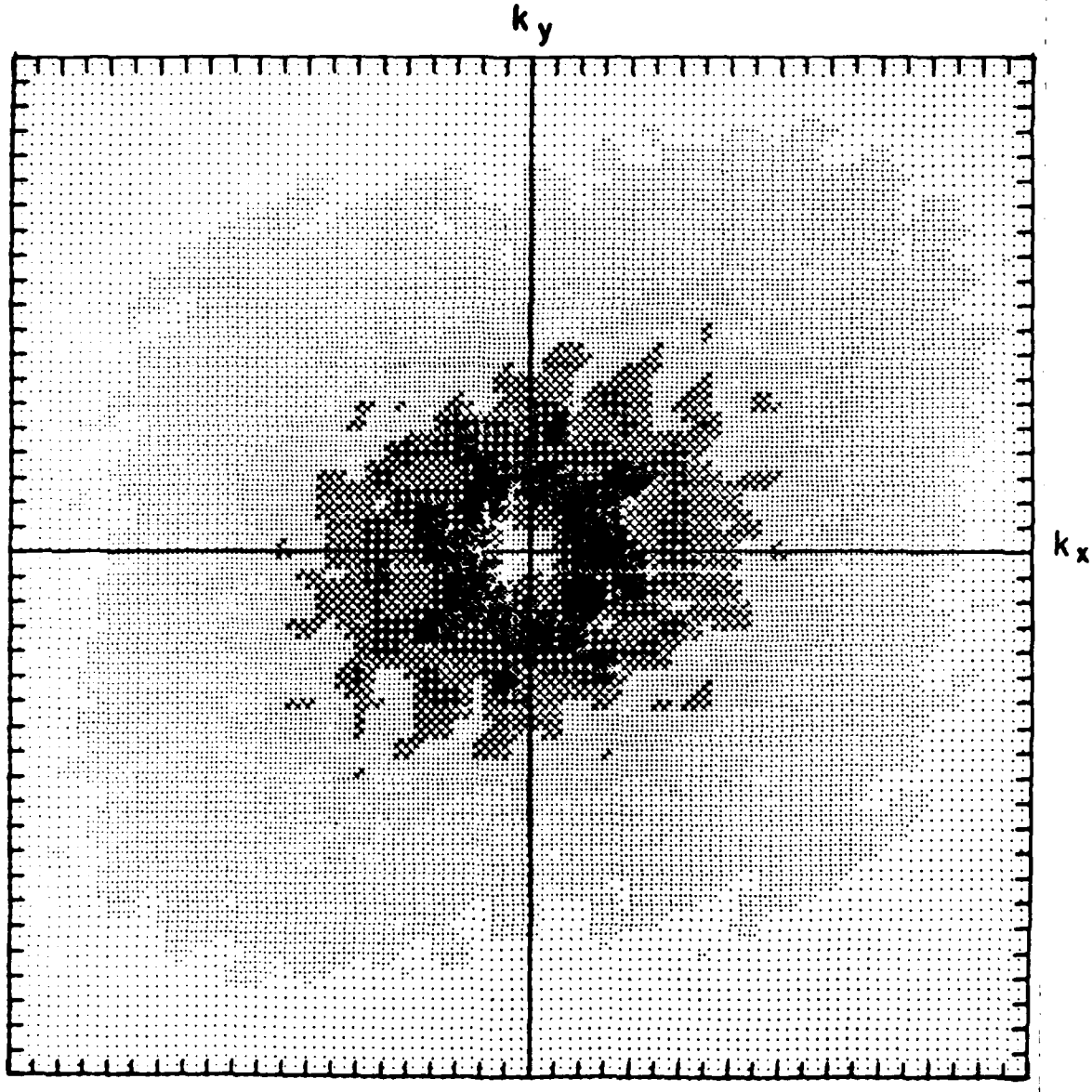

FIGURE 9

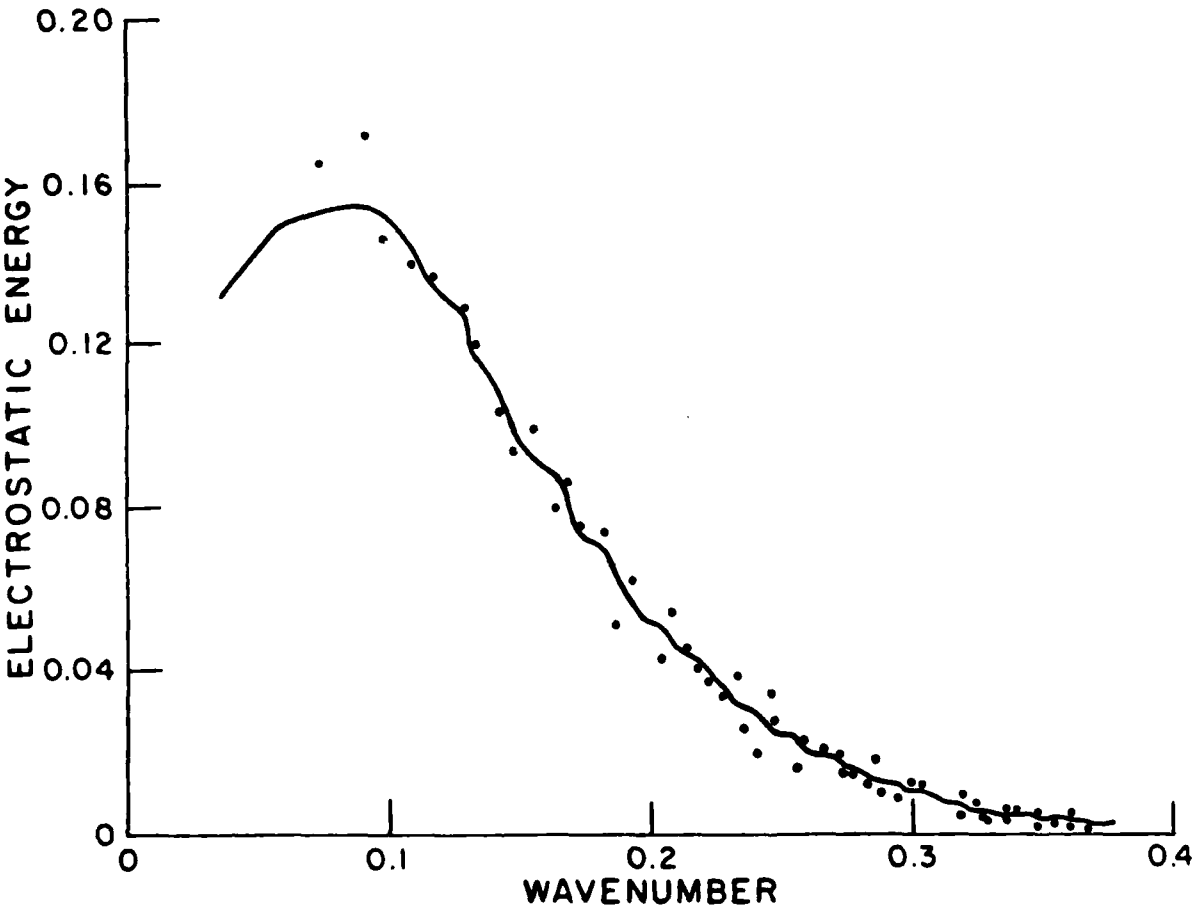
0.20
0.16
0.12
0.08
0.04
0
ELECTROSTATIC ENERGY
0
0.1
0.2
0.3
0.4
WAVENUMBER

FIGURE 10

AD-A129 320 PLASMA WAVE TURBULENCE AND PARTICLE HEATING CAUSED BY ELECTRON BEAMS RADI..(U) COLORADO UNIV AT BOULDER DEPT OF ASTRO-GEOPHYSICS M V GOLDMAN 01 JAN 83 CU-1533201

2/3

UNCLASSIFIED AFOSR-TR-83-0498 AFOSR-80-0022 F/G 20/9 NL

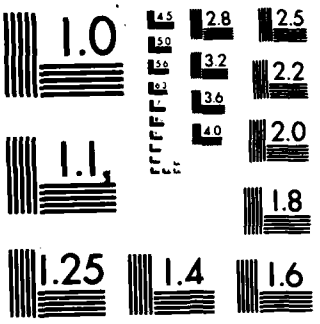

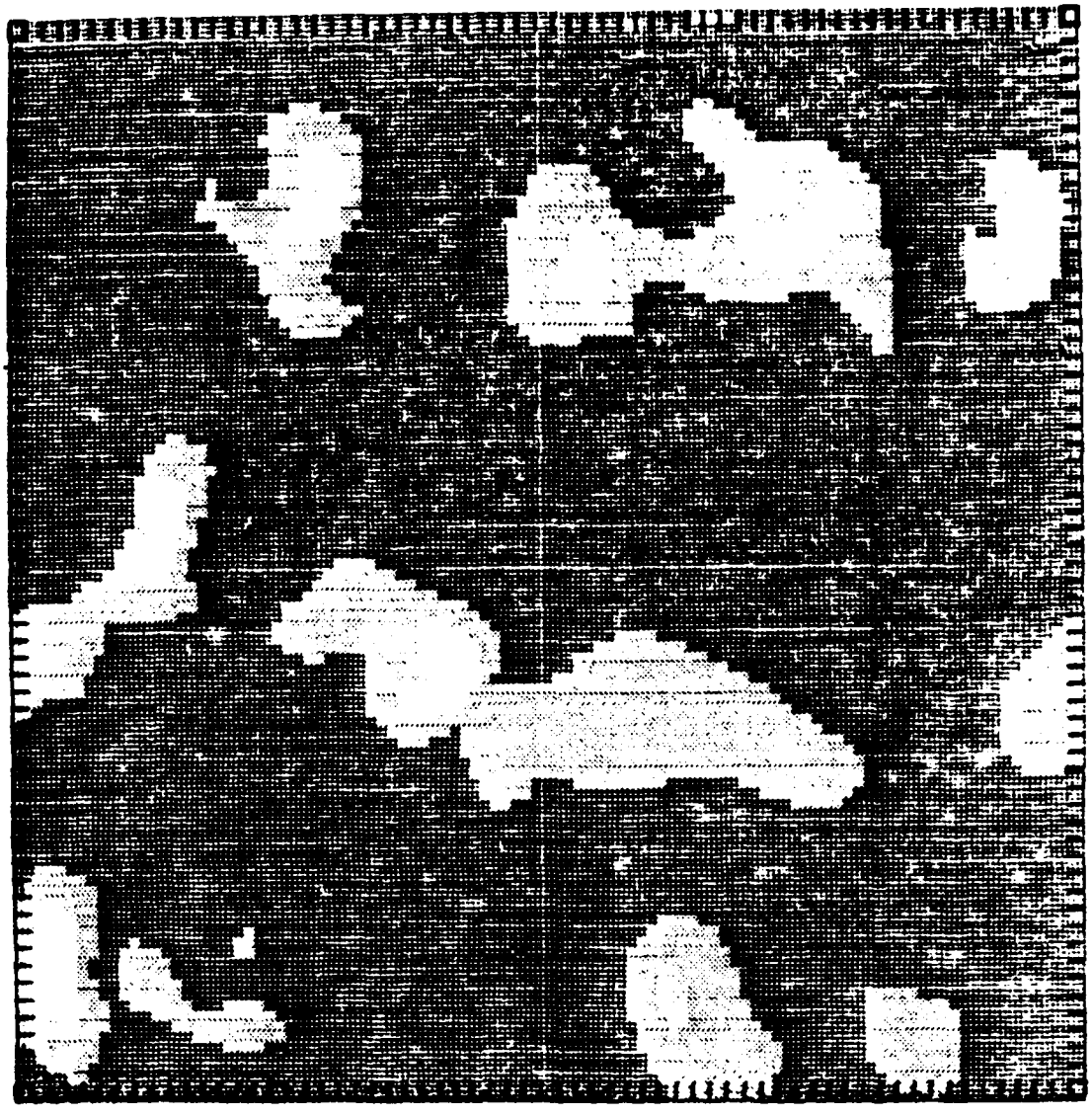

FIGURE 11

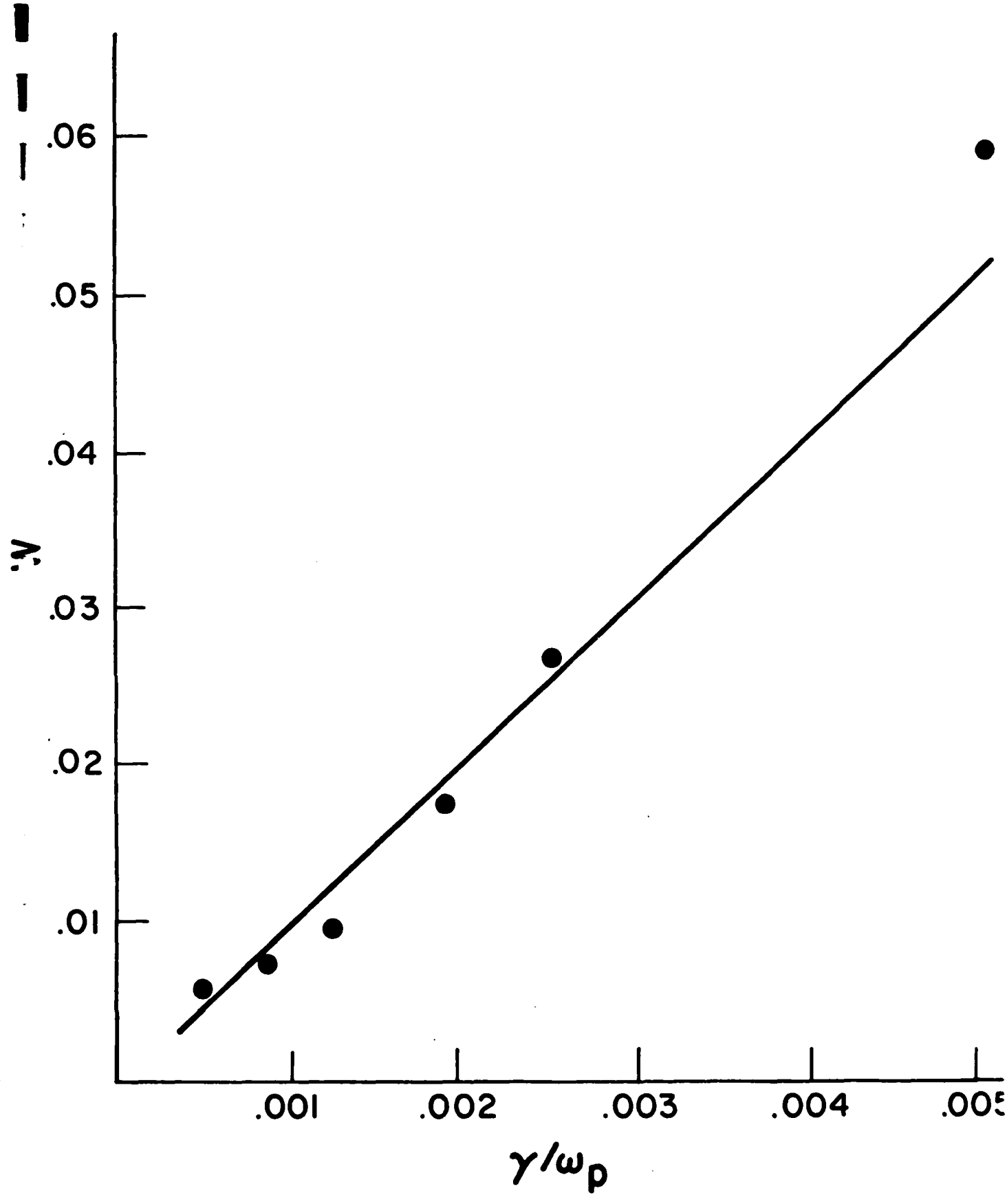

FIGURE 12

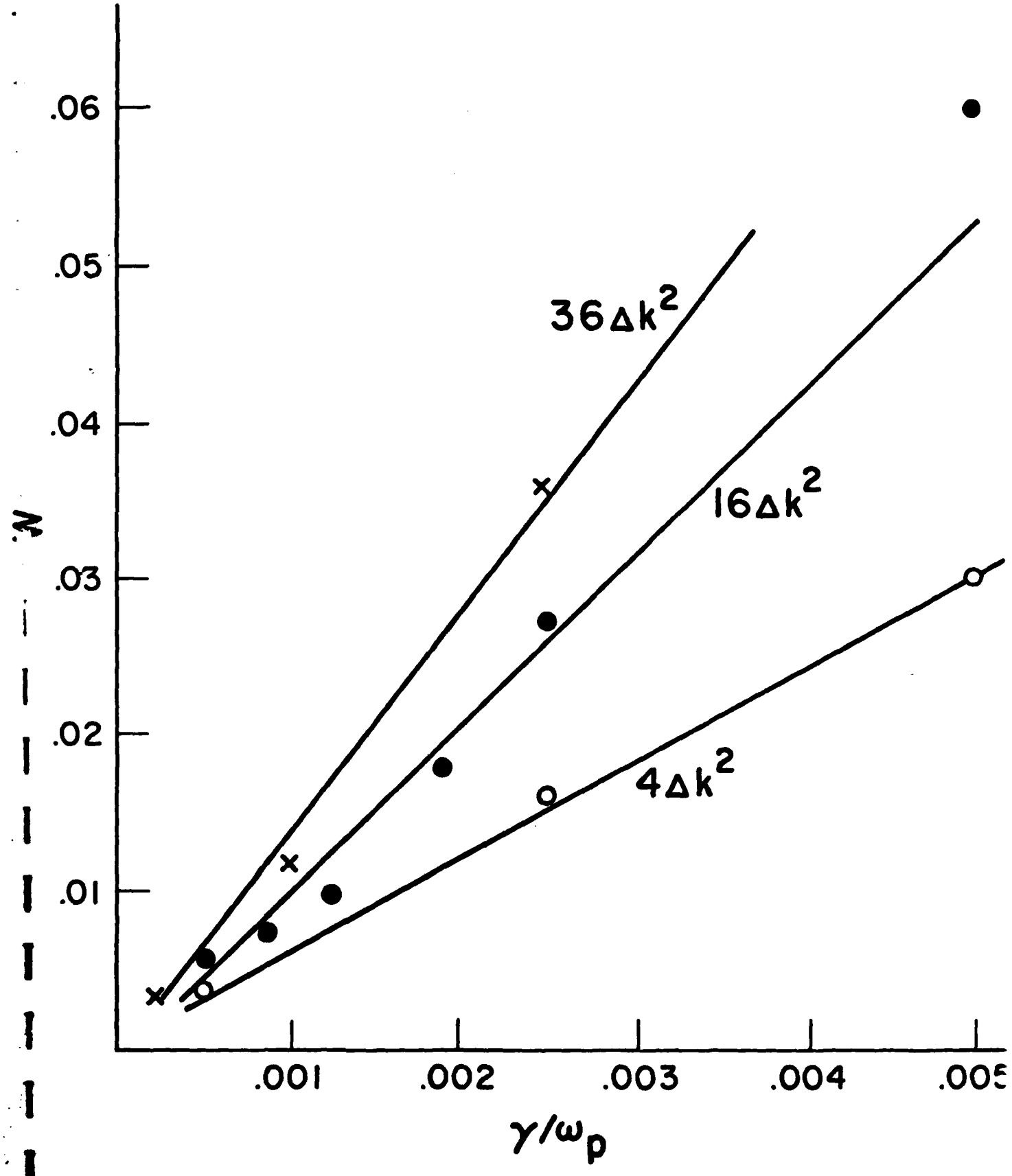

FIGURE 13

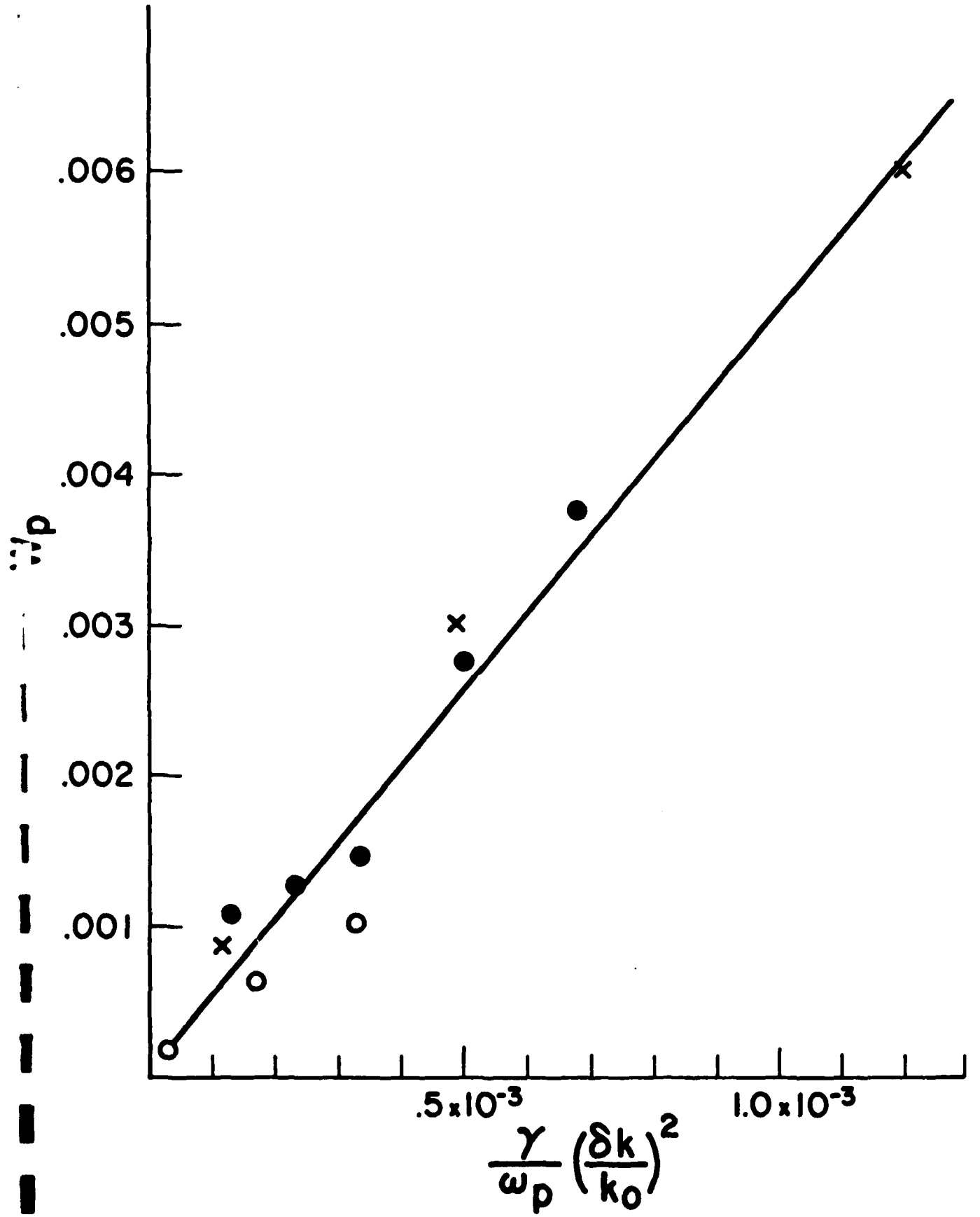
.006
.005
.004
.003
.002
.001
γ/ω_p
$.5 \times 10^{-3}$
1.0×10^{-3}
$\frac{\gamma}{\omega_p}\left(\frac{\delta k}{k_0}\right)^2$

FIGURE 14

APPENDIX C

C. "Backscatter Cascade of Beam-Modes off Ambient Density Fluctuations"

D.A. Russell and M.V. Goldman
Submitted to Physics of Fluids

Backscatter Cascade of Beam-Modes off Ambient Density Fluctuations

David A. Russell and Martin V. Goldman

Department of Astro-Geophysics

University of Colorado, Boulder, Colorado 80309

Abstract

We study the effects of a given non-thermal low-frequency density-fluctuation spectrum on the amplification of Langmuir waves by a "bump-on-tail" beam of electrons. The density-fluctuation spectrum is assumed to contain a uniform distribution of wavelengths ranging from much shorter than the beam mode wavelength to of the same order. This permits multiple large-angle (back) scatters to occur. One dimensional numerical solutions of the kinetic equations are found which yield criteria for linear saturation of the beam instability by a cascade of backscatters to high wavenumber. We also determine the relevant time scales and spectral shapes in both the stable and unstable regions. Linear damping and Cerenkov emission by a possible non-thermal tail of electrons is taken into account.

An application is made to the beam-modes observed simultaneously with density fluctuations off the Jovian bow-shock. It is shown that the observed level of density fluctuations is sufficient to saturate the unstable Langmuir waves, although non-thermal Landau damping may prevent a cascade to very high wavenumbers.

I. Introduction

Wave instabilities in plasmas rarely occur under the idealized background conditions assumed in textbook treatments.

In space plasmas, non-thermal conditions are often observed in both the ambient particle and wave spectra. Solar wind electron streams and the Langmuir waves they excite propagate through this non-thermal environment. Even slight non-thermal background features can greatly alter the linear evolution of the waves, and hence, possible subsequent nonlinear evolution.

In laboratory relativistic beam-plasma systems, return currents may excite low-frequency turbulence such as Buneman or ion-acoustic waves. The plasma waves excited by the relativistic beam may then see these modes as part of the background plasma and be affected or even saturated by the interaction.

In a recent theoretical treatment, Goldman and DuBois[1] studied the general problem of beam-plasma instability in the presence of low-frequency turbulence. Kinetic equations were derived for the evolution of Langmuir waves in the presence of a given stationary spectrum of low-frequency turbulence and a given stationary electron distribution function.

The kinetic equation was solved only for the case of a low-frequency spectrum containing wavelengths much longer than the wavelength of the beam-unstable modes. The Langmuir spectrum then became essentially isotropic due to multiple small-angle-scatter (angular diffusion) off the long-wavelength density-fluctuations. Since Langmuir waves oblique to a

bump-on-tail electron-distribution-function are damped rather than destabilized, a saturated steady state was created.

In the present work, we are concerned with the resonant effects of an ambient low-frequency spectrum of shorter wavelengths. A uniform distribution of wavelengths is assumed, ranging in size from the beam-mode wavelength ($\sim 2\pi v_b/\omega_p$) down to shorter wavelengths. The given spectrum is assumed to consist of ion-acoustic turbulence, and we take it to be one-dimensional and isotropic.

We find that Langmuir waves undergo a series of backscatters off the given spectrum. This cascade to higher wavenumbers continues until sufficient linear dissipation occurs, or until wavenumbers higher than a cut-off determined by the density spectrum cut-off are encountered. In the absence of a significant non-thermal electron tail at velocities below the "bump," the cascade continues up to wavenumbers which are on the order of a Debye wavenumber or half the maximum wavenumber of the density spectrum, whichever is smaller. However, a non-thermal tail on the ambient electron distribution can terminate the cascade at even lower wavenumbers, due to non-thermal Landau damping (with non-thermal Cerenkov emission also taken into account).

We explore numerically the conditions under which saturation of Langmuir-wave growth may occur. However, it is important to note that even when the instability is not saturated by

"linear" scattering off the given density fluctuations, such scattering may affect subsequent nonlinear evolution, since a broadened spectrum is created at the linear stage.

There are a number of subtle and even unexpected results which are elucidated in the present paper. Although it is well-known that nonlinear scatter off density fluctuations produces a cascade towards small k (we shall show why this is so in Section III, by resorting to simple "Golden Rule" arguments), the linear scatter will produce a cascade towards higher k.

A second surprising result has to do with the failure of a conventional estimate as to when the unstable beam-modes are saturated. The usual heuristic argument is to compare the rate of out-scatter to the growth rate. However, just because the out-scatter rate may be larger is no guarantee of saturation. This is because there are also scattering-in terms. In the absence of linear dissipation, there will always be as much in-scatter as there is out-scatter, so that scattering alone can never result in saturation. The estimation of when saturation can occur is therefore a subtle business involving the interplay of scatter and linear dissipation. In this paper we provide numerical criteria for saturation and find the proper time-scales for "net" out-scatter, taking in-scatter and dissipation into account.

One application of these results and one of the motivations for the present study has to do with Langmuir waves driven

by electron beams in the solar wind. There are two principal examples:

1. Beams originating at the sun during flare activity, and propagating out into interplanetary space where they excite Langmuir waves, which subsequently give rise to "Type III" or other radio-wave emission.

2. Beams created by quasi-perpendicular shocks such as planetary bow-shocks. Such beams go out along tangential magnetic field lines, and have been measured in elegant detail near the earth's bow shock. Near the Jovian bow-shock, the excited Langmuir waves have been studied by the Voyager 1 spacecraft, and observed to coexist with ambient low-frequency turbulence and apparently to cascade to higher wavenumbers.

We shall apply some of our numerical results to these problems, since the magnitude and shape of the density fluctuation spectrum, the shape of the electron distribution and beam, and the intensity of the Langmuir wave spectra are known in great detail in these examples. Our object will be to define thresholds for linear saturation and time-scales for cascade and to compare with experiment. We conclude that Langmuir waves are often observed at sufficiently low levels ($|\mathcal{E}|^2/4\pi n\Theta_e \ll 10^{-5}$) that density fluctuations as small as $\delta n/n \gtrsim 10^{-4}$ could have been responsible for their saturation. For more intense Langmuir waves, the saturation is probably nonlinear, but density fluctuations may still play a role in the early shaping of the spectrum.

The plan of this paper is as follows: In Section II, we summarize the results of space-craft measurements on electron-distribution functions, beam-excited Langmuir waves and associated low-frequency turbulence. The reader more interested in the general results of our calculations than in the phenomenology of the solar wind, may wish to skip Section II.

In Section III we write down the basic equations to be solved, and give a heuristic Golden Rule derivation which enables us to understand why the cascade goes to high k, and what are the conditions for neglect of nonlinear terms in the scatter. We also introduce our model of the density fluctuation spectrum and the electron velocity distribution.

In Section IV we study the solutions of the kinetic equations and describe the threshold that separates saturated from unbounded behavior in terms of the density fluctuations and the electron distribuition. Concluding remarks appear in Section V.

II. Review of Measurements of Beam-Excited Langmuir Waves and Simultaneous Low-Frequency Turbulence in the Solar Wind

A. Beam-waves near planetary bow-shocks

We begin with a concise summary of the Voyager 1 measurements in the vicinity of the Jovian bow shock.[2] Fig. 1 shows Langmuir waves excited by a beam of energy ∿10 keV. The waves are measured as the spacecraft moves towards the bow shock. The Langmuir waves are first observed when the spacecraft crosses the beam boundary, defined by a magnetic field line tangent to the bow shock. The beam electrons are carried out from the bow shock along this field line, so the beam propagates roughly orthogonal to the spacecraft and solar wind velocities. However, Langmuir wave packets receiving energy from the beam are convected by the solar wind towards the bow shock. Growth begins as the waves are swept into the beam region. The waves saturate and subsequently disappear when the bow shock is crossed. Since waves are continually swept in and out of the beam region we assume a steady-state spatially amplified and saturated spectrum of waves in the laboratory frame.

The spacecraft moves through this spatial region where measurements yield the time history shown in Fig. 1. Neglecting the wave-packet group velocity in comparison with the solar wind speed v_{sw}, a time interval Δt in the solar wind frame is related to a laboratory-frame spatial interval, Δx_{lf}, by $\Delta x_{lf} = v_{sw}\Delta t$. Assuming the Voyager spacecraft moves with a

laboratory frame velocity, v_V, essentially parallel to the solar wind, a time-interval, Δt_V, measured from the Voyager is related to Δt by

$$\Delta t_V = \frac{\Delta x_{lf}}{v_V} = \frac{v_{sw}}{v_V} \Delta t$$

In Fig. 1, we see that the total time of observation of Langmuir waves is $\Delta t_V^{obs} \approx 8$ minutes and that the initial rapid growth interval is $\Delta t_V^{gr} \approx 2$ minutes. Since $v_V \approx 17$ km/sec, and $v_{sw} \approx 400$ km/sec, we find

$$\Delta t_V^{gr} \approx 6 \text{ secs}$$

$$\Delta t_V^{obs} \approx 20 \text{ secs}$$

These times will be useful for purposes of comparison with the results of Section IV.

At the time marked A in Fig. 1, the observed Langmuir frequency spectrum (not shown) is very narrow (less than 1%), while at times marked B and C it has progressively broadened to around 10% of the plasma frequency. If this broadening is attributed to a cascade to higher wavenumbers, then this corresponds to a maximum Langmuir wavenumber of $k\lambda_D \approx 0.18$, where λ_D is the Debye length (about 18 meters).

A typical electric field strength from Fig. 1 is E = 100 μV/m. The mean background density and temperatures are n = 0.45 cm^{-3} and T = 3×10^4°K, so the usual dimensionless measure of the Langmuir wave energy density is quite low (i.e., linear, rather than nonlinear)

$$W \equiv \frac{E^2}{4\pi n k_B T} \approx 5 \times 10^{-7}$$

In Fig. 2, we see low-frequency waves, interpreted as ambient ion-acoustic wave turbulence, measured onboard the Voyager simultaneously with the beam-excited Langmuir waves. The low-frequency spectrum extends to around 500 Hz. Since $v_{sw} >> c_s$, (c_s = the ion-acoustic speed), the low-frequency dispersion relation is essentially $\omega = \underline{q} \cdot \underline{v}_{sw}$. At 500 Hz, an ion-acoustic wave propagating parallel to the solar wind would have $q\lambda_D = 0.14$. (The lower frequency part of the spectrum would give smaller values of $q\lambda_D$.) Ion-acoustic waves propagating parallel to the electron beam with wave number q_b would be at an angle near 90° to the solar wind so

$$q_b \lambda_D >> 0.14$$

Once again, the lower frequency part of the spectrum would give smaller values of $q\lambda_D$.

The integrated broadband electric field strength of the ion-acoustic fluctuation is found to be $E_{i.a.} \approx 10$ μV/m. This corresponds to a density fluctuation relative to the background density of

$$\frac{\delta n}{n} = \frac{eE_{ia}}{k_B T q} = \frac{7 \times 10^{-5}}{q\lambda_D}$$

Hence, with $q\lambda_D = 0.14$, we find

$$\frac{\delta n}{n} = 5 \times 10^{-4}.$$

Gurnett et al.[2] argue for a smaller value of $q\lambda_D$, based on a peak in the ion-acoustic spectrum at 100 Hz rather than 500 Hz, whereas we may argue for a larger value associated with q_b. Since the two effects oppose each other, it is not unreasonable to consider $\frac{\delta n}{n} = 5 \times 10^{-4}$ as a typical strength for the nonthermal low-frequency density fluctuations.

Finally, we remark that Gurnett et al. were the first to make the explicit suggestion that the observed broadening of the Langmuir spectrum may be due to multiple backscatter from the ambient non-thermal density fluctuations. One of the purposes of the present paper is to explore quantitatively the feasibility of this mechanism.

B. Nonthermal electron distributions

One may view the scattering of Langmuir waves off density fluctuations as a mechanism for shifting Langmuir energy density around in k-space. Of crucial importance are those shifts which take energy from a region where a (stationary) background beam can drive the waves unstable to a region where the background electrons can Landau damp the waves. Hence, the non-thermal distribution of electrons in the vicinity of the beam should be taken into account, so that the magnitude of the (non-thermal) Landau damping can be found and incorporated in the kinetic equations. Generally, in the solar wind, the electron distribution beyond a few hundred eV is highly non-thermal, and the associated Landau damping is much stronger for a Maxwellian

plasma at the (several-eV) temperature associated with the bulk of the electrons. (As we shall see, Cerenkov emission from the tail also needs to be taken into account.) Figure 3 shows a typical non-thermal distribution of high energy electrons in the solar wind. It is taken from ISEE-1 measurements in the vicinity of the earth's bow-shock.[3] Note the bump-on-tail at $v \approx -v_b = 21 \times 10^3$ km/sec, corresponding to a beam of energy $\sim$1 eV. Note also, the highly isotropic non-thermal tail at lower velocities. It is this region which is explored by Langmuir waves scattered to progressively higher k, since such waves have lower phase velocities. Numerical models of Landau damping based on Fig. 3 are incorporated into some of our solutions to the kinetic equations in Section IV. We also remark that such velocity distributions are common in interplanetary space remote from bow shocks. For example, Lin et al.[4] have consistently found such non-thermal tails in the solar wind both before and after the passage of streams of solar electrons associated with Type III solar radio wave emission. The temperature of the tail is typically from 10 to 1000 times that of the background plasma temperature.

C. Type III emissions

Langmuir waves have often been found in the solar wind in association with Type III solar radio-wave emission, and are thought to be associated with such emissions. The largest energy density ever found was on the order of

$$W_{max} = \frac{E^2}{4\pi n k_B T} \approx 4 \times 10^{-5}$$

whereas values two or more orders of magnitude smaller are much more common. Typical electron beams have energies like 25 keV, which correspond to $k\lambda_D \approx 10^{-2}$ for beam-resonant Langmuir waves. Hafizi et al.[5] and others have explored the nonlinear saturation of such waves.

Here, we remark that ion-acoustic waves are often independently excited in the solar wind, probably driven by heat flux instabilities.[6] Lower frequency density fluctuations are also observed. At the lowest observable frequencies ($\sim$100 Hz) the (Doppler-shift determined) wavenumbers of the ambient density fluctuations are at roughly the same wavenumber as the Langmuir waves. Typical intensities are $\delta n/n \approx 10^{-4}$. Hence, it is of interest to consider the possibility that the beam-driven Langmuir waves are saturated by large-angle scatter off ambient density fluctuations, particularly in the presence of the non-thermal electron-distribution-function tails commonly found in the solar wind. In Section IV we shall consider some examples of when this may be possible.

III. Kinetic Equations

A. General considerations

The kinetic equations which govern the evolution of Langmuir waves in the presence of a given stationary spectrum of ion-acoustic waves are well-known. A rigorous derivation has been given recently.[1] Since we are concerned here only with resonant three-wave interactions, we first present a short heuristic quantum-mechanical "derivation" based on "Golden Rule" arguments. This has the advantage of including nonlinear as well as linear scatter, so one condition for a completely "linear" derivation can easily be defined and the differences between the linear and certain nonlinear terms clearly understood.

We shall employ occupation numbers n^L and n^i to describe the "intensity" of the Langmuir waves and background ion-acoustic waves. They are defined as follows

$$\hbar\omega_{\underline{k}} n^L_{\underline{k}} = \langle|E^L_{\underline{k}}|^2\rangle/4\pi V \qquad (1a)$$

$$\hbar\Omega_{\underline{q}} n^i_{\underline{q}} = \langle|E^i_{\underline{q}}|^2\rangle/4\pi\lambda_D^2 q^2 V = nk_B T\langle|\delta n_{\underline{q}}|^2\rangle/n^2 V \qquad (1b)$$

Here,

$$\omega_{\underline{k}} = (\omega_p^2 + 3v_e^2 k^2)^{\frac{1}{2}}, \text{ and}$$

$$\Omega_{\underline{q}} = c_s q$$

are, respectively, the Langmuir and ion-acoustic frequencies, and $\langle|E^L_{\underline{k}}|^2\rangle/V$ and $\langle|E^i_{\underline{q}}|^2\rangle/V$ are the (ensemble average) spectral

functions of electric field fluctuations for the two kinds of waves (V is the "box volume," assumed to tend to infinity). The right sides of Eqs. (1) represent the spectral energy densities for the two kinds of waves. The spectrum of density fluctuations $<|\delta n_q|^2>/n_o^2 V$ has the integral

$$(\delta n/n_o)^2 = \int \frac{d^3q}{(2\pi)^3} \frac{<|\delta n_q|^2>}{n_o^2 V} \qquad (2)$$

A (position-independent) ensemble avarage is understood on the left. This result will be useful, since we shall often use $\delta n/n_o$ as a measure of the strength of the density fluctuations. Planck's constant, $\hbar$, in Eqs. (1) will play no role in any of our calculations.

The Feynman diagrams for the processes we study in this paper are shown in Fig. 4. The corresponding equation for the time rate of change of the occupation number $n^L_{\underline{k}}$ is

$$\partial_t n^L_{\underline{k}} =$$

$$- \int \frac{d^3q}{(2\pi)^2} |M|^2 \Big\{ \delta(\omega_{\underline{k}} - \omega_{\underline{k}_s} - \Omega_{\underline{q}}) \left[n^L_{\underline{k}}(n^L_{\underline{k}_s}+1)(n^i_{\underline{q}}+1) - (n^L_{\underline{k}}+1) n^L_{\underline{k}_s} n^i_{\underline{q}} \right]$$

$$+ \delta(\omega_{\underline{k}} - \omega_{\underline{k}_s} + \Omega_{\underline{q}}) \left[n^L_{\underline{k}}(n^L_{\underline{k}_s}+1) n^i_{\underline{q}} - (n^L_{\underline{k}}+1) n^L_{\underline{k}_s} (n^i_{\underline{q}}+1) \right] \Big\}$$

$$\underline{k}_s \equiv \underline{k} - \underline{q} \qquad (3)$$

The quantity $|M|^2$ is a matrix element squared. Its value will be written down later, in another form of the equation. The

integral over $\underline{q}$ represents a sum over final states. Momentum is conserved, because $\underline{k}_s \equiv \underline{k}-\underline{q}$. The delta functions are expressions of energy conservation for the two processes and their inverses ($\hbar$=1). In the first process an ion-acoustic wave is emitted (absorbed in the inverse process), while in the second process, an ion-acoustic wave is absorbed (emitted in the inverse process). The factors involving $n^L_{\underline{k}}$, $n^L_{\underline{k}_s}$ and $n^i_{\underline{q}}$ represent bose statistics. A factor $n^L_{\underline{k}}$ is inserted for an absorption, $(n^L_{\underline{k}}+1)$ for an emission, etc. Note the sign change for the inverse processes, in which a plasma wave at $\underline{k}$ is emitted, rather than absorbed. We have assumed an isotropic ion-acoustic spectrum (otherwise the $n^i_{\underline{q}}$, factors in the second square bracket are different from those in the first square bracket).

We combine terms and rewrite Eq. (3) as

$$\partial_t n^L_{\underline{k}} = -2(\gamma^{eff}_{\underline{k}}+\gamma^{n\ell}_{\underline{k}})n^L_{\underline{k}} + s^{eff}_{\underline{k}}, \tag{4}$$

where we have taken the semi-classical limit $n^L_{\underline{k}} >> 1$, and where

$$2\gamma^{eff}_{\underline{k}} \equiv \int \frac{d^3q}{(2\pi)^2} |M|^2 \left\{ \delta(R_-) + \delta(R_+) \right\} n^i_{\underline{q}} \tag{5a}$$

$$2\gamma^{n\ell}_{\underline{k}} \equiv \int \frac{d^3q}{(2\pi)^2} |M|^2 \left\{ \delta(R_-) - (R_+) \right\} n^L_{\underline{k}_s} \tag{5b}$$

$$s_{\underline{k}}^{eff} \equiv \int \frac{d^3q}{(2\pi)^2} |M|^2 \left\{ \delta(R_-) + \delta(R_+) \right\} n_{\underline{q}}^i n_{\underline{k}_s}^L \qquad (5c)$$

$$R_{\pm} \equiv \omega_{\underline{k}} - \omega_{\underline{k}_s} \pm \Omega_{\underline{q}} \qquad (5d)$$

These terms have the following physical interpretations. The effective "linear" out-scatter rate is given by $\gamma_{\underline{k}}^{eff}$. The effective in-scatter rate is given by $s_{\underline{k}}^{eff}$. The quantity $\gamma_{\underline{k}}^{n\ell}$ contains nonlinear (stimulated) out-scatter which we ignore in this paper. The term $-2\gamma_{\underline{k}}^{n\ell} n_{\underline{k}}^L$ is nonlinear because it is second-order in $n_{\underline{k}}^L$, the Langmuir wave occupation number ($\propto$ energy density). The other terms are all linear, but proportional to the ambient density fluctuation spectrum through $n_{\underline{q}}^i$.

We note that the nonlinear terms have been treated by many authors.[5] They give rise to a weak-turbulence cascade to lower wavenumbers because of the minus sign in Eq. (5b). To see why this is so, consider a one-dimensional problem. Then $R_- = 0$ implies $k_s \equiv k^- < k$ (the so-called Stokes process) and $R_+ = 0$ implies $k_s \equiv k^+ > k$ (the so-called anti-Stokes process). In order to get stabilization of an instability, we must have $\gamma_{\underline{k}}^{n\ell} > 0$. Hence, $n^L(k^-) > n^L(k^+)$ which explains why the spectrum must increase towards smaller wavenumbers.

In the linear term, $\gamma_{\underline{k}}^{eff}$ the two delta functions have the same sign, so there is no reason for the spectra only to cascade down. (This may be viewed as a simple consequence of the rules for Bose statistics.)

Even in the absence of any significant non-thermal density fluctuations (limit $n_{\underline{q}}^i$ small), the nonlinear term, $\gamma_{\underline{k}}^{n\ell}$ makes

a contribution. It represents scatter off the thermal level of ion-acoustic waves (the 1 in $n^i_{\underline{q}} + 1$). Nonlinear kinetic equation treatments usually neglect the terms proportional to $n^i_{\underline{q}}$. Our calcuation is complementary to these because it is linear, but does include scatter off a non-thermal level of density fluctuations (terms $\gamma^{eff}_{\underline{k}}$ and $s^{eff}_{\underline{k}}$ only).

It is easy to establish a necessary condition for the neglect of the nonlinear (stimulated out-scatter) term in Eq. (4). Comparing $2\gamma^{n\ell}_{\underline{k}}$ with $s^{eff}_{\underline{k}}$, we arrive at the requirement $n^L_{\underline{k}} << n^i_{\underline{k}}$, or, using eqn (1),

$$<|E^L_{\underline{k}}|^2>/(V4\pi n_o k_B T) << <|\delta n_{\underline{k}}|^2>\omega_p/(n_o^2 \Omega_{\underline{k}} V) \qquad (6a)$$

For ion-acoustic waves, $\omega_p/\Omega_{\underline{k}} \approx (M/m)^{\frac{1}{2}}/(k\lambda_D)$. In the problems that we consider, $k\lambda_D \approx 0.1$, and the normalized density fluctuations are $0(10^{-4})$. The RHS of (6a) is therefore of order 10^{-5}. For all of the stationary Langmuir spectra ($\partial_t n^L_{\underline{k}} \to 0$) that we have found numerically, the left hand side of (6a) is bounded above by 10^{-6}, thus justifying our neglect of this nonlinearity. (For unbounded behavior, the Langmuir wave energy diverges with increasing time so that (6a) is eventually violated.)

A nonlinearity not included in the rate equation (4) is due to the self-consistent evolution of δn in response to the ponderomotive force of the envelope electric field. This effect introduces a term in Eq. (4) that is also quadratic in $n^L_{\underline{k}}$ and includes the modulational instability (or self-focusing) of Langmuir solitary waves. This nonlinearity may

be ignored provided the threshold for modulational instability (collapse in 2 or more dimensions) is not exceeded:[5]

$$<|E^L_{\underline{k}}|^2>_{\Delta k}/(4\pi n k_B T) << 24(\Delta k)^2/k_D^2 \qquad (6b)$$

Here Δk is the width of a typical Langmuir wave packet and $<...>_{\Delta k}$ denotes an average over that packet. All of the Langmuir spectra that we study consist of pronounced spikes in k-space of various widths. In all cases observed, the RHS of (6b) is bounded below by 10^{-4}. For cases in which the spectrum reaches a stationary state ($\partial_t n^L_{\underline{k}} \to 0$), the LHS of (6b) is bounded above by 10^{-6}; so our neglect of this "ponderomotive" nonlinearity is also justified. (Again, for unbounded behavior (6b) is eventually violated, but perhaps not during times of interest in the solar wind problems addressed here. See Sec. IV C.)

Next, we write down the form of the kinetic equations to be solved in this paper. This amounts to working in terms of the spectral functions on the right side of Eqs. (1) rather than occupation numbers, and to explicitly writing down the matrix element for the interaction. A derivation based on the first Zakharov equation can be found in Ref. 1.

We shall also add in $\gamma_{\underline{k}}$ and $S_{\underline{k}}$ terms arising from the coupling to a passive background electron distribution function. The $\gamma_{\underline{k}}$ terms will include the bump-on-tail instability and the non-thermal Landau damping at higher k-values (lower phase velocities), and the $S_{\underline{k}}$ terms will include Cerenkov emission. Hence, even without the beam or density fluctuations, a steady-state non-thermal detailed balance is possible.

We now begin a convention which introduces dimensionless variables and relates them to dimensional variables (henceforth indicated with a "~") as follows:

$$t \rightarrow \tilde{t}\omega_p$$

$$\underline{r} \rightarrow (\tilde{\underline{r}}/\lambda_D)(2/3)^{\frac{1}{2}}$$

$$\delta n \rightarrow \delta\tilde{n}/2n_o$$

The kinetic equation will be expressed in terms of the Langmuir envelope field correlation function $\tilde{F}(\underline{k},t)$, defined by

$$\tilde{F}(\underline{k},t) = \frac{1}{V} \; <|\tilde{\mathcal{E}}_{\underline{k}}(t)|^2>,$$

where the complex envelope field $\tilde{\mathcal{E}}_{\underline{k}}$ is related to the total Langmuir electric field by

$$\tilde{\underline{E}}^L_{\underline{k}} = \tfrac{1}{2}\tilde{\mathcal{E}}_{\underline{k}} e^{-i\omega_p t} + \text{c.c.}$$

The kinetic equation is given by

$$\left(\partial_t + 2\gamma(\underline{k}) + 2\gamma^{\text{eff}}(\underline{k})\right)\tilde{F}(\underline{k},t) = \tilde{S}^{\text{eff}}(\underline{k},t) + \tilde{S}(\underline{k}) \quad (7a)$$

where the terms involving scatter off low-frequency density fluctuations are:

$$\gamma^{\text{eff}}(\underline{k}) \equiv \frac{\pi}{2}\int \frac{d^3q}{(2\pi)^3} C_q \mu_-^2 \left[\delta(R_+) + \delta(R_-)\right] \quad (7b)$$

$$\tilde{S}^{\text{eff}}(\underline{k}) \equiv \frac{\pi}{2}\int \frac{d^3q}{(2\pi)^3} C_q \mu_-^2 \left[\delta(R_+) + \delta(R_-)\right] \tilde{F}(\underline{k}-\underline{q},t) \quad (7c)$$

$$\mu_-^2 \equiv (\underline{k}\cdot(\underline{k}-\underline{q})/k|\underline{k}-\underline{q}|)^2 \quad (7d)$$

$$R_{\pm} \equiv |\underline{k}-\underline{q}|^2 - k^2 \pm c_s|\underline{q}|, \qquad c_s \equiv (2m/3M)^{\frac{1}{2}} \tag{7e}$$

$$C_{\underline{q}} \equiv \frac{1}{V} <|\delta n_{\underline{q}}|^2> \tag{7f}$$

The correlation function $C_{\underline{q}}$ describes the given external density fluctuations. Note that $R_{\pm}$ are now dimensionless and the expanded Langmuir dispersion relation has been employed.

The stationary linear damping (or growth), $\gamma(\underline{k})$, is related to a given electron distribution function, $f_e(\underline{v})$ by,

$$\gamma(\underline{k}) \equiv \frac{-\pi}{2n_o}\frac{\omega_p^2}{\tilde{k}^2}\int d^3\tilde{v}\,\underline{\tilde{k}}\cdot\partial_{\tilde{v}} f_e(\underline{v})\,\delta(\omega_p - \underline{\tilde{k}}\cdot\tilde{v}), \tag{8a}$$

and the corresponding Cerenkov emission is

$$S(\underline{k}) = 3\omega_p\,(32\pi n_o k^2)^{-1}\int d^3\tilde{v} f_e(\underline{v})\,\delta(\omega_p - \underline{\tilde{k}}\cdot\tilde{v}) \tag{8b}$$

(Here $f_e(\underline{v})$ has the units of length^{-3} x velocity^{-3}.) We now turn to further approximations relevant to the present calculation.

B. The model random medium

We consider an electron beam propagating through the plasma in the positive z-direction, and restrict our attention to density fluctuations which are a function only of z (see Fig. 5):

$$\delta n(\underline{r},t) = \delta n(z,t)$$

In one spatial dimension the density correlation function is given by

$$C_{\underline{q}} = \frac{(2\pi)^2}{L}\,\delta(q_x)\delta(q_y)\,\langle\delta n(-q_z)\,\delta n(q_z)\rangle. \qquad (9)$$

We define our random medium by taking density fluctuations having a flat, truncated, ensemble-averaged spectrum:

$$\frac{\langle\delta n(q_z)\delta n(-q_z)\rangle}{L} \equiv \begin{cases} \dfrac{\pi(DN)^2}{4Qm} & , \ |q_z| \le Q_m \\ 0 & , \ |q_z| > Q_m \end{cases} \qquad (10)$$

The value of $(DN)^2$ is determined by the constraint

$$\int \frac{d^3q}{(2\pi)^3}\, C_{\underline{q}} = (\delta\tilde{n}/\tilde{n}_o)^2$$

(This is Eq. (2) reexpressed in terms of dimensionless variables. An ensemble average on the right is omitted.) We find that

$$(DN)^2 = (\delta\tilde{n}/\tilde{n}_o)^2;$$

$(DN)^2$ is just the ensemble-averaged mean square density fluctuation, normalized to the ambient plasma number density.

Noticing that the angular factor μ_-^2 in Eqs. (7) serves to diminish Langmuir wave scattering at large angles to the z-axis, we set it equal to one. The final step in deriving the one-dimensional kinetic equation is to ignore the transverse structure of the electron distribution function:

$$f_e(\underline{v}) \equiv \delta(v_x)\delta(v_y)f(v_z).$$

With this assumption, $\mu_-^2 = 1$, and using Eqs. (9 and 10), Eqs. (7) yield the following linear, inhomogeneous equation for the evolution of $F(k_z,t)$:

$$\left[\partial_t + 2\gamma(k) + A(k) + B(k)\right]F(k,t) = A(k)F(-k+c_s,t) + B(k)F(-k-c_s,t) + S(k) \qquad (11a)$$

$$A(k) \equiv \begin{cases} \pi(DN)^2[8Q_m|2k-c_s|]^{-1} & \text{if } |2k-c_s| < Q_m \\ 0 & \text{if } |2k-c_s| \geq Q_m \\ & \text{or} \\ & \text{if } 2k = c_s \end{cases} \qquad (11b)$$

$$B(k) \equiv \begin{cases} \pi(DN)^2[8Q_m|2k+c_s|]^{-1} & \text{if } |2k+c_s| < Q_m \\ 0 & \text{if } |2k+c_s| \geq Q_m \\ & \text{or} \\ & \text{if } 2k = -c_s \end{cases} \qquad (11c)$$

We have suppressed the subscript on k_z and have normalized $\tilde{F}$ and $\tilde{S}$ to $8\pi\theta_e$, where θ_e is the electron temperature in energy units. In terms of our previous notation

$$2\gamma^{eff}(k) = A(k) + B(k)$$
$$S^{eff}(k,t) = A(k)F(-k+c_s,t) + B(k)F(-k-c_s,t).$$

A typical γ^{eff} is plotted in Fig. 6a.

The one-dimensional electron velocity distribution, f(v), consists of a Gaussian bump on the tail of a Maxwellian distribution, plus an exponential non-thermal component,

$$f_{NT}(v) \equiv \frac{n_{NT}}{2\Delta v_{NT}} \exp(-|v|/\Delta v_{NT}), \qquad (12)$$

chosen to simulate the conditions in the solar wind and other plasmas which are nonthermal at high energies (see Section II). In addition to the damping (or growth) rates that these distributions generate via Eq. (8), we include the effects of coulomb collisional damping on the Langmuir waves:

$$\gamma(k) = \gamma_L(k) + \gamma_B(k) + \gamma_{NT}(k) + \gamma_c$$

where

$$\gamma_L(k) = \left(\frac{\pi}{8}\right)^{\frac{1}{2}} \left|\frac{2}{3}k\right|^{-3} \exp(-3/4k^2) \quad \text{(Landau damping by thermal component)},$$

$$\gamma_B(k) = \Omega(v_B/\Delta v_B)\, z \exp(-z^2/2) \quad \text{(beam growth and damping)},$$

$$\Omega \equiv \left(\frac{\pi}{8}\right)^{\frac{1}{2}} n_B 3v_e^2/(2k^2 v_B \Delta v_B)$$

$$z \equiv (v_B/\Delta v_B)\left[(1.5)^{\frac{1}{2}} v_e\,(v_B|k|)^{-1} - \text{sign}(k)\right]$$

$$\gamma_{NT}(k) = n_{NT}\frac{3\pi}{8} k^{-2} (v_e/\Delta v_{NT})^2 \exp\left[-\sqrt{3}v_e\,(\sqrt{2}\Delta v_{NT}|k|)^{-1}\right]$$

(Landau damping by nonthermal component),

and

$$\gamma_c = (12\pi\sqrt{2\pi})^{-1}\, g\, \ln(12\pi g^{-1}) \quad \text{(collisional damping)}.$$

In the collisional damping rate above, g is the plasma parameter

$$g \equiv [n_o k_D^{-3}]^{-1} .$$

(For the solar wind and bow-shock plasmas that we consider, g is 0 (10^{-10}).) n_{NT} and n_B are, respectively, the non-thermal and beam number densities normalized to the ambient plasma number density. v_e is the electron thermal velocity; v_B is the mean velocity of beam electrons; Δv_B is the half-width of the beam; and Δv_{NT} is defined in Eq. (12).

The Cerenkov source term is given in one dimension by

$$S(k) = 3\omega_p (32\pi n_o k^2)^{-1} \int dv\ f(v)\delta(\omega_p - \tilde{k}\cdot\tilde{v}).$$

It follows that

$$S(k) = (\gamma_L(k)+\gamma_c)\cdot(4\pi)^{-1} + S_B(k) + S_{NT}(k),$$

where

$$S_B(k) = \Omega v_B \sqrt{6}\ |k|^{-1} \exp(-z^2/2) ,$$

and

$$S_{NT}(k) = n_{NT}\ 3\sqrt{3}v_e [64\sqrt{2}\pi\ \Delta v_{NT} |k|^3]^{-1} \exp[-\sqrt{3}v_e\ (\sqrt{2}\Delta v_{NT}|k|)^{-1}] ,$$

and we have added in a Bremsstrahlung emission term (proportional to γ_c). By far, most of the emission is from beam electrons. We plot $\gamma(k)$ and $S(k)$ for parameters typical of the solar wind in Figs. 6b and c, respectively.

For convenience, we list here all of the independent, dimensionless variables that characterize our problem.

Density Fluctuations:	DN^2, Q_m
Electron Beam:	n_B, v_e/v_B, $v_B/\Delta v_B$
Non-Thermal Component:	n_{NT}, $v_e/\Delta v_{NT}$

IV. Solutions of the Kinetic Equation

A. General Remarks

The Langmuir wave energy density at $\underline{\tilde{k}}$ is

$$d^3\underline{\tilde{k}}\ \tilde{W}(\underline{\tilde{k}}) \equiv d^3\underline{\tilde{k}}\ \theta_e F(k_z,t)\delta(k_x)\delta(k_y)\ . \qquad (13)$$

Therefore, the total wave energy density, normalized to $n_o\theta_e$ is

$$W(t) \equiv \int_{|\underline{\tilde{k}}|\le\tilde{k}_{max}<k_D} \frac{d^3\underline{\tilde{k}}}{(2\pi)^3}\frac{\tilde{W}(\underline{\tilde{k}})}{n_o\theta_e} = g(2/3)^{3/2}(2\pi)^{-2}\int_{-|k|_{max}}^{|k|_{max}} F(k,t)dk\ . \qquad (14)$$

The integration is only over those modes actually retained in our truncation of the Langmuir wave spectrum. We will truncate the spectrum at $|k|_{max} \approx 0.25$ (or $|\tilde{k}|_{max} \approx 0.2k_D$). Larger $|k|$-components are too heavily Landau-damped to affect the results for parameters appropriate to the solar wind problems. Furthermore, according to Eqs. (11 b and c), Langmuir wave components with $2|k| > Q_m + c_s$ evolve with no scatter; for such modes, Eq. (11a) is solved by the detailed balance result, $F(k) = S(k)\ [2\gamma(k)]^{-1}$. If these 'unscattered' modes are heavily Landau damped, they cannot contribute to the total wave energy. We will impose, therefore, the constraint

$$Q_m = 2|k|_{max} - c_s \qquad (15)$$

between our truncations of the density fluctuation spectrum and the Langmuir wave spectrum. (In fact, the Markoffian limit of the kinetic equation is justified only for those modes satisfying the resonance condition(s) $R_{\pm} = 0$ and hence only for scattered modes.)[1]

In the absence of a beam and non-thermal background ($n_B = 0 = n_{NT}$), the result of detailed balance is again the appropriate solution of Eq. (11a),

$$F(k,t) = S(k)/2\gamma(k) = \frac{1}{8\pi}$$

and

$$W(t) = g(2/3)^{3/2}(32\pi^3)^{-1} \cong 10^{-13},$$

regardless of the scattering. However, with an electron beam present, Langmuir wave energy is injected over some interval in k-space for which $\gamma(k)$ is negative. The energy in these 'pump' modes undergoes successive backscatterings (i.e. $k \rightarrow -k \pm c_s$), at a rate proportional to DN^2. Eventually some of the injected energy will be scattered into one of the dissipative regions of k-space where there is damping ($\gamma(k) > 0$, see Fig. 6b).

If the efficiency of the scattering is high enough, a <u>stationary state</u> will be reached in which wave energy is dissipated as fast as it is injected; i.e., the beam-plasma instability will be saturated (see Figs. 10):

$$F(k,t) \rightarrow F^o(k)$$
$$W(t) \rightarrow W^o$$

From Eqs. (11b and c) it is easy to see that scattering alone conserves energy:

$$\int 2\gamma^{eff}(k)F(k,t)dk = \int_{|k| \leq |k|_{max}} S^{eff}(k)dk$$

It follows from Eq. (11a) that all stationary states must satisfy

$$\int 2\gamma(k)F^{o}(k)dk = \int S(k)dk \ ,$$

thus generalizing the detailed-balance result given above.

If the efficiency of the scattering is too low, energy will be injected faster than it can be channeled into the sinks, and the total wave energy will diverge (see Fig. 11a):

$$W(t) \to \infty \ .$$

Under these conditions, nonlinear terms must be retained in the original kinetic equations.

There is a boundary in parameter space which separates the bounded behavior (stationary solutions) from the unbounded behavior. Next, we characterize, in more detail, the stationary solutions that lie below this threshold and introduce a simple method for approximating the threshold.

B. Stationary solutions and threshold

We search for stationary solutions by solving numerically the algebraic system

$$\underline{\underline{M}} \cdot \underline{F}^{o} = \underline{S} \qquad (16)$$

that results from Eq. (11a) when $\partial_t = 0$. Here, $\underline{F}^{o}$ is a vector defined by

$$(\underline{F}^{o})_j \equiv F^{o}(k_j) ,$$

where

$$|k_j| \leq |k|_{max} , \; j = 1,2,\ldots, N ,$$

and $k_{1,N} = \pm|k|_{max}$. (Typically, N = 241 and $|k_j - k_{j+1}| = 0.1\, c_s$.) To be physically acceptable ("realizable"), a solution of Eq. (16) must be positive for all k_j,

$$F^{o}(k_j) \geq 0 .$$

If such a solution exists, then all initial distributions that we examine are found to approach it with increasing time. When the parameters are such that the solution to Eq. (16) yields $F^{o}(k_j) < 0$ for some k_j, then our solution to the corresponding time-dependent equation, (11a), yields a total wave energy which diverges with increasing time, regardless of initial spectrum. Thus, the saturation threshold may be taken as that boundary in parameter space separating solutions of Eq. (16) with $F^{o}(k_j) \geq 0$ for all k_j from those solutions with $F^{o}(k_j) < 0$ for some k_j.

i) Case $n_{NT} = 0$

Consider first the case of no nonthermal component, ($n_{NT} = 0$). In Fig. 7, we plot the threshold curve as a function of beam growth rate ($\sim n_B (v_B/\Delta v_B)^2$) for a fixed level of density fluctuations (DN = 2×10^{-4}). Notice that the total wave energy at threshold is a weakly increasing function of beam density and beam width. Farther below threshold, total wave energies are significantly reduced from their threshold values.

Larger values of DN are required to saturate beams with higher n_B. Larger values of total wave energy at threshold occur in this limit. Langmuir wave spectra with total energies on the order of 10^{-7} were observed during the Voyager 1 fly-by of the Jovian bow shock.[2] If we choose $v_B/\Delta v_B = 2$, $v_e/v_B = .016$ $n_B = 8.55 \times 10^{-7}$, then our theory predicts DN = 2×10^{-3} to saturate the instability at threshold, with total wave energy $W^o = 2 \times 10^{-7}$. The measured values of DN (see Section II and Fig. 2) are on the order of 2×10^{-4}, which corresponds to Fig. 7. (The parameters n_B and Δv_B were not measured in the Voyager experiment.) For the chosen parameters, we find saturated total wave energies at least an order of magnitude smaller than those observed.

In Fig. 8 we plot $F^o(k)$ just below threshold at point 'P_1' in Fig. 7. Here the total wave energy, W^o, is 2.8×10^{-8}, and we note a significant scatter all the way out to wave numbers $|k|_{max} \approx 0.17\ k_D$. The pronounced spikes in the spectrum

occur at wave numbers in resonance with the fastest growing beam-unstable mode:

$$-k_o \pm c_s,\ k_o \pm 2c_s,\ -k_o \pm 3c_s,\ k_o \pm 4c_s \ldots$$

where k_o maximizes $|\gamma(k)|$ for growing modes. (Because we have chosen $v_e/v_B = 0.016 \cong c_s$, these resonances approximately overlap in pairs.) Scatter out to such high $|k|$-values is consistent with observations by Voyager 1, although W_o is roughly one tenth the observed energy.

ii) Case $n_{NT} \neq 0$

It is doubtful, however, that a simple bump-on-tail accurately models the electron velocity distribution function in the solar wind and off the bow shocks, as we have discussed in Section II. We use Eq. (12) to model the velocity distribution of the non-thermal electrons. Choosing $v_e/v_B = 0.016$ and $v_e/\Delta v_{NT} = 0.3$ results in non-thermally damped modes that are immediately adjacent to the beam-unstable modes in k-space, consistent with the observations off the earth's bow shock (cf. Figs. 3 and 6b).

It is natural to ask for the level of density fluctuations necessary to saturate the instability for different levels of the non-thermal component of the electron distribution function. In Fig. 9 we plot the threshold curve in the (n_{NT}, DN)-plane of parameter space for fixed beam parameters thought to be appropriate to the Jovian bow shock[2] and to Type III[4] conditions. As one would expect, larger non-thermal components require smaller levels of density fluctuation to saturate the instability.

Notice that the total wave energy at threshold is a weakly increasing (decreasing) function of DN (n_{NT}).

In Fig. 10a we plot $F^o(k)$ just below threshold at point 'P_2' in Fig. 9. Here the total wave energy, W_o, is 3×10^{-9} for a choice of non-thermal number density taken from terrestrial bow-shock observations. The scattering is only out to wave numbers of $|\tilde{k}| \cong 0.1\ k_D$. Again: below threshold, the stationary states have total wave energies significantly smaller than their threshold values.

iii) Conditions for saturation

Let us consider the physical origins of the stationary solutions. Clearly, it is impossible to find physical ($F^o(k_j) \geq 0$), stationary solutions of Eq. (11a) if $2\gamma + 2\gamma^{eff}$ is negative for some of the pump modes. Therefore, a necessary condition for saturation is

$$[2\gamma(k) + 2\gamma^{eff}(k)]\Big|_{beam} \geq 0 \ . \qquad (17)$$

(Obviously, if this is true for the beam-unstable modes, then it is true for all k-values.) This is not, however, a sufficient condition for saturation. If it were, we could identify the threshold condition as Min $[2\gamma(k) + 2\gamma^{eff}(k)] = 0$. Physically, condition (17) is not sufficient for saturation because some of the energy that is scattered out of the pump modes is scattered back into those modes. The net rate at which the pump modes are depleted must be positive for saturation. Threshold then can be identified by setting the minimum net rate for pump modes equal to zero. Of course, this minimum

net rate is obtained by solving Eq. (16) algebraically. However, it is instructive to do so for the case of only a few Langmuir wave components.

Suppose that the problem consisted only of the most unstable beam mode at k_o and the two modes coupled directly to it at $k_{1,2} \equiv -k_o \pm c_s$. Then Eq. (16) is easily solved, and we find that

$$(2\gamma_o + 2\hat{\gamma}_o^{eff})F_o^o = S_o \ ,$$

where

$$2\hat{\gamma}_o^{eff} \equiv 2\gamma_o^{eff} - A_o A_1 [2\gamma_1 + 2\gamma_1^{eff}]^{-1} - B_o B_2 [2\gamma_2 + 2\gamma_2^{eff}]^{-1} \ ,$$

and we have neglected the source terms at $k_{1,2}$. ($F_o^o \equiv F^o(k_o)$, $A_o \equiv A(k_o)$, etc.) Here we have defined a "renormalized" effective scattering-out rate, $\hat{\gamma}^{eff}$. Since all A's and B's are positive by definition (cf. Eqs. 11b and c), as are γ_1 and γ_2, we see clearly the destabilizing effects of the scatter back into the pump mode, i.e. $\hat{\gamma}_o^{eff} < \gamma_o^{eff}$.

For this 3-mode system the threshold condition is

$$2\gamma_o + 2\hat{\gamma}_o^{eff} = 0 \ . \qquad (18)$$

This reduces to the condition (17) in the limit of increasing damping of the scattered modes, $\gamma_{1,2} \to \infty$. However, if these modes are not heavily damped, as is likely to be the case,

we would have to include more than 3 modes in our truncation in order to reach sufficient dissipation to saturate the instability. As a rule, we keep adding modes to the truncation until we reach a k* such that

$$2\gamma(k^*) > 2\gamma^{eff}(k^*) \ .$$

Then the $\hat{\gamma}_o^{eff}$ that we obtain enables a good approximation to the threshold condition via Eq. (18). We will present a detailed analysis of this renormalization technique in a subsequent publication.

C. Time-dependent behavior

Starting from a reasonable initial Langmuir wave spectrum, the subsequent behavior will be either bounded or unbounded (i.e. requiring nonlinearity for saturation) depending on the parameters. We take as an initial spectrum, the solution of Eq. (16) with the beam turned off ($n_B = 0$, cf. Fig. 10b). Such initial conditions are particularly appropriate to the Jovian and terrestrial bow-shock problems in which the solar wind is convected into an almost orthogonal electron beam of finite extent parallel to the wind (see Fig. 5). Thus, in the rest frame of the solar wind (where our theory applies), we would see the beam suddenly turned on at t = 0. (Of course we can only assume a sharp beam boundary since we are not evolving the electron distribution in time.) Then we restore the beam ($n_B > 0$) and evolve Eq. (11a) with the full electron distribution function.

Such a scenario is also appropriate for describing Langmuir waves associated with Type III solar bursts, in which an electron beam streams through the ambient solar wind and excites Langmuir waves. However, the times of interest in Type III and bow-shock problems are quite different. In the bow-shock problems, the beam terminates abruptly at the shock front; so we are only interested in evolving the system for the time it takes a point at rest in the solar wind to travel from the beam front to the shock front. For the published Voyager 1 observations off Jupiter,[2] this is about 20 sec or 10^5 plasma periods. For the Type III observations,[4] the observation time is considerably longer (35 minutes in the frame of the ISEE-3 spacecraft). For a typical beam ($n_B = 10^{-6}$, $v_B/\Delta v_B = 3$, $v_e/v_B = 0.016$) and non-thermal component ($n_{NT} = 10^{-5}$, $v_e/\Delta v_{NT} = 0.3$) the evolution of the Langmuir wave spectrum just below threshold is summarized in Figs. 10. (We assume DN = 1.25×10^{-3} corresponding to point P_2 in Fig. 9). The elapsed time is 12×10^6 plasma periods (36 minutes at the Jovian bow shock), after which the total energy has reached <u>one half</u> of its final value (Fig. 10c).

Evidently, there is insufficient time available in the Jupiter problem for this stationary state to be observed. Therefore, in the context of that problem, the beam-plasma instability would be completely suppressed. However, here the level of density fluctuations is slightly larger than observed.

For the same beam and non-thermal component, but weaker density fluctuations (DN = 5×10^{-4}), we move above threshold to the case of unbounded behavior. In parameter space we are at point P_3 in Fig. 9. Here the evolution of the Langmuir wave spectrum for the first 12 million plasma periods is summarized in Figs. 11. The spectrum reaches energy levels at which nonlinear process, neglected in our theory, become important only at the end of the time interval (i.e. $W(t) = 10^{-5}$). Yet the scattering out is completed after a relatively short time. By 'completed' we mean the following:

Let $W_j(t)$ be the Langmuir wave energy contained between k_j and k_{j+1} where $F(k,t)$ has a local minimum at k_j. There is a spike in the spectrum between k_j and k_{j+1}. We define the efficiency of the scatter into $[k_j, k_{j+1}]$ as

$$f_j(t) \equiv W_j(t) \, [W_o(t)]^{-1}$$

where $W_o(t)$ is the energy under the beam-resonant spike at k_o. This is just the fraction of energy in the beam spike that is contained in the j-th spike. We observe that (for the chosen initial conditions) each f_j changes rapidly during roughly the first $2 \cdot 10^6$ plasma periods, after which the variation of F_j halts abruptly, and f_j is virtually constant for the remainder of the evolution. This is observed in all cases, for both bounded and unbounded behavior. The same is true of the fraction of the total energy contained in the beam-resonant spike. Thus, each spike receives a constant fraction of the total

wave energy long before the system either saturates or diverges. See Figs. 11c through e.

For the Type III and bow shock problems, the distinction between bounded and unbounded behaviors is irrelevant if the level of density fluctuations is sufficient to suppress the instability during the time that the plasma is exposed to the beam. This is the case in Figs. 11.

The suppressive effect of the scattering on the instability in the case of unbounded behavior can be observed by setting DN = 0. Doing so for the parameters in Figs. 11, we find that the total wave energy grows dramatically faster than in Fig. 11a due to the unabated exponential growth of the pump modes: after 12 million plasma periods W(t) is 2.6×10^{8}. Clearly, the instability is strongly suppressed when DN = 5×10^{-4} (as in Fig. 11a). Indeed, for much of the evolution W(t) has been held to acceptable levels for the application of our theory.

Therefore, in cases where the plasma is exposed to the beam for a finite time, observations of Langmuir spectra with significant components at higher $|k|$ and relatively small total wave energies (10^{-8}-10^{-6}) may be explained by the present theory even when that theory predicts time-asymptotic divergence of the wave energy.

V. Conclusions

We have studied the effects of a given, external spectrum of ion acoustic turbulence on the evolution of Langmuir waves in a beam-unstable plasma. Our theory is based on solving a linear kinetic equation for the spectral energy density of the Langmuir waves in one dimension. This equation includes the effects of Landau damping and growth for a given, stationary, non-thermal, electron distribution-function as well as the effects of scattering off the density fluctuations, which we have taken to have a flat spectrum. We find that the beam-plasma instability is saturated provided that the level of density fluctuations is sufficiently high. Then saturation results from the progressive back-scattering of beam-resonant wave energy into dissipative regions of k-space. In this case, a stationary spectrum is approached asymptotically in time by all initial spectra examined. If the level of density fluctuations is too low, the instability is not saturated, and the total wave energy diverges with increasing time.

In the case of bounded behavior and for parameters appropriate to the Jovian and terrestrial bow-shock environments as well as to Type III bursts, the saturated states are characterized by total wave energies ($W = 0(10^{-9} \rightarrow 10^{-7})$ well below the threshold at which nonlinear processes (neglected in our theory) become important ($W \sim 0(10^{-5})$). The stationary distributions demonstrate significant scatter of Langmuir wave energy out to wave numbers of from .1 to .2 k_D in magnitude, depending on the distribution of non-thermal electrons.

In the case of unbounded behavior, the scattering may suppress the growth of wave energy during beam-plasma interactions that occur over a finite interval of available time. Scattering to high-k components is completed much faster than the total wave energy diverges. Therefore, in the context of bow-shock and Type III problems, a broad spectrum of Langmuir waves may be observed at energy levels that favor the linear kinetic theory presented here, even when that theory predicts eventual divergence of the wave energy. For example, off the Jovian bow shock, the solar wind plasma is exposed to the electron beam for only about 20 sec (10^5 plasma periods) in the plasma frame. Yet, for parameters appropriate to this environment, the theory predicts that it takes the wave energy roughly 30 min to reach nonlinear levels if the density fluctuations are too weak to saturate the beam-plasma instability (cf. Fig. 11a). For early times, the wave energy is virtually constant and, if observed for only a short while, would give the impression of a stationary (saturated) Langmuir wave spectrum. For Type III bursts the beam-plasma interaction is observed to last longer. Here again, theory predicts that the time required for the wave energy to reach nonlinear levels is approximately 30 minutes in the solar wind frame.

We have characterized the threshold in parameter space that separates saturated from unsaturated behavior. Naturally, more powerful beams require larger levels of low-frequency turbulence to saturate the instability. However, the requisite threshold levels of turbulence are considerably lowered in the

presence of non-thermal electrons which provide dissipation over wide intervals in k-space. Recent measurements of the electron distribution off the earth's bow shock[3] indicate a strong non-thermal component in the electron velocity distribution. Such a component is generally present in the solar wind.[4] Consequently, relatively small levels ($\delta n/n_o = 0(10^{-4})$) of ion acoustic turbulence would suppress the beam-plasma instability for beams typical of the Jovian and terrestrial bow shocks.

ACKNOWLEDGMENT

We wish to acknowledge important interactions with F. Tappert and J. Weatherall, and helpful conversations with F. Scarf, R. Lin, D. Gurnett, and D. F. DuBois.

This work was supported by the Air Force Office of Scientific Research (Grant No. 80-0022), the National Aeronautics and Space Administration (Grant No. NAGW-91), by the National Science Foundation, Atmospheric Sciences Section (Grant No. ATM-7916837), and by the National Center for Atmospheric Research Computing Facility, to the University of Colorado. Support was also given by the Institute for Theoretical Physics, Santa Barbara, where the original ideas for this work were conceived.

References

1. M.V. Goldman and D.F. DuBois, Phys. Fluids 25, 1062 (1982).

2. D.A. Gurnett, J.E. Maggs, D.L. Gallagher, W.S. Kurth, and F.L. Scarf, J. Geophys. Res. 86, 8833 (1981).

3. R.R. Anderson, G.K. Parks, T.E. Eastman, D.A. Gurnett, and L.A. Frank, J. Geophys. Res. 86, 4493 (1981).

4. R.P. Lin, D.W. Potter, D.A. Gurnett, and F.L. Scarf, Astrophys. J. 251, 364 (1981).

5. B. Hafizi, J. Weatherall, M.V. Goldman, and D. Nicholson, Phys. Fluids 25, 392 (1982); D.R. Nicholson and M.V. Goldman, Phys. Fluids 21, 1766 (1978); W.L. Kruer and E.J. Valeo, Phys. Fluids 16, 675 (1973).

6. D.A. Gurnett, E. Marsch, W. Pilipp, R. Schwenn, and H. Rosenbauer, J. Geophys. Res. 84, 2029 (1979).

Figure Captions

Fig. 1. Langmuir waves excited by an electron beam of energy $\sim$ 10 keV, off the Jovian bow shock as observed by Voyager 1. (Gurnett et al., 1981)

Fig. 2. Ambient ion-acoustic wave turbulence measured by Voyager 1 simultaneous with the beam-excited Langmuir waves in Fig. 1. (Gurnett et al., 1981)

Fig. 3. A non-thermal distribution of high-energy electrons in the solar wind measured by ISEE-1 in the vicinity of the earth's bow shock. Note the electron beam at $v_{//} \cong -21$ km/s. (Anderson et al., 1981)

Fig. 4. Feynman diagrams for the scattering processes studied in this paper.

Fig. 5. Geometry of the beam-plasma interaction near a planetary bow shock.

Fig. 6. Coefficient functions in the kinetic equation.
(a) $\gamma^{eff}(k)$ vs k for $Q_m = .437$ and $DN = 1.25 \times 10^{-3}$.

(b) Total linear growth/damping rate, $\gamma(k) = \gamma_L(k) + \gamma_B(k) + \gamma_{NT}(k) + \gamma_c$ vs k, for $n_B = 10^{-6}$, $v_e/v_B = .016$, $v_B/\Delta v_B = 3$, $n_{NT} = 10^{-5}$, $v_e/\Delta v_{NT} = 0.3$.

(c) Linear spontaneous emission, S(k), due to the background particle distribution for parameters in Fig. 6b.

Fig. 7. Threshold as a function of beam-resonant growth rate, with no non-thermal damping. $n_{NT} = 0$, $DN = 2 \times 10^{-4}$, $Q_m = .437$, $v_e/v_B = .016$. (Note: γ growth $\sim n_B(v_e/\Delta v_B)^2$).

Fig. 8 The stationary distribution $F^o(k)$ just below threshold at point P_1 in Fig. 7. $v_B/\Delta v_B = 1.6$, $n_B = 2 \times 10^{-8}$, $W^o = 10^{-8}$.

Fig. 9 Threshold as a function of non-thermal electron and density fluctuation levels. $n_B = 10^{-6}$, $v_B/\Delta v_B = 3$, $v_e/v_B = 0.016$, $v_e/\Delta v_{NT} = 0.3$, $Q_m = .437$.

Fig. 10 Bounded behavior just below threshold at point P_2 in Fig. 9. $DN = 1.25 \times 10^{-3}$, $n_{NT} = 10^{-5}$. (Parameters are as in Fig. 6.)

(a) The stationary distribution $F^o(k)$. $W^o = 5.8 \times 10^{-9}$.

(b) Initial distribution function $F^o(k,t = 0)$. $W(t=0) = 5.6 \times 10^{-13}$

(c) The total wave energy, W(t). Elapsed time = 12×10^6 ω_p^{-1}.

(d) $F(k,t)$ at $t = 2.4 \times 10^5$

(e) $F(k,t)$ at $t = 3.36 \times 10^6$

(f) $F(k,t)$ at $t = 1.2 \times 10^7$

Fig. 11 Unbounded behavior above threshold at point P_3 in Fig. 9. $DN = 5 \times 10^{-4}$, $n_{NT} = 10^{-5}$.

(a) The total wave energy, W(t). Elapsed time = 12×10^6 ω_p^{-1}.

(b) The distribution function F(k) at $t = 3.36 \times 10^6$.

(c) The fraction of the total wave energy in the pump modes as a function of time.

Efficiencies: Energy in $[k_1,k_2]$ x [Energy in Pump Modes]$^{-1}$ as a function of time for

(d) $k_1 = -.03$ and $k_2 = .009$

(e) $k_1 = .085$ and $k_2 = .123$

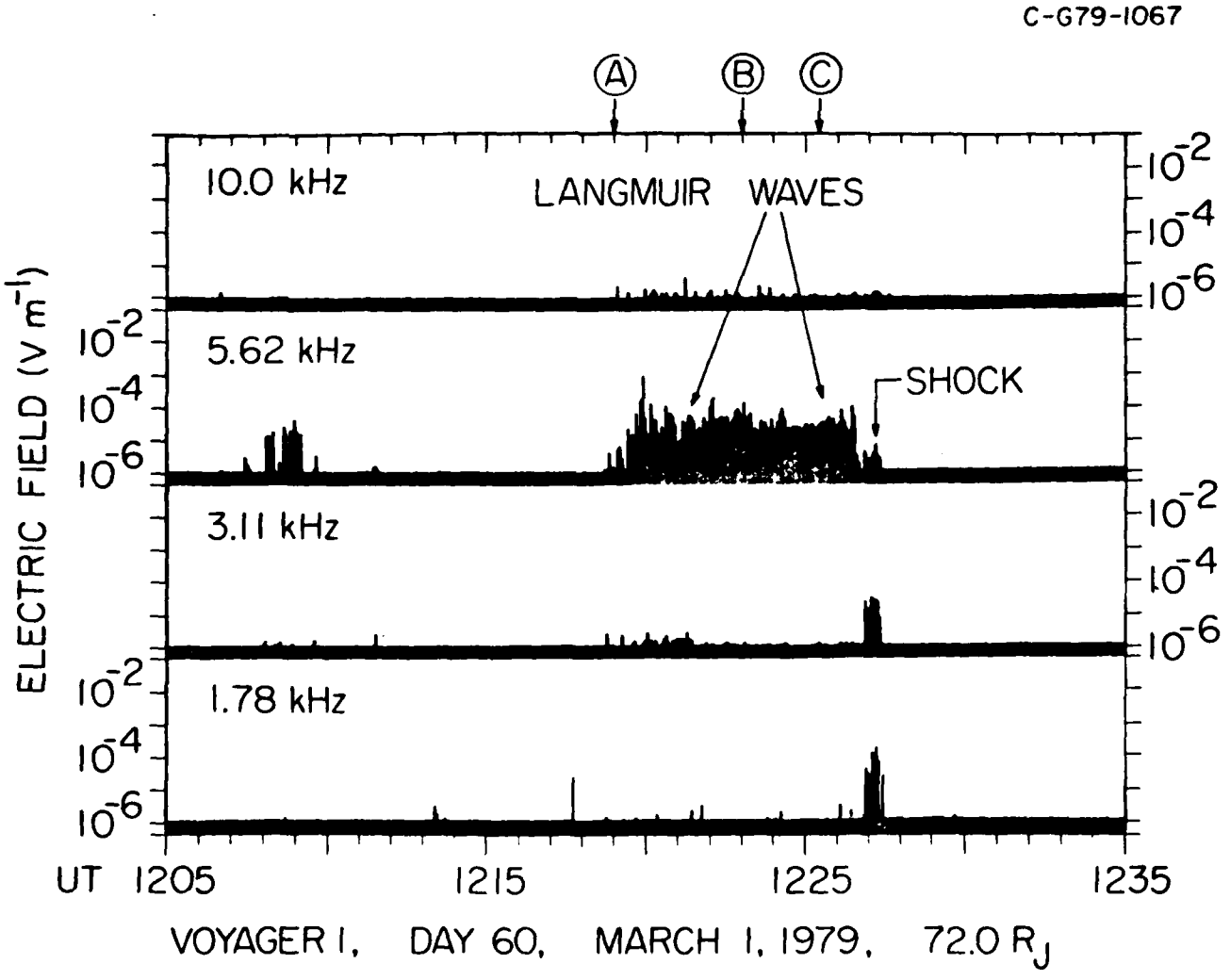
C-G79-1067
A
B
C
10.0 kHz
LANGMUIR WAVES
5.62 kHz
SHOCK
3.11 kHz
1.78 kHz
ELECTRIC FIELD (V m⁻¹)
10⁻²
10⁻⁴
10⁻⁶
UT 1205
1215
1225
1235
VOYAGER 1, DAY 60, MARCH 1, 1979, 72.0 R_J

Fig. 1

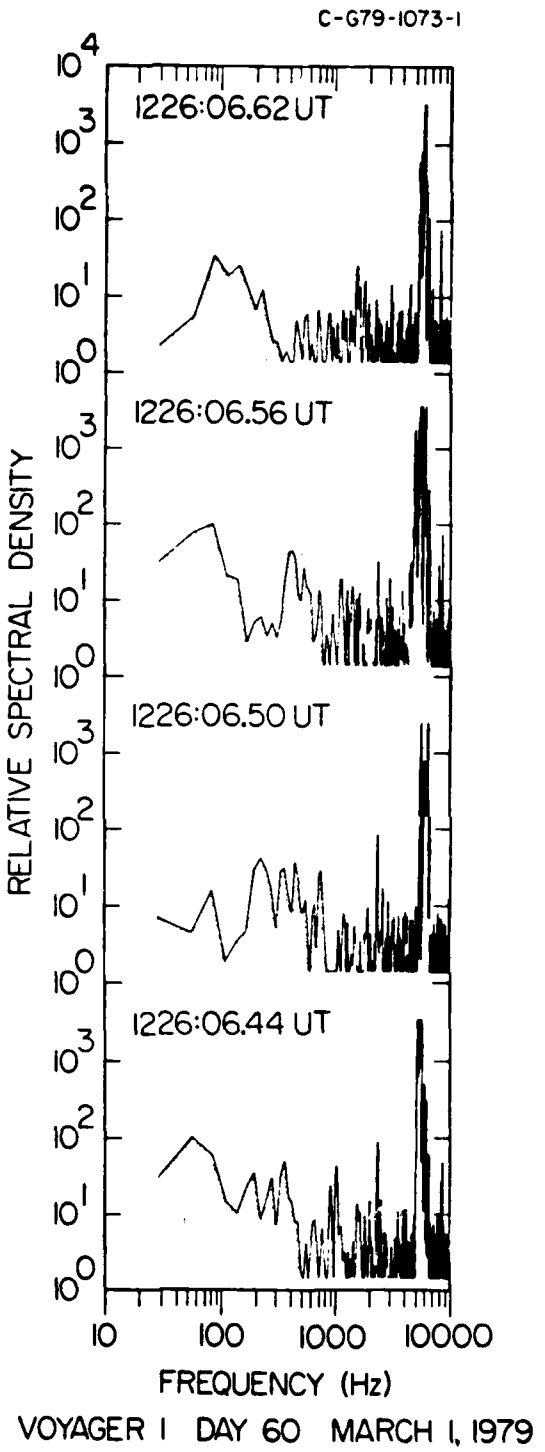
C-G79-1073-1
1226:06.62 UT
1226:06.56 UT
1226:06.50 UT
1226:06.44 UT
RELATIVE SPECTRAL DENSITY
FREQUENCY (Hz)
VOYAGER 1 DAY 60 MARCH 1, 1979

Fig. 2

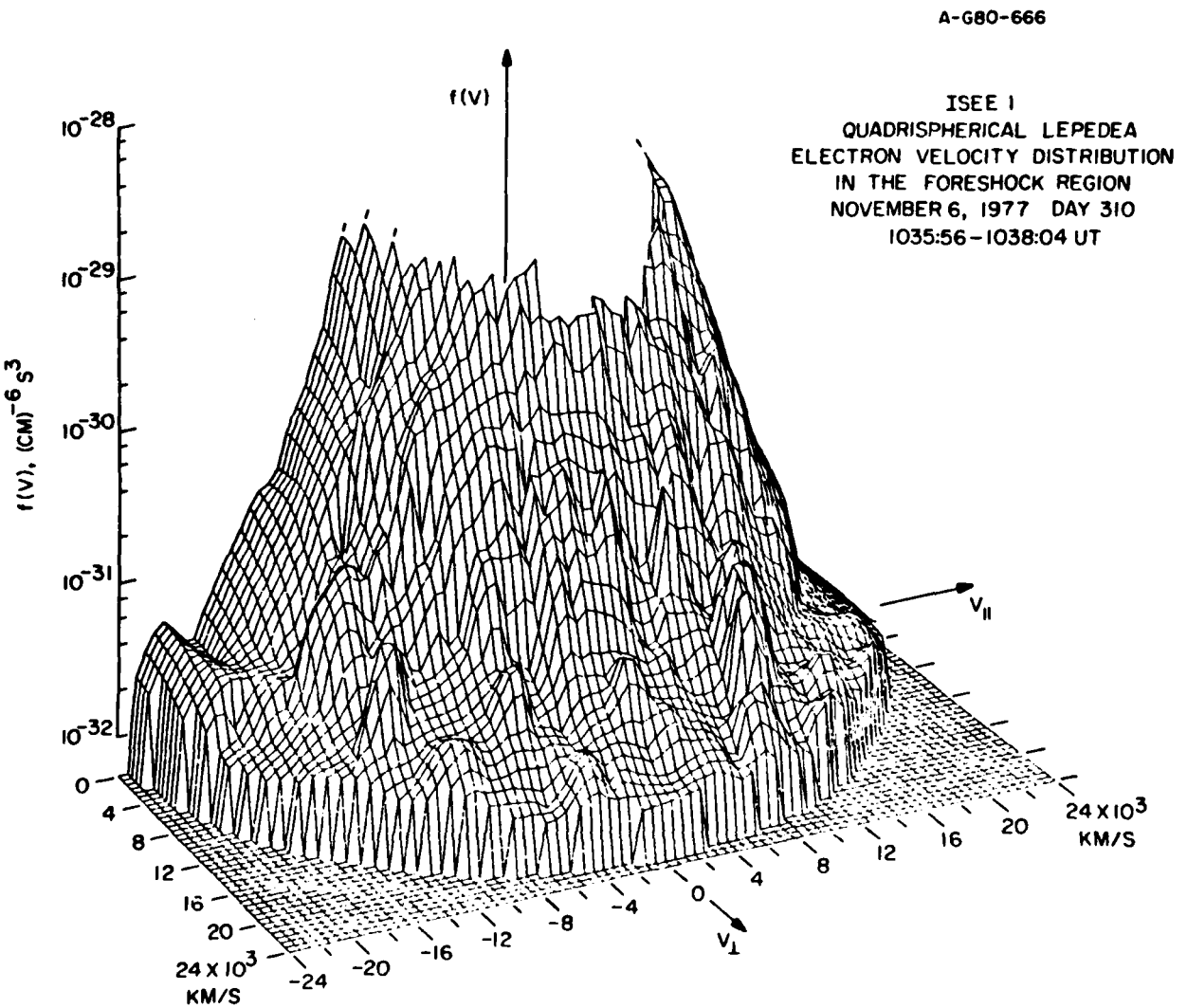
A-G80-666
ISEE 1
QUADRISPHERICAL LEPEDEA
ELECTRON VELOCITY DISTRIBUTION
IN THE FORESHOCK REGION
NOVEMBER 6, 1977 DAY 310
1035:56-1038:04 UT
f(V)
f(V), (CM)$^{-6}$S^3
10^{-28}
10^{-29}
10^{-30}
10^{-31}
10^{-32}
$V_{||}$
$V_\perp$
0
4
8
12
16
20
24 X 10^3
KM/S
-24
-20
-16
-12
-8
-4
0
4
8
12
16
20
24 X 10^3
KM/S

Fig. 3

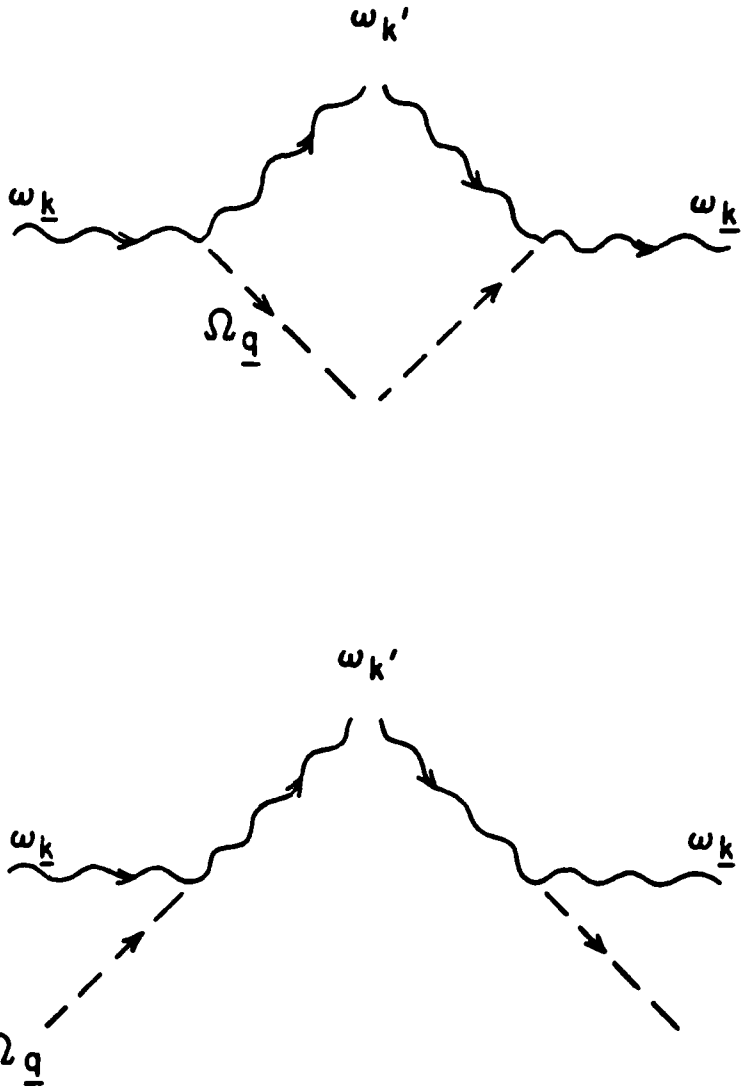
$\omega_{k'}$
$\omega_{\underline{k}}$
$\omega_{\underline{k}}$
$\Omega_{\underline{q}}$
$\omega_{k'}$
$\omega_{\underline{k}}$
$\omega_{\underline{k}}$
$\Omega_{\underline{q}}$

Fig. 4

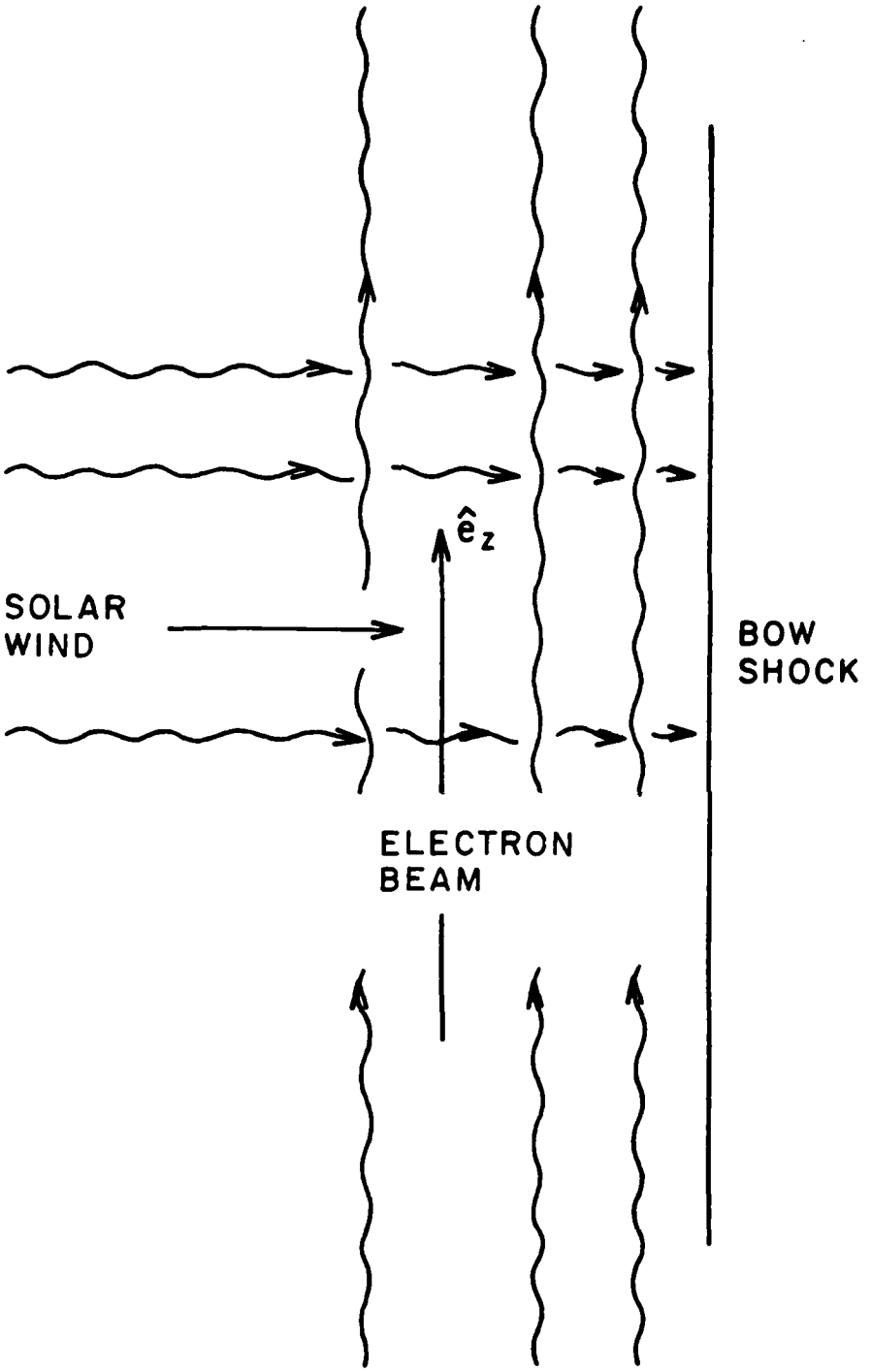

Fig. 5

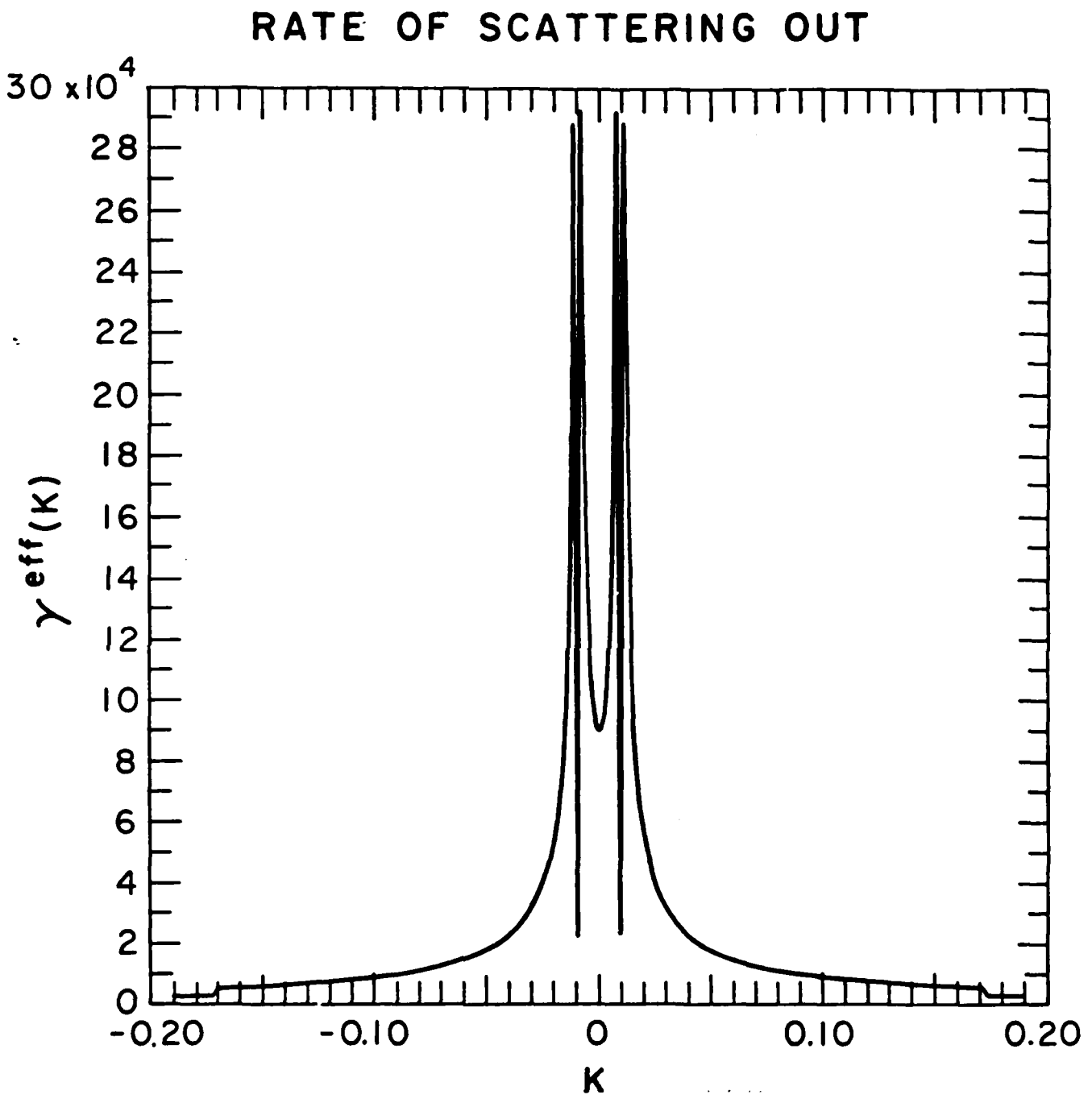
RATE OF SCATTERING OUT
30 x10^4
28
26
24
22
20
18
16
14
12
10
8
6
4
2
0
γ eff (K)
-0.20
-0.10
0
0.10
0.20
K

Fig. 6a

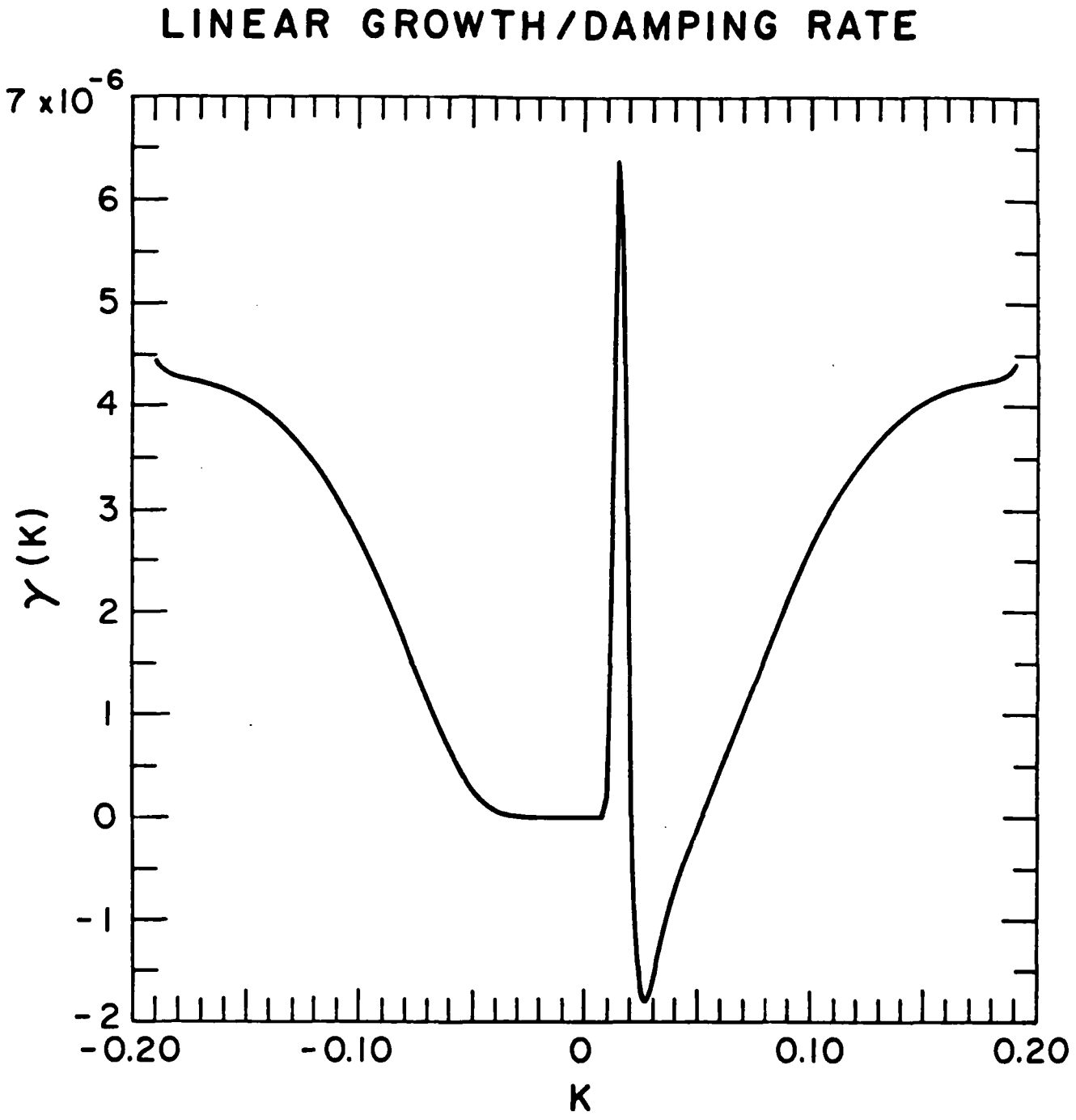
LINEAR GROWTH/DAMPING RATE
7 x10^-6
6
5
4
3
2
1
0
-1
-2
γ(K)
-0.20
-0.10
0
0.10
0.20
K

Fig. 6b

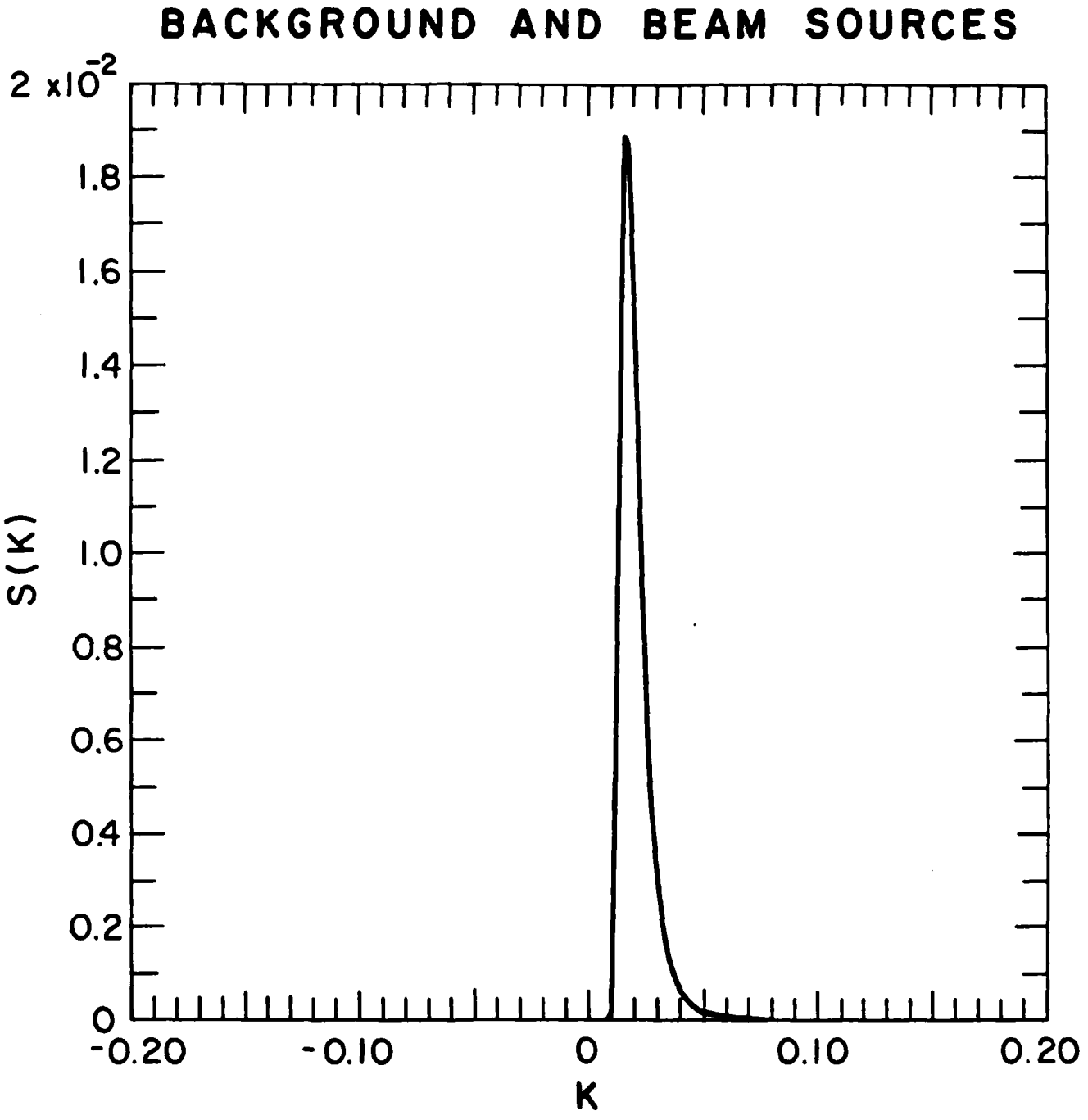
BACKGROUND AND BEAM SOURCES
2 x10⁻²
1.8
1.6
1.4
1.2
1.0
0.8
0.6
0.4
0.2
0
S(K)
-0.20
-0.10
0
0.10
0.20
K

Fig. 6c

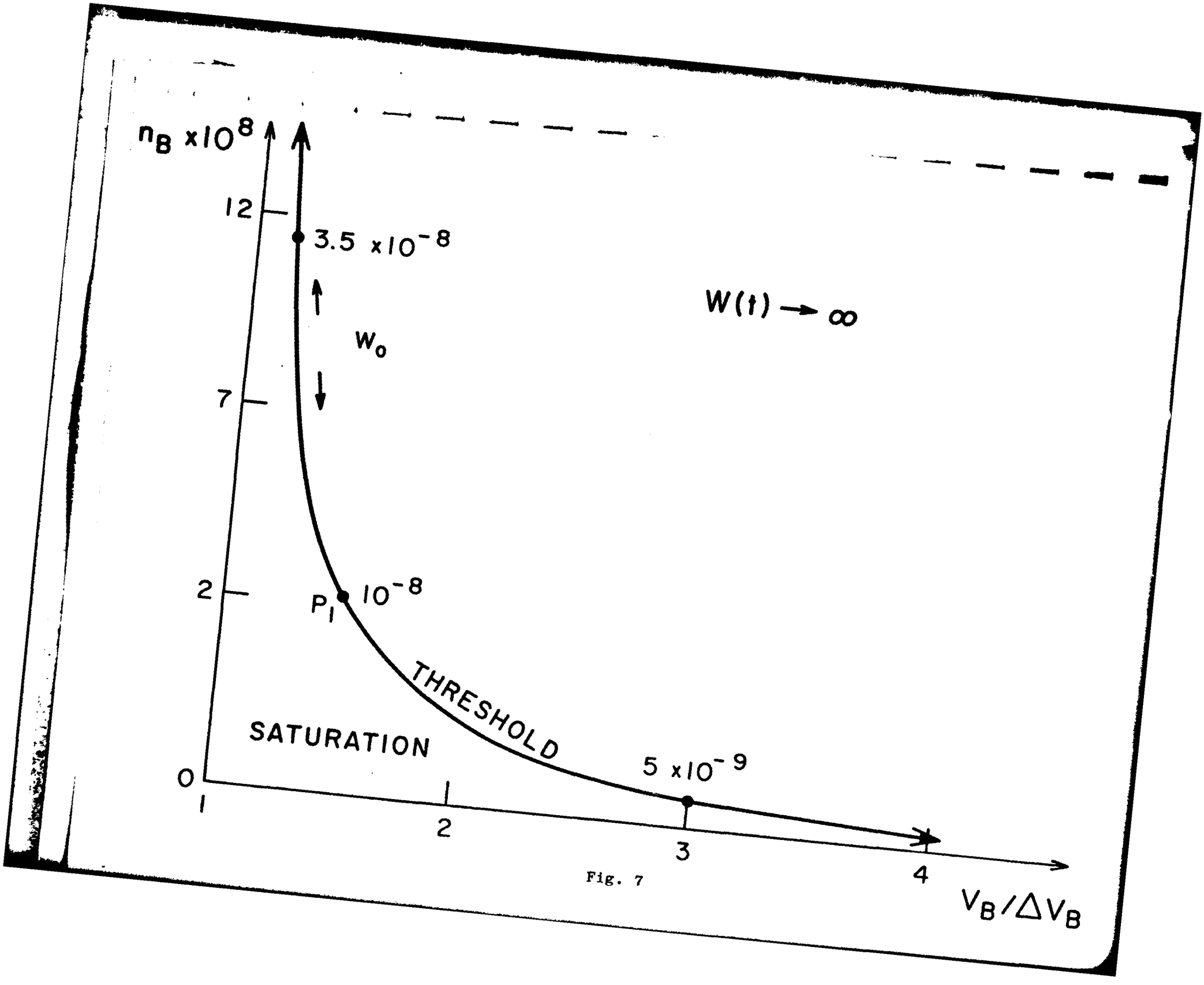
$n_B \times 10^8$
12
7
2
0
3.5×10^{-8}
W_o
$W(t) \to \infty$
P_1
10^{-8}
THRESHOLD
SATURATION
5×10^{-9}
1
2
3
4
$V_B/\Delta V_B$

Fig. 7

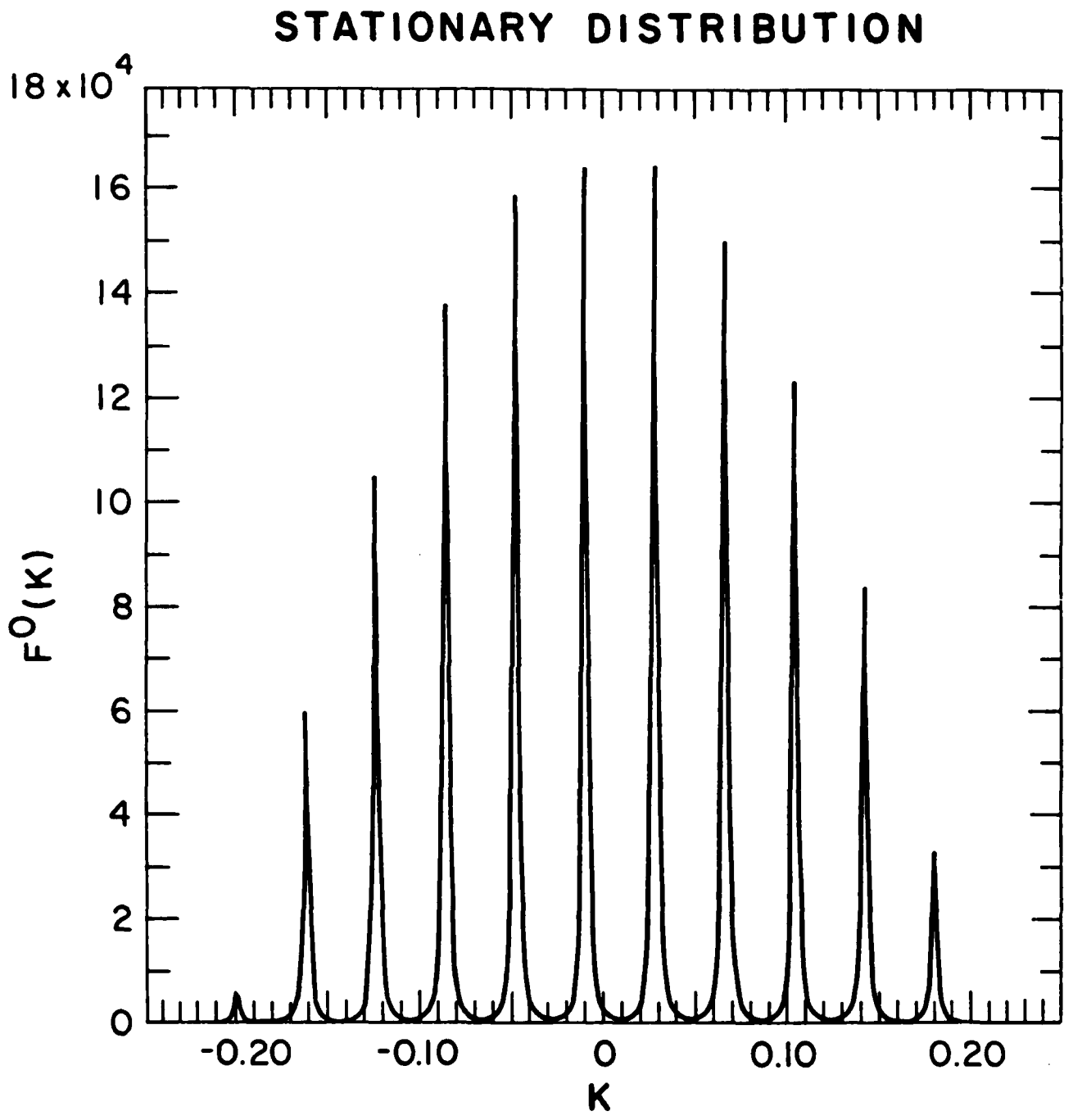
STATIONARY DISTRIBUTION
18 x 10^4
16
14
12
10
8
6
4
2
0
F^O(K)
-0.20
-0.10
0
0.10
0.20
K

Fig. 8

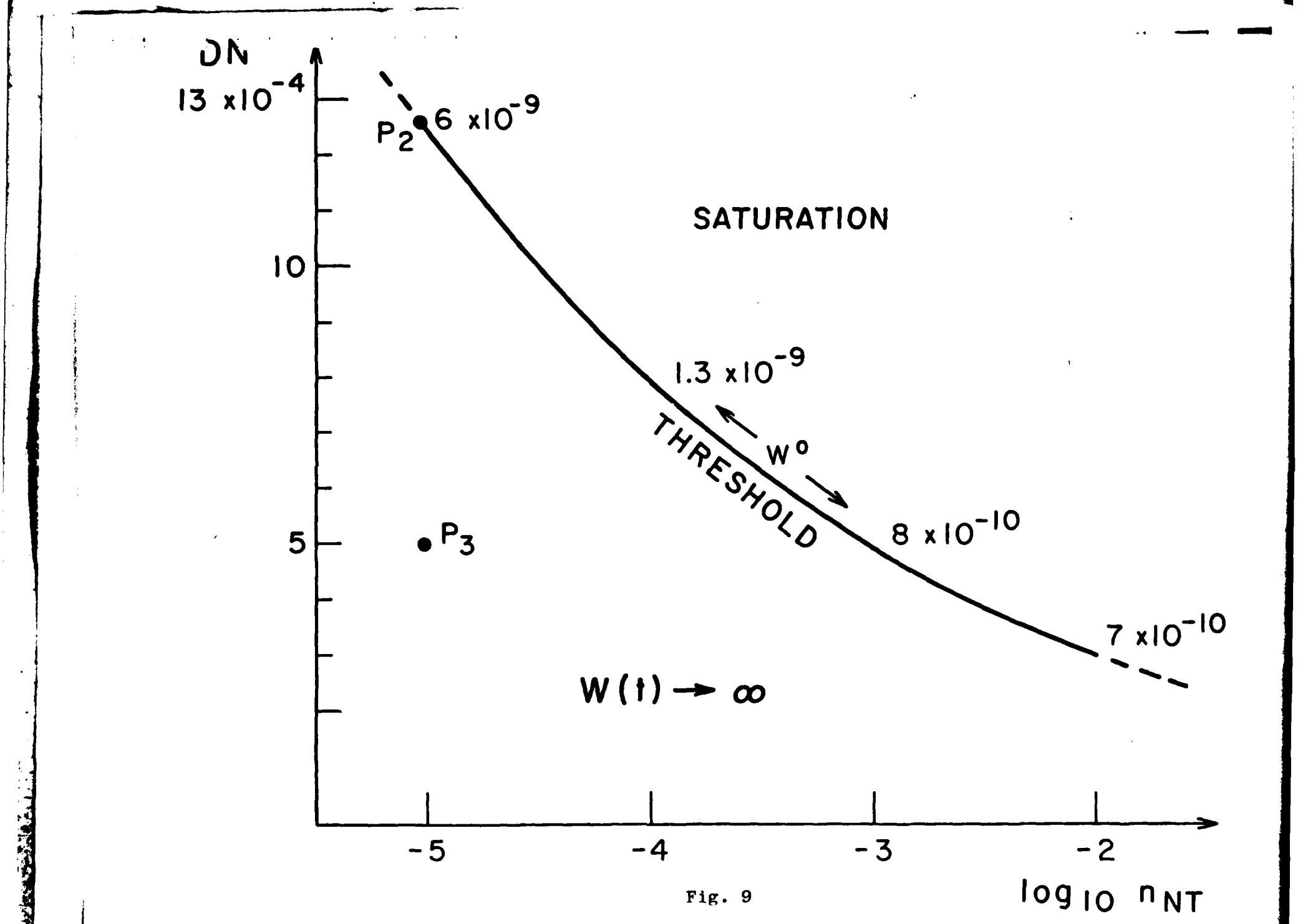
DN
13 x10^-4
10
5
P2
6 x10^-9
SATURATION
1.3 x10^-9
W°
THRESHOLD
8 x10^-10
7 x10^-10
P3
W(1) → ∞
-5
-4
-3
-2
log10 nNT

Fig. 9

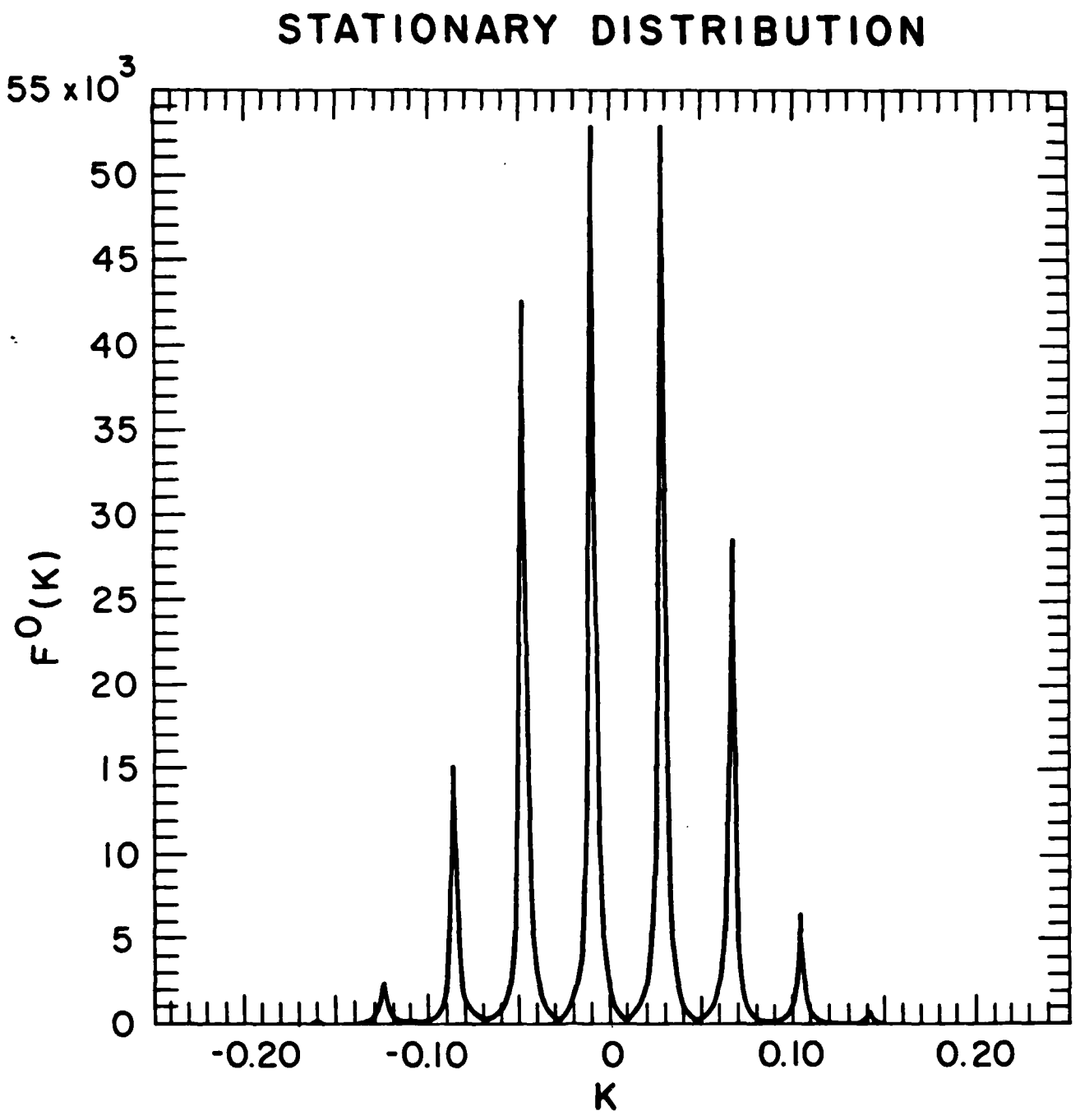
STATIONARY DISTRIBUTION
55 x10^3
50
45
40
35
30
25
20
15
10
5
0
F^0(K)
-0.20
-0.10
0
0.10
0.20
K

Fig. 10a

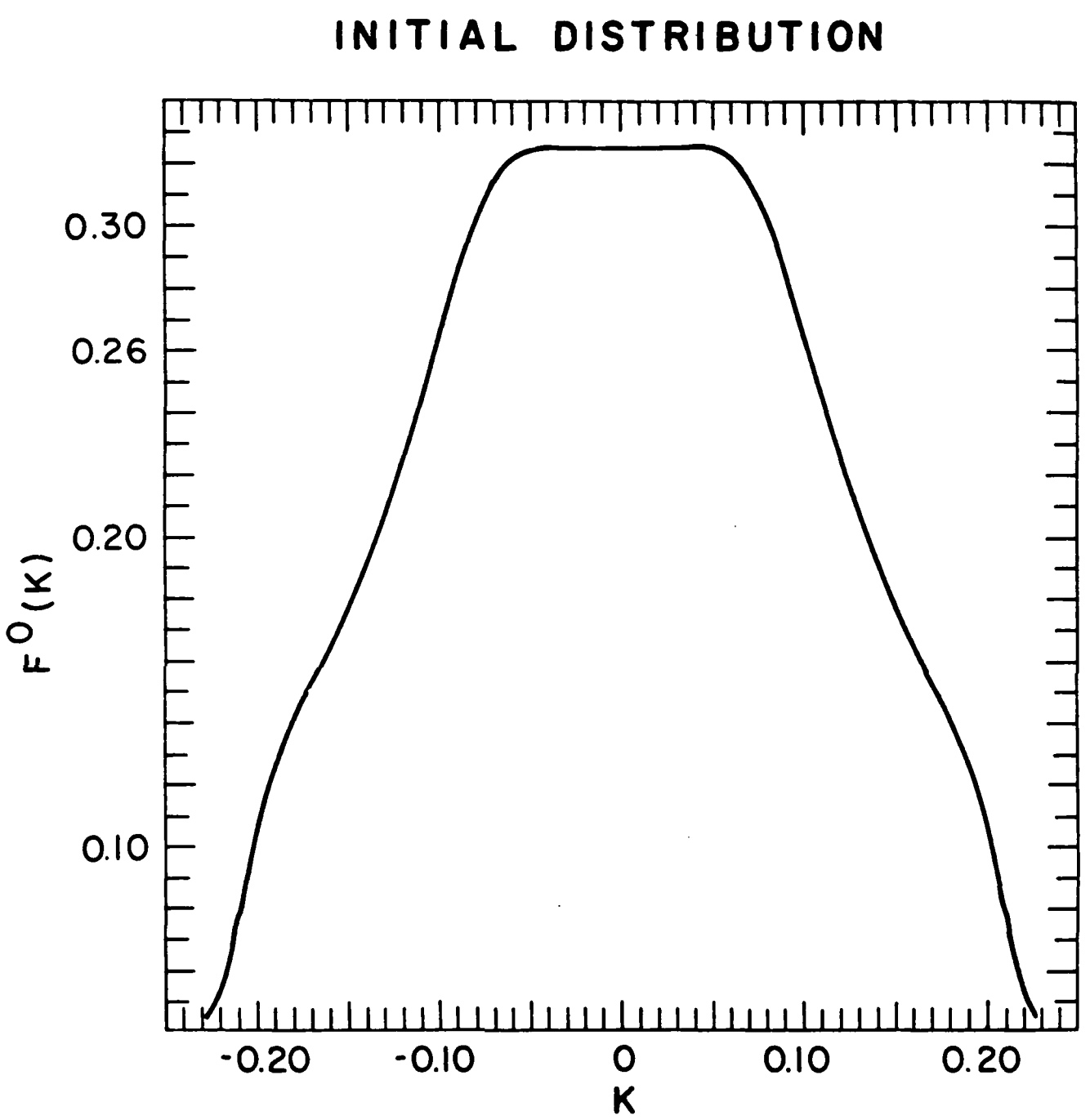

Fig. 10b

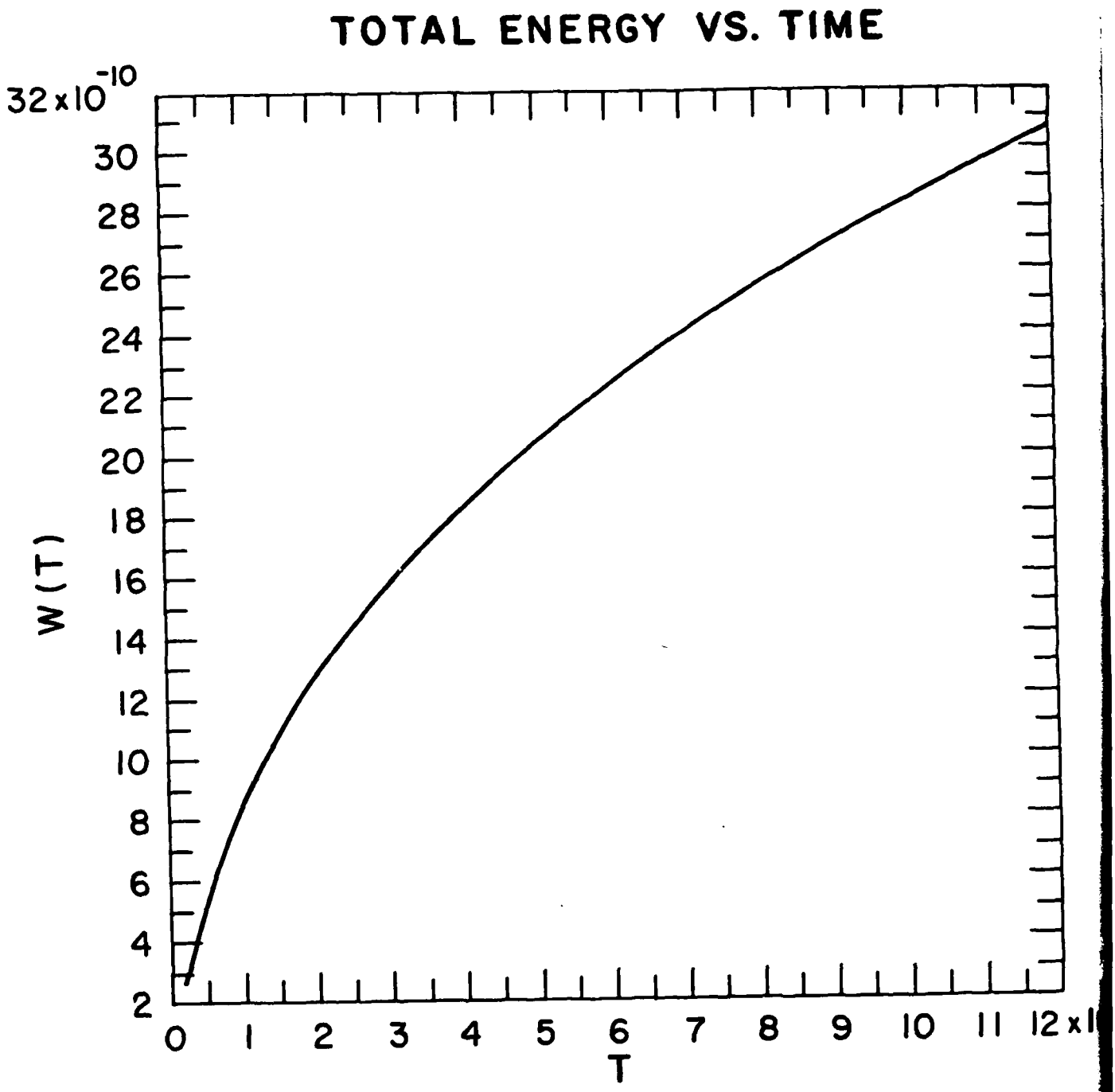
TOTAL ENERGY VS. TIME
32x10^-10
30
28
26
24
22
20
18
16
14
12
10
8
6
4
2
W(T)
0
1
2
3
4
5
6
7
8
9
10
11
12x1
T

Fig. 10c

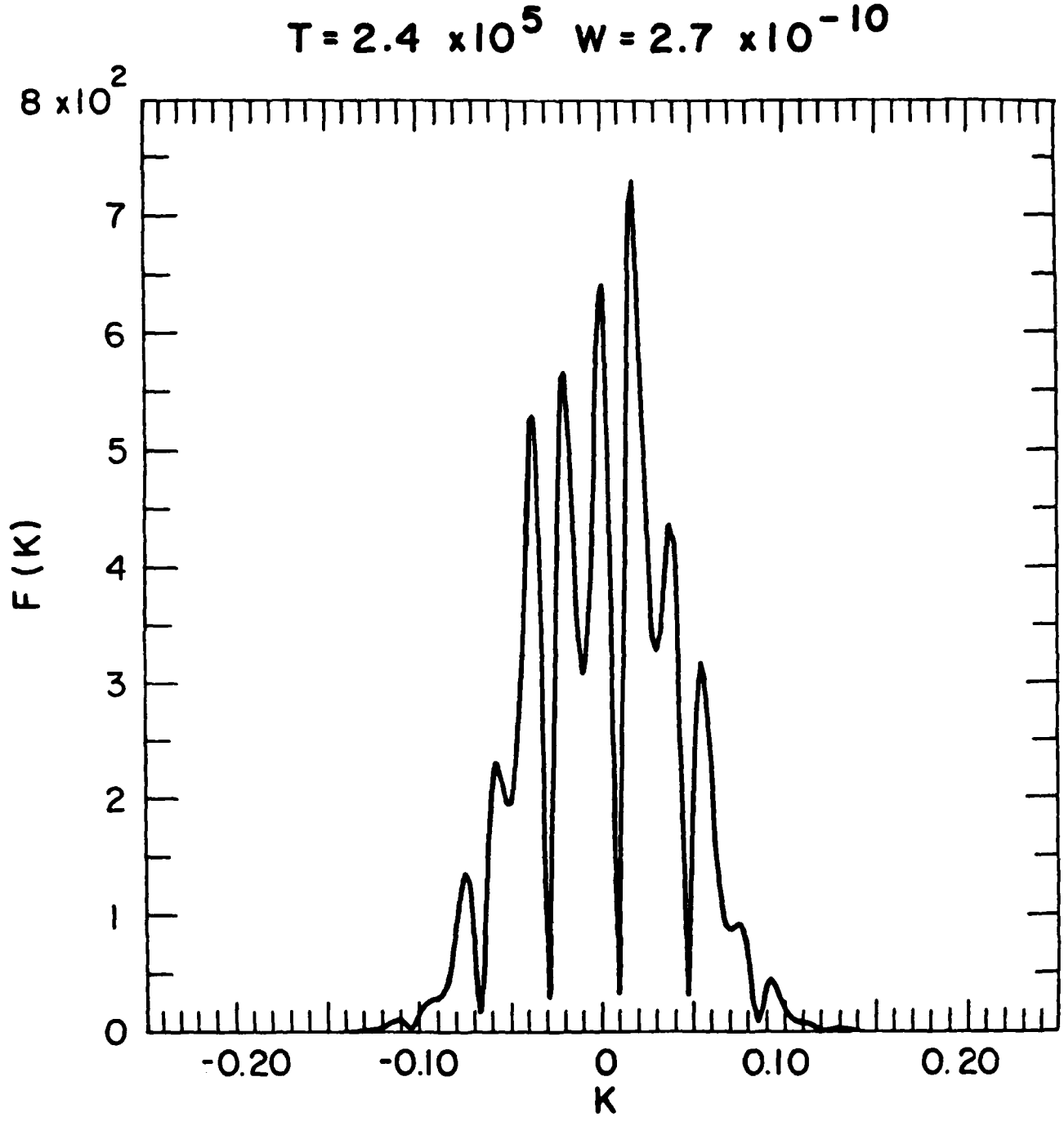

Fig. 10d

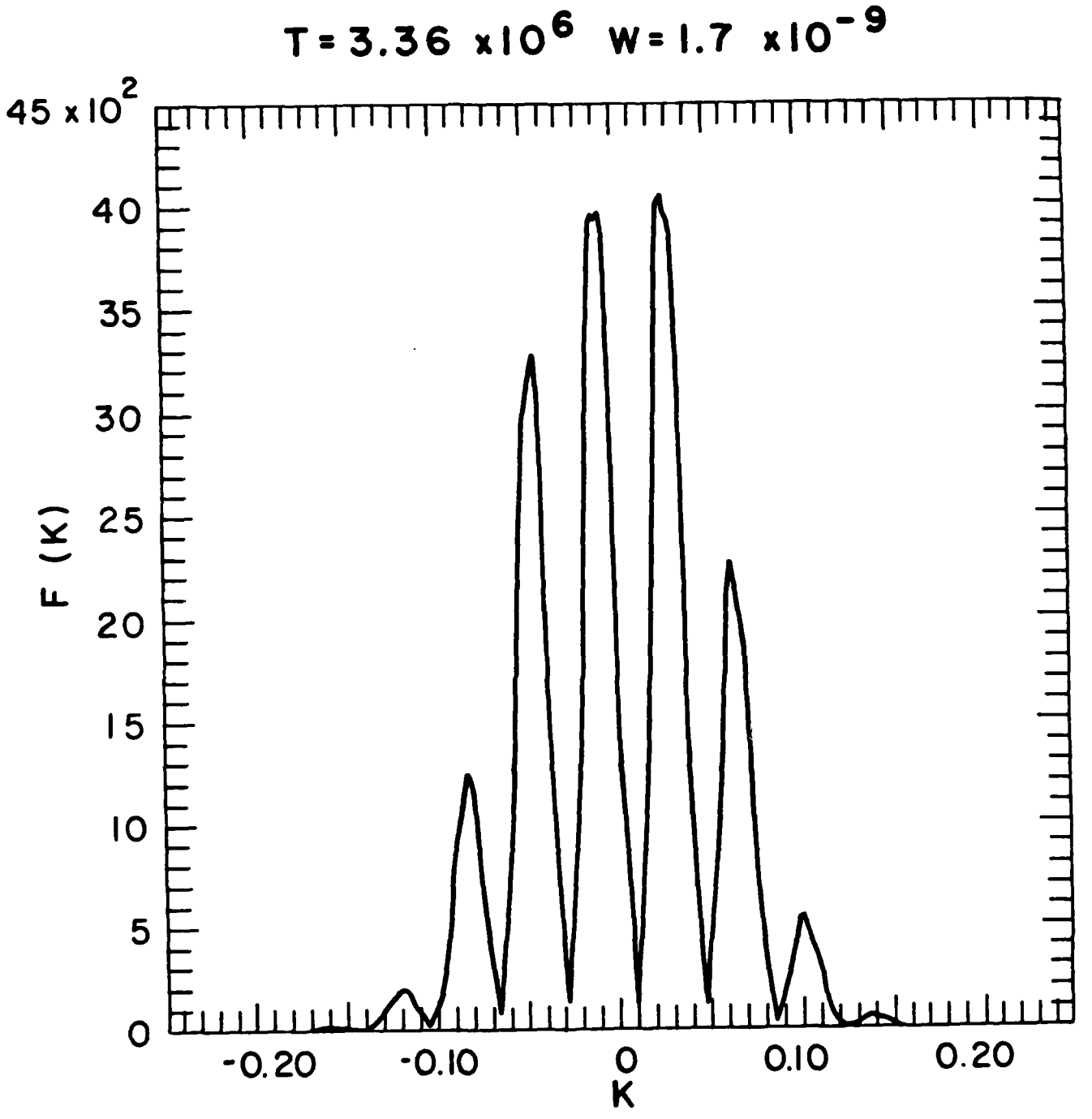
T = 3.36 x10^6 W = 1.7 x10^-9
45 x10^2
40
35
30
25
20
15
10
5
0
F (K)
-0.20
-0.10
0
0.10
0.20
K

Fig. 10e

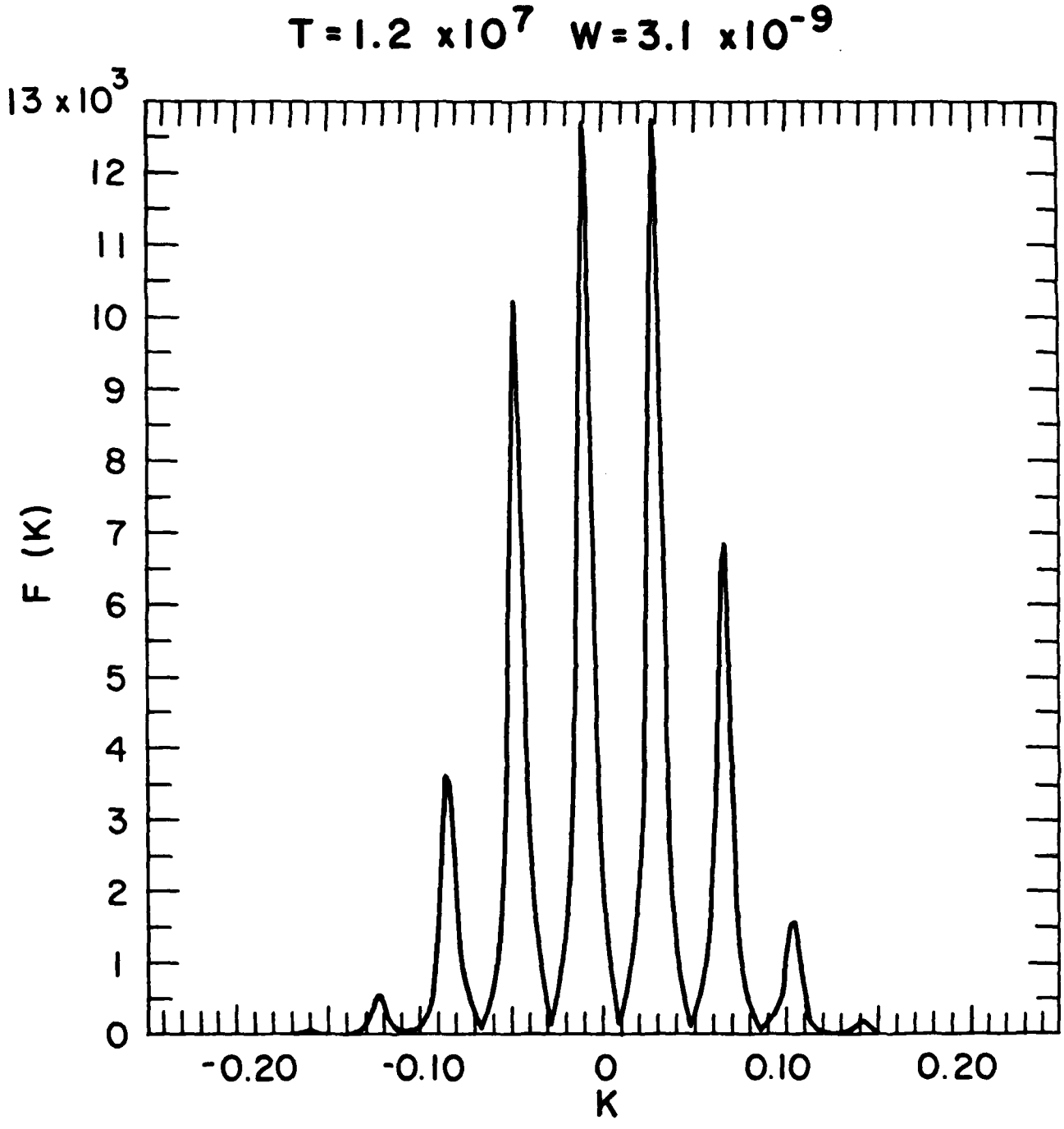
T = 1.2 x10^7 W = 3.1 x10^-9
13 x10^3
12
11
10
9
8
7
6
5
4
3
2
1
0
F (K)
-0.20
-0.10
0
0.10
0.20
K

Fig. 10f

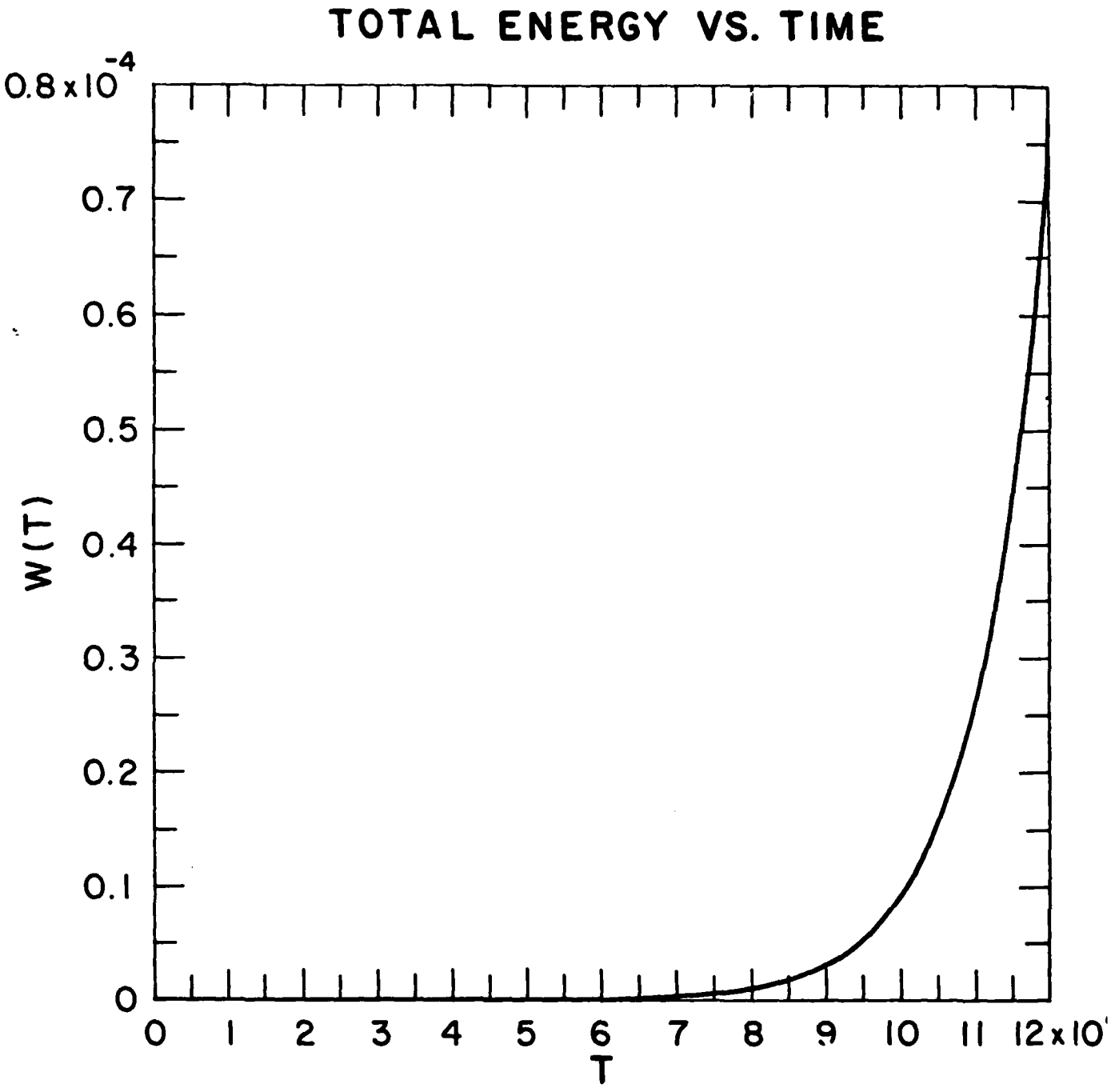
TOTAL ENERGY VS. TIME
0.8 x 10^-4
0.7
0.6
0.5
0.4
0.3
0.2
0.1
0
W(T)
0 1 2 3 4 5 6 7 8 9 10 11 12 x 10
T

Fig. 11a

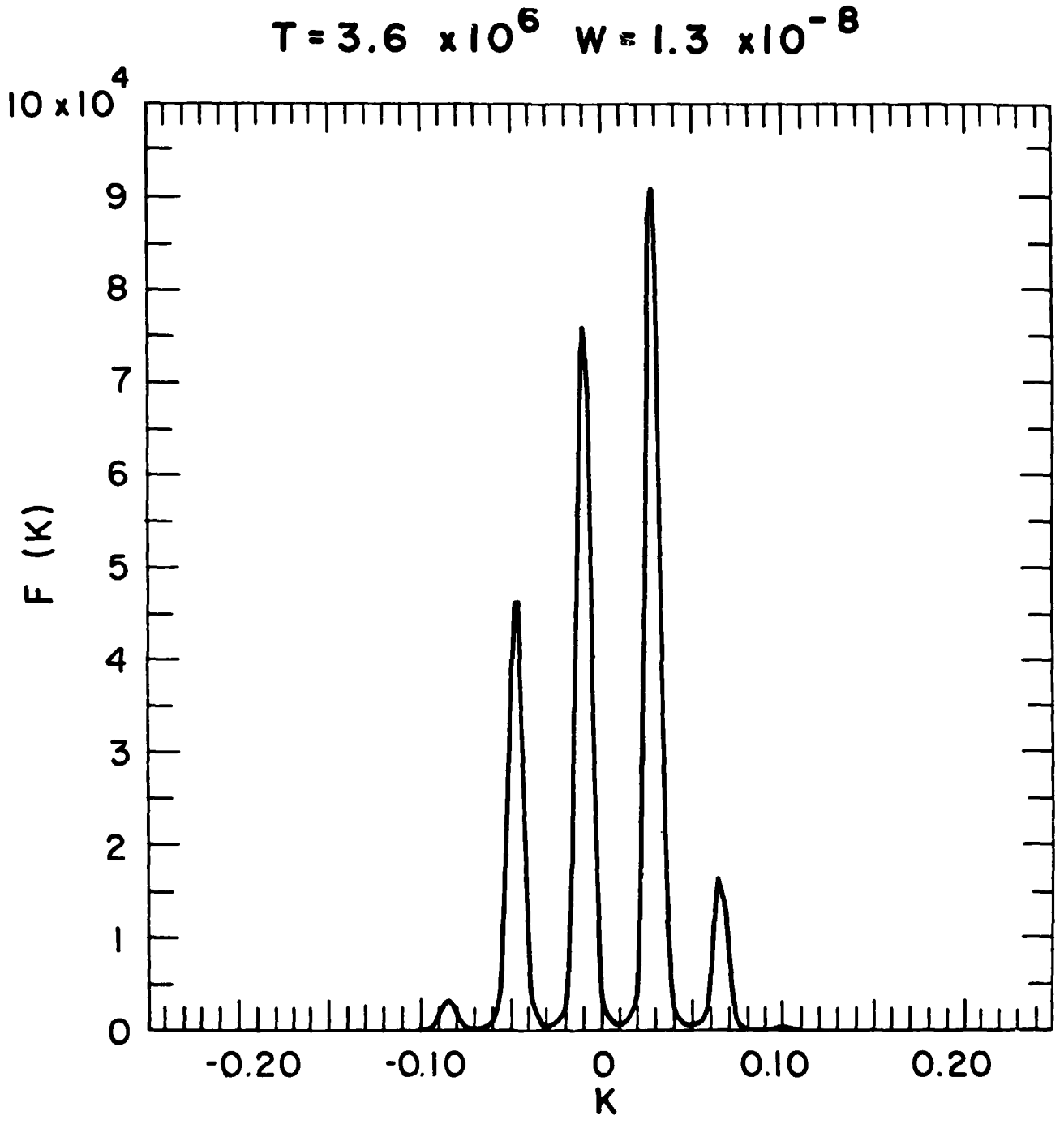

Fig. 11b

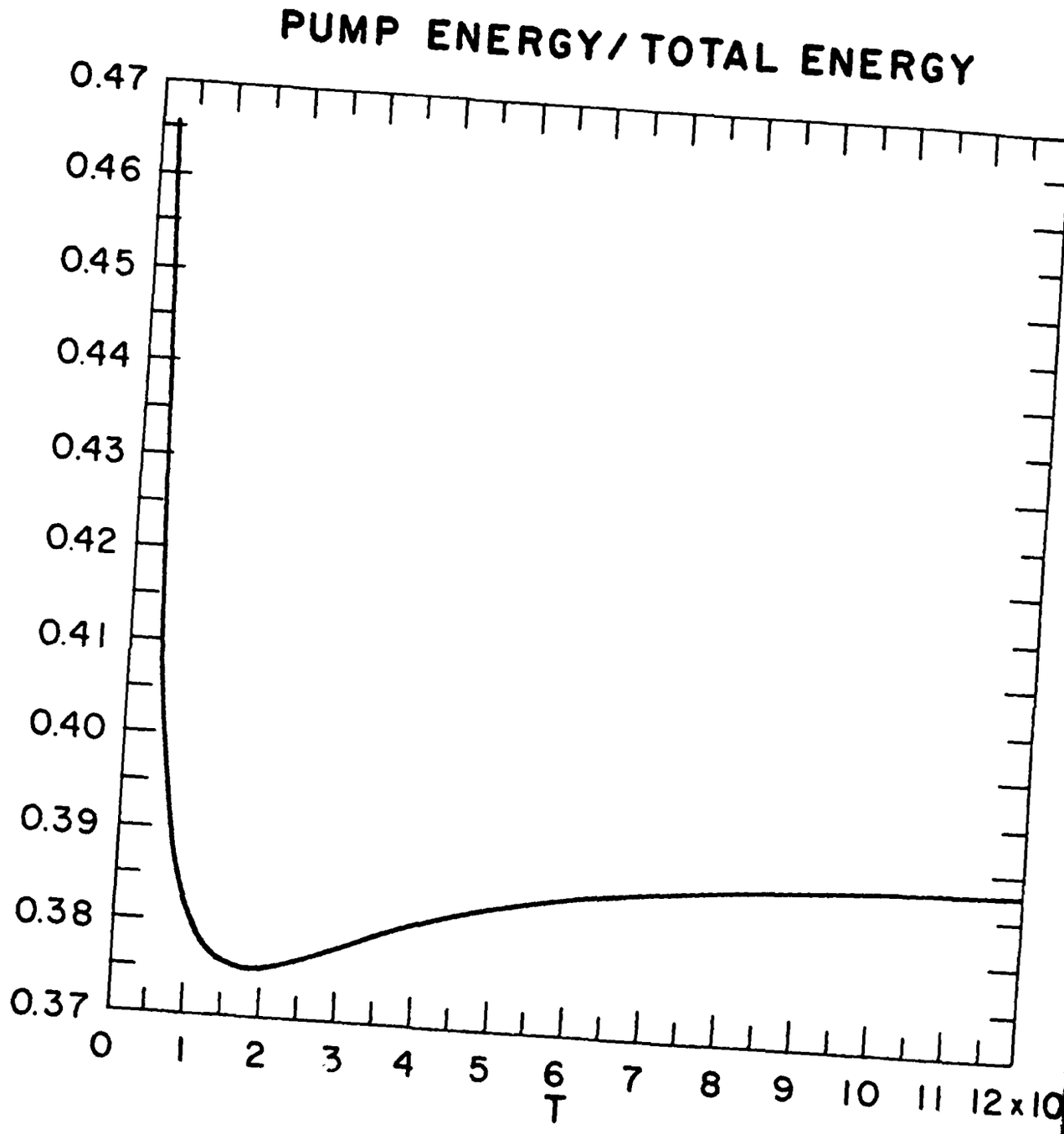
PUMP ENERGY/ TOTAL ENERGY
0.47
0.46
0.45
0.44
0.43
0.42
0.41
0.40
0.39
0.38
0.37
0
1
2
3
4
5
6
7
8
9
10
11
12x10
T

Fig. 11c

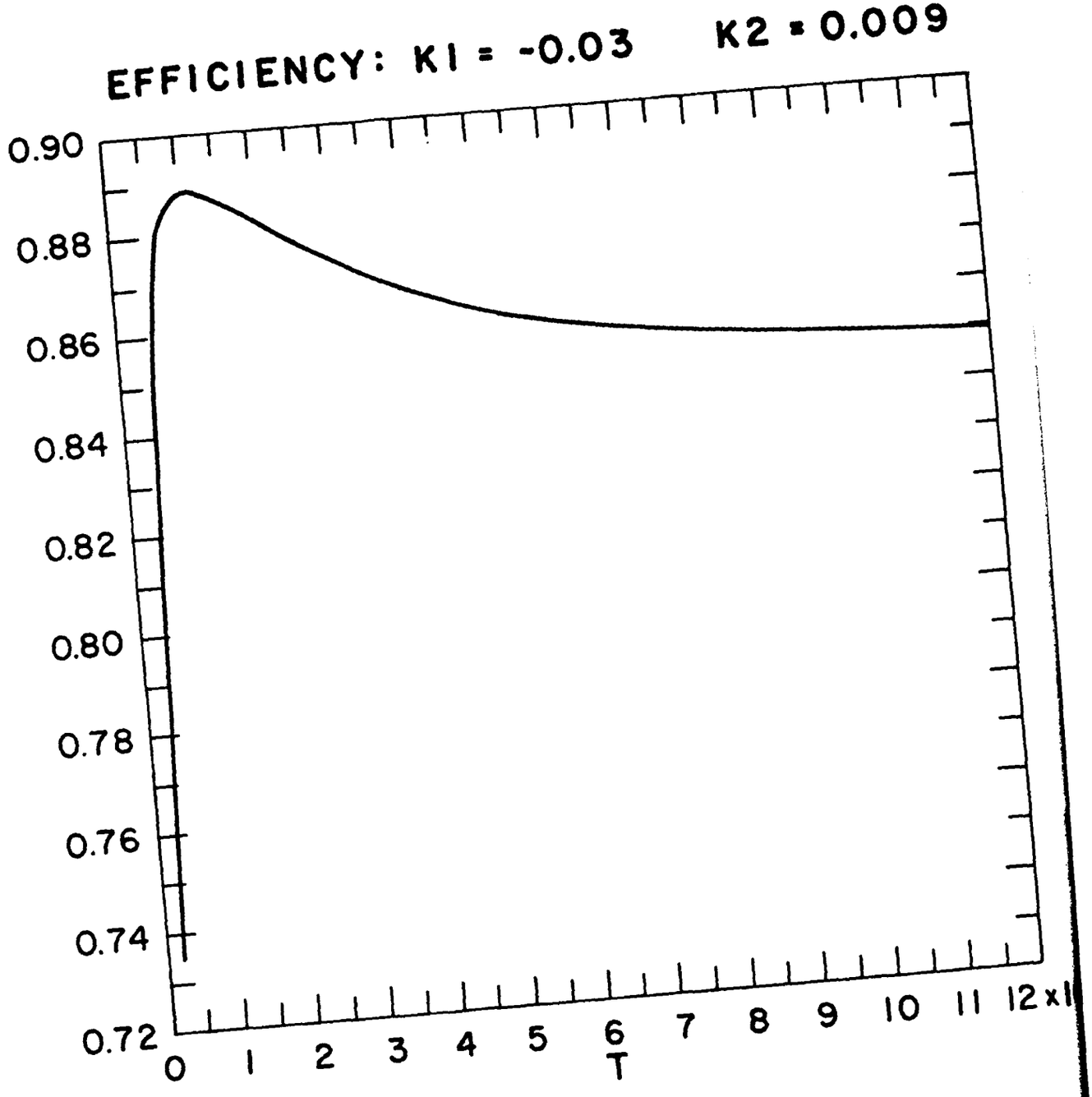
EFFICIENCY: K1 = -0.03 K2 = 0.009
0.90
0.88
0.86
0.84
0.82
0.80
0.78
0.76
0.74
0.72
0 1 2 3 4 5 6 7 8 9 10 11 12 x1
T

Fig. 11d

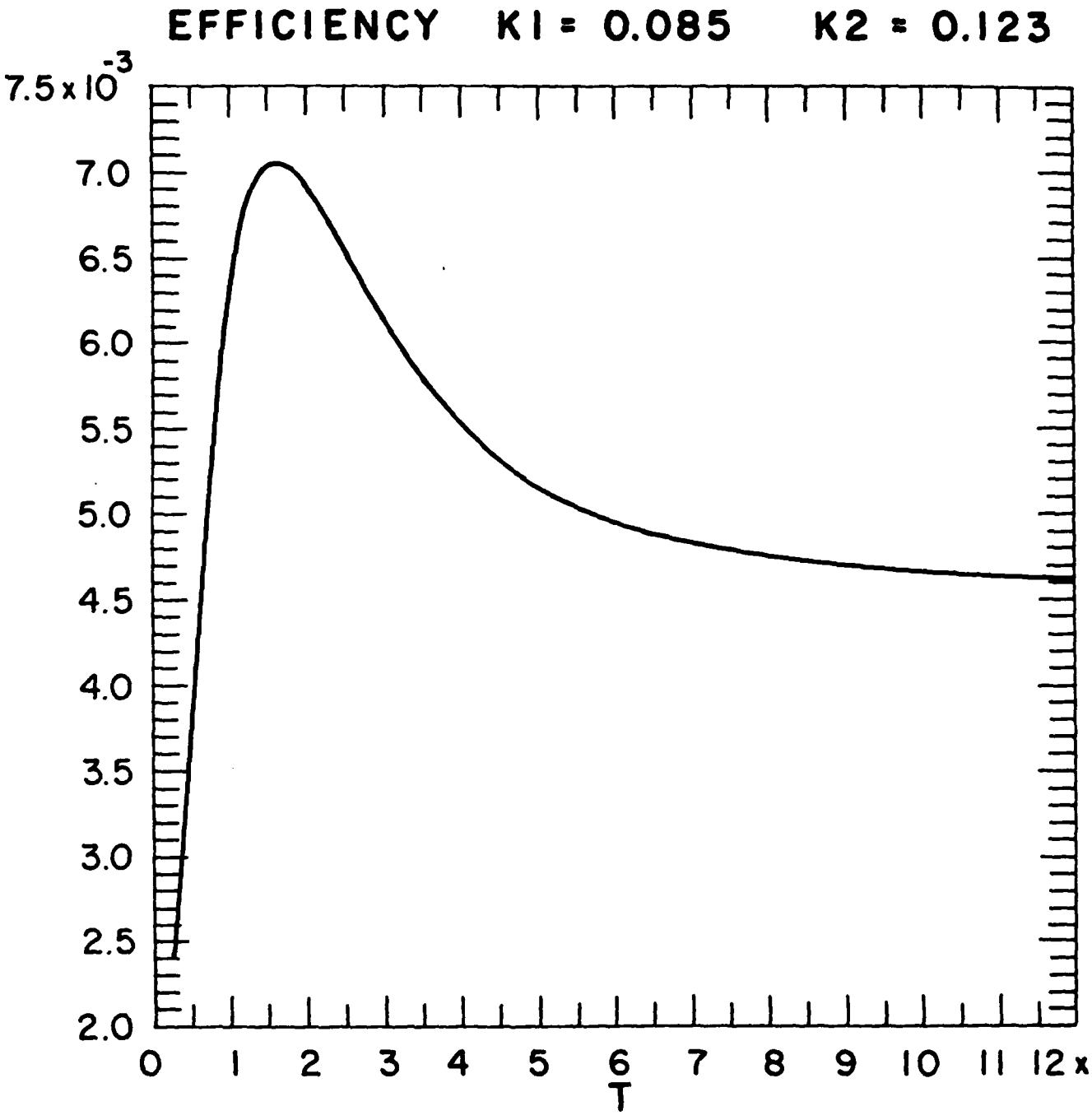
EFFICIENCY K1 = 0.085 K2 = 0.123
7.5 x 10^-3
7.0
6.5
6.0
5.5
5.0
4.5
4.0
3.5
3.0
2.5
2.0
0 1 2 3 4 5 6 7 8 9 10 11 12 x
T

Fig. 11e

APPENDIX D

D. "Preliminary Results Concerning Compton Conversion of Langmuir Waves into High Frequency Electromagnetic Waves in the Presence of an Ultra Relativistic Electron Beam"

David Newman
Preliminary report

PRELIMINARY RESULTS CONCERNING COMPTON CONVERSION OF LANGMUIR WAVES INTO HIGH FREQUENCY TRANSVERSE ELECTROMAGNETIC WAVES IN THE PRESENCE OF AN ULTRA RELATIVISTIC ELECTRON BEAM

David Newman

If a relativistic electron beam is injected into a plasma with a distribution of Langmuir waves, the Langmuir waves may scatter off electrons in the beam and in the process will be converted into transverse waves. Except for the conversion from longitudinal to transverse waves, this process is analogous to so-called inverse compton scattering. As a result of the kinematics of the scattering, the emitted transverse waves are strongly beamed in the forward direction (i.e. the direction of the beam electrons) and will have a frequency $\omega \gtrsim \gamma^2 \omega_{p_e}$ where $\gamma = \frac{E}{m_e c^2}$ is the relativistic parameter of the electrons (E is the energy of a beam electron).

Figure 1 depicts a typical scattering in the lab frame. The electron beam is taken to travel in the +x direction. The

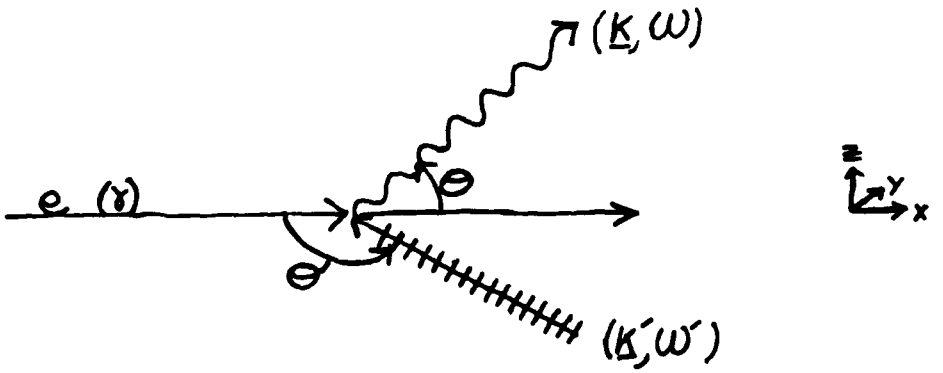

Fig. 1 Scattering geometry in lab frame. Langmuir wave ($\underline{k}'$,ω') scatters off electron in beam at angle θ' producing transverse wave ($\underline{k}$,ω) at angle θ. Electron experiences negligible recoil.

incident Langmuir wave has frequency ω' and a wave vector $\underline{k}'$ and is at angle θ' relative to the beam. The outgoing transverse wave is similarly characterized by ω, $\underline{k}$, and θ. (Properties of the incident wave will always be denoted by a ' superscript.) The z-axis will be chosen so that the scattered wave lies in the x-z plane (with $k_z > 0$). There is then another parameter of the scattering, namely the azimuthal angle about the beam axis between incident and scattered wave vectors, ϕ'. ϕ' is defined so that

$$\frac{k'_z}{|k'|} = \cos\phi'; \qquad \frac{k'_y}{|k'|} = \sin\phi'$$

It will be assumed that the frequency of the transverse wave $\omega >> \omega_p$ so that the dispersion relation is approximately that for photons in vacuum, i.e. $\omega = ck$ (from this point on, c will be set to 1). Thus, the scattered wave is characterized only by ω and θ.

In order to determine the scattered flux as a function of θ for a particular incident Langmuir wave, it is simplest to transform the scattering into a frame moving with the beam electrons. In this frame, the Langmuir wave scatters off of a stationary electron (see Figure 2). As argued by Gailitis and Tsytovich,[1] if the electron beam is ultra relativistic (i.e. $\gamma >> 1$), then scattering of Langmuir waves off of the bare electron is the only process which need be considered. (For a non-relativistic electron, scattering off the Debye cloud of the electron must be considered.)

[1] A. Gailitis & V.N. Tsytovich, Sov. Phys. JETP, 19, 1165 (1964).

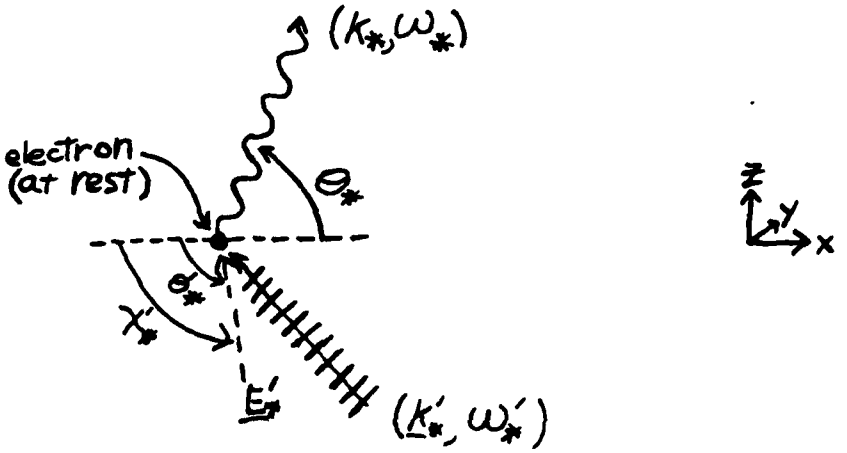

Fig. 2 Scattering geometry in electron frame. $\underline{E}'_*$, the electric field vector of the incident Langmuir wave, is no longer parallel to the wave vector $\underline{k}'_*$, but forms an angle, χ'_*, with the x(beam)-axis

The (*) subscripts in Figure 2 will be used to denote quantities in the electron rest frame. As depicted, the electric field in the electron rest frame of the Langmuir wave is no longer longitudinal, but forms an angle χ'_* with the x axis ($\chi'_* \neq \theta'_*$). An expression for χ'_* will be given below. In the Lorentz transformation, the Langmuir wave also picks up a transverse B field. However, the dipole approximation for the interaction of the electron with the fields of the incident wave will be used and the effect of the B field will be small relative to that of the E field.

The quantities in the two reference frames are related by the following relations (Lorentz transformations)

$$\omega'_* = \gamma(\omega' - \beta k' \cos\theta')$$

$$E'_{x_*} = E'_x = E'\cos\theta'$$

$$E'_{y_*} = \gamma E'_y = \gamma E'\sin\theta'$$

$$\tan\chi'_* = \frac{E'_{y_*}}{E'_{x_*}} = \gamma\tan\theta'$$

$$|E'_*|^2 = (\cos^2\theta' + \gamma^2\sin^2\theta')|E'|^2$$

$$\omega_* = \gamma\omega(1 - \beta\cos\theta)$$

$$\omega = \gamma\omega_*(1 + \beta\cos\theta_*)$$

$$\text{note: } \beta^2 = 1 - \frac{1}{\gamma^2}$$

The situation depicted in Figure 2 is that of classical Thompson scattering with the electron oscillating in the incident electric field and emitting electric dipole radiation. The classical formula holds provided there is negligible electron recoil (i.e. $h\omega'_* << m_e c^2$). By kinematics, $\omega'_* \sim \gamma\omega_p$, thus this condition is satisfied provided $\gamma \lesssim \frac{10^{20}s^{-1}}{\omega_p}$ which is essentially always the case.

The Thompson formula for the power radiated (per unit solid angle) in the electron rest frame is:

$$\frac{dP_*}{d\Omega_*} = r_o^2\sin^2\delta_* \frac{|E'_*|^2}{4\pi}$$

where $r_o = \frac{e^2}{mc^2}$ (the classical electron radius) and δ_* is the angle between in incident electric field and the scattered wave vector $\underline{k}_*$ (see Figure 3).

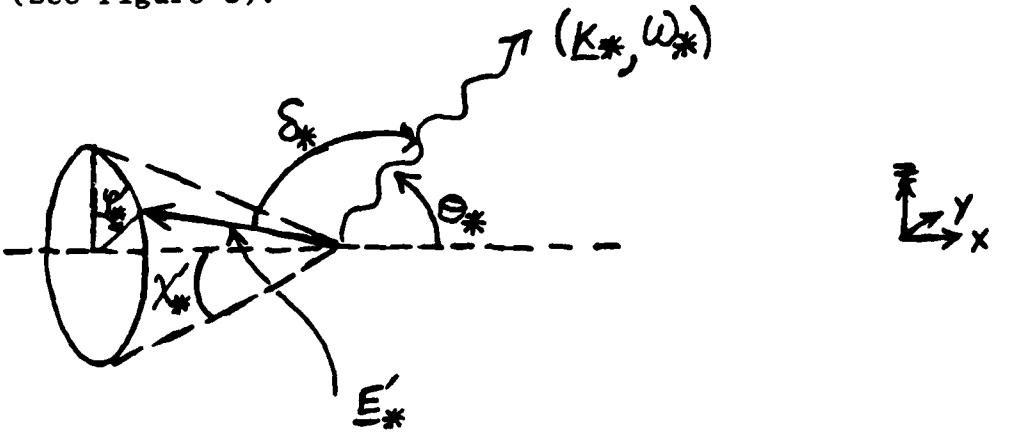

Fig. 3 Incident electric field vector $\underline{E}'_*$ lies on a cone of half opening angle χ'_* with azimuthal angle ϕ'_*. δ_* is the angle between $\underline{E}'_*$ and the wave vector of the emitted transverse wave $\underline{k}_*$ (note: $\underline{k}_*$ lies in the x-z plane)

$$\sin^2\delta_* = (1 - \cos^2\chi'_*\cos^2\theta_* - \sin^2\chi'_*\sin^2\theta_*\cos^2\phi'_* - $$
$$- 2\cos\chi'_*\cos\theta_*\sin\chi'_*\sin\theta_*\cos\phi'_*)$$

The Langmuir wave spectrum will be assumed to be azimuthally symmetric about the beam axis. Thus, $\sin^2\delta_*$ can be replaced by $\overline{\sin^2\delta_*}$ averaged over azimuthal angle ϕ'_*

$$\overline{\sin^2\delta_*} = \frac{1}{2\pi}\int_0^{2\pi} d\phi'_*\sin^2\delta_* = (1 - \cos^2\chi'_*\cos^2\theta_* - \frac{1}{2}\sin^2\chi'_*\sin^2\theta_*)$$

Defining $W_{\underline{k}'} = \frac{|E'|^2}{4\pi}$ as the energy density in the incident Langmuir wave in the lab frame, the power radiated per unit solid angle in the electron rest frame can be expressed as

$$\frac{dP_*}{d\Omega_*} = r_o^2\,\overline{\sin^2\delta}\;W_{\underline{k}'}\,\frac{|E'_*|^2}{|E'|^2}$$

$$= r_o^2 W_{\underline{k}'}(1 - \cos^2\chi'_*\cos^2\theta_* - \tfrac{1}{2}\sin^2\chi'_*\sin^2\theta_*)(\cos^2\theta' + \gamma^2\sin^2\theta')$$

Using $\tan\chi'_* = \gamma\tan\theta'$

$$\cos^2\chi'_*(\cos^2\theta' + \gamma^2\sin^2\theta') = \frac{\cos^2\theta' + \gamma^2\sin^2\theta'}{1 + \dfrac{\gamma^2\sin^2\theta'}{\cos^2\theta'}} = \cos^2\theta'$$

$$\sin^2\chi'_*(\cos^2\theta' + \gamma^2\sin^2\theta') = \frac{\cos^2\theta' + \gamma^2\sin^2\theta'}{1 + \dfrac{\cos^2\theta'}{\gamma^2\sin^2\theta'}} = \gamma^2\sin^2\theta'$$

Therefore,

$$\frac{dP_*}{d\Omega_*} = r_o^2 W_{\underline{k}'}(\cos^2\theta' + \gamma^2\sin^2\theta' - \cos^2\theta'\cos^2\theta_* - \tfrac{1}{2}\gamma^2\sin^2\theta'\sin^2\theta_*)$$

$$= r_o^2 W_{\underline{k}'}\left[\cos^2\theta'(1 - \cos^2\theta_*) + \gamma^2\sin^2\theta'(1 - \tfrac{1}{2}\sin^2\theta_*)\right]$$

The radiated power in the lab frame $\frac{dP}{d\Omega}$ can be expressed in terms of $\frac{dP_*}{d\Omega_*}$

$$\frac{dP(\theta,\phi)}{d\Omega} = \frac{|E(\ )|^2}{|E_*(\theta_*[\theta])|^2} \frac{dP_*(\theta_*[\theta],\phi)}{d\Omega_*}$$

since the Poynting flux is $\propto |E|^2$.

For a photon in vacuum, the magnitude of the E field Lorentz transforms like ω. Therefore

$$\frac{|E|^2}{|E_*|^2} = \frac{\omega^2}{\omega_*^2} = \frac{1}{\gamma^2(1 - \beta\cos\theta)^2}$$

Combining this with the previous expression for $\frac{dP_*}{d\Omega_*}$ and using:

$$\sin^2\theta_* = \frac{\sin^2\theta}{\gamma^2(1 - \beta\cos\theta)^2}$$

yields for the power radiated in the lab frame

$$\frac{dP}{d\Omega} = \frac{r_o^2 W_{\underline{k}'}}{2\gamma^4(1 - \beta\cos\theta)^4} \left[2\cos^2\theta'\sin^2\theta + \gamma^2\sin^2\theta'\left\{2\gamma^2(1 - \beta\cos\theta)^2 - \sin^2\theta\right\}\right.$$

Up to now, only the interaction of a single electron (characterized by γ) and one Langmuir wave (characterized by ω_p, k', θ', ϕ', $W_{\underline{k}'}$) has been considered.

Now, the effect of a beam of electrons (with distribution function $f(\varepsilon)$, but still uni-directional), and a distribution of Langmuir waves with $W_{\underline{k}'} \rightarrow \hat{W}(k',\theta')$ being the energy density per unit volume of moment ($\underline{k}'$) space will be treated.

If instead of a single Langmuir wave with energy density $W_{\underline{k}}$, there is a distribution of Langmuir waves with energy density per unit volume momentum space $\hat{W}(k',\theta')$, then what was previously referred to as $\frac{dP}{d\Omega}$ now becomes $\frac{dP}{d\Omega d\Omega' k'^2 dk'}$, i.e.

$$\frac{dP}{d\Omega d\Omega' k'^2 dk'} = \frac{r_o^2 \hat{W}(k',\theta')}{2\gamma^4(1-\beta\cos\theta)^4}\left[2\cos^2\theta'\sin^2\theta+\gamma^2\sin^2\theta'\left\{2\gamma^2(1-\beta\cos\theta)^2-\sin^2\theta\right\}\right]$$

In order to calculate e.g. induced emission probabilities, it is necessary to know the power radiated per unit volume of phase space (this will be proportional to dN_ω/dt where N_ω is the phase space density of photons.)

The power radiated per unit volume of phase space is

$$\frac{1}{\omega^2}\frac{dP}{d\Omega d\omega} = \frac{1}{\omega^2}\int_0^{2\pi} d\phi' \int dk' k'^2 \frac{dP}{d\Omega k'^2 dk' d\phi' d\cos\theta'} \left|\frac{d\cos\theta'}{d\omega}\right|$$

where $\frac{d\cos\theta'}{d\omega}$ is determined from the kinematic constraints

$$\gamma(\omega' - \beta k'\cos\theta') = \omega'_* = \omega_* = \gamma\omega(1 - \beta\cos\theta)$$

with θ, k', ω' held constant.

Thus $\left.\frac{d\cos\theta'}{d\omega}\right|_{k',\theta} = \frac{-(1 - \beta\cos\theta)}{\beta k'}$

$$\frac{1}{\omega^2}\frac{dP}{d\Omega d\omega} = \frac{\pi r_o^2}{\omega^2\gamma^4(1 - \beta\cos\theta)^3}\int k'dk'\hat{W}(k',\theta')\left[2\cos^2\theta'\sin^2\theta + \gamma^2\sin^2\theta'\left\{2\gamma^2(1 - \beta\cos\theta)^2 - \sin^2\theta\right\}\right]$$

Here θ' is no longer an independent variable, but is a function of ω,θ and k',ω'.

At this point, two simplifying assumptions will be introduced. Both of these assumptions will have to be relaxed when treating the case of an arbitrary Langmuir wave spectrum, but are employed here primarily in order to bring the situation treated here into correspondence with the case treated by Kaplan and Tsytovich.[2,3]

1. It will be assumed that the spectral density of Langmuir waves in the lab frame is isotropic. Thus:

$$\hat{W}(k',\theta') = \hat{W}(k') = \frac{W(k')}{4\pi k'^2}$$

Here W(k') is the Langmuir energy density per interval dk'.

2. It will be further assumed that the Langmuir waves have a phase velocity $\frac{\omega'}{k'} << c$ so that

$$\omega'_* = \gamma(\omega' - \beta k'\cos\theta') \cong -\beta\gamma k'\cos\theta'$$

Both of these assumptions would be invalid if the Langmuir spectrum were excited by the electron beam for then the Langmuir waves would be i) preferentially aligned with the beam (anisotropic), and ii) in resonance with the beam, i.e. $\omega' \cong \underline{k}'\cdot v$ where for relativistic electrons $v \cong c$. This is in contrast with assumption 2. This contradiction could only be avoided if there were some mechanism to scatter the resonant waves into a region of higher wave numbers. If the beam of relativistic electrons has an energy distribution

[2]S.A. Kaplan & V.N. Tsytovich, Sov. Phys. Uspekhi 12, 42 (1969)

[3]S.A. Kaplan & V.N. Tsytovich, Plasma Astrophysics, Pergamon Press, New York (1973)

$f(\varepsilon)$, $[\varepsilon = \gamma m_e]$ then the density of photons per volume of phase space will be generated at a rate (spontaneously)

$$\left.\frac{dN_\omega}{dt}\right|_{spont} = \int\left[\frac{(2\pi)^3}{\omega}\,\frac{1}{\omega^2}\,\frac{dP}{d\Omega d\omega}\right] f(\varepsilon)d\varepsilon$$

$$= \frac{2\pi^3 r_o^2}{\omega^3}\int \frac{dk'}{k'}\,W(k')\int d\varepsilon f(\varepsilon)\,\frac{1}{\gamma^4(1-\beta\cos\theta)^3}$$

$$\left[2\cos^2\theta'\sin^2\theta + \gamma^2\sin^2\theta'\left[2\gamma^2(1-\beta\cos\theta)^2 - \sin^2\theta\right]\right]$$

Once the rate of the spontaneous process is known, induced emission and reabsorption rates can be determined. In the interaction being considered, conservation of energy requires the electron after the scattering to have energy $\varepsilon_2 = \varepsilon + \omega' - \omega$ (note: $\hbar = 1$).

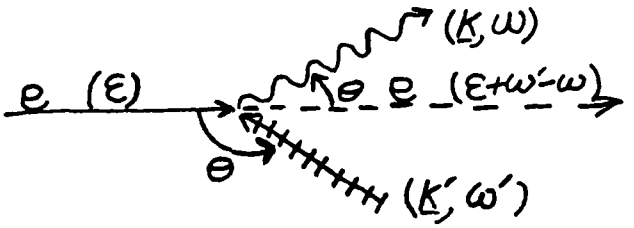

Fig. 4 Scattering geometry in lab frame showing change in the energy of recoil electron by the amount $(\omega'-\omega)$

Since the scattering of interest is that for which $\omega >> \omega'$, $\varepsilon_2 \cong \varepsilon - \omega$.

The electron will also be deflected through some angle δ, but $\delta_{max} \sim \frac{\gamma^2\omega'^2}{m^2c^4} \sim \frac{\gamma^2\omega_p^2}{10^{40}s^{-2}} <<< 1$ (this is similar to the condition for the scattering to be Thompson). This deflection angle can be safely ignored.

The inverse reaction to the one pictured above is:

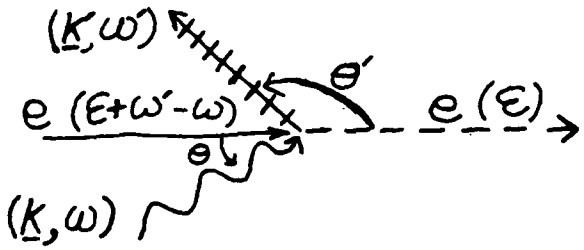

Fig. 5 Time reversed scattering process of the one pictured in Figure 4

Let the forward reaction have rate (spontaneous and induced)

$$R_+ = \int \sigma f(\varepsilon) N_{\underline{k}'} (1 + N_{\underline{k}}) d\varepsilon$$

and the reverse reaction have rate

$$R_- = \int \sigma f(\varepsilon-\omega) N_{\underline{k}} (1 + N_{\underline{k}'}) d\varepsilon$$

where σ is defined so that $\int \sigma f(\varepsilon) N_{\underline{k}'} d\varepsilon = \left.\frac{dN_{\underline{k}}}{dt}\right|_{spont}$

The total rate

$$\left.\frac{dN_{\underline{k}}}{dt}\right|_{tot} = R_+ - R_- = \int d\varepsilon \sigma \left[f(\varepsilon) N_{\underline{k}'} + \left(f(\varepsilon) - f(\varepsilon-\omega) \right) N_{\underline{k}'} N_{\underline{k}} - f(\varepsilon-\omega) N_{\underline{k}} \right]$$

Thus:

$$\left.\frac{dN_{\underline{k}}}{dt}\right|_{tot} \cong \left.\frac{dN_{\underline{k}}}{dt}\right|_{spont} + \int d\varepsilon \sigma \left[\omega \frac{\partial f}{\partial \varepsilon} N_{\underline{k}'} - f(\varepsilon-\omega) \right] N_{\underline{k}}$$

$$= \left.\frac{dN_{\underline{k}}}{dt}\right|_{spont} + \gamma^t N_{\underline{k}}$$

It will be assumed that $N_{\underline{k}'}$ is sufficiently large so that

$$\int d\varepsilon \sigma \omega \frac{\partial f}{\partial \varepsilon} N_{\underline{k}'} >> \int d\varepsilon \sigma f(\varepsilon-\omega)$$

i.e. the semiclassical approximation.

Then $\gamma^t \cong \int d\varepsilon \sigma\omega \frac{\partial f}{\partial \varepsilon} N_{\underline{k}'}$.

Thus, the expression for γ^t can be determined from the expression for $\left.\frac{dN_{\underline{k}}}{dt}\right|_{spont}$ by making the substitution

$$f(\varepsilon) \rightarrow \omega \frac{\partial f(\varepsilon)}{\partial \varepsilon}$$

For a distribution of Langmuir waves

$$\gamma^t = \frac{2\pi^3 r_o^2}{\omega^2} \int \frac{dk'}{k'} W(k') \int d\varepsilon \frac{\partial f(\varepsilon)}{\partial \varepsilon} \frac{1}{\gamma^4 (1 - \beta\cos\theta)^3} \left[2\cos^2\theta' \sin^2\theta \right.$$
$$\left. + \gamma^2 \sin^2\theta' \left(2\gamma^2 (1 - \beta\cos\theta)^2 - \sin^2\theta \right) \right]$$

Doing integration by parts on the ε integral and assuming $f(\varepsilon)\Big|_o^\infty = 0$

$$\gamma^t = \frac{4\pi^3 r_o^2}{\omega^2} \int \frac{dk'}{k'} W(k') \int d\varepsilon f(\varepsilon) \frac{\partial}{\partial \varepsilon} \left[\frac{1}{\gamma^4 (1 - \beta\cos\theta)^3} \left(\cos^2\theta' \sin^2\theta \right.\right.$$
$$\left.\left. + \gamma^2 \sin^2\theta' \left(2\gamma^2 (1 - \beta\cos\theta)^2 - \sin^2\theta \right) \right) \right]$$

$$\cos^2\theta' = \frac{\omega^2 (1 - \beta\cos\theta)^2}{k'^2} \qquad \sin^2\theta' = 1 - \frac{\omega^2 (1 - \beta\cos\theta)^2}{k'^2}$$

employing assumption 2, $\omega' << k'c$.

If $\gamma << 1$, then the majority of scattered waves will come out in the forward direction. (Essentially ½ of the radiation will come out in a cone of opening angle $\theta_o = \frac{1}{\gamma}$.)

Because of this beaming effect, a small angle approximation for θ can be employed ($\cos\theta \rightarrow (1 - \frac{\theta^2}{2})$, $\sin\theta \rightarrow \theta$) also, $\beta \cong 1 - \frac{1}{2\gamma^2}$

$$(1 - \beta\cos\theta) \cong \left[1 - (1 - \frac{1}{2\gamma^2})(1 - \frac{\theta^2}{2}) \right] = \tfrac{1}{2}(\frac{1}{\gamma^2} + \theta^2) - \tfrac{1}{4}\frac{\theta^2}{\gamma^2}$$

since $\theta \sim \frac{1}{\gamma} << 1$ the last term can be ignored.

$$(1 - \beta\cos\theta) \approx \frac{1}{2\gamma^2}\left[1 + (\theta\gamma)^2\right] = \frac{1}{2\gamma^2}(1 + \alpha^2) \qquad \text{(def of } \alpha\text{)}$$

γ^t now becomes

$$\gamma^t \approx \frac{-2\pi^3 r_o^2}{\omega^2}\int\frac{dk'}{k'}\,W(k')\int d\varepsilon f(\varepsilon)\,\frac{\partial}{\partial\varepsilon}\left[\frac{4\gamma^2}{(1+\alpha^2)^3}\left\{\gamma^2\left(1 - \frac{\omega^2(1+\alpha^2)^2}{4\gamma^4 k'^2}\right.\right.\right.$$

$$\left.\left.\left.\left(\frac{(1+\alpha^2)^2}{2\gamma^2} - \theta^2\right) + 4\left(\frac{\omega^2(1+\alpha^2)^2}{4\gamma^4 k'^2}\right)\theta^2\right\}\right]$$

$$= \frac{-2\pi^3 r_o^2}{\omega^2}\int\frac{dk'}{k'}\,W(k')\int d\varepsilon f(\varepsilon)\frac{\partial\varepsilon}{\varepsilon}\left[\frac{4\gamma^2}{(1+\alpha^2)^3}\left[\left(1 - \frac{\omega^2(1+\alpha^2)^2}{4\gamma^4 k'^2}\right)(1+\alpha^4)\right.\right.$$

$$\left.\left. + 4\left(\frac{\omega^2(1+\alpha^2)^2}{4\gamma^4 k'^2}\right)\theta^2\right]\right]$$

The above expression for γ^t can be compared with the expression found by Kaplan & Tsytovich [Sov. Phys.-Uspekhi 12, 42 (1969)] equation 8.24.

$$\gamma^t_{(K\&T)}\,[= -\mu(\omega,\theta)] = \frac{16\pi^3}{\omega^2}\,r_o^2\int W(k')\,\frac{dk'}{k'}\int d\varepsilon\,\frac{\partial f}{\partial\varepsilon}\,\frac{\gamma^2}{(1+\alpha^2)^4}$$

$$\left[\left(1 - \frac{\omega^2(1+\alpha^2)^2}{4\gamma^4 k'^2}\right)(1+\alpha^4) + \left(\frac{\omega^2(1+\gamma^2)^2}{\gamma^4 k'^2}\right)\alpha^2\right]$$

This differs from the result found above by:

1. an overall additional factor of $\dfrac{2}{(1+\alpha^2)}$
2. an additional factor of γ^2 in the last term.

Starting with

$$\gamma^t = \frac{-8\pi^3 r_o^2}{\omega^2}\int W(k')\,\frac{dk'}{k'}\int d\varepsilon f(\varepsilon)\,\frac{\theta}{m}\,\frac{\partial}{\partial\alpha}\,\frac{\alpha^2}{\theta^2(1+\alpha^2)^3}\left[(1+\alpha^4)\right.$$

$$\left. - \frac{\omega^2\theta^4}{4k'^2}\,\frac{(1+\alpha^2)^2(1+\alpha^4)}{\alpha^4} + \frac{\omega^2\theta^6}{k'^2}\,\frac{(1+\alpha^2)^2}{\alpha^4}\right]$$

which employs the fact that $\frac{d}{d\varepsilon} = \frac{\theta}{m}\frac{d}{d\alpha}$ where again $\alpha = \gamma\theta$.

Explicitly performing the differentiation:

$$\frac{1}{m\theta}\frac{\partial}{\partial\alpha}\left[\frac{\alpha^2(1+\alpha^4)}{(1+\alpha^2)^3} - \frac{\omega^2\theta^4}{4k'^2}\frac{(1+\alpha^4)}{4(1+\alpha^2)} + \frac{\omega^2\theta^6}{k'}\frac{1}{4(1+\alpha^2)}\right]$$

$$= \frac{1}{m\theta}\left[\frac{2\alpha}{(1+\alpha^2)^4}(3\alpha^4 - 2\alpha^2 + 1) - \frac{\omega^2\theta^6}{k'^2}\left(\frac{\alpha^4 - 2\alpha^2 - 1}{\alpha^3(1+\alpha^2)^2}\right) - \frac{2\omega^2\theta^6}{k'^2}\right.$$

$$\left.\left(\frac{2\alpha^2+1}{(1+\alpha^2)^2\alpha^3}\right)\right]$$

Recalling that $\cos^2\theta' = \frac{\omega^2(1-\beta\cos\theta)^2}{k'^2} \cong \frac{\omega^2(1+\alpha^2)^2}{4\gamma^4k'^2} = \frac{\omega^2(1+\alpha^2)^2\theta^4}{4\alpha^4k'^2}$

$$\frac{1}{m\theta}\frac{\partial}{\partial\alpha}[\quad]$$

$$= \frac{1}{m\theta}\left[\frac{2\alpha}{(1+\alpha^2)^4}\left[\left[(3\alpha^4 - 2\alpha^2 + 1) - (\alpha^4 - 2\alpha^2 - 1)u^2 - 4(2\alpha^2+1)\theta^2u^2\right]\right]\right]$$

where $u = \cos\theta' \qquad 0 \le u \le 1$

$$= \frac{2\varepsilon}{m_e^2}\left[\frac{1}{(1+\alpha^2)^4}\left[(3\alpha^4 - 2\alpha^2 + 1) - (\alpha^4 - 2\alpha^2 - 1)u^2 - 4(2\alpha^2+1)\theta^2u^2\right]\right]$$

The last term inside the brackets is much smaller than the first two because of the extra factor of θ^2 (by assumption $\theta << 1$) and is also of a lower power in α and will hence be further suppressed when $\alpha > 1 \rightarrow \theta > \frac{1}{\gamma}$.

Dropping this third term, the expression for γ^t now becomes:

$$\gamma^t = \frac{-16\pi^3r_o^2}{\omega^2m_e^2}\int W(k)\frac{dk'}{k'}\int d\varepsilon f(\varepsilon)\left[\frac{\varepsilon}{(1+\alpha^2)^4}\left[\alpha^4(3-u^2\gamma) - 2\alpha^2(1-u^2)\right.\right.$$

$$\left.\left. + (1+u^2)\right)\right]$$

If the electron distribution is concentrated at energy ε_*, then $f(\varepsilon) \equiv n_b \delta(\varepsilon - \varepsilon_*)$ where n_b is the electron density in the beam. In this case:

$$\gamma^t = \frac{-32\pi^3 r_o^2 n_b}{\omega^2 m_e^2} \int W(k') \frac{dk'}{k'} \varepsilon_* \left[\frac{1}{(1 + \alpha_*^2)^4} \left\{ \alpha_*^4 (3 - u^2) - 2\alpha_*^2 (1-u^2) + (1 + u^2) \right\} \right]$$

where $\alpha_* = \frac{\varepsilon_* \theta}{m}$

note: u is an implicit function of k' for given ω, θ, γ and must be kept under the k' integral.

There will be growth [$\gamma^t > 0$] if the expression in brackets becomes negative. This never occurs for any values of the parameters α and u.

This is in stark contrast to the result claimed by Kaplan and Tsytovich (plotted in Fig. 6; this corresponds to Fig. 3 from reference 2) although there is agreement within a factor of 2 with the value of γ^t at forward scattering ($\alpha \approx 0$) [Eq. 8.25, ref. 2].

It should be further noted that Fig. 6 does not seem to come directly from the integrand of (8.24). Differentiating the energy dependent terms in (8.24) yields

$$\gamma^t_{K\&T} = \frac{-32\pi^3 r_o^2}{\omega^2 m_e^2} \int W(k) \frac{dk'}{k'} \int d\varepsilon f(\varepsilon) \left[\frac{\varepsilon}{(1 + \alpha^2)^5} \left\{ (1 - \alpha^2)^3 + u^2(1 + 3\alpha^2 - 9\alpha^4 + \alpha^6) \right\} \right]$$

Although the sign of the term in brackets does reverse near $\alpha = 1$, the maximum value of $|\gamma^t|$ for $\gamma^t > 0$ is at most $\sim$7% the value of $|\gamma^t|$ at $\alpha = 0$ (when $\gamma^t < 0$). This occurs when $u^2 = 1$ (i.e. $\cos\theta' = 1$; Langmuir wave in line with electron beam traveling in opposite direction). When $u = 0$, $|\gamma^t > 0|_{max}$ <1% $|\gamma^t < 0|_{max}$. Thus, there seems to be no way to attain a maximum growth rate as large as the reabsorption rate at $\theta = 0$ which is implied by Fig. 6.

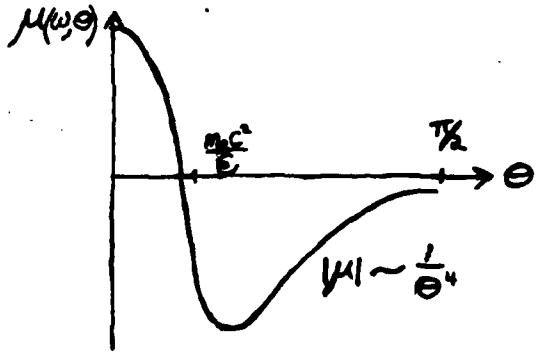

Fig. 6 Growth rate as function of angle from Kaplan & Tsytovich (Ref. 2 Fig. 3). Negative values imply growth ($\gamma^t \sim -\mu(\omega,\theta)$)

Conclusions and Tentative Results of Subsequent Investigation

It has been found that if the restriction $\omega_p << k_L c$ is imposed on the incident Langmuir wave spectrum, amplification via induced emission is impossible for all values of the scattering angles (θ' and θ). This is in contrast to the results cited by Kaplan and Tsytovich (Refs. 2 & 3), under the assumption $\omega_p << k_L c$ to the effect that growth will occur for transverse waves emitted at an angle $\theta \gtrsim 1/\gamma$ to the electron beam.

The restriction $\omega_p/k_L c << 1$ is physically unsuitable for beams which excite Langmuir waves with phase velocities near ω_p/c. We have relaxed this restriction and found a new expression for γ^t which has $\omega_p/k_L c$ as an additional parameter. Preliminary calculations indicate that growth ($\gamma^t > 0$) is possible for certain scattering geometries when $\omega_p^2/k_L c > 1$. All of the configurations yielding growth appear to require the incident Langmuir wave vectors to be parallel, or nearly parallel, to the electron beam. (Such a scattering configuration is kinematically forbidden when $\omega_p/k_L c < 1$.)

The maximum possible frequency for the emitted radiation due to the scattering of a Langmuir wave off a parallel electron beam is

$$\omega_{max} = \gamma^2 \omega' \cong \gamma^2 \omega_p$$

This maximum value is only attainable in the limit $\omega_p/k_L c >> 1$. Thus, the above scattering geometry is incapable of producing

emission at frequencies $\omega \gtrsim 3\gamma^2\omega_p$, such as may have been observed by Benford, in his relativistic beam experiments.

The complete determination of the induced emission growth coefficient $\gamma^t(\omega,\theta)$ requires an integration over the incident Langmuir wave spectrum. A particular spectrum, e.g. one resulting from beam induced Langmuir turbulence, must be specified. Such a spectrum would, in general, not be isotropic and would introduce an added element of complexity to the required integration. This integration would, however, have to be undertaken numerically even in the isotropic case for all but the simplest of Langmuir wave spectra.

Although growth is predicted for emission due to the scattering of Langmuir waves with wave vectors parallel to the beam axis, the contribution due to Langmuir waves coming from other directions (having a negative growth coefficient) will have the effect of reducing, or even reversing, the sign of the integrated growth rate. Thus, it is necessary to determine the Langmuir spectrum and perform the required integration in order to determine whether amplification due to induced emission is sufficient to produce the observed emission rates.

One other effect must be taken into account. The true electron beam is not unidirectional, but rather has an angular spread of $\sim 15°$ (in the experiment of Benford et al.). The beam spread will affect the growth rate calculations in two ways. First, the Langmuir wave spectrum generated by the beam will be modified, and second, the beam angular distribution must be integrated over. Consideration of beam spread effects could lead to further reduction or reversal of the growth rate.

APPENDIX E

E. "Solitons and Ionospheric Modification"

J.P. Sheerin, J.C. Weatherall, D.R. Nicholson, G.L. Payne, M.V. Goldman, and P.J. Hansen
Submitted to Journal of Atmospheric and Terrestrial Physics (March, 1982)

U. of Iowa 82-6

Solitons and Ionospheric Modification

J. P. SHEERIN,[1] J. C. WEATHERALL,[2] D. R. NICHOLSON,[1] G. L. PAYNE,[1] M. V. GOLDMAN,[2] and P. J. HANSEN[1]

Submitted to J. Atmos. Terr. Phys.

March 1982

[1]Department of Physics and Astronomy, University of Iowa, Iowa City, Iowa 52242, U.S.A.

[2]Astro-Geophysics Department, University of Colorado, Boulder, Colorado 80309, U.S.A.

ABSTRACT

The possibility of Langmuir soliton formation and collapse during ionospheric modification is investigated. Parameters characterizing former facilities, existing facilities, and planned facilities are considered, using a combination of analytical and numerical techniques. At a spatial location corresponding to the exact classical reflection point of the modifier wave, the Langmuir wave evolution is found to be dominated by modulational instability followed by soliton formation and three-dimensional collapse. The earth's magnetic field is found to affect the shape of the collapsing solition. These results provide an alternative explanation for some recent observations.

INTRODUCTION

Modification of the ionosphere by intense radio waves launched from the earth's surface continues to be an active area of experimental and theoretical research; reviews can be found in the November 1974 issue of Radio Science [9 (11), 1974], in the articles by FEJER (1975, 1979), and in the book by GUREVICH (1978). The important role of nonlinear wave effects during ionospheric heating is by now well established, and these effects have at least qualitatively explained many of the observational phenomena.

The purpose of this report is to explore the possibility that three-dimensional Langmuir soliton collapse occurs during ionospheric heating. This possibility was first introduced by PETVIASHVILI (1975, 1976), who emphasized the importance of the geomagnetic field. Previous analytic theories of nonlinear wave interaction during ionospheric modification, as summarized in FEJER (1975, 1979), and in NICHOLSON (1977), have mainly concentrated on three-wave parametric instabilities; see, for example, BEZZERIDES and WEINSTOCK (1972), CHEN and FEJER (1975), DuBOIS and GOLDMAN (1972), KRUER and VALEO (1973), and PERKINS et al. (1974). Most of these theories have neglected the four-wave parametric instability also known as the modulational instability or oscillating two-stream

instability, despite the fact that this instability was the one discussed in the original paper of PERKINS and KAW (1971) introducing the significance of parametric instabilities to ionospheric modification.

In this paper, we treat the evolution of Langmuir waves at the exact reflection point of the modifier wave, the point where the modifier frequency is exactly equal to the plasma frequency ($z = 0$ in Fig. 1). At this spatial point, it is well known (CHEN, 1974) that only the four-wave oscillating two-stream instability can occur. Previous theories using three-wave parametric instabilities are appropriate to spatial locations somewhat closer to the earth, including the location where the maximum amplitude of the standing heater wave occurs. The competition among three-wave interactions, four-wave interactions, and soliton formation at these lower altitudes will be treated by us in future work. Here, we numerically solve a nonlinear wave equation for parameters appropriate to modern modification facilities (e.g., the Platteville facility). We find that the Platteville modifier wave is intense enough to excite an oscillating two-stream instability which evolves into a set of three-dimensional collapsing solitons. Because of collisional damping, these solitons do not collapse catastrophically to a singularity, but rather undergo a period of virulent collapse followed by exponential damping due to collisions.

In the next section, we review the wave equation which describes nonlinear Langmuir waves in the absence of a magnetic field, and solve it for parameters appropriate to the Platteville facility. In the succeeding section, the effects of the geomagnetic field are added; this results in a significant change in the shape of the collapsing solitons. In the final section, conclusions are presented and the possible application of the results to explain certain observational facts is discussed.

AD-A129 320 PLASMA WAVE TURBULENCE AND PARTICLE HEATING CAUSED BY ELECTRON BEAMS RADI..(U) COLORADO UNIV AT BOULDER DEPT OF ASTRO-GEOPHYSICS M V GOLDMAN 01 JAN 83 CU-1533201

UNCLASSIFIED AFOSR-TR-83-0498 AFOSR-80-0022 F/G 20/9 NL

3/3

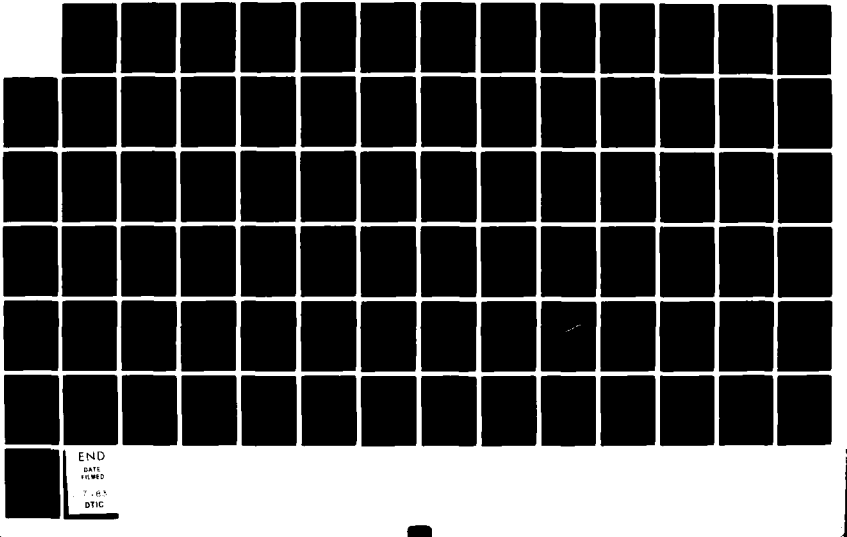

END

DATE FILMED

7-83

DTIC

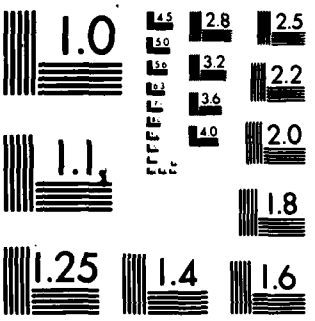

SOLITON COLLAPSE IGNORING THE GEOMAGNETIC FIELD

The equations describing the nonlinear evolution of Langmuir waves were introduced by ZAKHAROV (1972) and are known as the Zakharov equations. From NICHOLSON et al. (1978), these are

$$(i\partial_t + i\nu_e/2 + \nabla^2)\nabla \cdot \underline{E}(\underline{x},t) = \nabla \cdot (n\,\underline{E}) \quad , \tag{1}$$

$$(\partial_t^2 + \nu_i\partial_t - \nabla^2)n(\underline{x},t) = \nabla^2|\underline{E}|^2 \quad , \tag{2}$$

together with $\nabla \times \underline{E} = 0$, where $\underline{E}(\underline{x},t)$ is the low-frequency envelope of the total high-frequency electric field $\underline{E}^{TOT}(\underline{x},t) = \underline{E}(\underline{x},t)\exp(-i\omega_e t)$ plus the complex conjugate; $n(\underline{x},t)$ is the deviation of the ion density from its average value n_0; ω_e is the background plasma frequency; ν_e (ν_i) is the high (low) frequency phenomenological energy damping rate (twice the amplitude damping rate); the sound speed $c_s = [(\gamma_i T_i + \gamma_e T_e)/m_i]^{1/2}$, where γ_e (γ_i) is the electron (ion) specific heat ratio characteristic of low-frequency oscillations; T_e (T_i) is the electron (ion) temperature; and $\underline{x} = (x,y)$ and t represent space and time; all in dimensionless units. Their relation to dimensional variables, signified by a tilde, is given by

$$t = \left(\frac{2\eta}{3}\right)\left(\frac{m_e}{m_i}\right)(\omega_e \tilde{t}) \quad ,$$

$$(x,y) = \frac{2}{3}\left(\frac{\eta\, m_e}{m_i}\right)^{1/2}\left(\frac{\tilde{x},\tilde{y}}{\lambda_e}\right) \quad ,$$

$$n = \left(\frac{3m_i}{4\eta\, m_e}\right)\left(\frac{\tilde{n}}{n_0}\right) \quad ,$$

$$E = \frac{1}{\eta}\left(\frac{m_i}{m_e}\right)^{1/2}\left(\frac{3\tilde{E}^2}{16\pi n_0 T_e}\right)^{1/2} \quad ,$$

$$\nu_{e,i} = \left(\frac{3}{2\eta}\right)\left(\frac{m_i}{m_e}\right)(\tilde{\nu}_{e,i}/\omega_e) \quad , \qquad (3)$$

where the electron Debye length $\lambda_e = (T_e/m_e\omega_e^2)^{1/2}$ and the dimensionless ratio $\eta = (\gamma_e T_e + \gamma_i T_i)/T_e$. The physical effects contained in (1) and (2) have been discussed by ZAKHAROV (1972), by NICHOLSON et al. (1978), and by many others.

We consider parameters (NICHOLSON, 1977) characteristic of ordinary-mode nighttime heating by the Platteville, Colorado, facility. The heater frequency is taken to be $\omega_0/2\pi = 4.9$ MHz so that the reflection point occurs at an electron density $n_0 = 3 \times 10^5$ cm^{-3} approximately 300 km above the earth's surface; $T_e = T_i =$ 0.1 eV; electron collision frequency due to ions and neutrals (high-frequency amplitude damping rate) $\nu_e/2\omega_e = 2 \times 10^{-5}$; power density incident at the base of the ionosphere 50 $\mu W/m^2$; ionospheric density scale length 50 km. We are interested in the electric field of the

ordinary-mode heater wave at the exact reflection point where $\omega_e = \omega_0$ ($z = 0$ in Fig. 1). Here, the heater electric field is along the geomagnetic field with an effectively infinite wavelength. The formulae of GINZBURG (1964), taking into account the Airy enhancement of the heater wave as shown in Fig. 1, predict an electric field of 1.0 V/m for the stated power density. A natural measure of the intensity of this field is the ratio $W = |\tilde{E}|^2/4\pi n_0 T_e$ of electric field energy density to background kinetic energy density; for these parameters we have $W = W_0 = 4.4 \times 10^{-4}$ at the initial time.

The electrons are isothermal with respect to the low-frequency response, $\gamma_e = 1$. The adiabatic compression is one dimensional and $\gamma_i = 3$ and thus $\eta = 4$. The low-frequency damping coefficient is quite large due to ion Landau damping in an equal temperature plasma. We adopt a simple model damping which after Fourier transformation is $\nu_i(\underline{k}) = 2|\underline{k}|$.

Following NICHOLSON et al. (1978), a stability analysis of the heater field yields a threshold for a purely growing instability

$$|E_0|^2 = \nu_e/2 \quad , \tag{4}$$

or in dimensional units for the present parameters, $E_0 = 0.6$ V/m, well below our value of $E_0 = 1.0$ V/m.

In order to determine the nonlinear evolution of the oscillating two-stream instability, we solve the Zakharov equations (1) and (2) numerically in two spatial dimensions. The numerical technique is described in NICHOLSON et al. (1978) and in NICHOLSON and GOLDMAN (1978). The initial electric field consists of the "pump" electric field with wave number zero pointing in the x-direction, representing the heater field, and small random electric fields at all other wave numbers in the two-dimensional wave number grid. The initial density perturbation is zero. All electric field components are subject to the linear damping $\nu_e/2$, except for the pump electric field which has zero linear damping.

At time $\omega_e\tilde{t} = 4.4 \times 10^5$ or $\tilde{t} = 0.014$ s, the unstable modes have exponentiated sufficiently from their initial noise levels that the absolute value of the total electric field, Fig. 2, shows regions of substantially enhanced field and substantially depressed field.

The regions of intense field begin to collapse, so that at $\omega_e\tilde{t} = 7.9 \times 10^5$ or $\tilde{t} = 0.026$ s (Fig. 3) they have become even more intense. At this time, the low-frequency density variation n (Fig. 4) has minima in the same spatial locations as the maxima of the electric field amplitude in Fig. 3. This is as expected for the oscillating two-stream instability and the subsequent soliton collapse.

At the final time of this run, $\omega_e \tilde{t} = 8.9 \times 10^5$ or $\tilde{t} = 0.029$ s, the collisionally damped solitons are quite prominent (Fig. 5). The relative electric field energy density W/W_o vs. time throughout the run is displayed in Fig. 6. After time $\omega_e \tilde{t} = 7 \times 10^5$, the unstable modes take a substantial fraction of energy from the original $\underline{k} = 0$ pump mode; this energy is subsequently lost due to collisional damping. The net damping is always slower than the collisional damping rate (dashed line in Fig. 6) because a substantial fraction of the total wave energy continues to reside in the undamped $\underline{k} = 0$ mode at each time. The collisional damping in this case acts fast enough to prevent the collapse of the solitons to such small spatial regions that the accuracy of the computer code is lost.

The numerical work described here is in two spatial dimensions, while the actual solition collapse during ionospheric heating occurs in three spatial dimensions. Thus the spatial dimensions of the solitons, and the maximum energy density in the center of the solitons, may differ by factors of two or more in the actual physical situation from those obtained here. However, the time scales involved are probably very close in the two-dimensional and three-dimensional cases.

Before discussing the implications of these results for ionospheric heating, we proceed in the next section to add the effect of the geomagnetic field. This results in significant quantitative

differences; the overall qualitative scenario, however, remains unchanged.

SOLITON COLLAPSE INCLUDING THE GEOMAGNETIC FIELD

The earth's magnetic field is such that the electron gyrofrequency Ω_e is roughly $\Omega_e/\omega_e = 1/3.5$ for the parameters of interest. For linear Langmuir waves with a wave number component k_y perpendicular to the magnetic field, the dispersion relation is

$$\tilde{\omega}^2 = \omega_e^2(1 + 3\tilde{k}^2\lambda_e^2 + \frac{\Omega_e^2}{\omega_e^2}\sin^2\theta) \quad , \tag{5}$$

where $\theta = \tan^{-1}(k_y/k_x)$. Thus we include the effect of the geomagnetic field in our numerical calculation by making the following replacement of the dimensionless Fourier representation of the operator $-\nabla^2$ in (1):

$$k^2 \rightarrow k^2 + \frac{3}{4\eta}\frac{\Omega_e^2}{\omega^2}\frac{m_i}{m_e}\sin^2\theta \quad . \tag{6}$$

With modification (6) to our computer program, we repeat the calculation of the previous section. Since only wave numbers with small values of k_y are predicted to grow, and since we are limited

by computer resources to a grid of 64 x 64 points, we resolve the behavior in configuration space by choosing $L_y/L_x = 50$.

Figure 7, analogous to Fig. 3 in the unmagnetized case, shows the electric field in configuration space at $\omega_e\tilde{t} = 7.9 \times 10^5$ or $\tilde{t} = 0.026$ s. The maximum energy densities here are actually twice as large as in the unmagnetized case. We interpret this as follows. In the magnetized case, the spatial configuration is much more one-dimensional than in the unmagnetized case. It is well known that dispersion is more effective in inhibiting one-dimensional collapse than in inhibiting two-dimensional collapse. Thus, in the magnetized case, the unstable oscillating two-stream modes can remain in phase with the pump for a longer time. This allows them to absorb more of the pump energy than in the unmagnetized case; at a slightly later time, when the waves do decouple from the pump and begin to collapse, they have a somewhat greater intensity than in the unmagnetized case. This effect is helped by the fact that the magnetized solitons involve the collapsing energy from a spatial volume roughly 50 times larger than in the unmagnetized case; thus, it is not surprising that the intensity at the very center of a collapsing soliton is larger in the magnetized case.

Figure 8 shows the relative electric field energy density vs. time for the entire magnetized run. The energy dissipation at late times is even closer to the collisional damping rate than in the unmagnetized case (Fig. 6), consistent with our previous

interpretation of a greater efficiency in the conversion of pump energy to unstable mode energy in the magnetized case.

CONCLUSIONS AND IMPLICATIONS

We have demonstrated numerically that the ordinary mode Platteville modifier is intense enough to cause an oscillating two-stream instability at its exact reflection point. This instability leads to regions of spatially localized intense electric field which become collisionally damped collapsing solitons. The time scale for collapse is a few milliseconds. The spatial scale of the collapsing solitons is about one meter along the geomagnetic field, and, because of the geomagnetic field, about one-hundred meters or less perpendicular to the geomagnetic field.

Our results lend an intriguing interpretation to an important observational fact. It has been observed that when the modifier at Arecibo is turned on, the intensity of the plasma-line echo is initially quite intense (MULDREW and SHOWEN, 1977); this phenomenon is called "plasma-line overshoot." According to linear theory, this result is difficult to understand, since it requires Langmuir waves created by the modifier to travel up or down in an essentially vertical direction. However, the unstable oscillating two-stream instability of the present paper, and the parametric decay instability of the earlier theories of ionospheric modification reviewed in the introduction, both produce Langmuir waves travelling

predominantly along the geomagnetic field, not in the vertical direction. However, this difficulty does not occur if one has three-dimensional collapsing solitons. These nonlinear entities contain all wave number components, not merely the ones allowed by the linear Langmuir wave dispersion relation. Thus, at least qualitatively, the three-dimensional collapsing solitons of the present paper could lead to a substantial plasma-line intensity. An estimate of the plasma-line intensity due to soliton collapse will appear in future work. A more extensive version of the present work can be found in WEATHERALL et al. (1982).

ACKNOWLEDGMENTS

This work was supported by the National Science Foundation, Grant Nos. ATM81-11126 and ATM79-18778, by NASA Grant No. NSG-7632, and by USDOE Grant No. DE-AC02-76ET53034. The work of two of us (M.G. and J.W.) was also supported by the National Science Foundation, under ATM79-16837 and ATM80-20426, by the Air Force Office of Scientific Research under Contract F49620-76-C-0005, and by NASA NAGW-91. We thank the National Center for Atmospheric Research, supported by the National Science Foundation, for computer time used in this research. Part of this work was performed while two of us (M.G. and D.N.) were the guests of the Aspen Institute for Physics and Astrophysics, whose hospitality is appreciated.

REFERENCES

BEZZERIDES B. and WEINSTOCK J.	1972	Phys. Rev. Lett. 28, 481.
CHEN F. F.	1974	Introduction to plasma physics, Plenum, New York.
CHEN H. C. and FEJER J. A.	1975	Phys. Fluids 18, 1809.
DuBOIS D. F. and GOLDMAN M. V.	1972	Phys. Fluids 15, 919.
FEJER J. A.	1975	Philos. Trans. R. Soc. London, Ser. A 280, 151.
FEJER J. A.	1979	Rev. Geophys. Space Phys. 17, 135.
GINZBURG V. L.	1964	The propagation of electromagnetic waves in plasmas, Pergamon, Oxford.
GUREVICH A.	1978	Nonlinear phenomena in the ionosphere, Springer, Berlin-New York.
KRUER W. L. and VALEO E. J.	1973	Phys. Fluids 16, 675.
MULDREW D. B. and SHOWEN R. L.	1977	J. Geophys. Res. 82, 4793.
NICHOLSON D. R.	1977	J. Geophys. Res. 82, 1839.
NICHOLSON D. R. and GOLDMAN M. V.	1978	Phys. Fluids 21, 1766.

NICHOLSON D. R., GOLDMAN M. V., HOYNG P. and WEATHERALL J. C.	1978	Astrophys. J. 223, 605.
PERKINS F. W. and KAW P. K.	1971	J. Geophys. Res. 76, 282.
PERKINS F. W., OBERMAN C. and VALEO E. J.	1974	J. Geophys. Res. 79, 1478.
PETVIASHVILI V. I.	1975	Fiz. Plazmy 1, 28 [Sov. J. Plasma Phys. 1, 15].
PETVIASHVILI V. I.	1976	Fiz. Plazmy 2, 450 [Sov. J. Plasma Phys. 2, 247].
WEATHERALL J. C., SHEERIN J. P. NICHOLSON D. R., PAYNE G. L., GOLDMAN M. V. and HANSEN P. J.	1982	J. Geophys. Res. 87, 823.
ZAKHAROV V. E.	1972	Zh. Eksp. Teor. Fiz. 62, 1745 [Sov. Phys.-JETP 35, 908].

FIGURE CAPTIONS

Fig. 1. Standing wave pattern of the heater electric field and direction of the geomagnetic field over Platteville, Colorado.

Fig. 2. Contours of absolute value of electric field in configuration space at $\omega_e \tilde{t} = 4.4 \times 10^5$ or $\tilde{t} = 0.014$ s. The spatial region shown is that used by the computer program, with L_x corresponding to $\tilde{L}_x/\lambda_e = 7400$ or $\tilde{L}_x = 32$ m, and $\tilde{L}_y = 64$ m. Contour 2 corresponds to the initial electric field energy density W, contour 1 is 3% below the initial value, and contour 3 is 3% above the initial value.

Fig. 3. Contours of absolute value of electric field in configuration space at $\omega_e \tilde{t} = 7.9 \times 10^5$ or $\tilde{t} = 0.026$ s. Contour 1 corresponds to $W = 2.4 \times 10^{-4}$, contour 2 to $W = 9.7 \times 10^{-4}$, and contour 3 to $W = 2.2 \times 10^{-3}$. Other parameters are the same as in Fig. 2.

Fig. 4. Low-frequency density variation in configuration space at time $\omega_e \tilde{t} = 7.9 \times 10^5$ or $\tilde{t} = 0.026$ s. Contour 1 corresponds to a zero density variation, contour 2 corresponds to $\tilde{n}/n_0 = -0.002$ or $\tilde{n} = -600$ cm^{-3}, and contour 3 (in four places, unmarked on figure) corresponds to $\tilde{n}/n_0 = -0.004$ or $\tilde{n} = -1200$ cm^{-3}. Other parameters as in Fig. 2.

Fig. 5. Contours of absolute value of electric field in configuration space at $\omega_e \tilde{t} = 8.9 \times 10^5$ or $\tilde{t} = 0.029$ s. Contour 1 corresponds to $W = 1.4 \times 10^{-4}$, contour 2 to $W = 5.4 \times 10^{-4}$, and contour 3 (in three places, unmarked) to $W = 1.2 \times 10^{-3}$. Other parameters as in Fig. 2.

Fig. 6. Log_{10} of the relative electric field energy density W/W_0 vs. time for the entire unmagnetized run. The dashed line shows the rate of energy decay which would occur if all modes were collisionally damped. The actual decay is slower than this because at each time a significant fraction of the wave energy is in the undamped $\underline{k} = 0$ mode.

Fig. 7. Contours of absolute value of electric field in configuration space at $\omega_e \tilde{t} = 7.9 \times 10^5$ or $\tilde{t} = 0.026$ s, for the magnetized case. Contour 1 corresponds to $W = 5.4 \times 10^{-4}$, contour 2 to $W = 2.2 \times 10^{-3}$, and contour 3 to $W = 4.9 \times 10^{-3}$. Note that this figure has been compressed by a factor of 25 in the vertical direction.

Fig. 8. Log_{10} of the relative electric field energy density W/W_0 vs. time for the entire magnetized run. The dashed line shows the rate of energy decay which would occur if all modes were collisionally damped. The actual decay is slower than this because at each time a significant fraction of the wave energy is in the undamped $\underline{k} = 0$ mode.

C-G81-223

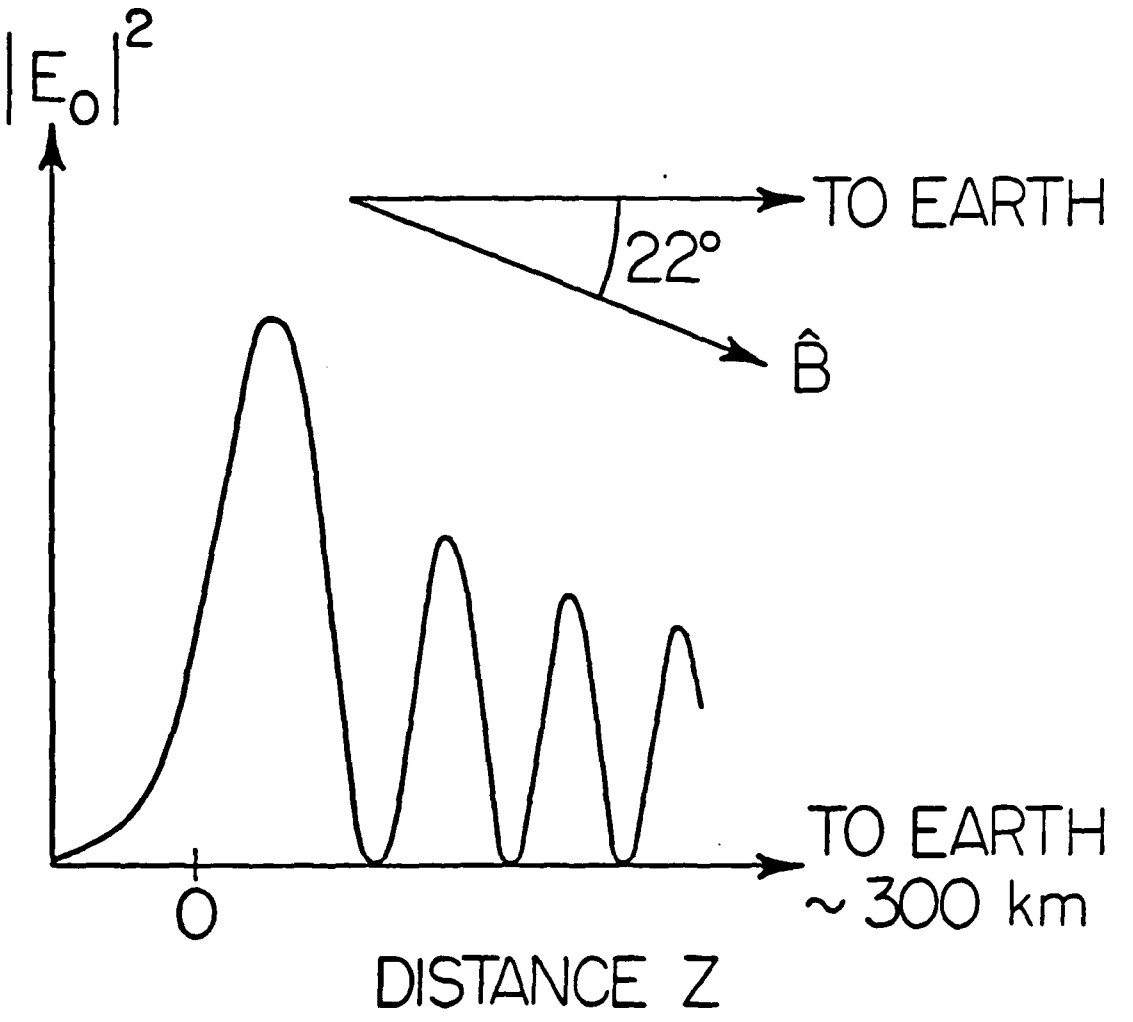

Fig. 1

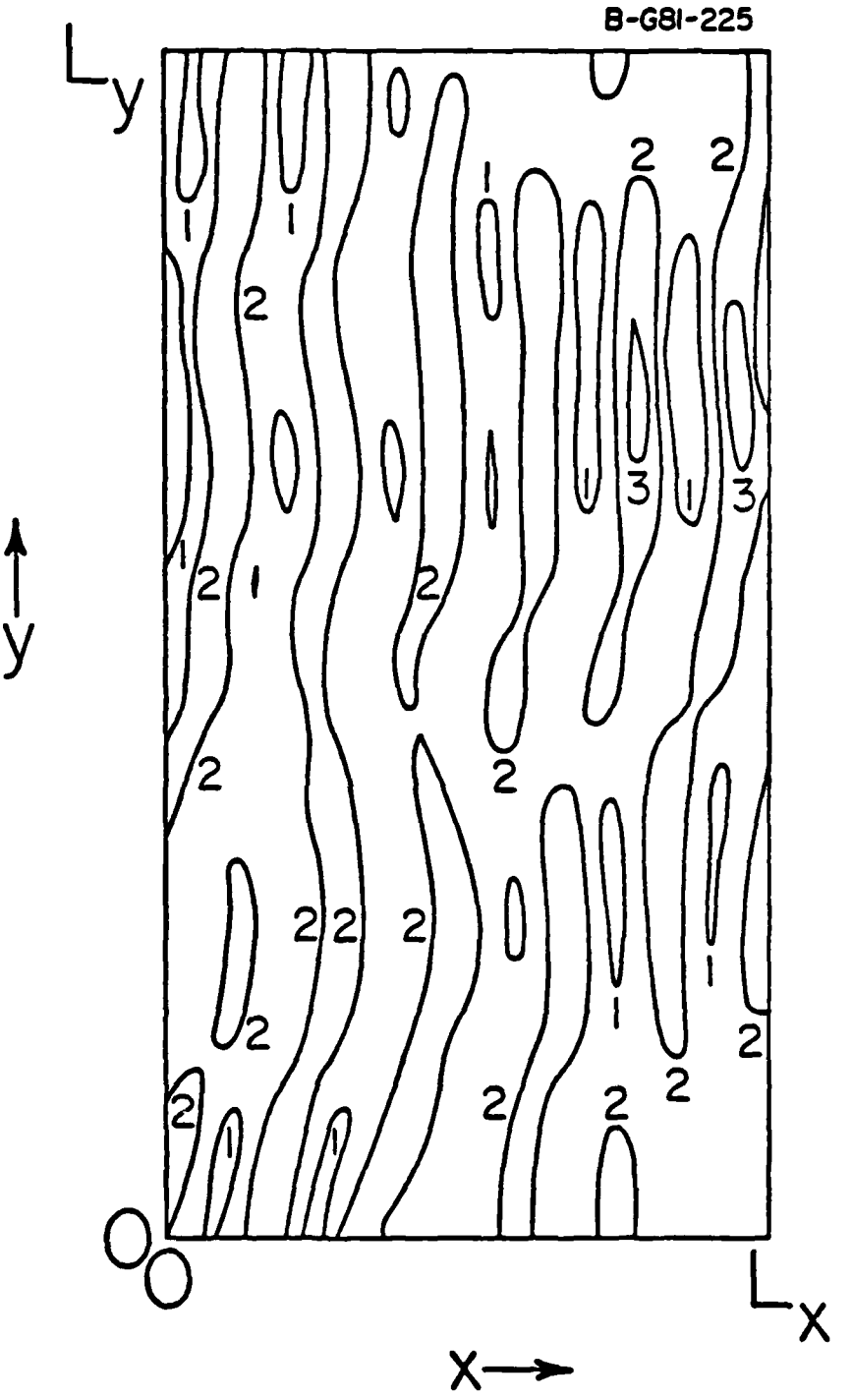

Fig. 2

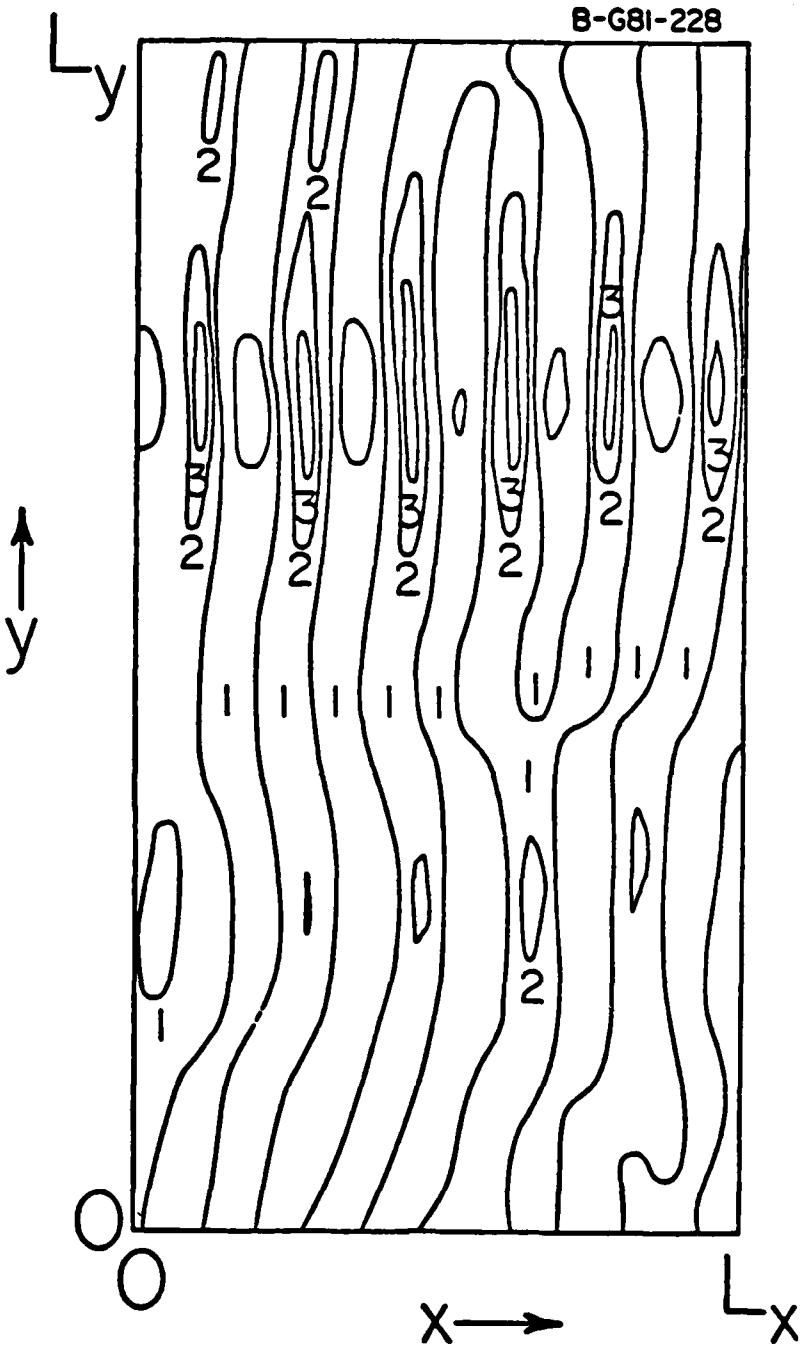

Fig. 3

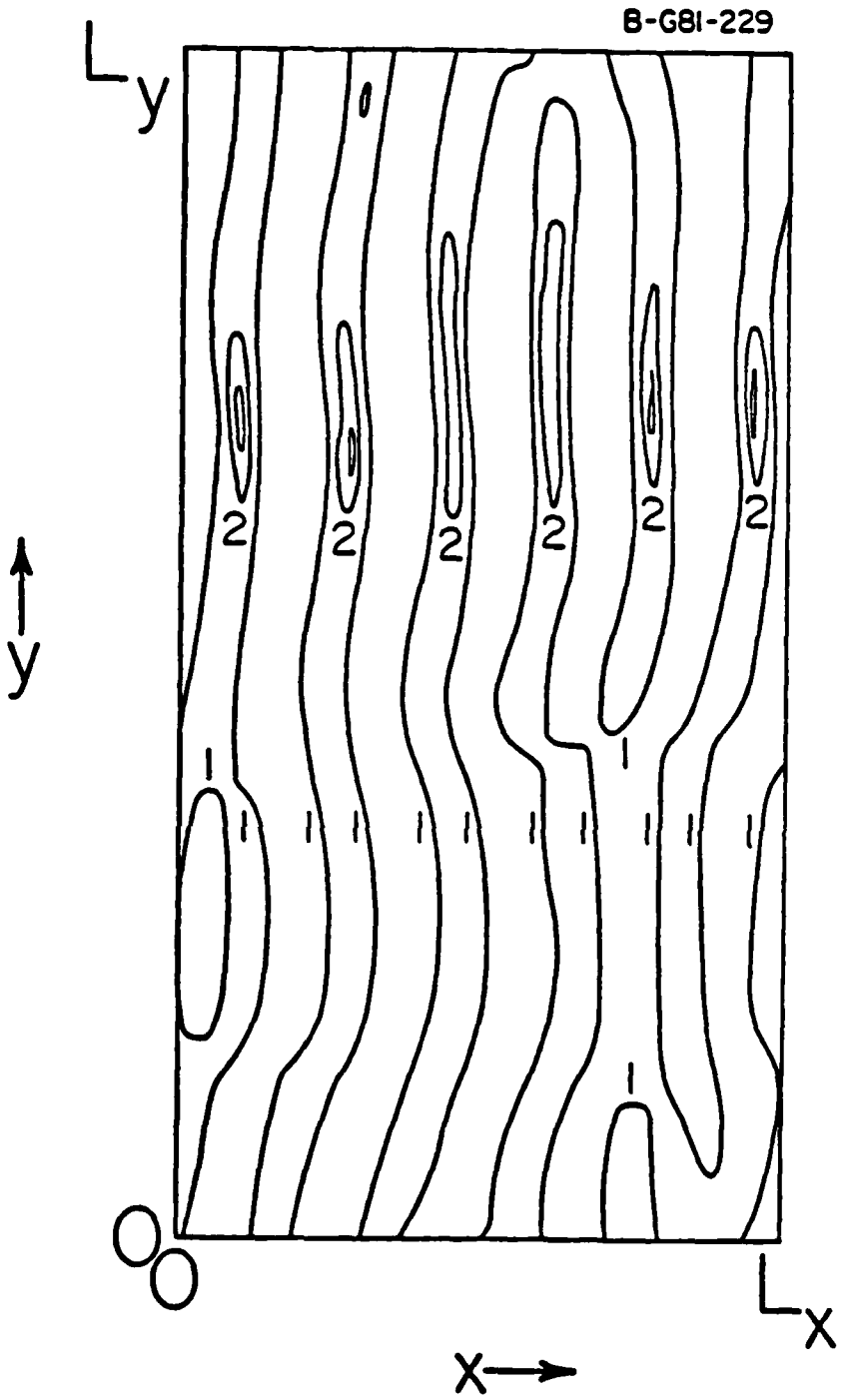

Fig. 4

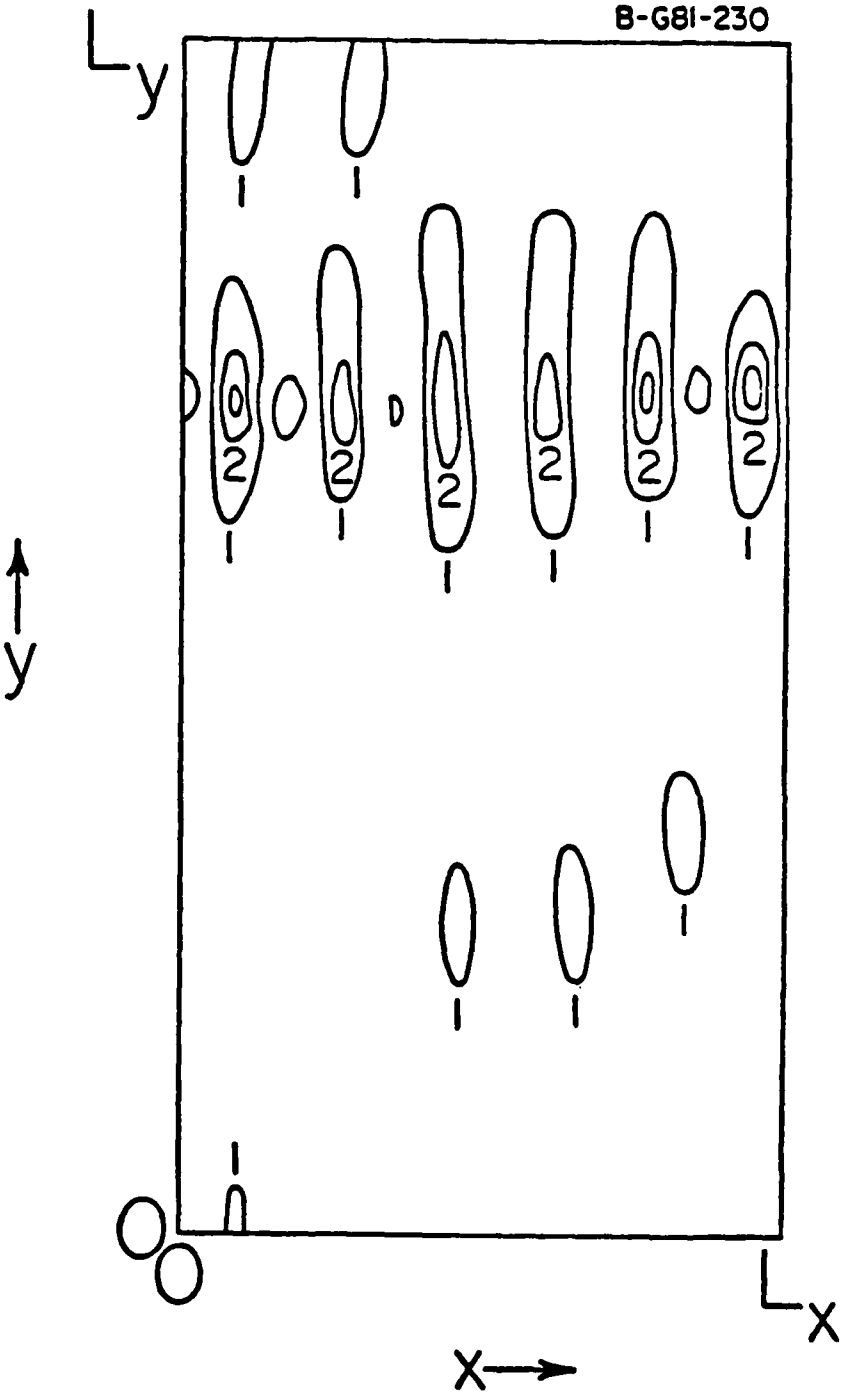

Fig. 5

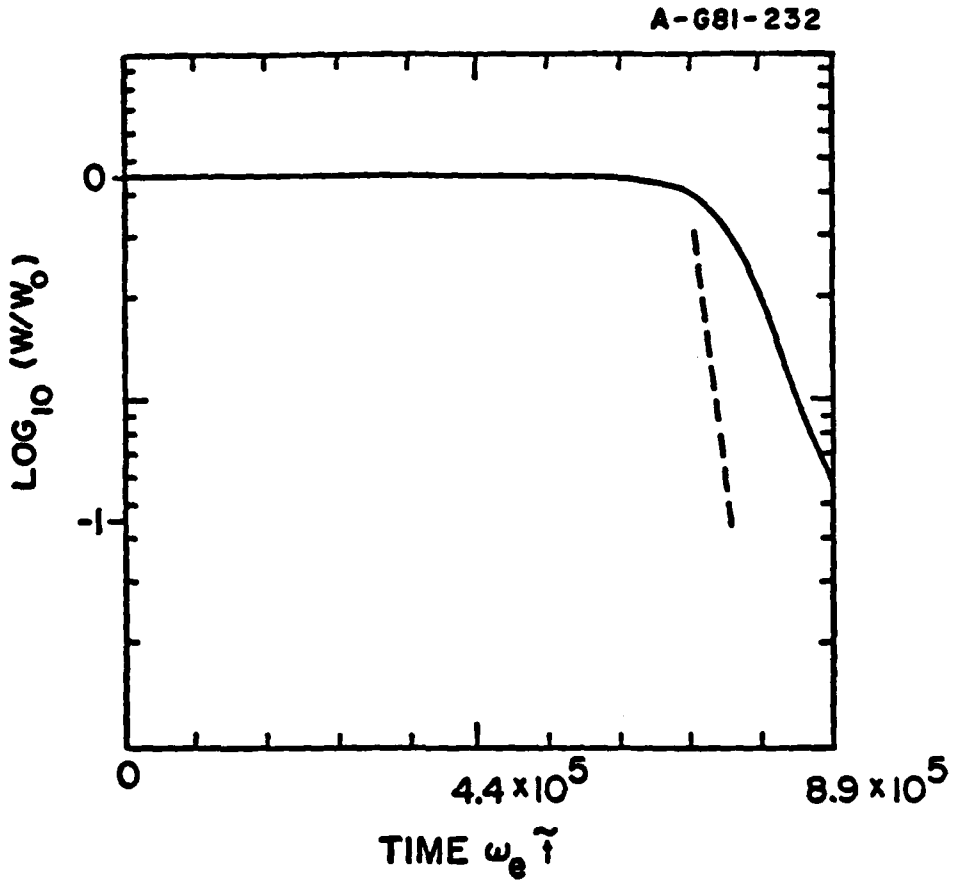

Fig. 6

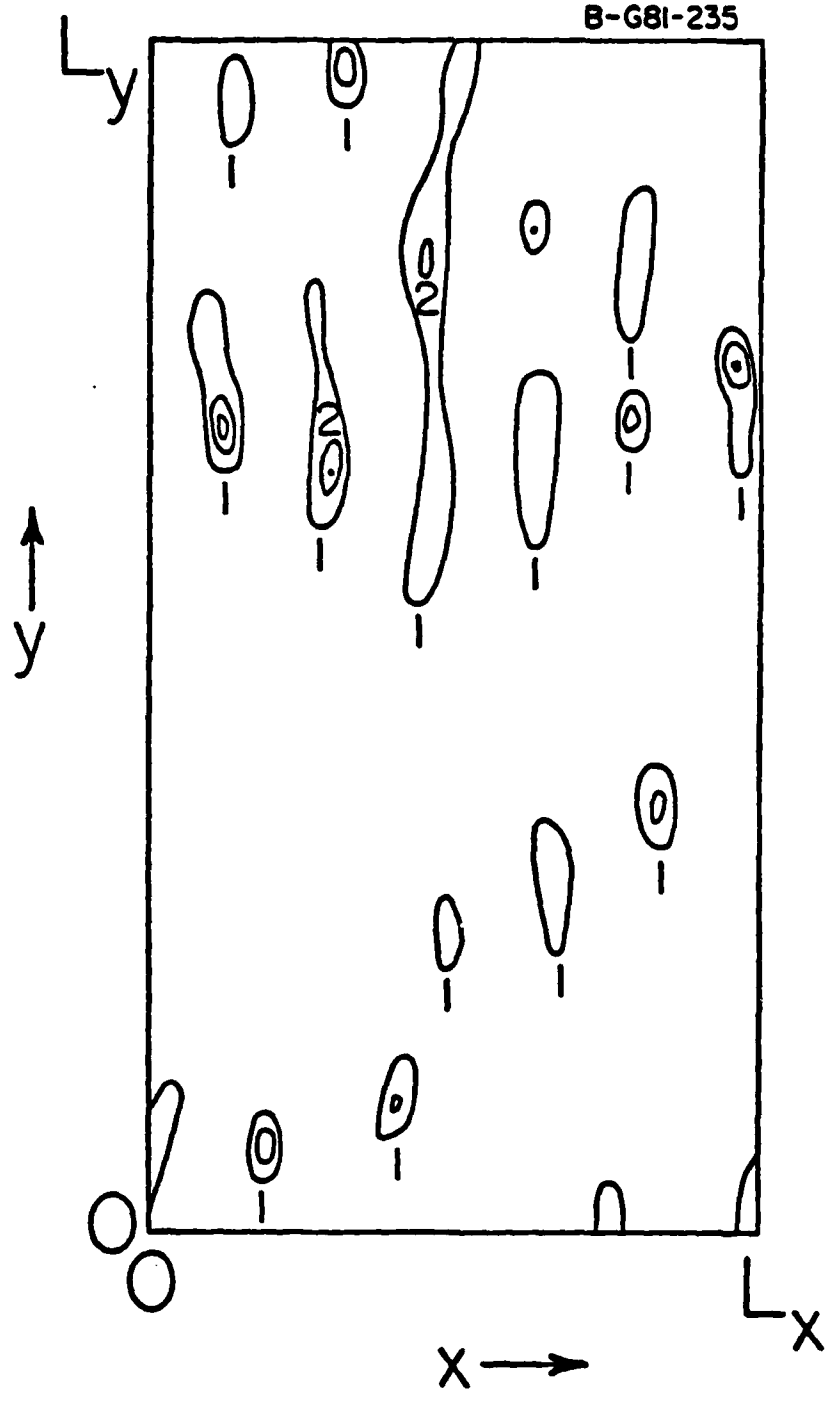

Fig. 7

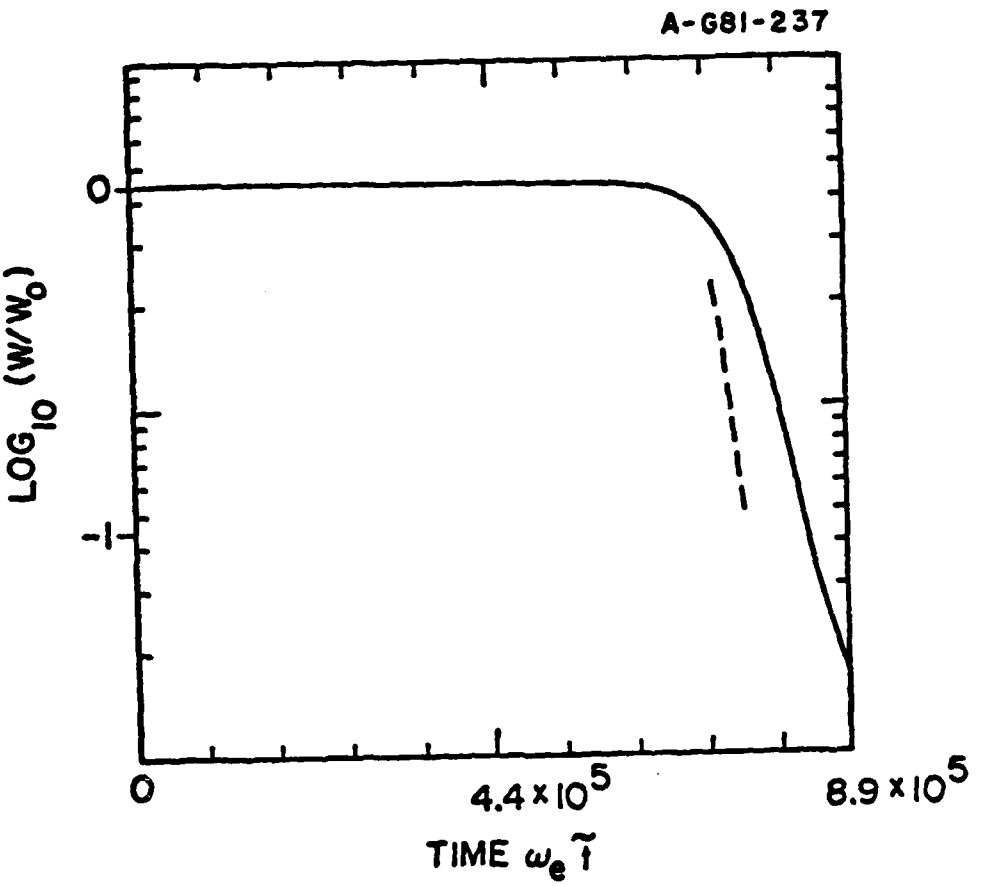
A-G81-237
0
-1
$LOG_{10}(W/W_0)$
0
4.4×10^5
8.9×10^5
TIME $\omega_e \tilde{t}$

Fig. 8

APPENDIX F

F. "Beam-Plasma Interactions in a Positive Ion-Negative Plasma"

T. Intrator, N. Hershkowitz, and R.A. Stern
Submitted to Physics of Fluids

BEAM-PLASMA INTERACTIONS IN A POSITIVE ION-NEGATIVE PLASMA

Tom Intrator, Noah Hershkowitz

Department of Nuclear Engineering

University of Wisconsin

Madison, Wisconsin 53706

Raul Stern

Department of Physics, Astro Geophysics

University of Colorado

Boulder, Colorado 80309

Abstract

An electron free plasma consisting of negative ions (SF_6^-) and positive ions (Ar^+) and negligible neutral-ion collision frequencies has been created in the laboratory. This plasma has a mass ratio of approximately 3.5 similar to many computer Particle-In-Cell simulated systems. A fluid description of this Positive and Negative Ion Confinement (PANIC) plasma is given and compared to experimental measurements of a beam-plasma instability for both beam species and a wide range of beam energies. The fluid dispersion relation and most growing mode are predicted to be insensitive to many parameters of the PANIC beam-plasma system, and found to be consistent with the data.

I. Introduction

Many problems in plasma physics are not amenable to analytic methods of solution, and therefore direct computer calculations of plasma properties are attempted. For practical reasons, computer Particle-In-Cell simulations frequently specify the mass ratio of their particle species to be near unity instead of several thousand [e.g. 1836 for the (H^+, e^-) plasma]. In this paper we describe a laboratory plasma that corresponds to such simulation mass ratios. It consists of positive ions (Ar^+, mass $m_+ \sim 40$ amu), negative ions (SF_6^-, mass $m_- \sim 140$ amu), and virtually no electrons. This Positive and Negative Ion Confinement (PANIC) plasma has a mass ratio of $m_-/m_+ \sim 3.5$, and is contrasted with the electron-ion plasma in Table 1. Table 1

Here we describe an experimental measurement of beam-plasma interactions in the PANIC plasma. A Double Plasma (DP)[1] device was designed to allow ion beams of either species to be injected from one half of the machine into a "target" plasma in the other half. Single chamber versions of such plasmas have been described by Wong et al.[2] and Hershkowitz and Intrator[3]. A serious problem in such devices is that reactive fluorine radicals from the (Ar^+, SF_6^-) plasma corrode the entire vacuum system. Thus experimental data is at the expense of system longevity (gauges, pumps, chambers, etc.). The results from this experiment are interpreted with the aid of an unmagnetized fluid model which allows a simple analysis of this beam-plasma system and includes the

influence of the unusual mass ratio. For the PANIC beam-plasma-instability, a dispersion relation and most growing frequency are predicted and experimentally confirmed.

Interest in beam-plasma interactions in unmagnetized plasmas is not new, and indeed dates back to the earliest investigations of unmagnetized electron-ion-beam systems. Electron beams[4] and ion beams[5,6] can interact with the plasma, depending on whether the beam velocity is in the vicinity of a sound speed (c_s) or an electron thermal velocity (v_e). These interactions are respectively, the beam driven ion-acoustic wave and the beam-plasma instability.[7] Although there have been many experimental investigations of these interactions in electron-ion systems, there have been few of negative ion-positive ion plasmas.[8] The negative ion-positive ion plasma has rarely been the subject of experiments[8] or theory.[9] Wong et al.[2] used a grid to drive "fast ion acoustic" instability in a negative ion-positive ion plasma. A study of the beam-plasma instability in a PANIC plasma is the subject of this paper.

An outline of the fluid model is given in Section II. This approximation yields a simple description of the various normal modes of the PANIC plasma, which can then be compared with the analogous modes in the more familiar ion-electron plasma. Details of the experimental apparatus and techniques are given in Section III. Experimental data for a PANIC beam excited instability are shown in Section IV, discussions and conclusions are given in Sections V and VI.

II. The Fluid Model and the PANIC Plasma

A. Fluid Approximation

The three fluid (two background plus beam) approximation leads to an expression for the background density perturbation

$$\frac{n_{s1}}{n_s} = ikE_1 \frac{q_s}{m_s(\omega^2 - \Gamma_s k^2 v_s^2)} \tag{1}$$

which can be inserted into Poisson's equation to give a dielectric response function

$$\varepsilon(k,\omega) = 1 - \frac{\omega_{p+}^2}{\omega^2 - \Gamma_+ k^2 v_+^2} - \frac{\omega_{p-}^2}{\omega^2 - \Gamma_- k^2 v_-^2} \tag{2}$$

$$- \frac{\omega_{pb}^2}{(\omega - kv_b)^2 - k^2 v_{bth}^2} - \frac{\omega_{pe}^2}{\omega^2 - k^2 v_e^2}$$

The density is denoted by n_s, the wavenumber by k, the self consistent electric field by E_1, species charge by q_s, mass by m_s, and wave frequency by ω. Thermal velocities are v_+, v_-, v_e, v_{bth} for +, -, electron and beam species, and v_b is beam velocity. The subscript 1

indicates a first order perturbed quantity. The plasma frequencies $\omega_{ps} = (4\pi e^2 n_s/m_s)^{1/2}$ are subscripted +, e, b, e for positive ions, negative ions, beam ions or electrons, respectively. The value of Γ_s depends on the type of perturbation (e.g. isothermal or adiabatic). Solutions of $\varepsilon(k,\omega) = 0$ give the dispersion relations for electrostatic waves and can be found analytically for the small wavenumber limit, where we choose $\Gamma_s = 1$.

B. Sound Wave

At $\varepsilon(k,\omega) = 0$, the dispersion relation has a "low" frequency root

$$\frac{\omega^2}{\omega_{p+}^2} \approx \frac{\alpha - M}{1 + M}\left(\frac{k}{k_{D+}}\right)^2 + \left[\frac{\alpha}{1 + M} - \frac{(\alpha + M)(\alpha + 1)}{(1 + M)^2} + \frac{(\alpha + M)^2}{2(1 + M)^3}\right]\left(\frac{k}{k_{D+}}\right)^4 \qquad (3)$$

where $\alpha \equiv v_-^2/v_+^2$, the mass ratio $M \equiv m_+/m_-$, and the k in (3) is normalized to the Debye wavenumber $k_{D+} \equiv (4\pi e^2 n_+/T_+)^{1/2}$.

The dispersion relation becomes

$$\omega/\omega_{p+} \sim \pm\, \theta \frac{k}{k_{D+}} \frac{v_-}{v_+} \qquad (4)$$

where $\theta = [(1 + M/\alpha)/(1 + M)]^{1/2} + \mathcal{O}(k^2/k_{D+}^2)$. This sound wave always travels at a phase velocity a little larger than the thermal velocity of the slower ion. The thermal velocity is $v_- = \alpha^{1/2} v_+$ so that for

temperatures satisfying $1 \lesssim T_-/T_+ \lesssim 3$ the corresponding range for α is $0.3 \lesssim \alpha \lesssim 1.0$. Now θ ($1.0 \lesssim \theta(\alpha) \lesssim 1.2$) can be interpreted as the ratio of the sound wave phase velocity (v_ϕ^{sound}) to the heavier ion thermal velocity (v_-) (i.e. $\theta = v_\phi^{sound}/v_-$). In the electron-ion plasma, ion acoustic waves travel at slightly greater than the sound speed $c_s \equiv \sqrt{T_e/m_i}$, which is the analogue of θv_- in the PANIC plasma. In the limit of equal thermal velocities, numerical calculations give $\lim_{\alpha \to 1} \theta(\alpha,k) = 1$, to all orders in k.

C. Density Perturbations and Wave Propagation

In both types of plasmas (electron-ion and PANIC), the positive and negative species oscillate in phase with respect to each other, with alternating regions of bunching and rarefaction. The heavier particles drag along the lighter ones, and thermal motions of the latter enables them to shield fields from the bunched heavy ions. Thermal motion of the heavier species as well as the mutual repulsion of the (now incompletely shielded) bunched charges tends to spread out these regions of compression. The heavier ions overshoot their lighter neighbors because of inertia, regenerate compressions and rarefactions, and thence renew the wave. For the two-ion PANIC plasma, masses and thermal velocities and mutual reaction times become nearly the same for the two species.

D. The Plasma Oscillation

The plasma oscillation root of the two ion dispersion relation (2 background species, no beam) is given by the "high" frequency solution

$$\frac{\omega^2}{\omega_{p+}^2} \sim (1 + M)\left[1 + \frac{1 + \alpha M}{(1 + M)^2}\frac{k^2}{k_{D+}^2} + \ldots\right] \tag{5}$$

Choosing M = 0.29 for the $Ar^+ - SF_6^-$ plasma gives:

$$\omega \sim \omega_p\left[1 + 0.3\,\frac{k^2}{k_{D+}^2}\,(1 + 0.3\alpha) + \ldots\right] \tag{6}$$

Where $\omega_p \equiv [\omega_{p+}^2 + \omega_{p-}^2]^{1/2} = 1.14\,\omega_{p+}$. As expected, these "Langmuir" solutions exhibit a low frequency cut off near the plasma frequency ω_p. For the case of no collisions, the two charge species oscillate 180° out of phase with respect to each other.

E. Beam Modes for Electron-Ion Plasmas

Adding an ion beam with density much smaller than the background gives rise to new features in the electron-ion plasma response. For example, the "bump on tail" distribution of Fig. 1a is a typical velocity distribution function for an ion-electron plasma with a small ion beam. In the limit that the background ion thermal velocity (v_{ion}) and beam "bump" velocity (v_b) are very far apart ($v_{ion} \ll v_b$), they do not interact, and ion acoustic waves are observed at $v_\phi \approx \pm c_s$, symmetric

about the background ion distribution. The background electrons provide the restoring force for the wave displacements, and have a very wide velocity distribution ($v_b << v_e$) that is essentially invariant for a change of rest frame. With this in mind, a Galilean transformation from the ion background to beam rest frame can be made. Now the same type of "ion-acoustic" wave will be seen at phase velocities symmetric about the beam velocity ($v_\phi \approx v_b \pm [n_b/n_o]^{1/2} c_s$). The nomenclature for the "fast" ("slow") beam mode at $v_\phi = v_b \ (\pm) \ (n_b/n_o)^{1/2} c_s$ is taken from this feature. For small beam velocities $v_b \sim c_s$ (e.g. Fig. 1b) two modes between the ion "bumps" coalesce and form a growing-damping conjugate pair of modes. For the case of the PANIC plasma, there is no frame invariant background ion distribution, so that this reasoning does not apply to the two-ion beam driven sound wave. Fig. 1a, 1b

Another beam driven mode is known as the beam-plasma instability. The beam velocity must be larger than the largest thermal velocity in the system and less than the Langmuir wave phase velocity for the "fast" and "slow" beam modes to couple and form this instability.

F. The Effect of Beams on the PANIC Plasma

When a beam fluid is added to the PANIC plasma and electron impurities included, the dielectric response function is, from (2):

$$\varepsilon(k,\omega) \approx 1 - \frac{1}{\omega_*^2 - \Gamma k_*^2} - \frac{M_- n_-}{\omega_*^2 - \Gamma k_*^2 \alpha} - \frac{M_b n_b}{(\omega_* - k_* v_{b*})^2 - k_*^2 v_{bth*}^2} + \frac{n_e}{k_*^2} \qquad (7)$$

where the dimensionless quantities of frequency (ω_*), wavenumber (k_*), beam velocity (v_{b*}), beam thermal velocity (v_{bth*}), mass (M) and density (n) are normalized to plasma frequency (ω/ω_{p+}), Debye wavenumber (k/k_{D+}), positive ion mass ($M_- \equiv m_+/m_-$, $M_b \equiv m_+/m_b$), and positive ion density ($n_- = n_-/n_+$, $n_b = n_b/n_+$, $n_e = n_e/n_+$), respectively. The subscripts +, -, b, e denote Ar^+, SF_6^-, beam and electron species. Since we will only consider ion waves of phase velocity much less than the electron thermal velocity, $\omega << kv_e$ is neglected in the electron term. Charge neutrality requires that $n_- = 1 \pm n_b$. Typical PANIC velocity distributions are shown in Fig. 2a for $v_b >> v_+$ and in Fig. 2b where $v_b \gtrsim v_+$. Fig. 2a,2b

The roots of Eq. (7) were calculated numerically for complex ω vs. real k and real ω vs. complex k, with very similar results. The parameters that could affect these results include beam velocity, beam density, beam temperature, background temperature and electron impurity. Dispersion relations and most-growing frequencies were found to be insensitive to the following parameter ranges: $0.01 < k_* < 1$, $1 < v_{b*} < 10$, $0 < v_{bth*} < 2$, $0.1 < n_b < 0.2$, and $0 < n_e < 0.002$. The case of complex ω vs. real k corresponds to spatially periodic, temporally growing perturbations[10] and is consistent with the experimentally observed unstable real frequency. Numerical solutions for this case are shown in Fig. 3, a graph of ω vs. k, showing fast and slow beam modes coupled to form a beam-plasma mode, and Fig. 4, a graph of ω vs. k showing the slow beam mode coupling to a sound wave for small beam velocity. Fig. 5 is a graph of phase velocity (v_ϕ) versus beam velocity (v_b) showing the various

Fig. 3

Fig. 4

background plasma modes (Langmuir and sound waves) and beam modes (fast and slow beam modes) as a function of beam velocity. The coupled modes indicate the identical real parts of growing-damping conjugate pairs of roots. Fig. 6 is similar except that it corresponds to the case of real ω vs. complex k. The dielectric function is symmetric as $(v_b, v_\phi) \rightarrow (-v_b, -v_\phi)$ so that there is point symmetry about the origin on a linear graph of v_ϕ versus v_b such as Fig. 7. Note that any vertical line crosses the six zeroes of $\varepsilon(k,\omega)$ from equation (2).

Fig. 5

Fig. 6

Fig. 7

The phase velocity versus beam velocity representation of the PANIC beam-plasma system (Figs. 5-7) reveals two modes that are independent of the beam velocity. These are the sound wave with phase velocity $v_\phi \sim \omega_p/k$. However, these roots are not continuous. For example, one can follow the sound wave root on Fig. 7 in the direction of the v_b axis, as it curves upwards and becomes the fast beam wave root, while the slow beam wave root levels off and acquires the phase velocity of the sound wave. It is clear that no two roots cross, although wave properties <u>do</u> switch from one root to another.

The modes that do depend on the beams are the "fast" ("slow") beam modes, so named because their phase velocities are slightly faster (slower) than the beam for very large beam velocities (i.e. $v_b > \omega_p/k$). For smaller values of v_b, the fast and slow beam modes coalesce into a growing-damping conjugate pair with equal real phase velocities $v_\phi \sim 0.9\ v_b$. This is the beam-plasma instability that has been observed in the laboratory PANIC DP device, for beam velocities in the range $2 < v_{b*} < 10$. Details are given in the following section.

G. Dispersion Relation for Beam-Plasma Instability

For the beam-plasma instability in the PANIC beam system, the dispersion relation is found numerically to be

$$\omega = \xi k v_b \tag{8}$$

in one dimension, where $0.8 < \xi < 1.0$ is an empirical parameter of order unity. When one extends the problem to three dimensions, the beam velocity $\vec{v}_b$ defines a preferred direction with which we can establish a coordinate system. The dispersion relation of Eq. (8) only depends on the projection of $\vec{k}$ on $\vec{v}_b$, so another parameter, the angle between $\vec{k}$ and $\vec{v}_b$, must also be measured experimentally (i.e. $\omega = \xi \vec{k} \cdot \vec{v}_b$).

Many parameters in this system can be varied, with little or no change in ξ. Typical results are shown in Fig. 8, which is a graph of v_ϕ/v_b versus wavenumber k/k_{D+}, for several values of beam density. A search over the possible values for beam velocity [$1 < v_{b*} < 10$], beam density [$0.1 < n_b < 0.3$] and temperatures [$0 < T_b/T_+ < 4$ for beam; $1 < T_-/T_+ < 3$ for background] was conducted. All parameters were allowed to vary, yet remarkably $0.8 < v_\phi/v_b < 1.0$. Thus the qualitative nature of the beam waves does not appear to be sensitive to any of these parameters. Fig. 8

H. Growth Rates

There are two growth rates of interest: γ, the absolute growth rate which competes with damping processes that occur in real time and the relative growth rate γ/ω which competes against damping phenomena on plasma period time scales (ω_p^{-1}). The relative growth rate was used in this analysis.

The frequency at which the relative growth rate is maximum is predicted to be

$$0.5 < \omega[(\gamma/\omega)_{max}]/\omega_{p+} < 0.6 \qquad (9a)$$

where the ion plasma frequency $\omega_{p+}(s^{-1}) = 33 n_+^{1/2}(cm^{-3})$. The linear growth must compete with ion-neutral collision frequency[11] $\nu_{+n} \sim 2.2 \times 10^7$ P_o (Torr) $T_+^{1/2}$(eV) and Coulomb collision frequency[11] $\nu_{+-} \sim 9.7 \times 10^{-7}$ n (cm^{-3}) $T_e^{-3/2}$ (eV). The data will show that $\nu_{+n} < \nu_{+-} << \omega_{p+}$ for this experiment. The wavenumbers that correspond to this most growing region are

$$0.1 < k[(\gamma/\omega)_{max}]/k_{D+} < 0.3 \qquad (9b)$$

where the Debye wavenumber is $k_{D+}(cm^{-1}) = 1.4 \times 10^{-3}[n_+(cm^{-3})/T_+(eV)]^{1/2}$.

A computer search over ω, k, v_b, n_e, n_b, T_-/T_+, T_b/T_+ yielded only the small variations shown in Eqs. (9) for ω and k at $(\gamma/\omega)_{max}$.

I. Electrons

Analytically a small electron impurity is insignificant to the PANIC-beam dispersion relation (7) except in the limit of small wavenumbers. If we set the $\varepsilon(k,\omega)$ of Eq. (7) to zero, with phase velocity ($v_{\phi^*} = \frac{\omega/k}{v_+}$) then

$$k_*^2 + n_e = \frac{1}{v_{\phi^*}^2 - 1} + \frac{m_+/m_-(1 \mp n_b)}{v_{\phi^*}^2 - \alpha} + \frac{n_b}{(v_{\phi^*} - v_{b^*})^2 - T_b/T_+} \qquad (10)$$

For the typical laboratory PANIC plasma data, the electron fraction is small $10^{-4} < n_e < 10^{-3}$ so that Eq. (10) differs from the case for $n_e = 0$ only for $n_e \gtrsim k_*^2$, or $k/k_{D+} \lesssim 0.03$. For the following experiments, the wavenumbers that correspond to the most growing modes are $k/k_{D+} \sim 0.2$-0.3, well away from the electron dominated regime. The effect of electrons on the fluid model two ion plasma oscillation is explicitly displayed in Figs. 3 and 4.

III. The Experiments and Apparatus

The PANIC plasma (Ar^+, SF_6^-) is generated by attaching cold electrons[2,3,12] to SF_6 gas in an Ar^+-cold electron plasma via the resonant reaction $e^- + SF_6 \rightarrow SF_6^-$. The cross section for electron attachment to SF_6 has a maximum for cold electrons with energy near 0.1 eV[13]. The PANIC

plasma experiment operates at neutral pressure low enough so that collisions with neutral particles will not dominate the collective behavior of the plasma.[12] The neutral pressure was $P_o \lesssim 6 \times 10^{-5}$ Torr and typical PANIC ion temperature was $T_+ \lesssim 0.2$ eV. From this the ion-neutral collision frequency can be estimated at[11] $\nu_{+n} \lesssim 500\ s^{-1}$. The plasma density of $n \sim 10^8\ cm^{-3}$ gives a Coulomb collision frequency[11] $\nu_{+-} \sim 1000\ s^{-1}$. The plasma is "collisionless" in the sense that $\nu_{+n} < \nu_{+-} << \omega_{p+}$ and both are much less than the frequencies of interest.

A laboratory steady state beam-plasma interaction was maintained in a Double Plasma (DP)[1,3,12] consisting of a 40 litre multidipole line cusp confinement device,[14] containing two separate PANIC plasmas at different and controllable plasma potentials. A beam of ions was injected from one half of the PANIC DP to the other. Beams with densities equal to 10% of the background target density could be created. Fig. 9a shows the PANIC DP with cold electron sources, individually biased target anode, and the beam control grid between targets. The grid can be biased to potentials as shown for example in Fig. 9b to transmit single beam species. Electrostatic probes were used to determine plasma density and temperature, beam energy and density, and also the wavefront arrival time for the beam driven disturbances. The probes were 0.6 cm diameter tantalum discs that could be moved in three dimensions, with two choices of orientation (facing towards and away from the beam). By simultaneously triggering data acquisition on a reference probe and movable search probes, a graph of phase versus spatial location of unstable waves was

Fig. 9a,9b

constructed in three dimensions. This yielded information about frequency, wavelength and damping. The data were found to be in good agreement with the fluid theory prediction.

IV. Data

A dominant frequency is observed for the PANIC beam-plasma instability, and is probably the non-linearly saturated most unstable frequency (ω_I). The value of ω_I is consistent with the fluid model prediction of a most growing mode at $\omega_I = \omega[(\gamma/\omega)_{max}] \sim 0.6\ \omega_{p+} \sim 0.5\ \omega_p$. The data give a best fit to $\omega \approx (0.5 \pm 0.1)\omega_p$ given in Fig. 10, a graph of noise frequency (f_I) versus plasma frequency (f_p). Fig. 10

The wavelength measurements are consistent with the dispersion relation (including electrons), $\omega_I = \xi \vec{k} \cdot \vec{v}_b$. The value of the parameter ξ has the range $0.8 \lesssim \xi \lesssim 1.0$ from the fluid approximation for the beam-plasma mode. Fig. 11 is a graph of f_I versus $v_b/\lambda_{I\parallel}$, where v_b is the beam velocity and $\lambda_{I\parallel}$ is the wavelength corresponding to the projection of $\vec{k}$ on $\vec{v}_b$. A straight line fit to the data cannot distinguish between $\xi = 0.9$ and $\xi = 1.0$. Fig. 11

It is interesting to note that waves are driven obliquely to the beam direction on occasion. Data in Fig. 11 show that the cosine factor is not always equal to one.

These data indicate that beam driven noise of the fluid beam-plasma instability type is indeed observed. The fluid relative growth rate has a gentle maximum as a function of wavenumber at the frequency $\omega_I \equiv \omega[(\gamma/\omega)_{max}]$. Evidently this is enough of a maximum to generate a reasonably monochromatic instability for a given beam velocity and plasma density. The saturation level of the turbulent fluctuations could be made smaller than $\delta n/n \sim 10^{-3}$. The beam driven waves propagated several wavelengths before damping out. Note that the group velocity is identical to the phase velocity for this wave (i.e. it is non-dispersive).

The electron impurity population can be inferred from a Langmuir trace of the PANIC plasma, such as Fig. 12. This shows a current vs. voltage characteristic of an electrostatic probe in the plasma, where the saturation current $I_{*SF_6^-}$ - (I_{*Ar^+}) of the negative (positive) species is measured down (up) from the inflection point on the Langmuir trace. The electron free PANIC plasma characteristic should have saturation currents $I_{*SF_6^-}/I_{*Ar^+} = (m_{Ar^+}/m_{SF_6^-})^{1/2} \sim 0.6$. The electrons add to the measured negative saturation current to give an estimate of $n_e/n_- \approx 4 \times 10^{-4}$. Upper limits on the temperature of the ion species can be determined from a typical Langmuir trace like Fig. 12. The slopes of Ar^+ and SF_6^- portions of the curve are not the same. Typically the temperature of the heavier species ($T_{SF_6^-}$) was seen to be warmer than the Argon temperature (T_{Ar^+}) ($T_{SF_6^-} \approx 0.2$ eV, $T_{Ar^+} \approx 0.1$ eV). These approximate temperatures correspond to thermal velocity ratio $\alpha = v_-^2/v_+^2 \sim 0.45 - 0.65$.

Fig. 12

In Fig. 13 a Langmuir trace shows the "source" plasma potential and "target" characteristics, including the target plasma potential and beam "bump" contribution. Fig. 13

V. Discussion

The fluid model of the PANIC-beam system predicts that a beam-plasma instability exists for beam velocity $2 \lesssim v_b/v_+ \lesssim 10$. For the PANIC plasma, the data verify that waves of this nature can indeed be driven by beams. The dispersion relation of the beam mode is predicted by fluid calculations and observed to be $\omega_I = \xi \vec{k} \cdot \vec{v}_b$, where $0.8 < \xi < 1.0$, and the unstable frequency is $\omega_I \sim 0.5\ \omega_p$. In a previous experiment Wong et al.[2] drove waves in a negative ion-positive ion plasma with a toneburst grid, using approximately 1 volt ($e\phi \sim 4\ T_e$). In that experiment the waves were at $0.4\ \omega_{p+}$ but were identified as "fast ion acoustic" waves.

In the PANIC experiment, the neutral pressure was near $P_o \sim 6 \times 10^{-5}$ Torr, with result that neutral collisions did not dominate the collective behavior of the plasma. For plasma frequencies typically $\omega_{p+} \sim 10^4$-$10^6\ s^{-1}$, $\nu_{+n}/\omega_{p+} \lesssim 10^{-2}$. The electron impurity is shown to be less than 0.1% of background.

This PANIC-DP experiment demonstrated the existence of a beam driven mode in an unambiguous fashion. A reasonable range of parameters was explored in beam velocity ($v_b/v_+ \sim 1.4$ - 10) and wavelength ($\lambda_I \sim 0.3$-10 cm) for both beam species. Plasma frequencies range from 50kHz to 800 kHz (Figs. 8, 9). This corresponds to PANIC plasma densities from $n_o = 5 \times 10^6$ - $3 \times 10^8\ cm^{-3}$.

VI. Conclusion

A Positive And Negative Ion Confinement (PANIC) plasma has been considered from the fluid model point of view, and also created in the laboratory as an $Ar^+ - SF_6^-$ plasma with virtually no free electrons. With this plasma, a beam-plasma instability was driven and observed experimentally. The PANIC plasma has a mass ratio of $m_-/m_+ \sim 3.5$, which corresponds to the typical simulated plasma systems of computer Particle-In-Cell techniques.

The fluid approximation has been used to show that this PANIC plasma exhibits two-ion plasma oscillations, sound waves and unstable beam modes. One such beam instability is reported here. The sound wave speed c_s corresponds to v_-, the thermal velocity of the slower and heavier PANIC ion (SF_6^-). A mass ratio of order unity has the consequence that the sound waves and plasma oscillations occur at frequencies less than an order of magnitude apart. After an ion beam was added to the dispersion relation, two beam driven modes were predicted by the fluid solutions. These were named "fast" and "slow" beam modes, due to phase velocity respectively faster or slower than the beam velocity (v_b). For slow beam velocities $v_b \sim v_-$, the slow beam mode can couple to a sound wave. For large enough beam velocities ($2 < v_b/v_+ < 10$) the fast and slow beam modes coalesce into a complex conjugate pair, with one member growing and the other damping. This mode has been experimentally observed in steady state. All these fluid modes have been classified on a graph of wave

phase velocity versus beam velocity. The PANIC- beam system was shown to exhibit behavior analogous to that of the better known electron-ion-beam systems.

Of the two PANIC beam unstable modes predicted by this fluid model, one has been observed in the laboratory, using a PANIC-DP device. This beam-plasma instability has a dispersion relation given from numerical solutions to the fluid equations $\omega = \xi \vec{k} \cdot \vec{v}_b$, where the coefficient $0.8 < \xi < 1.0$ is insensitive to the many parameters including wavenumber, beam velocity, beam and background temperature, beam density, and electron impurity fraction. The frequency at which maximum relative growth rate occurs was predicted to be $\omega(\gamma/\omega)_{max} \sim 0.5\ \omega_p$, and confirmed by experiment. The values for most unstable ω and k are also insensitive to the many salient parameters.

Electrostatic probes were used to measure the unstable frequencies, wavelengths, and spatial propagation of waves. The data agree well with the fluid predictions. This experiment was carried out at low neutral pressures and density fluctuation levels, so that waves did not need to be driven by a grid[2] and wave damping from neutral collisions or turbulence was not a problem. A wide selection of beam velocities and densities, of either PANIC species (Ar^+ or SF_6^-) was available inside the Double Plasma (DP) device.

VII. Acknowledgments

This work has been supported by NASA grant number NAGW-275, Air Force grant number F29601-81-K-0018, and NSF grant number ECS-8203965.

REFERENCES

[1] H. Ikezi, R.J. Taylor, Phys. Rev. Lett., 24, 206 (1970).

R.J. Taylor, K.R. MacKenzie, H. Ikezi, Rev. Sci. Instrum., 43, 1675 (1972).

[2] A.Y. Wong, G. Mamas, D. Arnush, Phys. Fluids, 18, 1489 (1975).

[3] N. Hershkowitz, T. Intrator, Rev. Sci. Instr., 52, 1629 (1981).

[4] I. Langmuir, Gen. Electric. Rev., 27, 449 (1924).

J.R. Pierce, Journ. Appl. Phys., 19, 231 (1948).

G.D. Boyd, L.M. Field, R.N. Gould, Phys. Rev., 109, 1393 (1958).

R.J. Briggs, Electron-Stream Interactions with Plasmas, MIT Press, Cambridge, MA (1964).

[5] B. Fried, A.Y. Wong, Phys. Fluids, 9(6), 1084 (1966).

[6] R.J. Taylor, F.V. Coroniti, Phys. Rev. Lett., 29 (1), 34 (1972).

N. Hershkowitz, T. Romesser, G.Knorr, C.K. Goertz, Phys. Rev. Lett., 33, 754 (1974).

[7] S. Ichimaru, Phys. Fluids, 5 (10), 1264 (1962).

[8] M. Bacall, G.W. Hamilton, A.M. Bruneteau, H.J. Doucet, J. Taillet, Rev. Sci. Instrum., 50, 719 (1979).

M. Bacall, G.W. Hamilton, Phys. Rev. Lett., 42, 1538 (1979).

M. Seidl, A. Pargellis, Phys. Rev. B (USA), 26, 1 (1982).

M. Bacall, H.J. Doucet, Vacuum (GB), 24, 595 (1974), Conf. on Negative Ions, Liverpool, Lancastershire, England.

H.J. Doucet, R. Rouille, Vacuum (GB), 24, 527 (1974), Conf. on Negative Ions, Liverpool, Lancastershire, England.

Ehlers, K.W., Leung, K.N., Rev. Sci. Instrum., 51, 721 (1980).

[9] N. D'Angelo, S.V. Goeler, T. Ohe, Phys. Fl., 9, 1605 (1966).

[10] R.W. Gould, Phys. Rev. 136, A991 (1964).

[11] D.L. Book, NRL Plasma Formulary, Naval Research Laboratory, Washington, D.C. (1980).

[12] T. Intrator (thesis) Univ. Colorado, Boulder (1982).

[13] R.K. Asundi, J.D. Craggs, Proc. Phys. Soc., 83, 611 (1964).

[14] R. Limpaecher, K.R. MacKenzie, Rev. Sci. Instr., 44, 726 (1973).

A. Lang, N. Hershkowitz, J. Appl. Phys., 49, 4707 (1978).

FIGURE CAPTIONS

Fig. 1. A plot of typical velocity distribution function for an electron-ion-ion beam plasm, with $v_b >> c_s$. (a) Beam velocity v_b is the center velocity of the beam and c_s is the ion-acoustic sound speed. (b) $v_b \sim c_s$; the slow beam mode and ion-acoustic root couple.

Fig. 2. Maxwellian velocity distribution function of PANIC plasma with beam. (a) For $v_b >> v_+$. (b) For $v_b \sim v_+$, the beam-sound wave is the analogue of beam driven "ion- acoustic" modes.

Fig. 3. ω versus k showing coupled beam plasma mode for $v_b/v_+ = 6$. Fast and slow beam modes are coupled here. Two growth rates are also plotted. The relative growth rate (γ/ω) is germane to this problem, although absolute growth rate (γ) is given as well.

Fig. 4. ω versus k showing the slow beam mode coupling to a sound wave, and γ/ω for $v_b/v_+ = 1.3$.

Fig. 5. Phase velocity versus beam velocity for a typical fluid model solution to the PANIC plasma with beam excitation. The beam driven sound wave is shown for $v_b \sim v_+$, and for beam velocities much greater than thermal velocities, the beam-plasma mode is shown with growth rate γ/ω. The general features are not very dependent on any other parameter of the plasma-beam system.

Fig. 6. Phase velocity versus beam velocity for the PANIC fluid model, showing the results for real ω-complex k to be very similar to the case of complex ω-real k. Note that $\omega > \omega_p$ in order that the "Langmuir" wave can exist.

Fig. 7. A linear graph of phase velocity versus beam velocity, showing all six roots of the PANIC- beam system.

Fig. 8. Graph of phase velocity/beam velocity vs. wavenumber for the PANIC plasma. The dispersion relation $\omega/\underset{\sim}{k}\cdot\underset{\sim}{v}_b \approx 1$ is insensitive to the beam density for the wavenumber of interest ($0.1 < k_* < 0.3$).

Fig. 9. (a) Schematic of the PANIC double plasma device (DP).
(b) Potential versus distance in the DP, showing the grid modulation of beam flux crossing the source to target.

Fig. 10. A graph of the experimentally observed most growing frequency (f_I) versus plasma frequency (f_p). The best straight line fit gives $0.5 \lesssim f_I/f_p \lesssim 0.6$, in agreement with the fluid model, for the frequency of the fastest growing beam-plasma mode.

Fig. 11. A graph of experimental data showing the dispersion relation for the beam plasma instability. f_I is plotted against v_b/λ_I in the parallel (to the beam) direction. The best straight line fit is consistent with $\omega \sim 0.9(\pm 0.1)kv_b$.

Fig. 12. Typical Langmuir trace from the PANIC plasma, showing saturation currents, with the inflection point of the "knee" for each contribution.

Fig. 13. Langmuir traces of source (bottom) and target plasmas (top) showing the target beam "bump" to a SF_6^- beam injected from the source. When the target probe is biased more negatively than ϕ_{pS}, the beam contribution is "turned off." Beam energy is $E_b = e(\phi_{pT} - \phi_{ps}) \sim 3.8$ eV. For slow trace sweeps like this, noise is averaged out giving the "thick" lines.

TABLE 1

CHARACTERISTICS OF LABORATORY PLASMAS

Parameters	Electron-Ion	PANIC
Mass Ratio	1836:H^+/e^- 74000:Ar^+/e^-	3.5:SF_6^-/Ar^+
Plasma Frequency $2\pi f_p = \sqrt{4\pi e^2 n/m}$	10^7 - 10^{10} Hz $f_{pe} >> f_{pi}$	$f_{p+} \sim f_{p-} <$ MHz $f_{p+} \sim 33[n_+(cm^{-3})]^{1/2}$
Temperatures	kT_e = 0.1 - 4.0 eV $T_e > T_i$	$T_+ \sim T_- \sim$ 0.1 - 0.3 eV
Density	$n = 10^6 - 10^{12}$ cm^{-3}	$n = 10^5 - 10^9$ cm^{-3}
Debye length $\lambda_D \sim 740\sqrt{T/n}$	$\lambda_D \sim 10^{-3} - 10^{-1}$ cm	$\lambda_D \sim 10^{-2}$ - 1 cm
Waves	Langmuir Ion Acoustic	Plasma Oscillation Sound Waves

Fig. 1

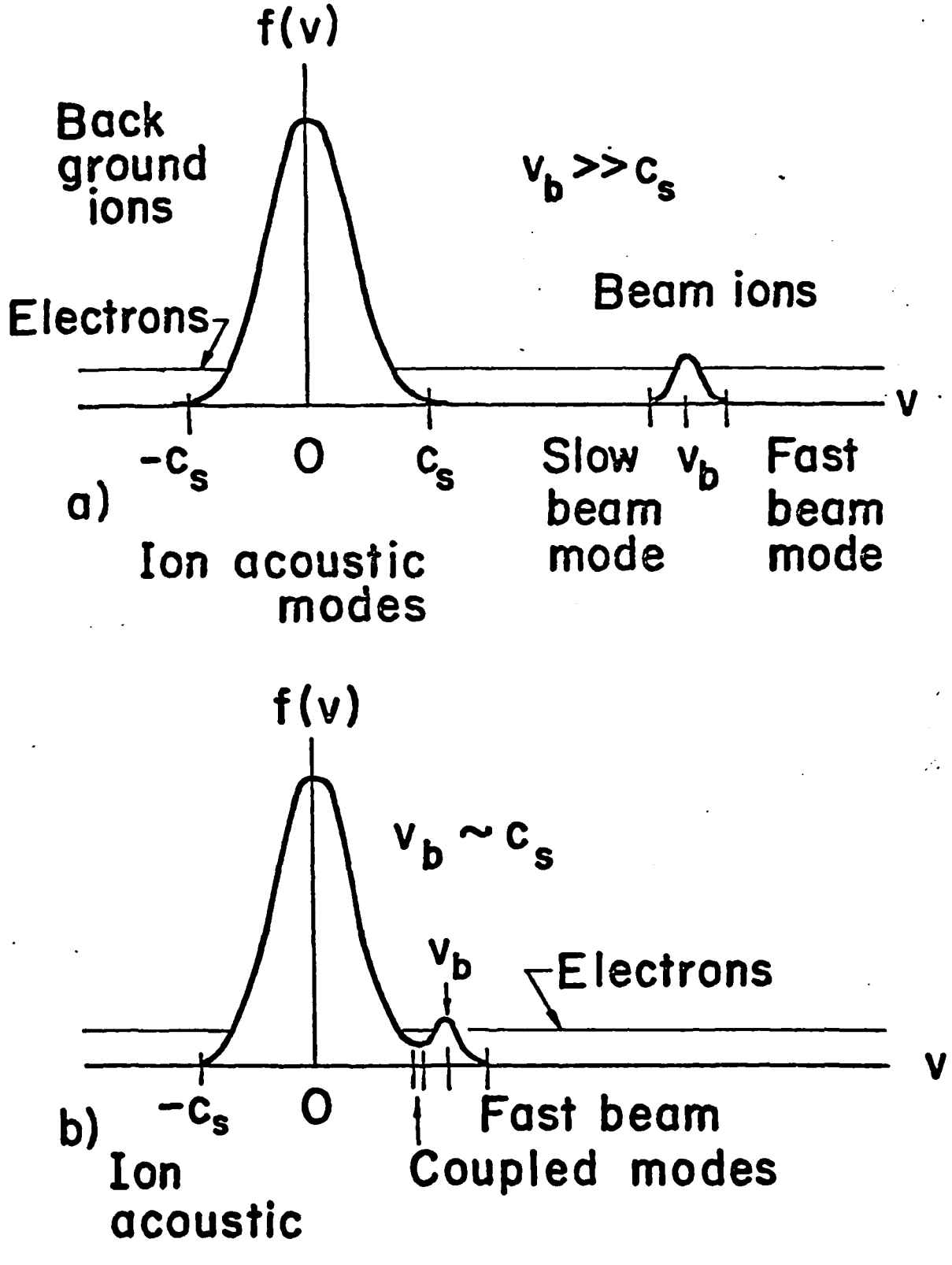
f(v)
Back ground ions
$v_b >> c_s$
Beam ions
Electrons
v
$-c_s$
0
c_s
Slow beam mode
v_b
Fast beam mode
a)
Ion acoustic modes
f(v)
$v_b \sim c_s$
v_b
Electrons
v
$-c_s$
0
Fast beam
b)
Ion acoustic
Coupled modes

Fig. 2

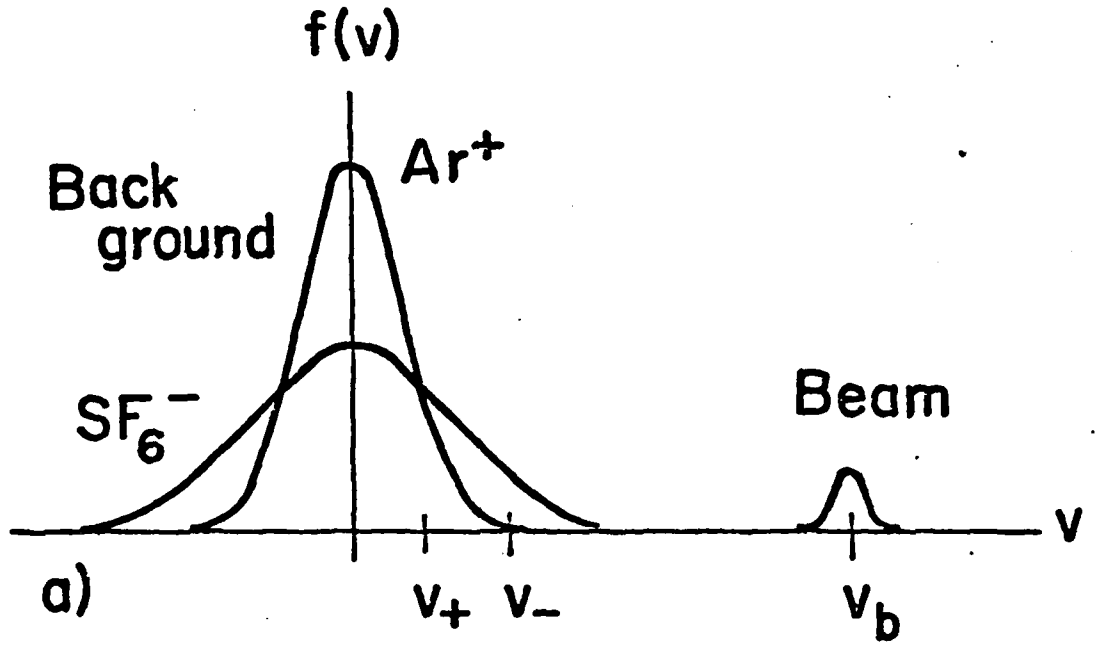

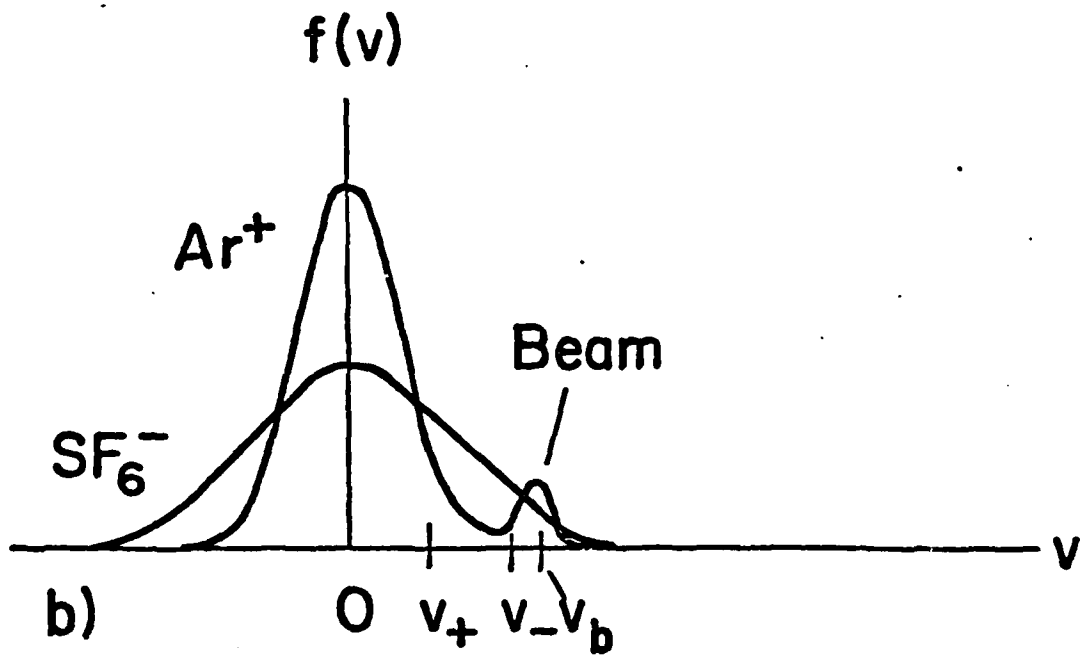

Fig. 3

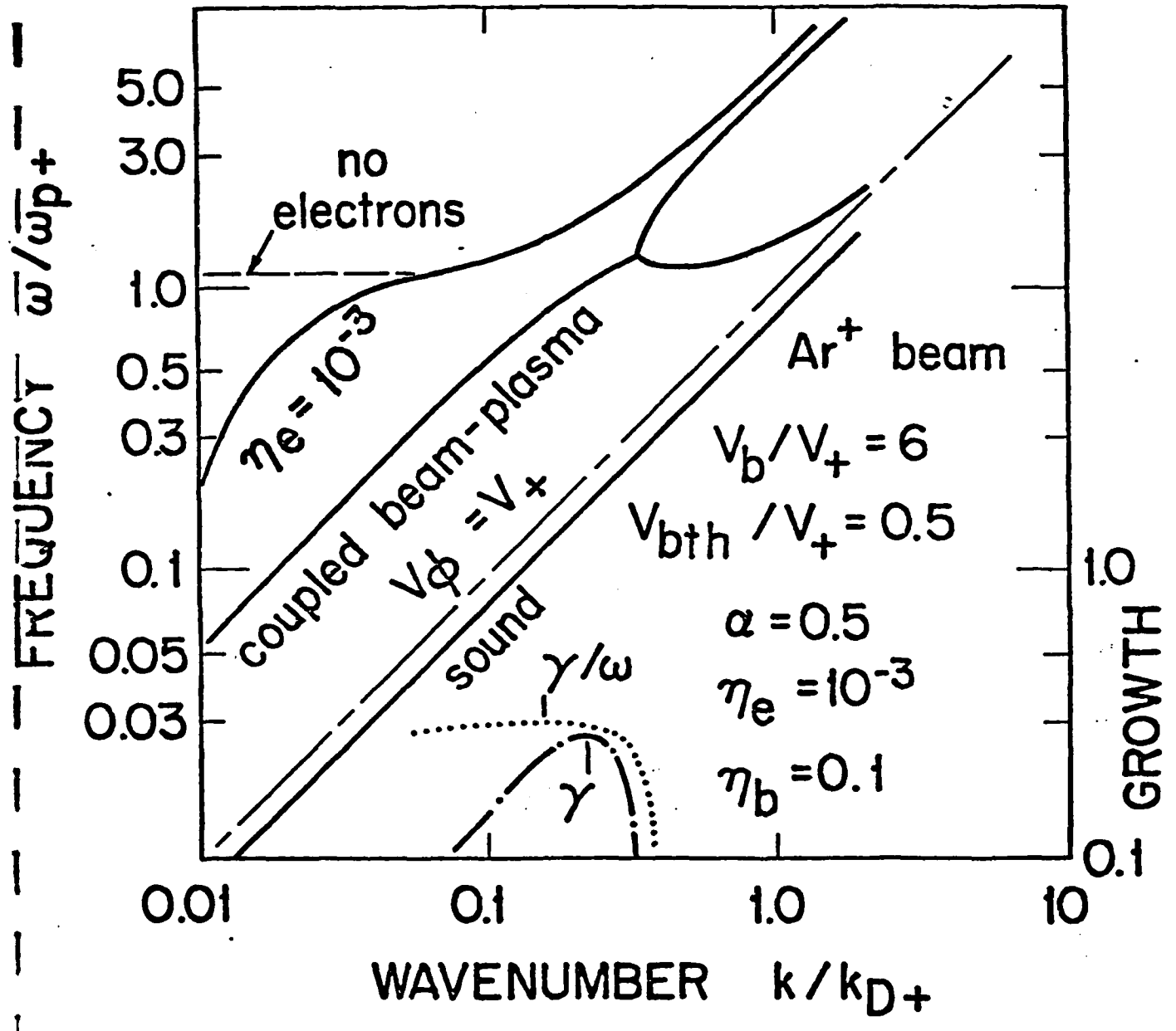
FREQUENCY ω/ω_{p+}
5.0
3.0
1.0
0.5
0.3
0.1
0.05
0.03
no electrons
$\eta_e = 10^{-3}$
coupled beam-plasma
$V_\phi = V_+$
sound
γ/ω
γ
Ar^+ beam
$V_b/V_+ = 6$
$V_{bth}/V_+ = 0.5$
$\alpha = 0.5$
$\eta_e = 10^{-3}$
$\eta_b = 0.1$
1.0
0.1
GROWTH
0.01
0.1
1.0
10
WAVENUMBER k/k_{D+}

Fig. 4

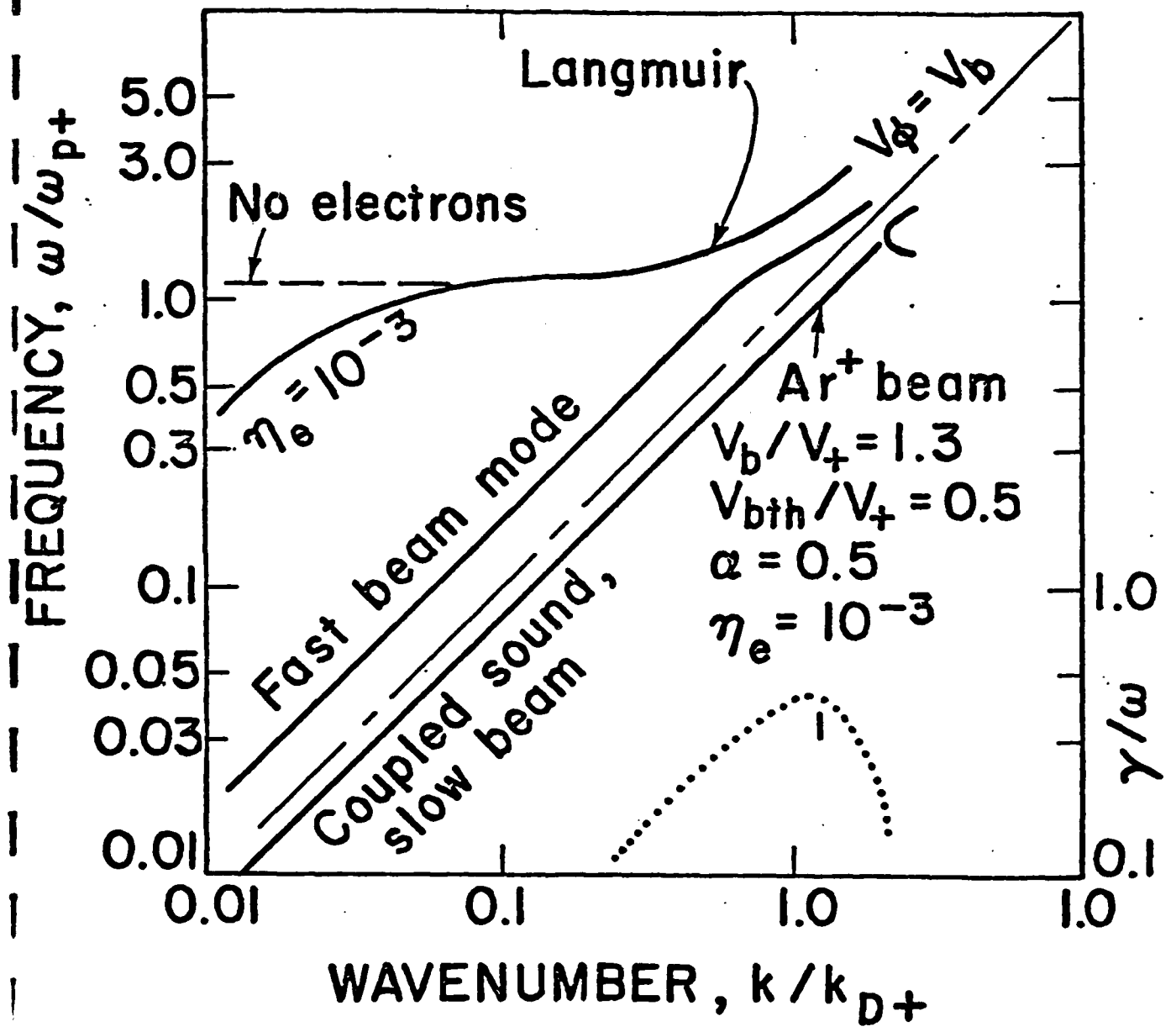
Langmuir
$V_\phi = V_b$
No electrons
$\eta_e = 10^{-3}$
C
Ar^+ beam
$V_b/V_+ = 1.3$
$V_{bth}/V_+ = 0.5$
$\alpha = 0.5$
$\eta_e = 10^{-3}$
Fast beam mode
Coupled sound, slow beam
I
FREQUENCY, ω/ω_{p+}
5.0
3.0
1.0
0.5
0.3
0.1
0.05
0.03
0.01
γ/ω
1.0
0.1
0.01
0.1
1.0
1.0
WAVENUMBER, k/k_{D+}

Fig. 5

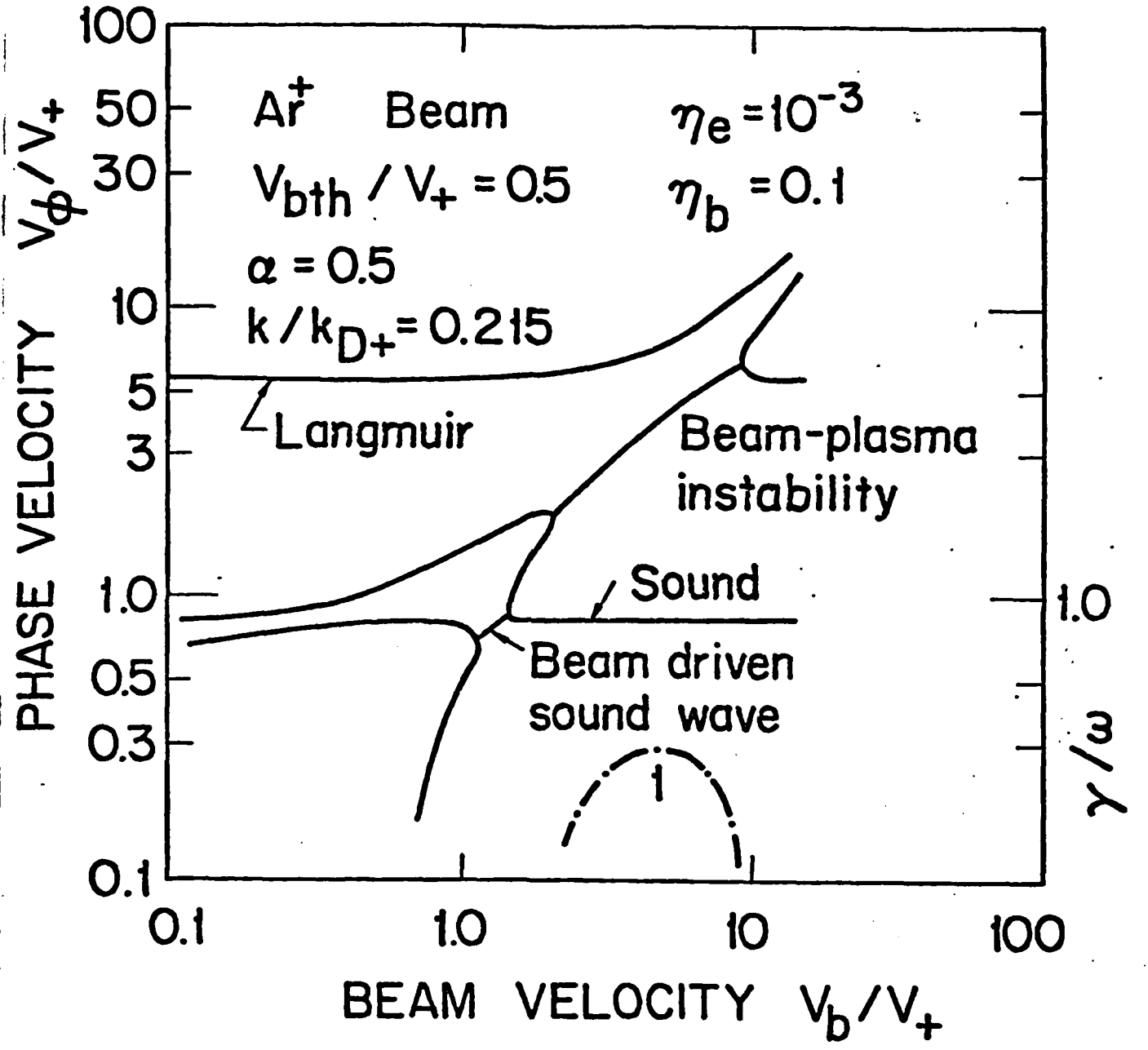
100
50
30
10
5
3
1.0
0.5
0.3
0.1
PHASE VELOCITY V_ϕ / V_+
Ar^+ Beam
$V_{bth} / V_+ = 0.5$
$\alpha = 0.5$
$k / k_{D+} = 0.215$
$\eta_e = 10^{-3}$
$\eta_b = 0.1$
Langmuir
Beam-plasma instability
Sound
Beam driven sound wave
1
1.0
γ / ω
0.1
1.0
10
100
BEAM VELOCITY V_b / V_+

Fig. 6

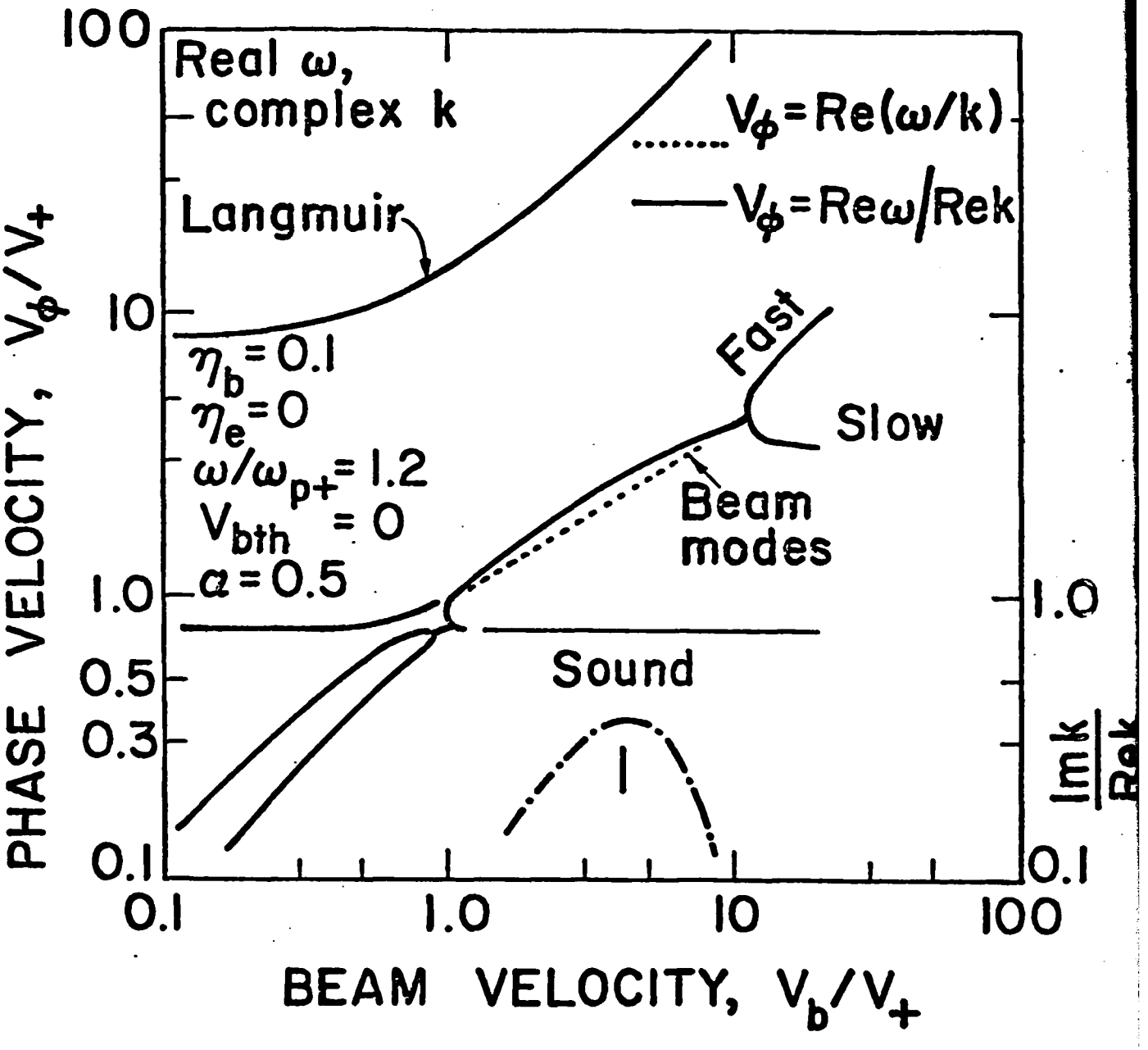
Real ω,
complex k
$V_\phi = Re(\omega/k)$
$V_\phi = Re\omega/Rek$
Langmuir
Fast
Slow
$\eta_b = 0.1$
$\eta_e = 0$
$\omega/\omega_{p+} = 1.2$
$V_{bth} = 0$
$\alpha = 0.5$
Beam modes
Sound
100
10
1.0
0.5
0.3
0.1
0.1
1.0
10
100
PHASE VELOCITY, V_ϕ/V_+
BEAM VELOCITY, V_b/V_+
$\frac{Imk}{Rek}$

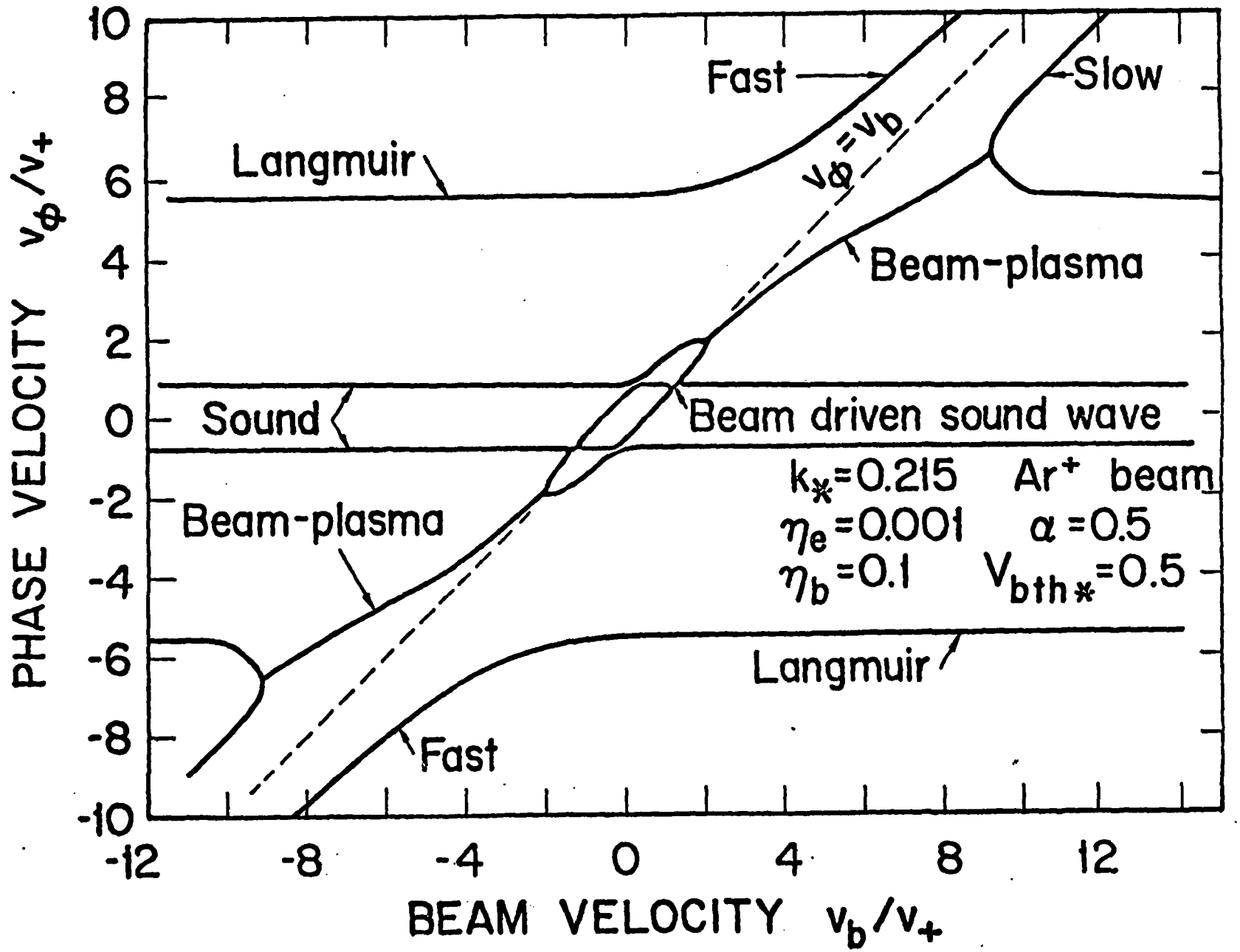
PHASE VELOCITY v_ϕ/v_+
BEAM VELOCITY v_b/v_+
10
8
6
4
2
0
-2
-4
-6
-8
-10
-12
-8
-4
0
4
8
12
Fast
Slow
Langmuir
$v_\phi = v_b$
Beam-plasma
Sound
Beam driven sound wave
$k_* = 0.215$ Ar^+ beam
$\eta_e = 0.001$ $\alpha = 0.5$
$\eta_b = 0.1$ $V_{bth*} = 0.5$
Beam-plasma
Langmuir
Fast

Fig. 7

Fig. 8

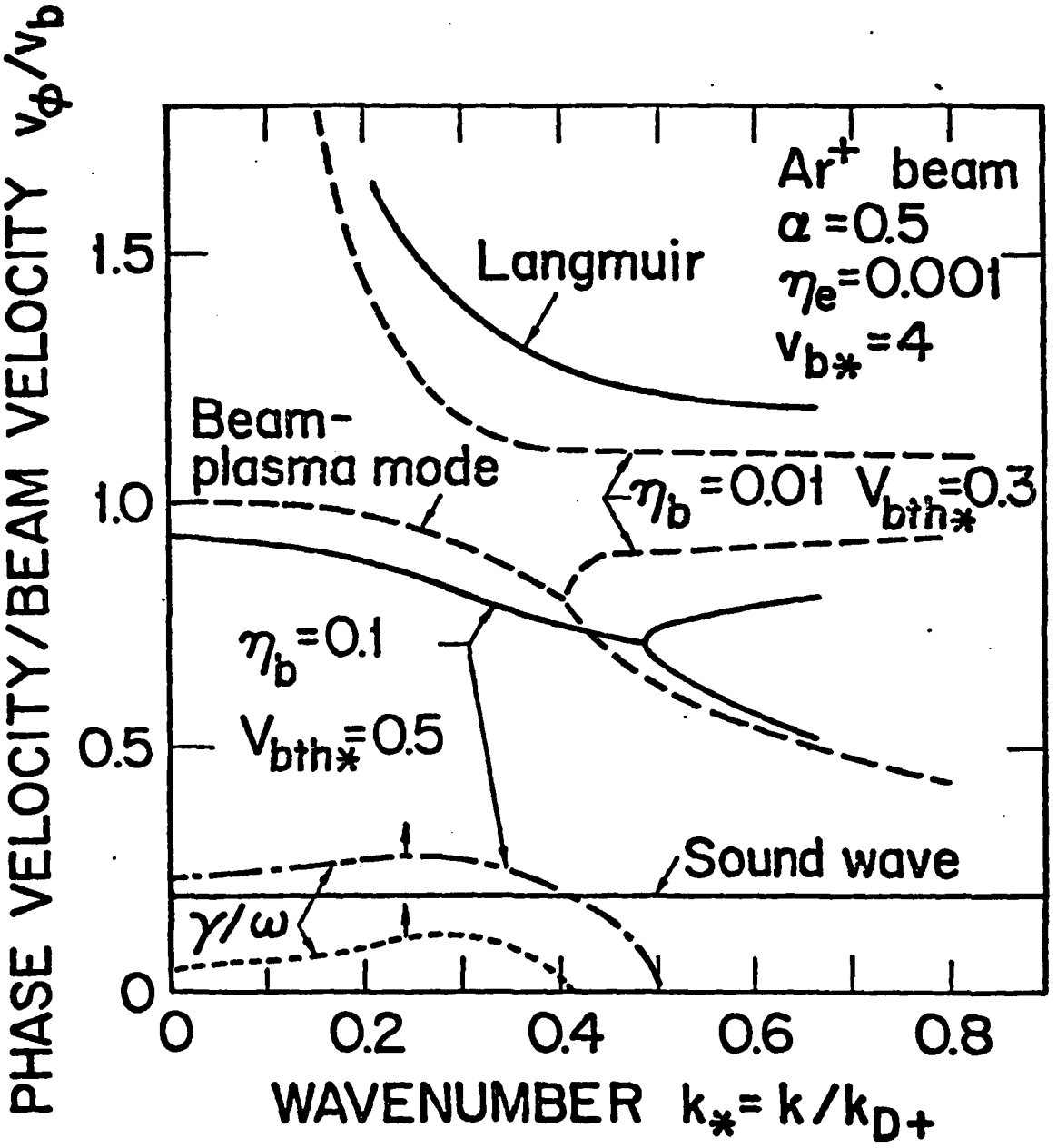
PHASE VELOCITY/BEAM VELOCITY v_ϕ/v_b
1.5
1.0
0.5
0
0
0.2
0.4
0.6
0.8
WAVENUMBER $k_* = k/k_{D+}$
Ar^+ beam
$\alpha = 0.5$
$\eta_e = 0.001$
$v_{b*} = 4$
Langmuir
Beam-plasma mode
$\eta_b = 0.01$ $V_{bth*} = 0.3$
$\eta_b = 0.1$
$V_{bth*} = 0.5$
Sound wave
γ/ω

Fig. 9

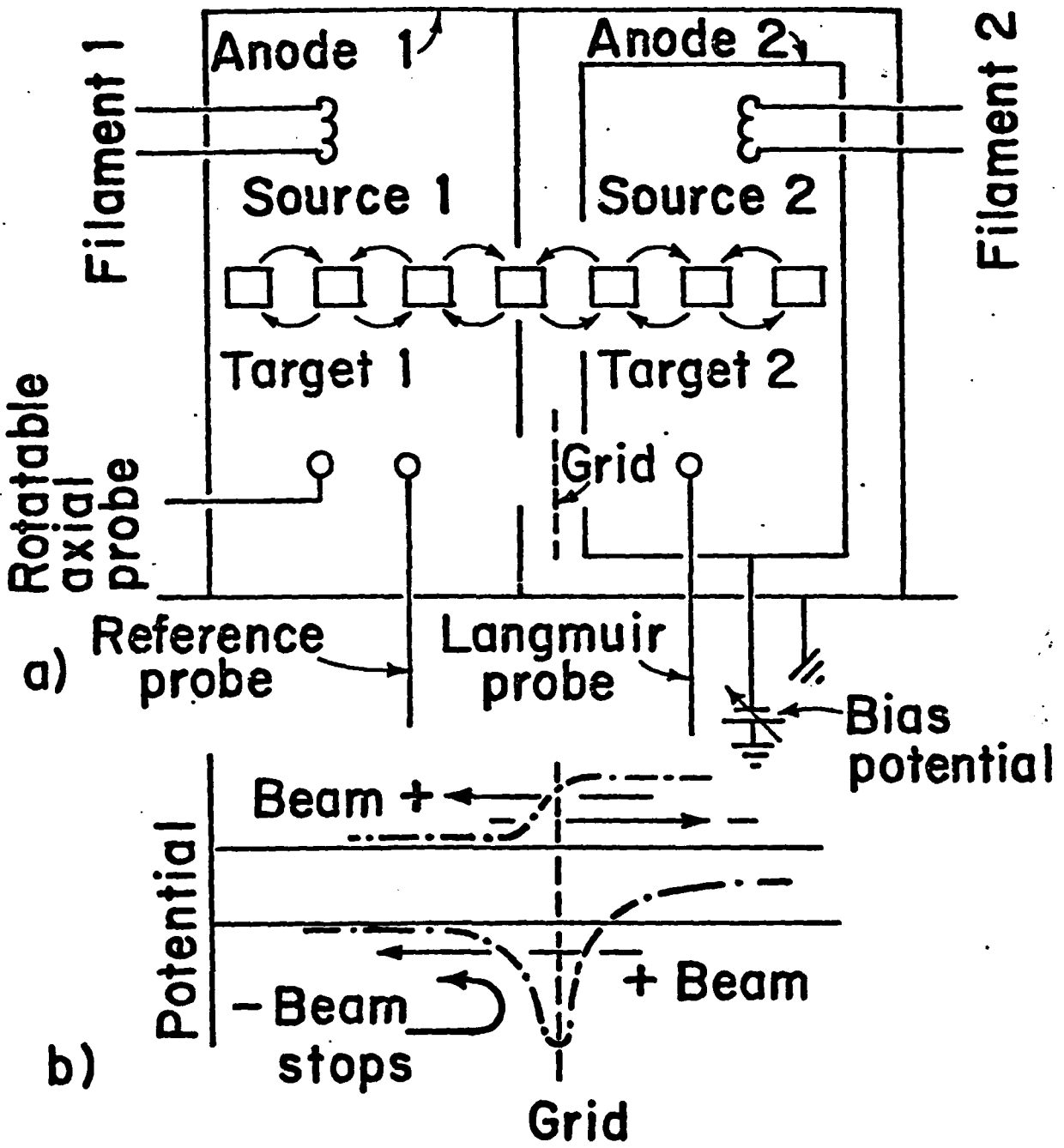
Anode 1
Anode 2
Filament 1
Filament 2
Source 1
Source 2
Target 1
Target 2
Grid
Rotatable axial probe
Reference probe
Langmuir probe
Bias potential
a)
Beam +
Potential
+ Beam
- Beam stops
b)
Grid

Fig. 10

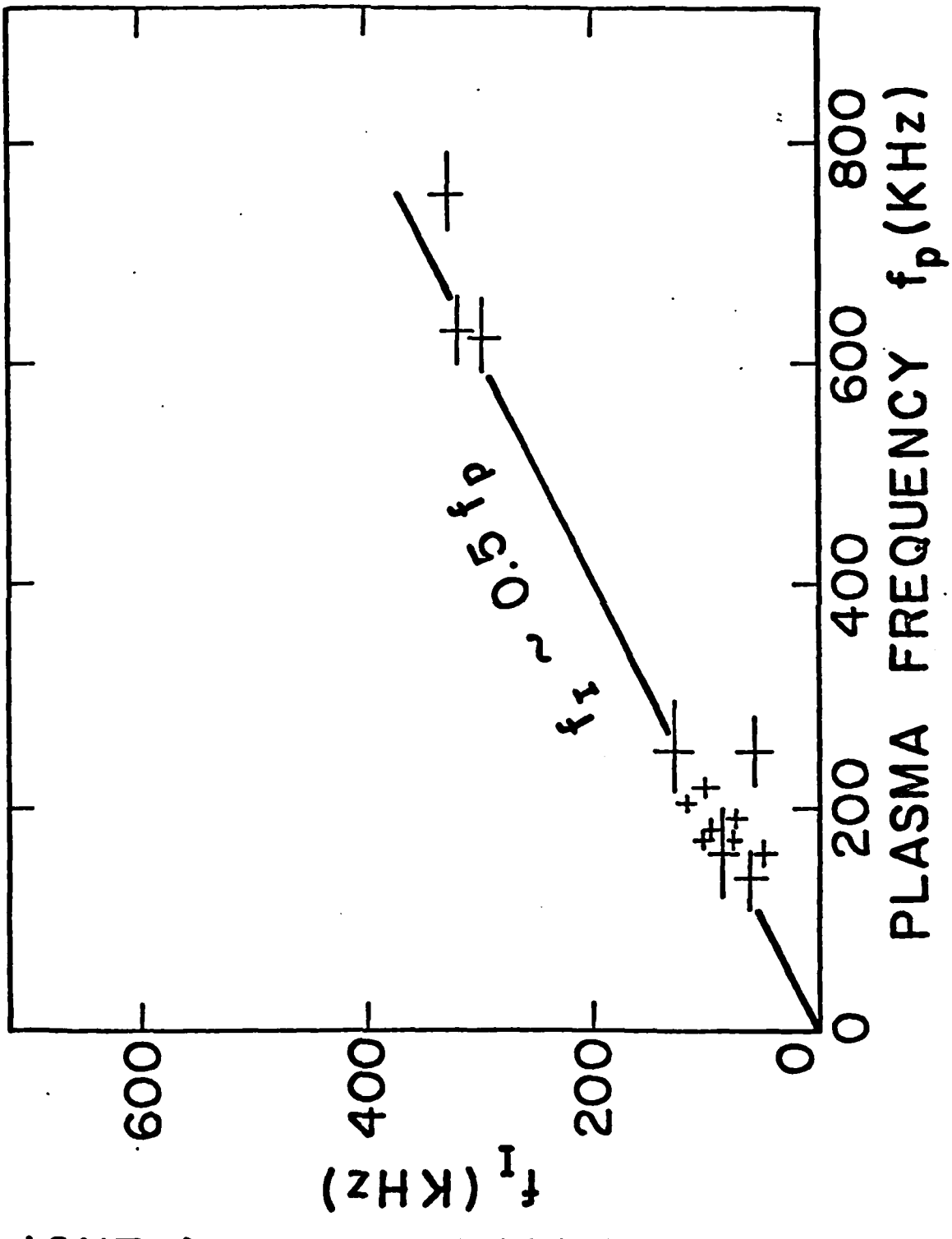
MOST UNSTABLE FREQUENCY
f_I (KHz)
600
400
200
0
PLASMA FREQUENCY f_p(KHz)
0
200
400
600
800
$f_I \sim 0.5 f_p$

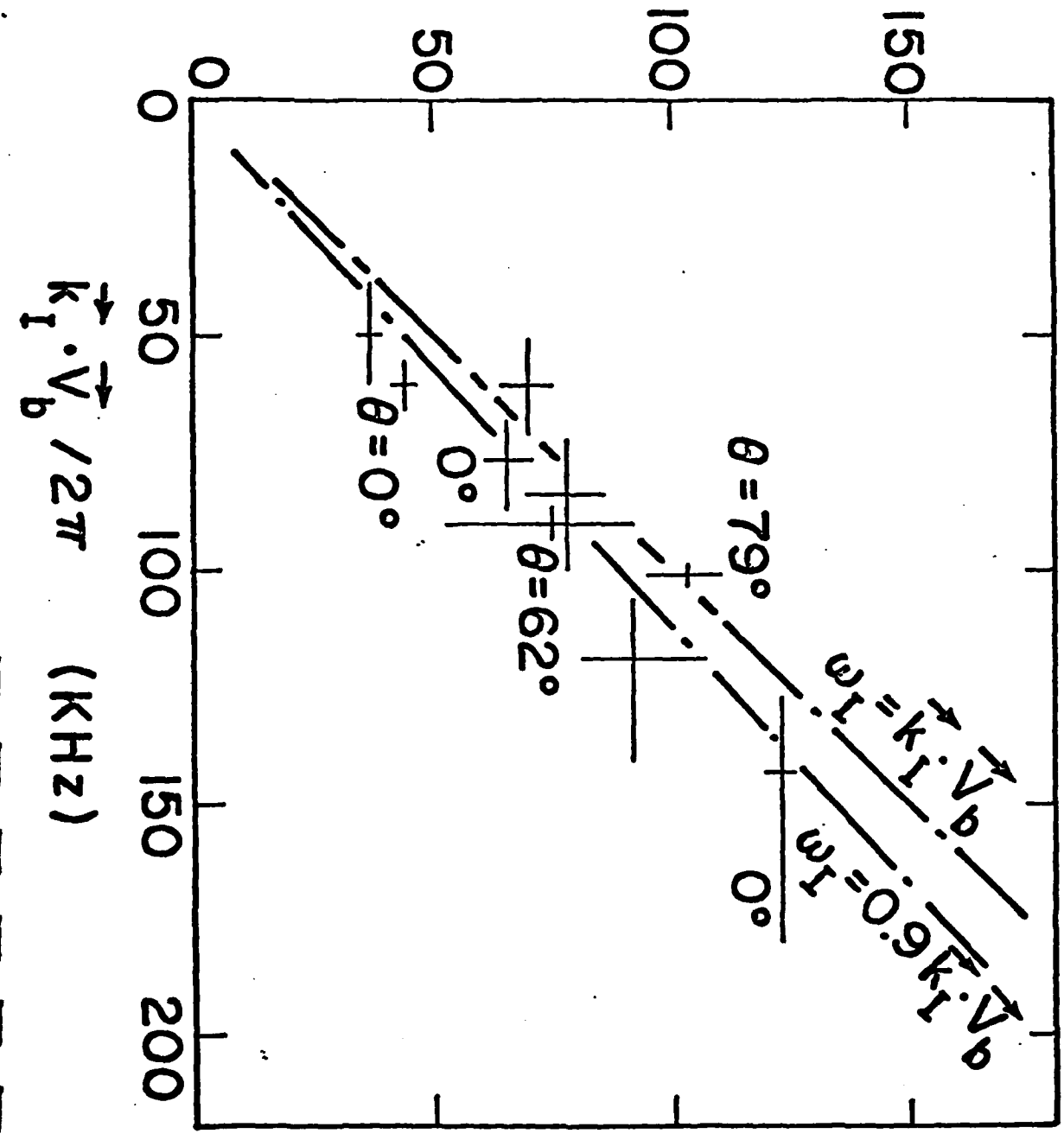
FREQUENCY OF INSTABILITY
f_I (KHz)
0
50
100
150
200
$\vec{k}_I \cdot \vec{V}_b / 2\pi$ (KHz)
$\theta = 0°$
$\theta = 62°$
$\theta = 79°$
$\omega_I = \vec{k}_I \cdot \vec{V}_b$
$\omega_I = 0.9 \vec{k}_I \cdot \vec{V}_b$

Fig. 11

Fig. 12

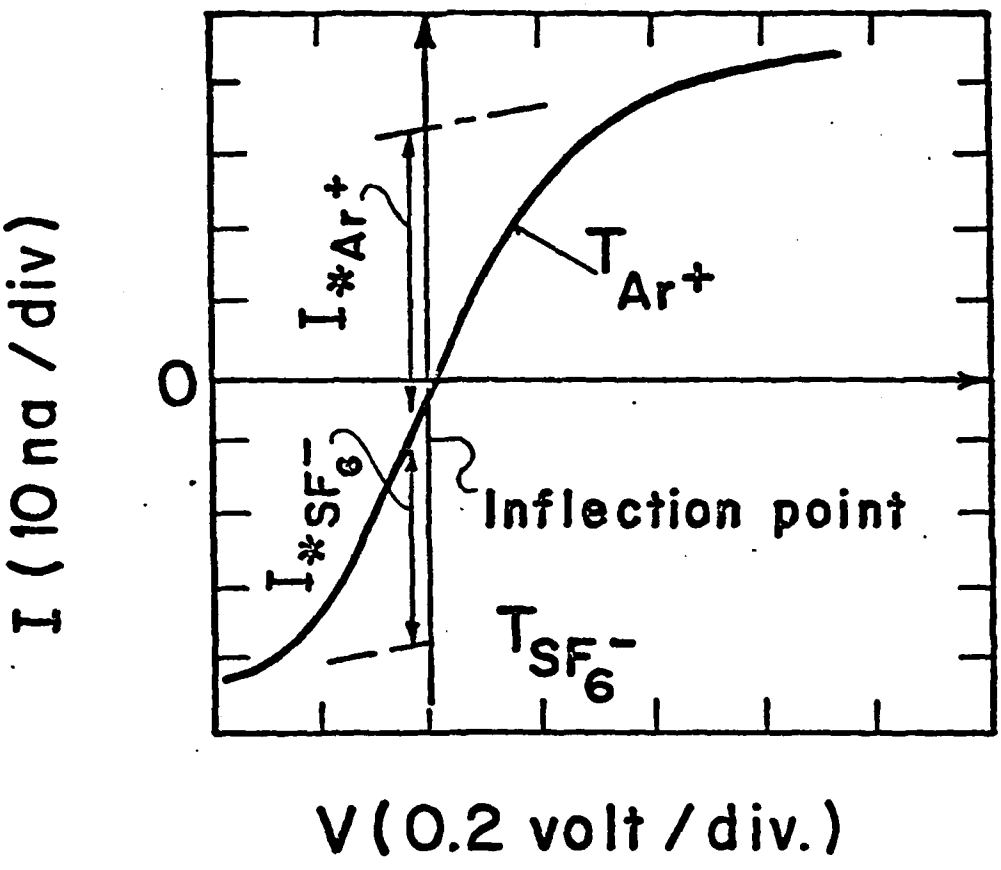

Fig. 13

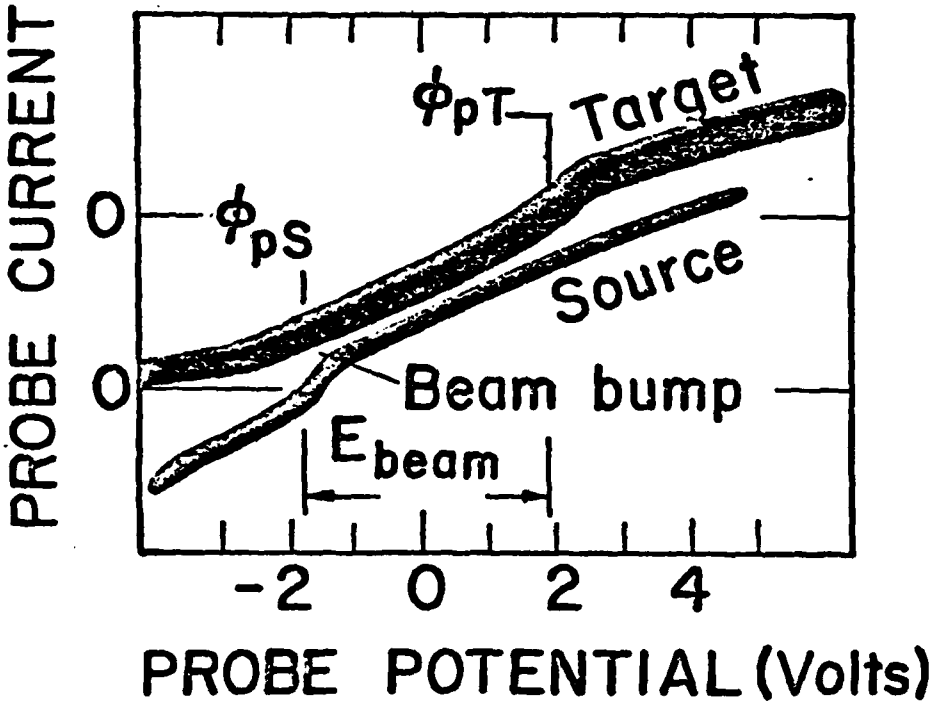
PROBE CURRENT
0
0
ϕ_{pT}
Target
ϕ_{pS}
Source
Beam bump
E_{beam}
-2
0
2
4
PROBE POTENTIAL (Volts)

APPENDIX G

G. "Intense Ion Transport in Electrostatic Ion Cyclotron Waves"

R.A. Stern and N. Rynn
Proceedings of the 1982 International Conference on Plasma Physics (October, 1982)

1.

INTENSE ION TRANSPORT IN ELECTROSTATIC ION-CYCLOTRON WAVES

R. A. STERN, University of Colorado, Boulder, CO 80309 &
N. RYNN, University of California, Irvine, CA 92717

ABSTRACT

A series of experiments documenting in detail the cross-magnetic field ion motion caused by intense electrostatic ion cyclotron waves is described. Using novel laser diagnostics, we observe large-scale ion heating and diffusion as well as the formation of pathological phase-space distributions.

INTRODUCTION

Electrostatic Ion Cyclotron Waves (EICW), the lowest-frequency eigenmodes of a magnetized plasma, are amongst the easiest to destabilize and consequently occur in a large variety of configurations, including tokomaks, mirrors, the magnetosphere and isotope separation schemes[1]). They have an appreciable oscillating electric-field component directed across the static magnetic field B. We describe intense ion heating and diffusion across B, driven by the oscillating electric field.

EXPERIMENTAL CONFIGURATION

Experiments were carried out in Q-machine plasmas[2]) using BaII, KII and CsII; and in ArII diffusion plasmas of the ECRH type. Typically, a 50% ionized plasma column 5 cm. in diameter is used, with $n_i = n_e = 10^8$ to 10^{10} cm^{-3}. The magnetic field is uniform to a few % and ranges from 1.5 to 8 KG. Ion temperatures are of order 0.2 eV; electron temperatures range from 0.2 eV in Q machines to 5 eV in the diffusion plasmas. The

2. EICW were excited by electron currents with the Drummond-Rosenbluth growth rate: $\gamma \approx (V_d/V_{th})^{\cdot}(T_e/T_i)$, where V_d and V_{th} are the electron drift and thermal speeds, respectively. Oscillating potential excursions in the wave ranged up to 2 V peak to peak.

DIAGNOSTICS

The ion distribution velocity function $F(\underline{v},\underline{r},t)$, was obtained through the use of laser-induced fluorescence techniques[3]). These methods resolve v to within 0.1 and 0.01 of the ion thermal speed; and define a diagnosed volume of order 1 mm^3 , which is scanned across the plasma. Time resolution to within a small fraction of the wave period w_{ci}^{-1} was achieved. A new method--Optical Tagging (OT)--was devised to follow the diffusion of ions[4]). In OT, ions are optically pumped by tunable lasers from one long-lived quantum state to another, and re-interrogated by another laser beam at a different point in space-time.

SUMMARY OF RESULTS

We describe experiments where the destabilizing electron current was generated by inserting a small-diameter electrode (e.g. 0.6 cm.) into the plasma. This localizes the current to an unstable filament aligned with B and of same diameter as the electrode, because of the small particle gyro-radii.

GROSS DENSITY CHANGES: As the destabilizing current increases, a dramatic loss of both electron and ion density occurs within the filament. In the limit, the residual density is only 20% of the initial value.

A corresponding increase in the density of the surrounding plasma is observed. Using OT, we follow the transport of ions which originate in the filament and diffuse all the way to the column edge, i.e. over cross-magnetic field distances one to two orders of magnitude larger than the background ion gyro-radii.

DYNAMICS OF EXPELLED IONS: Spatially and temporally resolved measurements[5]) of the distribution function of ejected ions reveal two components: a nearly Gaussian, heated and static (in time) population, amounting to about 1/3 of the diffused species, with temperatures up to 5 times the background value; and a dynamic component, 100% density modulated in synchronism with the EICW frequency, with central energies of order 1-2 eV and narrow velocity spread. This beam component is assymetric in velocity space; and also localized in radius to a region surrounding the unstable filament and distant from it by about one beam gyro-radius. The beam is found to rotate azimuthally in the direction of the diamagnetic ion current. Using OT to follow particle orbits expelled from the filament, we verify that this beam represents the net circulation of ions expelled radially from the filament with the peak energy of the potential oscillations, and undergoing magnetron rotation due to the $v \times B$ force.

MULTI-FILAMENT INTERACTION: The interaction between two unstable filaments was observed. When one strongly-driven "pump" filament is brought radially close to a marginally

4.

destabilized "target" filament, we find that the EICW intensity in the latter is decreased, and in the limit supressed entirely. This process is ascribed to the net export of hot ions out of the "pump" filament and into the "target", thereby increasing T_i and decreasing the net growth rate. This suggests that a system of many filaments will be unstable, since the more intense filaments will "export" more hot ions than they receive, quench surrounding filaments, and grow stronger still. This may be responsible for the broader width of EICW spectra in large-diameter unstable plasmas.

CONCLUSIONS: We have demonstrated a new type of wave-particle interaction with complex dynamics, occurring over scales many orders of magnitude more intense than conventional processes.

1) TFR Group, Phys. Rev. Lett. 41, 113 (1978); F. H. Coensgen, et al., ibid 35, 1051 (1975); F. S. Mozer, et al., ibid 38, 292 (1977); J. M. Dawson, et al., ibid 37, 1547 (1976), and E. S. Weibel, ibid 44, 377 (1980).

2) N. Rynn, Rev. Sci. Instru. 35, 40 (1964).

3) R. A. Stern and J. A. Johnson, III, Phys. Rev. 34, 1548 (1975); R. A. Stern, D. L. Correll, H. Bohmer and N. Rynn, ibid 37, 833 (1976).

4) to be published.

5) R. A. Stern, D. N. Hill and N. Rynn, Phys. Rev. Lett. 47, 792 (1981).

APPENDIX H

H. "Direct Ion Transport Measurements by Optical Tagging"

R.A. Stern, D.N. Hill, and N. Rynn
Accepted for publication in Physics Letters A

DIRECT ION TRANSPORT MEASUREMENT BY OPTICAL TAGGING

R. A. Stern*, D. N. Hill and N. Rynn

Department of Physics
University of California
Irvine, California 92717

UCI Technical Report #82-61 August 1982

Abstract

Optical pumping of long-lived quantum states is used to identify groups of ions in phase space and follow their transport. The principles and variants of a novel diagnostic method, as well as new physical aspects and applications, including space-dependent line-narrowing, are demonstrated.

We present a new non-perturbing diagnostic technique which directly measures particle transport with high space-time resolution, and some results obtained through its use. Optical tagging, the application of optical pumping to particles with appreciable kinetic motion, requires a multilevel quantum system comprising at least one long lived state. Tagging adds to the argument of the velocity distribution function $f(r,v,t)$ the definition of the quantum state B; i.e., $f(r,v,t,;B)$ has a "memory". It is therefore an extension and advance beyond laser fluorescence spectroscopy[1], since the complete phase-space history of particle motion is disclosed. In this communication we summarize the basic and technical aspects of optical tagging, and demonstrate interdisciplinary results: the measurement of the distribution function without scanning or dispersive optics, a velocity selection process applicable in spectroscopy as well as remote magnetic-field measurements, and the measurement of "anomalous" cross-magnetic field transport in a plasma.

The technique is demonstrated using two laser beams and a 3-level system with 2 long-lived levels O and B, as in Figure 1. A "pump" (P) laser is tuned to the transition O - A. It decreases the density ρ_o of O-state ions, and ultimately increases the density ρ_B of the B-state. A "search" (S) laser, located at the diagnosed point is tuned to any transition which has either O or B as a lower level. The S-beam induces fluorescence with intensity I proportional to ρ_o or ρ_B, as chosen. It contains a "tagged" component I_T whose magnitude depends on P. This second component, reflecting ion transport from the location of P to S can be

extracted from I by modulating the P beam intensity or frequency and using synchronous detection methods.

The experiments were carried out in a single-ended Q-machine at the University of California, Irvine[2], Fig. 1. A highly ionized Ba II plasma column is produced by contact ionization of Barium atoms on a 5 cm. dia. rhenium-coated hot plate. A magnetic field B < 7 kG perpendicular to the plate confines the charged particles to a column about 5 cm. dia. The background pressure is 10^{-6} Torr. Plasma densities are kept below 10^{10} cm^{-3}, and ion and electron temperatures are about 0.2 eV., so that collisions are negligible. The O, A and B states are respectively the $6^2S_{1/2}$ ground level, $6^2P_{1/2}$ excited and $5^2D_{3/2}$ metastable levels. The P-beam, a single mode scanning dye laser with output < 60 mW was tuned to the O-A transition at 4934 Å. A large f-number lens and photomultiplier pick up the fluorescence, I, induced by the S-beam at the intersection of its optical axis and the beam, defining a diagnosed volume of about 1 mm^3. The lens and S-beam are mechanically coupled and can be scanned across the plasma.

Two distinct modes of operation for Optical Tagging are demonstrated here. (1) "Dark" signals are obtained if the S-beam is tuned to a transition whose lower level is the O state. Here the fluorescence induced by the S-beam is reduced because the P-beam has depopulated the O-state initial density ρ_o; i.e., I_T is negative. (2) "Bright" signals are obtained if the S-beam is tuned to a transition whose lower level is the B-state. Now P has increased ρ_o; i.e., I_T is positive.

In Figure 2 (a) - (b), the P-beam is chopped at 1 kHz, while

S is on continuously. In Fig. 2(a), the S-beam is tuned to the same wavelength as P. During the on-periods of the P-beam, the top trace shows I decreasing ("Dark" pulse) by 75%. The lower trace shows I with the S-beam turned off. Residual light at 4934 Å during the P on-period represents elastic scattering from the chamber walls, and verifies that P was on when the S-induced fluorescence is reduced. In Fig. 2(b) the S-beam is tuned to 5854 Å, inducing transitions from the metastable level. With P on, I increases ("bright" pulse) by about 350%. With P off, I falls to its background value, which represents fluorescence from the background metastable density, roughly 10%.

Transport is measured most simply by pulsing the P-beam with a risetime shorter than the particle transit time τ between the P and S-beam positions. This method is illustrated in Figures 2(c) and (d). Here we measure ion drift parallel to the magnetic field, by axially displacing S 2.5 cm away from P, which is positioned 80 cm from the hot plate. The scheme used is "bright" pulse. Trace (c) monitors P, which has a risetime of about 0.1 μsec $<< \tau$. Trace (d) displays the intensity I of the S-beam induced fluorescence, with the "bright" pulse appearing 20 μsec after the P switch-on. It rises much more gradually ($\tau_R \approx 5$ μsec.), and decays more slowly than the P-beam. The rise-and-fall profiles of I represent the distribution of axial velocities due to the finite temperature of the ions, even though P is transverse and cannot select axial speeds. Independent verification is provided by monitoring the fluorescence directly induced by a narrow-band P beam parallel to B, as a function of wavelength.

This confirms that $f(v\|B)$ has an axial drift of about 10^5 cm/sec ($\sim$ 10 μs/cm), and a width of the same extent corresponding to trace (d).

Optical line narrowing or ion velocity filtering can be obtained by making use of the vector properties of optical tagging. In a magnetic field, velocity and position are coupled so that velocity selection by lasers defines phase-space trajectories. We demonstrate this process using parallel P and S beams (which define the y-axis) normal to the magnetic field (z axis). When tuned to the same frequency ω, both beams resonante only with ions whose local velocity y-component v_y has the value $v_{yo} = (\omega - \omega_o)c/\omega$, where ω_o is the resonance for stationary particles. Consider ions initially resonant with P, moving towards S with a speed v_z. Over the axial separation Δz between beams, their v_y changes from v_{yo} to $v_y(\Delta z) = v_{yo}\cos\Phi + v_{xo}\sin\Phi$, where $\Phi = \Omega_c \Delta z/v_z$, and Ω_c is the cyclotron frequency. "Tagged" ions are that sub-class which resonates again with S; i.e., for which $v_y(\Delta z) = v_{yo}$. This condition requires $v_{xo} = v_{yo}(1-\cos\Phi)/\sin\Phi$. If the a-priori prababilities of v_{yo}, v_{xo} are Maxwellian with a temperature T, for instance, it follows that the tagged particle velocity distribution at S will be proportional to: $\exp - (v_{yo}^2 + v_{xo}^2)/T = \exp - 2v_{yo}^2/T(1+\cos\Phi)$. The temperature now has a coefficient ≤ 1; i.e., space-dependent line-narrowing has taken place. Note that two velocity components, v_{yo} and v_{xo}, have been selected by two lasers; this would require 3 lasers in the most recent version of velocity-selective optical pumping schemes.[3]

This process is illustrated in Figure 3. The beams are displaced along the magnetic field axis and their wavelength scanned in synchronism. Trace (a) shows the tagged fluorescence I_T. The narrow resonance corresponds to a Ba II "temperature" T* of about 60°K. For comparison, trace (b) shows the fluorescence of the background ions, corresponding to the full ion temperature, about 2,000°K. The resonances emerging on the side of the central peak in the narrowed trace (a), shown magnified and smoothed in the dashed sections, represent the hyperfine structure of Ba II in a magnetic field, visible even though the S laser is normal to the magnetic field. Finally, trace (c) plots the spatial variation in tagged linewidth, specifically the effective temperature $T^* = T(1 + \cos\Phi)/2$, which accurately fits our model. This velocity selection enables the Zeeman effect to be measured with much increased precision. It provides a new method for remotely measuring the local magnetic field in plasmas, or the hyperfine structure of ions, without the monochromaticity required in beam-injection schemes.[4]

Using optical tagging, transport processes which change both the velocity and position of particles can be diagnosed for the first time. An elementary scheme employs an S-beam scanned in space only, large enough in bandwidth to resonate with all particle velocities. Here we know the initial velocity and position of the ions, and measure their final positions, irrespective of final velocities.

The process we study is the cross-magnetic field scattering of ions caused by electrostatic waves (anomalous diffusion). These are excited by inserting a 2 cm. dia. electrode across the plasma,

with a positive bias relative to the hot-plate. The resulting instability has a strong radial electrostatic field component, causing strong ion heating.[5] The corresponding transport is measured by tagging ions at the center of the current filament, and scanning the S-beam across the plasma. Figure 4 shows the tagged intensity I_T (density profile of diffused particles) as a function of radius, for increasing excitation voltages. The traces document particle transport extending to the column edge. Due to radial weighting, the number of ions diffused to the edge of the plasma is much larger, proportionally, than appears from the raw data.

In the inset of Figure 4 is plotted the mean radius R_T determined from the radially weighted density profiles. Also shown is the increase in the mean Larmor radius R_L, calculated from the Doppler profile obtained via laser-induced fluorescence. The correspondence of the two radii would indicate that the over-all nature of the process is thermal: the "swelling" of the Larmor orbits is caused by ion heating by the waves. Although exact comparison with theory is beyond our scope, we note that this data provides the most detailed information yet available on ion transport.

In summary, the basic principles of optical tagging as well as new results and techniques have been described. This method is particularily suitable for collisionless (hot) plasmas, where transport occurs due to wave processes which do not alter the quantum state of tagged ions.

This work was supported by the National Science Foundation under Grant No. 80-09809.

Footnotes and References

*Visiting Professor, 1982-83, Centre de Recherches en Physique des Plasmas, Ecole Polytechnizue Federale, CH-1007 Lausanne, Switzerland. Permanent address: University of Colorado, Boulder, CO 90309.

1. A comprehensive overview can be found in: Laser Spectroscopy IV, H. Walther and K. W. Rothe, Eds. Springer-Verlag, New York 1979. Application to plasmas was first discussed conceptually by R. M. Measures, Journ. Appl. Phys. 39, 5232 (1968) and D. Dimock, E. Hinnov and L. C. Johnson, Phys. Fluids 12, 1730 (1969); and demonstrated experimentally in R. A. Stern and J. A. Johnson III, Phys. Rev. Lett. 34, 1548 (1975); R. A. Stern, D. L. Correll, H. Böhmer, and N. Rynn, Phys. Rev. Lett. 37, 833 (1976).
2. N. Rynn, Rev. Sci. Instrum. 35, 40 (1964).
3. L. Julien, M. Pinard and F. Laloe, Phys. Rev. Letts. 47, 564 (1981).
4. N. J. Wiegart, U. Rebhan and H.-J. Kunze, Physics Letts. 90A, 190 (1982).
5. N. Rynn, D. R. Dakin, D. L. Correll, and G. Benford, Phys. Rev. Letts. 33, 765 (1974).

Figure Captions

Figure 1. Top: Physical Principle. O,A,B, quantum states. Continuous lines: laser-pumped transitions. Wavy lines: spontaneous transitions. Bottom: Experimental Configuration.

Figure 2. Signal Modes. Vertical: tag signal intensity, linear scale, arbitrary units. Horizontal: time, linear scales indicated. (a) "Dark" signal, (b) "Bright" signal, direct PMT output. (c) Input signal monitor, (d) Tag signal, averaged.

Figure 3. Line Narrowing. Vertical: tagged signal intensity, linear scale, arbitrary units. Horizontal: wavelength, total scan shown 7.7 GHz. (a) tagged signal at cyclotron orbit midpoint. (b) untagged signal. Dashed: selected parts of (b), amplified and integrated. Insert: apparent temperature T* vs. axial laser separation Φ.

Figure 4. "Anomalous" Diffusion. P-beam at center, r = 0. Vertical tagged signal, linear scale, arbitrary units. Horizontal: radial position of S-beam. Excitation in volts as a parameter. Inset: Change in Thermal (ion Larmor), R_L, and Transport, R_T, radii versus excitation voltage.

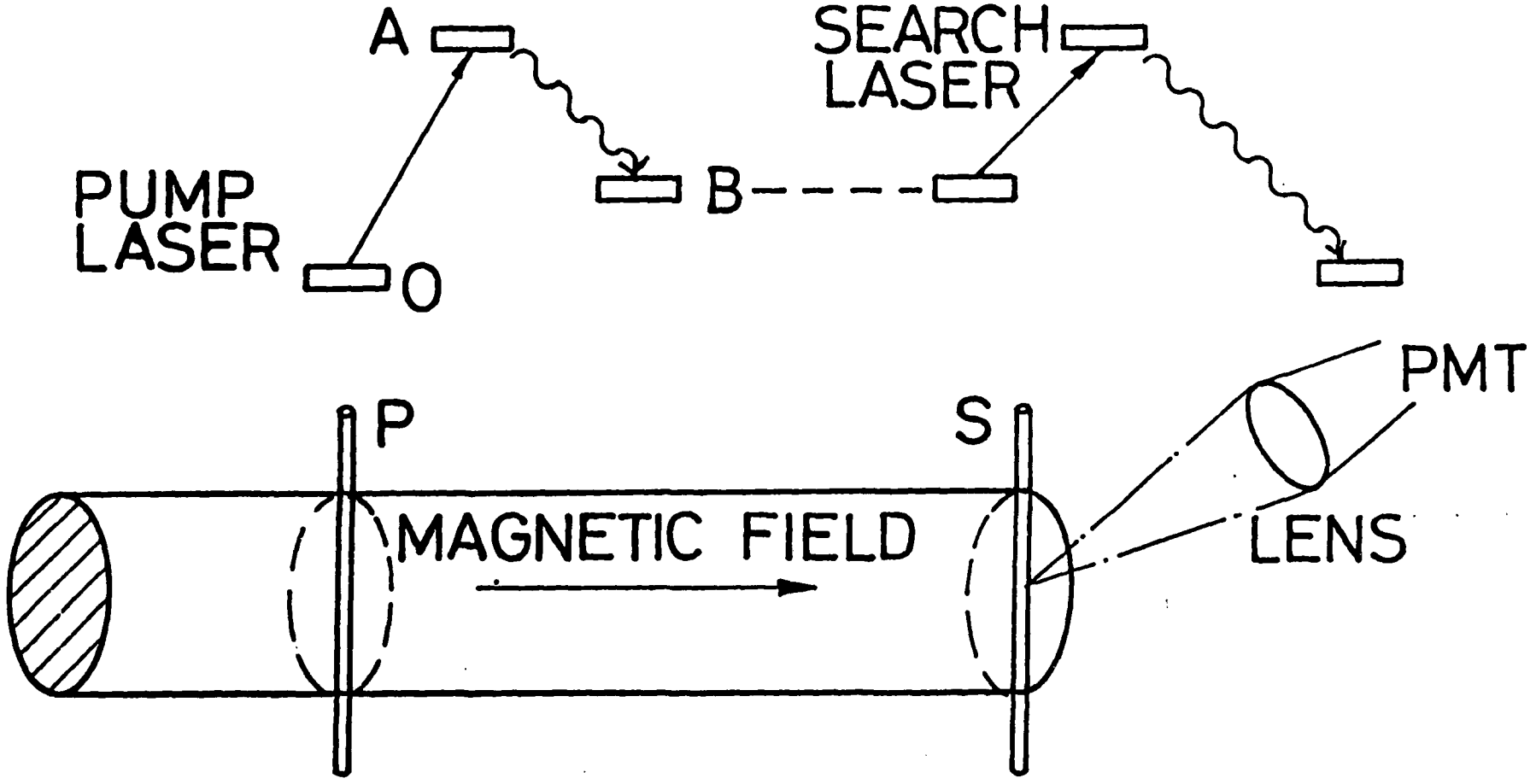
A
SEARCH
LASER
PUMP
LASER
O
B
PMT
P
S
MAGNETIC FIELD
LENS

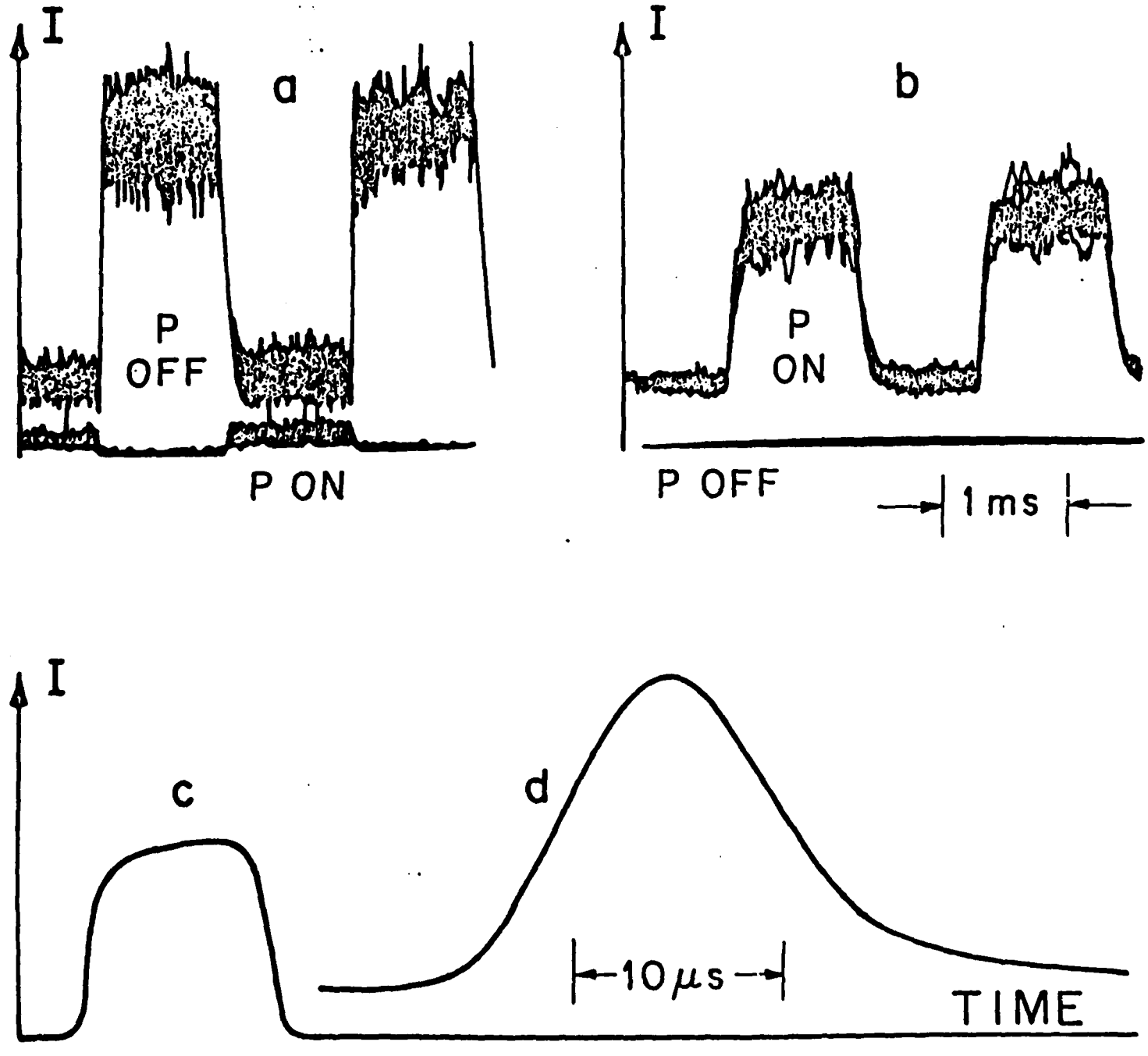
I
a
P
OFF
P ON
I
b
P
ON
P OFF
1 ms
I
c
d
10 μs
TIME

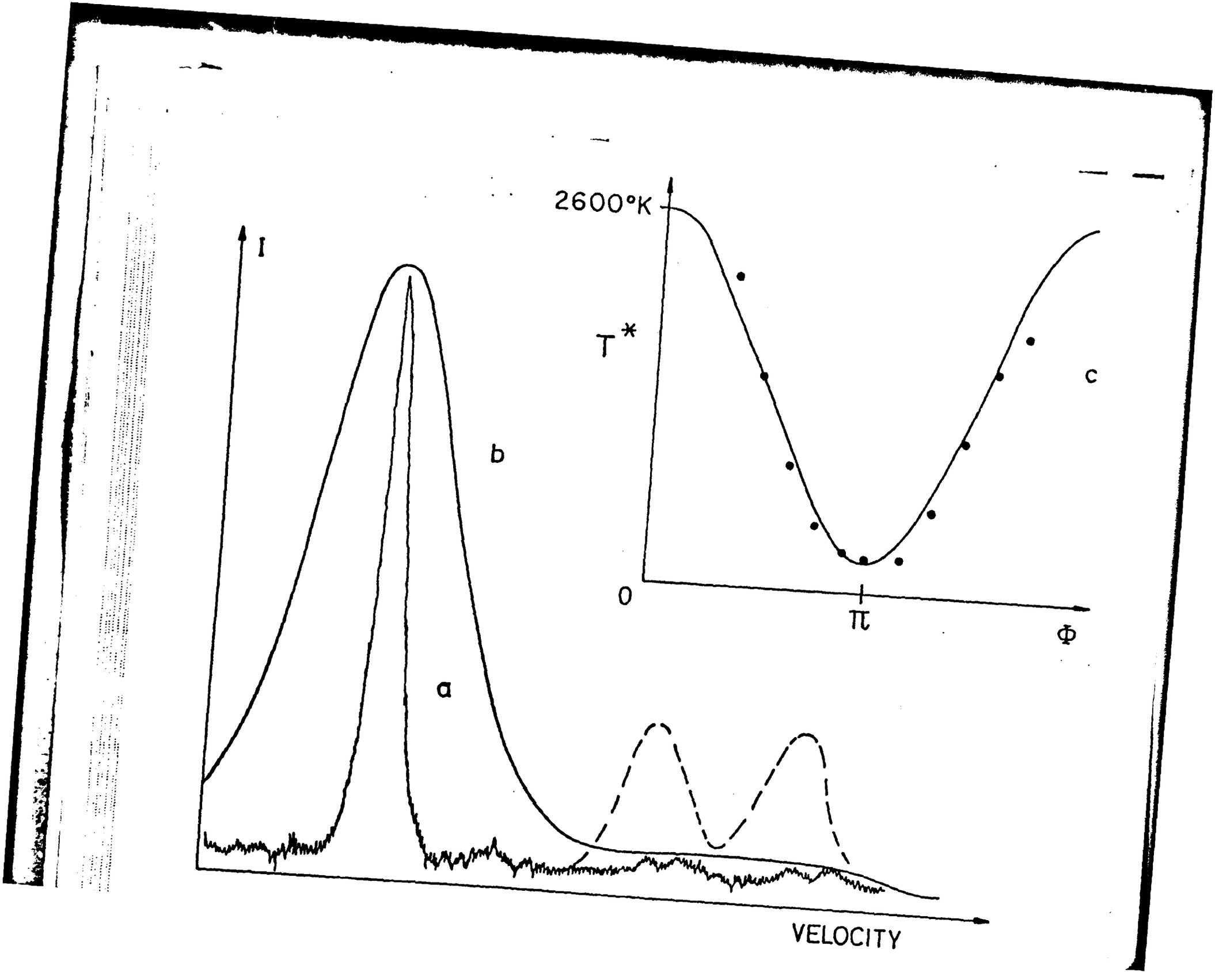
2600°K
T*
0
π
Φ
c
I
b
a
VELOCITY

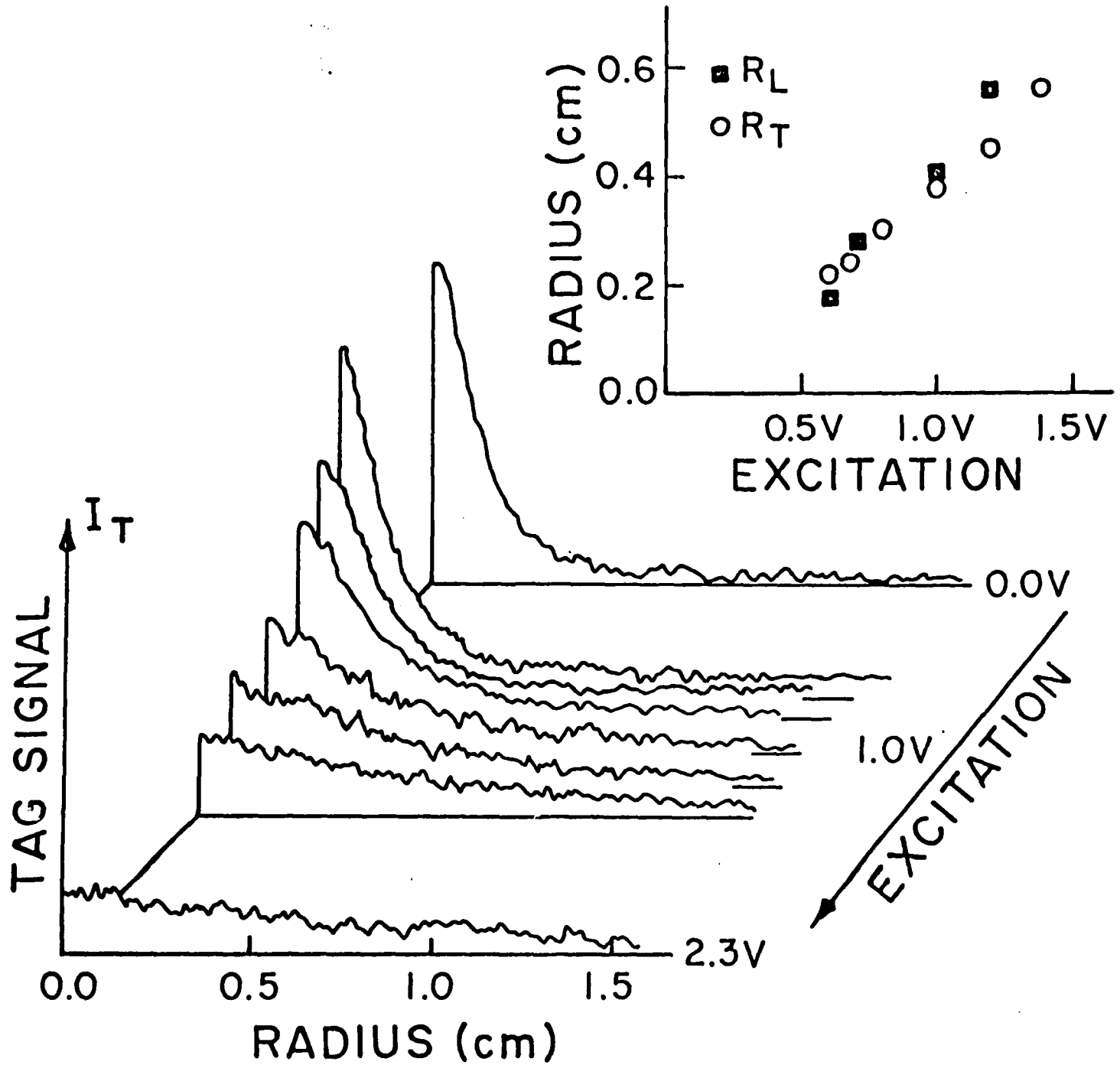
RADIUS (cm)
0.6
0.4
0.2
0.0
R_L
R_T
0.5V
1.0V
1.5V
EXCITATION
I_T
TAG SIGNAL
0.0V
1.0V
2.3V
EXCITATION
0.0
0.5
1.0
1.5
RADIUS (cm)

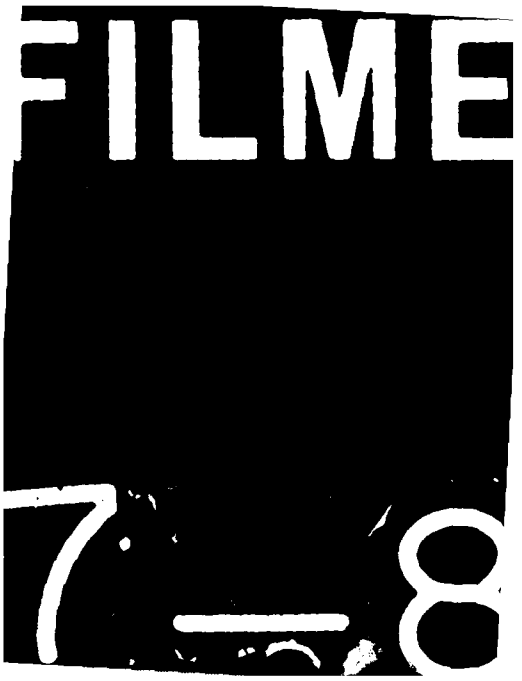
FILME